Naturally-Occurring Asbestos in Southern Nevada

Brenda J. Buck[1]
Rodney V. Metcalf[1]
Brett T. McLaurin[2]

[1]Department of Geoscience, University of Nevada Las Vegas, 4505 South Maryland Parkway, Las Vegas, Nevada 89119-4010
[2]Department of Environmental, Geographical and Geological Sciences, Bloomsburg University of Pennsylvania, 400 East Second Street, Bloomsburg, Pennsylvania 17815, USA

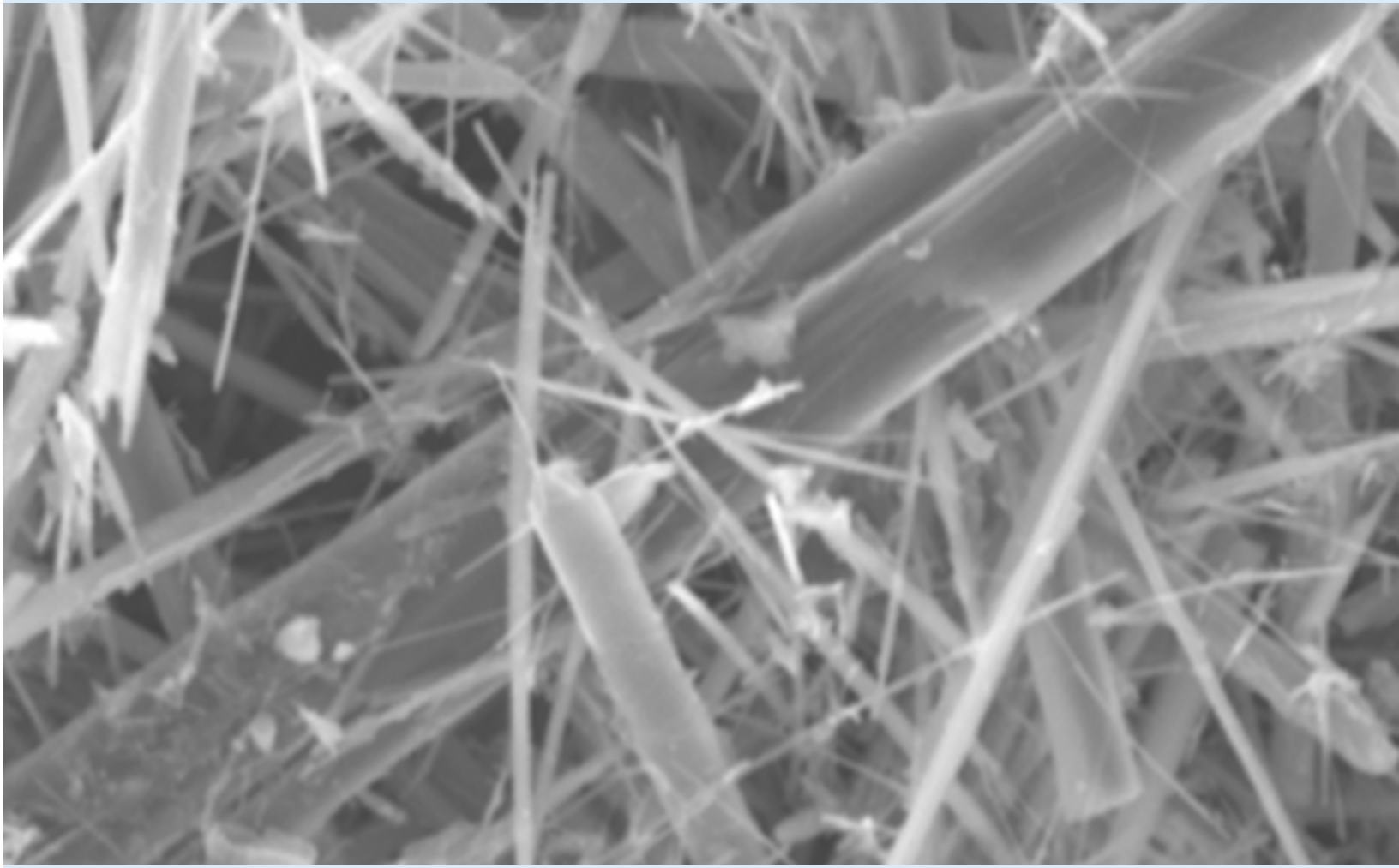

Final Report to Bureau of Land Management
for Task Agreement Number L13AC00237
December 2018

Cover Photo: SEM image of naturally-occurring amphibole asbestos from sample S5 near Searchlight Nevada.

The views and conclusions contained in this document are those of the authors and should not be interpreted as representing the opinions or policies of the U.S. Government. Mention of trade names or commercial products does not constitute their endorsement by the U.S. Government.

(This page intentionally left blank)

Table of Contents

Acknowledgements

Numerous people contributed many hours of hard work to collect the data contained within this report. We would especially like to thank all of the students who collected data to contribute to this report (in alphabetical order):

Isabella Aquino, undergraduate research, UNLV
Tomo Austin, M.S. graduate student, UNLV
Anabel Castro, undergraduate research, UNLV
Anay Gomez, undergraduate research, UNLV
Laekyn Kelley, undergraduate research, UNLV
Dara Laczniak, undergraduate research, UNLV
Samantha Lockhart, undergraduate research, UNLV
Jesus Solis-Leon, undergraduate research, UNLV
Meg Sumner-Moore, Bryn Mawr, summer undergraduate research, UNLV
Anna Urso, Depauw University, summer undergraduate research, UNLV

We thank Lisa Christianson (BLM) for her management of this project. We also thank UNLV staff for their hard work helping with administrative tasks: Elizabeth Smith, Maria Rojas, Cynthia Irwin, Terry Spell (Dept Chair). A very special thanks to Amanda Bengtson (Williams) at SWCA Environmental Consultants for statistical analyses.

Chapter 1:

Life Cycle of Asbestos

Rodney V. Metcalf[1]
Brenda J Buck[1]
Brett T. McLaurin[2]

[1]Department of Geoscience, University of Nevada Las Vegas, 4505 South Maryland Parkway, Las Vegas, Nevada 89119-4010
[2]Department of Environmental, Geographical and Geological Sciences, Bloomsburg University of Pennsylvania, 400 East Second Street, Bloomsburg, Pennsylvania 17815, USA

Introduction

In recent years there has been increased awareness of the potential health risks from environmental exposures to asbestos and asbestos-like minerals present as natural components in rocks, sediments, and soils. These exposures can be caused from, both occupational and non-occupational activities. The term **naturally-occurring asbestos** (NOA) has been used to describe such asbestos occurrences (including non-regulated fibrous minerals with known toxicity) (e.g. Harper, 2008). Here we introduce a new term, “commercially-modified asbestos” (CMA) to describe asbestos minerals that have been mined, processed, refined, and manufactured into products. The contrast between CMA and NOA points to important distinctions when considering the life cycle of asbestos for (1) fiber populations (size and morphology), (2) in assessing toxicity (related, in part, to morphology), (3) in understanding potential differences in human exposure pathways, (4) in developing appropriate monitoring strategies and risk assessment models, and (5) in improving diagnostic protocols (e.g. patient histories).

Our first paper reporting NOA in Clark County (Buck et al, 2013) caused considerable turmoil. This was in part because our reported locations were in the path of the I-11/Boulder City Bypass project (now completed), but also because asbestos was thought to form under a limited set of geologic conditions, ones that were well-understood and predictable. Because the geologic setting in southern Nevada was not one where asbestos would be predicted, our paper demonstrated a shortcoming in scientists’ understanding of how and where asbestos minerals form. That lack of understanding stemmed, in part, from the fact that much of what we knew about asbestos came from large, commercially exploitable asbestos ore deposits, which are typically rare. The concern is that asbestos minerals may be present in areas scientists had not previously considered as a potential source for environmental exposure to asbestos minerals.

What Is Asbestos?

In its most restrictive sense, asbestos is a commercial and regulatory term applied to six fibrous (asbestiform) minerals: the serpentine mineral chrysotile, and the fibrous varieties of five amphibole minerals, tremolite, actinolite riebeckite, cummingtonite-grunerite, and anthophyllite. Although initial recognition of the negative effects of asbestos inhalation came from heavy occupational exposures, years of research has clearly demonstrated that lower levels of exposure, including non-occupational exposure, can produce similar negative health outcomes. In recent decades research has shown that exposure to fibrous amphiboles outside the regulatory definition, e.g. winchite at Libby, Montana (US EPA, 2014), fluoro-edenite at Biancavilla, Italy (Comba et al., 2014), and to fibrous zeolite minerals, e.g. erionite in Cappadocia, Turkey (Carbone et al, 2011) represents a health risk equal to or greater than exposure to regulated asbestos minerals.

Asbestos-Related Health Concerns

Exposure to fibrous amphiboles can cause asbestosis, lung, ovarian, and larynx cancer, mesothelioma, pleural fibrosis, and possibly other health effects including depressed immune function, cardiovascular disease and gastrointestinal cancer (Aust et al., 2011; Antonio et al., 2011; Case et al., 2011; Pfau et al., 2014; Plumlee et al., 2006). Many of the characteristics believed to contribute to the ability of asbestos to cause disease include their fibrous shape, high surface area, and resistance to chemical and biological degradation (Aust et al., 2011; Plumlee et al., 2006). Toxicity is related to fiber width, length, aspect ratio, surface area, and surface chemical composition (Aust et al., 2011). Separable fibers longer than 5 μm with aspect ratios ≥ 3:1, and those that contain iron (Fe) are considered to be more toxic (Aust et al., 2011; Antonio et al., 2011; Case et al., 2011).

Overview of the Life Cycle of Asbestos

Here we present a model for the Life Cycle of Asbestos that seeks to track asbestos from petrogenesis of primary asbestos and asbestos-like minerals (defined as fibrous minerals with known or suspected toxicity), through all stages of the extraction (industrial) and/or liberation (natural) of asbestos minerals. The goal of the life cycle model is a better understanding of the occurrence of asbestos and asbestos-like minerals in both occupational and non-occupational settings, and to aid in the recognition of pathways to human exposures.

The Life Cycle model is illustrated in Figure 1-1. In the model, colored boxes represent physical materials and the solid arrows represent processes that link the groups of physical materials, these processes are identified in red text next to the arrows (Figure 1-1). The word “Modified” is use in the Life Cycle model to emphasize that these processes, whether industrial (mining, processes etc.) or natural (weathering, erosion, transport etc) are likely capable of altering the morphology (size & shape) of *individual* asbestos mineral particles and of the *populations* of asbestos mineral particles.

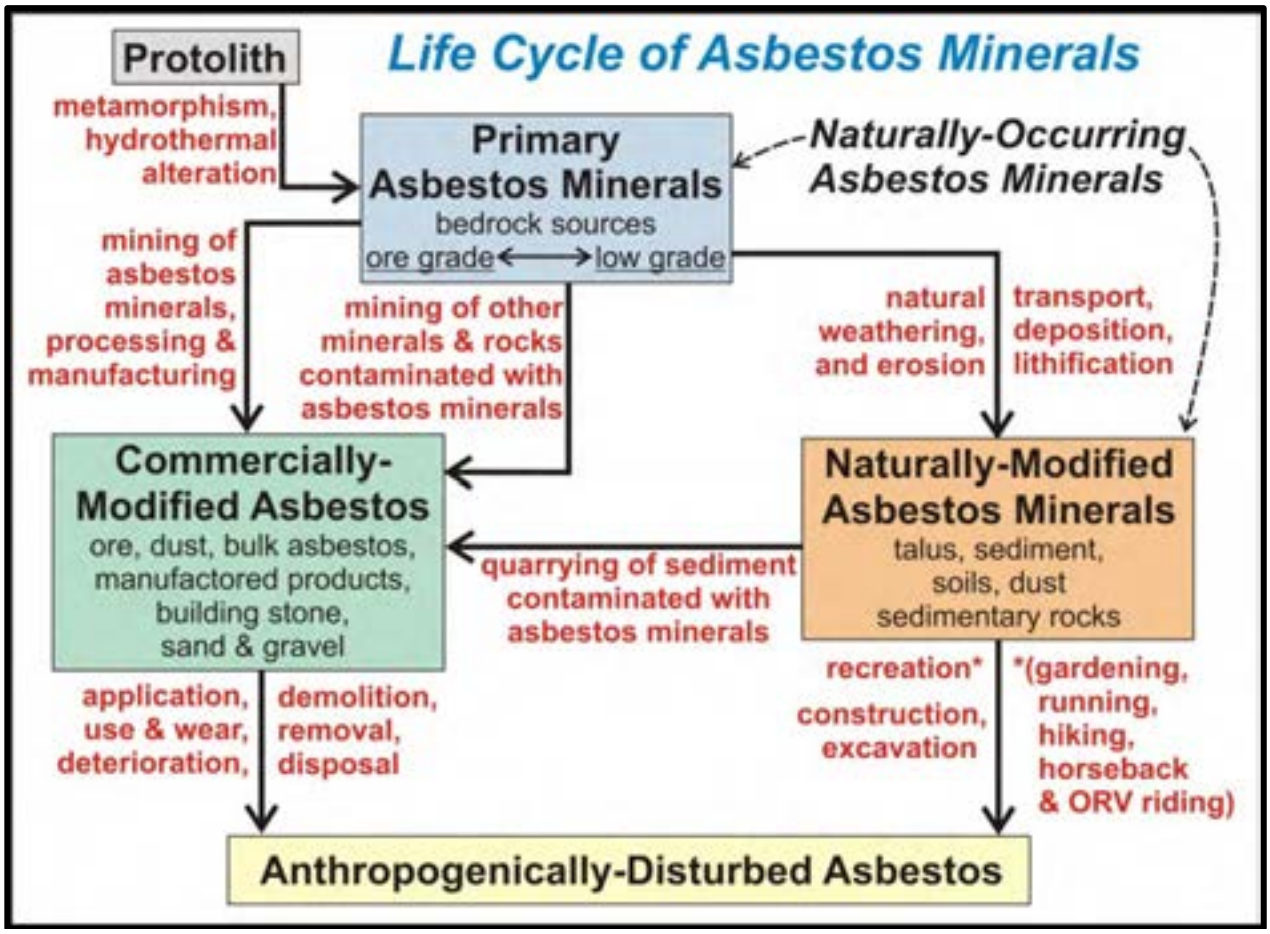

Figure 1-1. Life cycle model for asbestos minerals; boxes represent physical materials, arrows with red text denotes processes which move asbestos minerals through the environment. See text for further details.

Primary Asbestos Minerals refer to all bedrock sources of asbestos and asbestos-like minerals. Asbestos and asbestos-like minerals form via metamorphism, hydrothermal alteration and/or metasomatism of a **Protolith** (defined as a pre-existing rock). Common sources of commercial (regulated) asbestos include: altered ultramafic and mafic rock types, altered carbonate rocks, and altered banded iron formations (Van Gosen 2007). Fibrous amphiboles have also be found in alkalic mafic/ultramafic igneous intrusive complexes (e.g. Rainey Creek Complex, Libby MT, Meeker et al., 2003) and carbonatites associated with REE mineralization (Van Gosen, 2007). Recently fibrous amphiboles have been reported from hydrothermally altered granitic plutons along the Nevada-Arizona border near Hoover Dam (Buck et al., 2013; Metcalf and Buck, 2015), in granitic plutons in northern Italy (Lucci et al, 2018), and volcanic rocks on the flanks of the Mt Etna volcano near Biancavilla, Italy (Burragato et al, 2005). The primary source of naturally-modified asbestos may have lower concentrations of primary

asbestos minerals compared to richer deposits mined for commercial asbestos although localized areas may have high concentrations.

Commercially-Modified Asbestos (CMA) is produced when asbestos minerals are extracted from bedrock sources rocks during commercial mining operations and then turned into products (Figure 1-1). The most obvious example of CMA are asbestos products such as tiles, auto-brakes, insulation, fire retardants, cement binders, etc. These products are produced when are asbestos ores (rocks with high concentrations of asbestos minerals) are mined, processed (crushed), separated, and sorted for different applications, then manufactured into products. The six regulated asbestos minerals were those that were being commercially mined and made into products when regulations were first written in the late 1970s. Much of our understanding of the genesis, human exposure pathways, particle morphology, toxicity, and even the minerals considered asbestos, come from the exploitation of commercial asbestos deposits.

Within the Life Cycle model, *commercially-modified asbestos* also may include asbestos or asbestos-like minerals that contaminate *other commercially extracted ores***,** and may be present at concentrations likely below that of ore grade asbestos (Figure 1-1). The most notable example of this type of CMA is vermiculite ore contaminated with fibrous amphibole asbestos (winchite, richterite, magnesio-riebeckite) at Libby, Montana (Meeker et al., 2006). Finally, commercially-modified asbestos could include *industrial rocks and minerals* such as building stone, sand and gravel, but likely at concentrations well below that of ore grade asbestos deposits; volcanic quarry stone contaminated with the fibrous amphibole fluoro-edenite at Biancavilla, Italy (Burragato et al, 2005) is a notable example of this type of CMA.

Naturally-Modified Asbestos Minerals refer to asbestos and asbestos-like minerals that have been liberated from primary outcrops by natural processes of weathering and erosion, soil formation, transport (wind or water), deposition, and lithification into clastic sedimentary rock (Figure 1-1). These materials include talus, alluvium, soils, sedimentary rocks formed from these materials, and dust. These naturally-modified asbestos materials are the greatest source of environmental human exposure via dust.

Naturally-Occurring Asbestos is a term applied to fibrous minerals with known or suspected toxicity that are present as a natural component of rocks and soils, and may include fibrous minerals that do not meet the regulatory definitions of asbestos (Harper, 2008; Metcalf and Buck, 2015). Within the Life Cycle model both *primary asbestos minerals* and *naturally-modified asbestos minerals* are considered to constitute *naturally-occurring asbestos*. Recognizing the presence of naturally-occurring asbestos minerals is critical to understanding potential human exposure pathways, and to developing appropriate monitoring strategies and risk assessments plans.

Finally, the Life Cycle model includes a category called **Anthropogentically-Disturbed Asbestos** which is meant to emphasize human interactions with both *commercially-modified asbestos* and *naturally-modified asbestos minerals*. This designation and the processes that connect it to CMA and NMA is intended to draw attention to the various pathways for human exposure related to either occupational or non-occupational activities of the general population. A good example is off-road-vehicle driving, see Chapter 5 in this report.

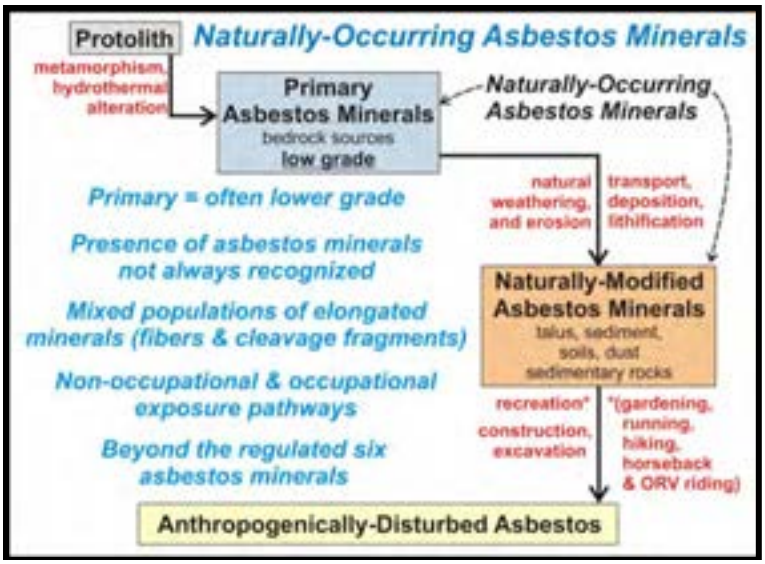

Figure 1-2. Portion of the Asbestos Life Cycle model that deals with naturally-occurring asbestos.

Naturally-Occurring Asbestos in Clark County and Adjacent Areas

Asbestos-bearing materials in Clark County (including BLM lands) and adjacent areas fit into the *naturally-occurring asbestos* portions of the Life Cycle model (see Figure 1.2). One example in Clark County of *Primary asbestos minerals,* are those found in fractured, faulted and hydrothermally altered portions of Miocene-age (17-12 million years) plutons (igneous magma that solidified in the subsurface). These plutons form a north-south belt along the Nevada-Arizona border south of Lake Mead (Figure 1.3). Immediately following pluton solidification a hydrothermal fluid-flow fracture system was established, as plutons were faulted, uplifted, and exposed to erosion at the earth's surface. Altered NOA-bearing Miocene plutonic rocks were being eroded at the earth's surface within two millions years of pluton solidification (Metcalf and Buck, 2015; Felger et al., 2014). Erosion of uplifted NOA-bearing Miocene plutons produced *naturally-modified asbestos materials* now found in Miocene to recent (12 million years to present) alluvial fans that surround areas of uplifted plutons. It is the NOA-bearing alluvial fans (e.g. soils) that carry the greatest risk of NOA exposure to humans because (1) asbestos fibers can become more easily airborne when soils containing NOA are disturbed as compared to bedrock, (2) people tend to have more interactions with the

landscape in areas containing soils as compared to bedrock, and (3) the footprint of NOA-containing soils is larger than that of bedrock (see Chapter 4). During the course of this project, we also learned that hydrothermal alteration of other lithologies, specifically Precambrian age (~14.1.7 billion years) plutonic and metamorphic rocks, could produce NOA as well. We used our understanding of the genesis of primary asbestos minerals and the role of natural processes to modify and redistribute NOA into alluvial fans, as a guide our sampling strategies during this project.

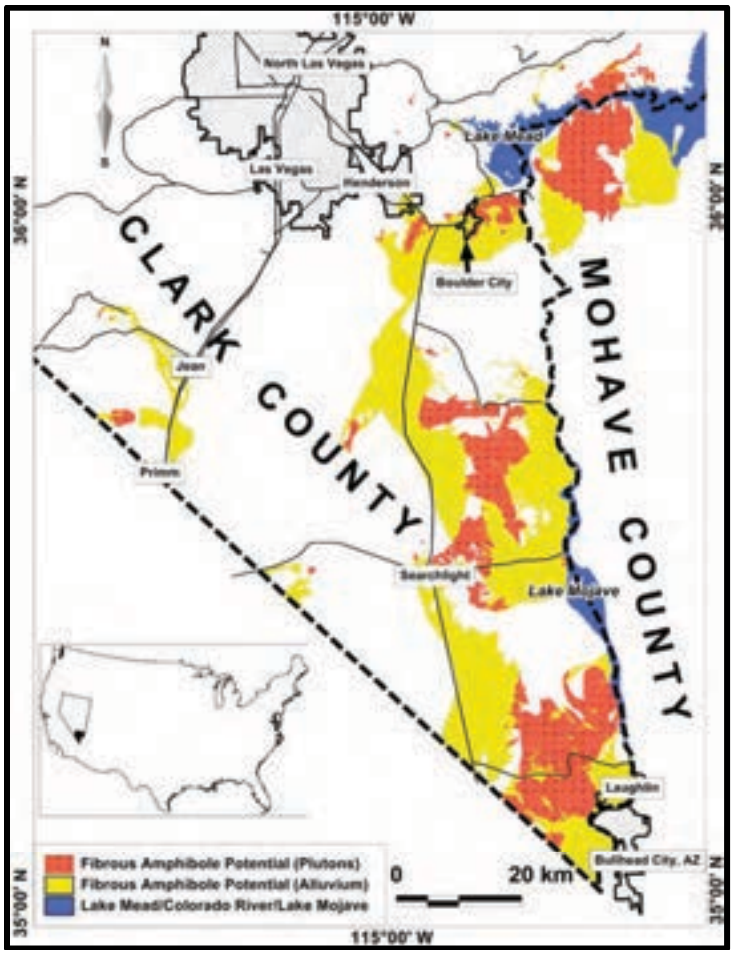

Figure 1-3. NOA potential map (from Buck el al., 2013) based on distribution of Miocene age plutons (source of Primary Asbestos Minerals) and Miocene to recent alluvium eroded from plutons.

References

Anatao, V. C., Larson, T.C. & Horton, D.K., 2012, Libby vermiculite exposure and risk of developing asbestos-related lung and pleural diseases: Current Opinion in Pulmonary Medicine v. 18, p. 161-167.

Aust, A.E., Cook, P.M. & Dodson, R.F., 2011, Morphology and chemical mechanisms of elongate mineral particle toxicities: Journal of Toxicology and Environmental Health, Part B v. 14, p. 40-75.

Buck, B.J., Goossens, D. Metcalf, R.V., McLaurin, B., Ren, M., and Freudenberger*, F., 2013, Naturally occurring asbestos: Potential for human exposure, southern Nevada USA, *Soil Science Society of America Journal,* 77:2192-2204. doi:10.2136/sssaj2013.05.0183

Burragato, F., Comba, P., Baiocchi, V., Palladino, D.M., Gianfagna, A., Paoletti, L., and Pasetto, R. (2005) Geo-volcanlogical, mineralogical, and environmental aspects of quarry materials related to pleural neoplasm in the area of Biancavilla, Mount Etna (Eastern Sicily, Italy). Environmental Geology 47, 855-868, DOI: 10.1007/s00254-004-1217-7.

Carbone, M., Baris¸, Y. I., Bertino, P., Brass, B., Comertpay, S., Dogan, A. U., et al. (2011). Erionite exposure in North Dakota and Turkish villages with mesothelioma. *Proceedings of the National Academy of Sciences of the United States of America,* 108(33), 13618–13623.

Case, B.W., Abraham, J.L., Meeker, G., Pooley, F.D., Pinkerton, K.E., 2011, Applying definitions of “asbestos” to environmental and “low-dose” exposure levels and health effects, particularly malignant mesothelioma. Journal of Toxicology and Environmental Health, Part B v. 14, p. 3-39.

Comba, P., Scondotto, S., Musmeci., L. (2014) The fibres with fluoro-edenitic composition in Biancavilla (Sicily, Italy): Health impact and clues for environmental remediation. Ann Ist Super Sanità Vol. 50, No. 2: 108-110, DOI:0.4415/ANN_14_02_01

Harper, M. 2008. 10th Anniversary critical review: Naturally occurring asbestos. *J. Environ. Monit.* 10:1394–1408.

Lucci, F., Ventura, G.D., Conte, A., Nazzari, M., Scarlato, P. (2018) Naturally Occurring Asbestos (NOA) in Granitoid Rocks, A Case Study from Sardinia (Italy). Minerals, 8, 442; doi:10.3390/min8100442.

Meeker, G., A. Bern, I. Brown_eld, H. Lowers, S. Sutley, T. Hoefen, and J. Vance. 2003. The composition and morphology of amphiboles from the Rainy Creek Complex near Libby, Montana. Am. Mineral. 88:1955–1969.

Meeker, G., H. Lowers, G. Swayze, B. Van Gosen, S. Sutley, and I. Brownfield. 2006. Mineralogy and morphology of amphiboles observed in soils and rocks in El Dorado Hills, California. USGS Open-File Rep. 2006-1362. USGS, Reston, VA.

Metcalf, R.V., and Buck, B.J., 2015, Genesis and health risk implication of an unusual occurrence of NaFe3+-amphibole: *Geology* v. 43, p. 63-66, doi:10.1130/G36199.1

Pfau, J.C., K.M. Serve, and Noonan, C.W., 2014. Autoimmunity and asbestos exposure. *Autoimmune Dis,* p. 782045.

Plumlee G.S., Morman S., & Ziegler T., 2006, The toxicological geochemistry of earth materials: An overview of processes and the interdisciplinary methods used to understand them: Reviews Mineralogy and Geochemistry, v. 64, p. 5-57.
US Environmental Protection Agency (EPA), 2014. Toxicological Review of Libby Amphibole Asbestos. EPA/635/R-11/002F

Van Gosen, B.S., 2007. The geology of asbestos in the United States and its practical applications. *Environmental & engineering Geoscience* v. XIII, No. 1, pp. 55-68.

Chapter 2:

Chemical Classification of Naturally-Occurring Asbestos

Rodney V. Metcalf[1]
Brenda J Buck[1]
Brett T. McLaurin[2]

[1]Department of Geoscience, University of Nevada Las Vegas, 4505 South Maryland Parkway, Las Vegas, Nevada 89119-4010
[2]Department of Environmental, Geographical and Geological Sciences, Bloomsburg University of Pennsylvania, 400 East Second Street, Bloomsburg, Pennsylvania 17815, USA

Introduction

Asbestos and naturally-occurring asbestos (NOA) are defined by (1) *morphology* (fibrous shape and size) and (2) *mineral classification* which is based on the chemical composition of minerals, specifically the mineral formula. Serpentine asbestos (chrysotile) has a nearly fixed mineral formula (little chemical variation), amphibole group minerals, however, exhibit wide variability in chemical formulae. In this study we used the scanning electron microscope (SEM) with energy dispersive spectroscopy (EDS) to observe and measure the morphology of individual NOA particles obtained from rock and soil.

Amphiboles

Amphiboles (Figure 2-1) are hydrous silicate minerals formed of double-wide chains of oxygen-sharing $[SiO_4]^{4-}$ tetrahedra elongate in the c-crystallographic direction (double chain tetrahedra are linked by shared O^{2-} anions forming a polymer structure of Si_4O_{11}). The general formula of amphibole group minerals is $A_{0-1}B_2C_5T_8O_{22}(OH)_2$ (Table 2.1). A layer of octahedral cations (surrounded by and bonded to six O^{2-} that comprise the C-sites) are sandwiched between two double-wide silicate chains forming a TOT "I-beam" unit; I-beams are bound together by cations on the B-site. Cations are distributed in the amphibole structure as follows: T = Si^{4+} ±Al^{3+}, C = Mg^{2+}, Fe^{2+}, Al^{3+}, and Fe^{3+}, B = Ca^{2+}, Na^{1+}, Mg^{2+}, and/or Fe^{2+} for end-member amphiboles, and A-site can be empty (vacancy) or partially to completed filled with Na^{1+} and/or K^{1+}. The large number of possible cation substitutions across numerous cation sites allows for considerable compositional variation (called solid solution), thus amphiboles comprise a large mineral group with over 70 individual mineral species (names).

In this study we employed an amphibole classification system based on recommendations and nomenclature of the International Mineralogical Association (Leake et al., 1997) referred to herein as IMA97. The IMA97 classification divides

amphiboles into four main subgroups based on B-site cation occupancy: calcic amphiboles ($Ca_B \geq 1.5$ cations), sodic-calcic amphiboles ($Na_B = 0.5\text{-}1.5$), sodic ampbiboles ($Na_B > 1.5$ cations), and Mg-Fe amphiboles ($[Ca+Na]_B < 1$, $[Mg+Fe]_B > 1$). Each of these groups are further subdivided based on T-site occupancy (amount of Al^{3+} substituting for Si^{4+}), Mg# (defined as Mg/[Mg + Fe^{2+}] per formula), and on the A-site occupancy.

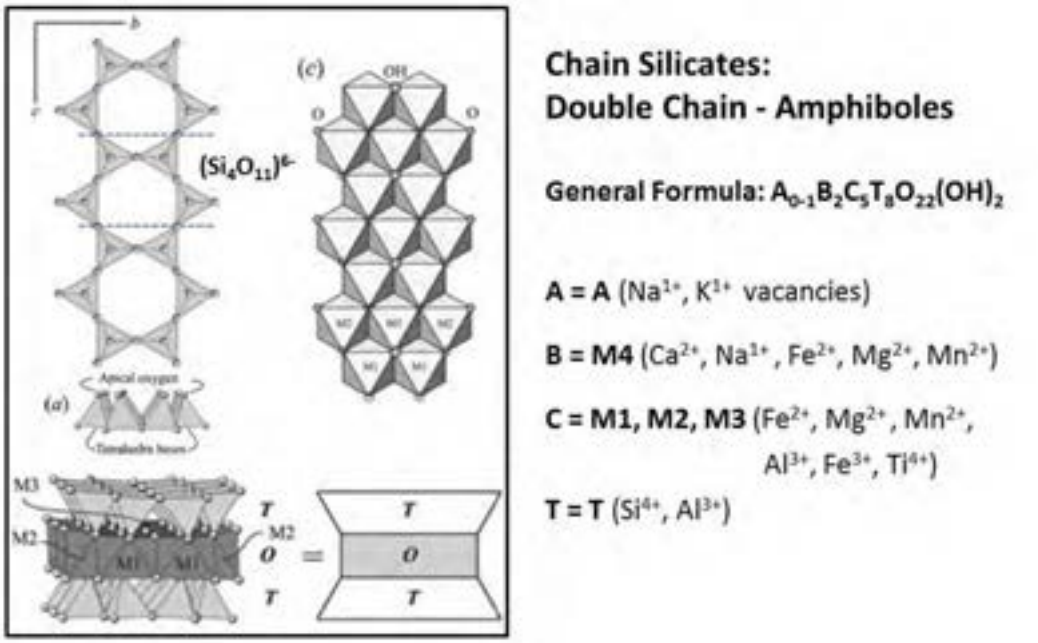

Figure 2-1. Formula, atomic structure and cation distribution in amphibole group minerals.,

EPMA-WDS Amphibole Data Sets Collected on Polished Rock Thin-Sections

The state-of-the-art method for acquiring mineral chemical data is the Electron Probe Micro-Analyzer (EPMA) using Wavelength Dispersive Spectrometers (WDS) x-ray detectors; this method is *fully quantitative* when data is collected in situ using polished thin-sections of rock samples. Chemical data from the EPMA-WDS analyses are reported as weight percent oxides (wt% SiO_2, Na_2O etc.). In order to classify the mineral these oxide data are converted into a structural (chemical) formula through a complicated calculation procedure following recommendations in IMA97. The calculation used is referred to as 23-oxygen normalization. Some amphiboles contain

both FeO (Fe^{2+}) and Fe_2O_3 (Fe^{3+}) but the EPMA-WDS analysis method cannot measure Fe valance states and reports all Fe as FeO (Fe^{2+}). When significant amounts of Fe_2O_3 (Fe^{3+}) are present it impacts the quality of the 23-oxygen normalization calculation. IMA97 outlines a procedure (based on six possible versions of a cation normative calculation) that sets the minimum and maximum amounts of Fe^{3+} allowed for each individual analysis, the averaged value is then used to convert an amount of FeO to Fe_2O_3 prior to the 23-oxygen normalization calculation (see Appendix 2 in Leake et al., 1997 for details). We developed an Excel spreadsheet to make these calculations using EPMA-WDS data.

As part of this project we used EPMA-WDS to collect quantitative analyses of amphibole in polished thin-sections made from NOA-bearing hydrothermally altered rocks collected on or adjacent to BLM lands in Clark County, Nevada. We refer to this data set as the *altered Nevada data set*. We also include a companion data set from NOA-bearing altered Miocene plutonic rocks (Wilson Ridge pluton) in Mohave County, Arizona. This data set, which we refer to as the *altered Arizona data set*, includes previously published data (Metcalf and Buck, 2015; Pfau et al 2017) plus additional data collected in a companion study. Finally we present amphibole analyses from unaltered Miocene plutonic rocks, specifically unaltered portions of the Miocene Wilson Ridge pluton (data used in Metcalf, 2004) and unaltered Precambrian gneiss (Beshears, 2016). Our Excel spreadsheet was used to calculate full 23-oxygen normalized structural formulae (including calculated Fe^{3+}) on all of these analyses; these results then were used to assign each analysis an IMA97 mineral name and plot on the appropriate IMA97 classification diagram (Figures 2.2-2.5).

The *altered Nevada data set* includes a total of 547 analyses collected from 11 individual samples, nine samples of NOA-bearing Miocene plutonic rocks and three samples of NOA-bearing Precambrian gneiss. Prior to collecting data on the EPMA, polished thin-sections were examined and photographed on the petrographic (optical) microscope and areas for EPMA analysis selected. Results for the altered Nevada data set are shown in Figure 2-2. The majority of the altered Nevada analyses yielded calcic amphibole formulas including actinolite (54%), magnesiohornblende (33%), edenite (2%), and pargasite (2%). One sample (a Precambrian gneiss) yielded Mg-Fe-Mn amphibole formulas for the mineral cummingtonite (67%). The remainder of the *altered Nevada data set* also includes several analyses with sodic-calcic compositions (winchite, magnesiokatophorite, taramite).

The *altered Arizona data set* includes 507 analyses from 11 samples; all samples are from the Miocene Wilson Ridge pluton, Mohave County, Arizona. Results for the altered Arizona data set are plotted in Figure 2-3. Sodic-calcic and sodic compositions make up a large portion of the data set, including winchite (41%), magnesioriebeckite (8%) and richterite (3%). Calcic amphiboles, including actinolite (26%), magnesiohornblende (21%), and edenite (1%) make up the remainder of the *altered Arizona data set*.

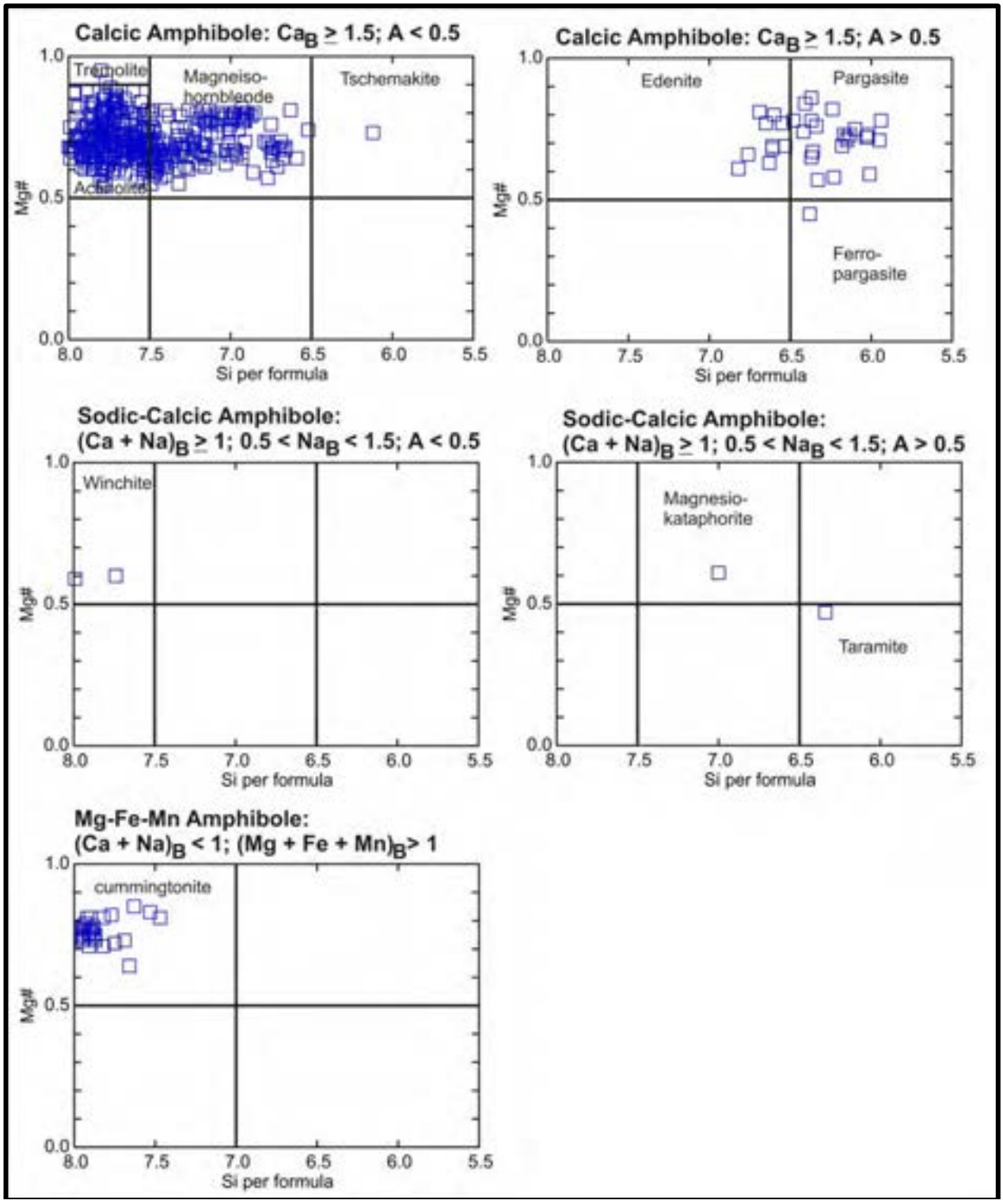

Figure 2-2 Amphibole classification diagrams (Leake et al., 1997) showing EPMA-WDS data set for altered rocks from Clark County, Nevada (BLM lands).

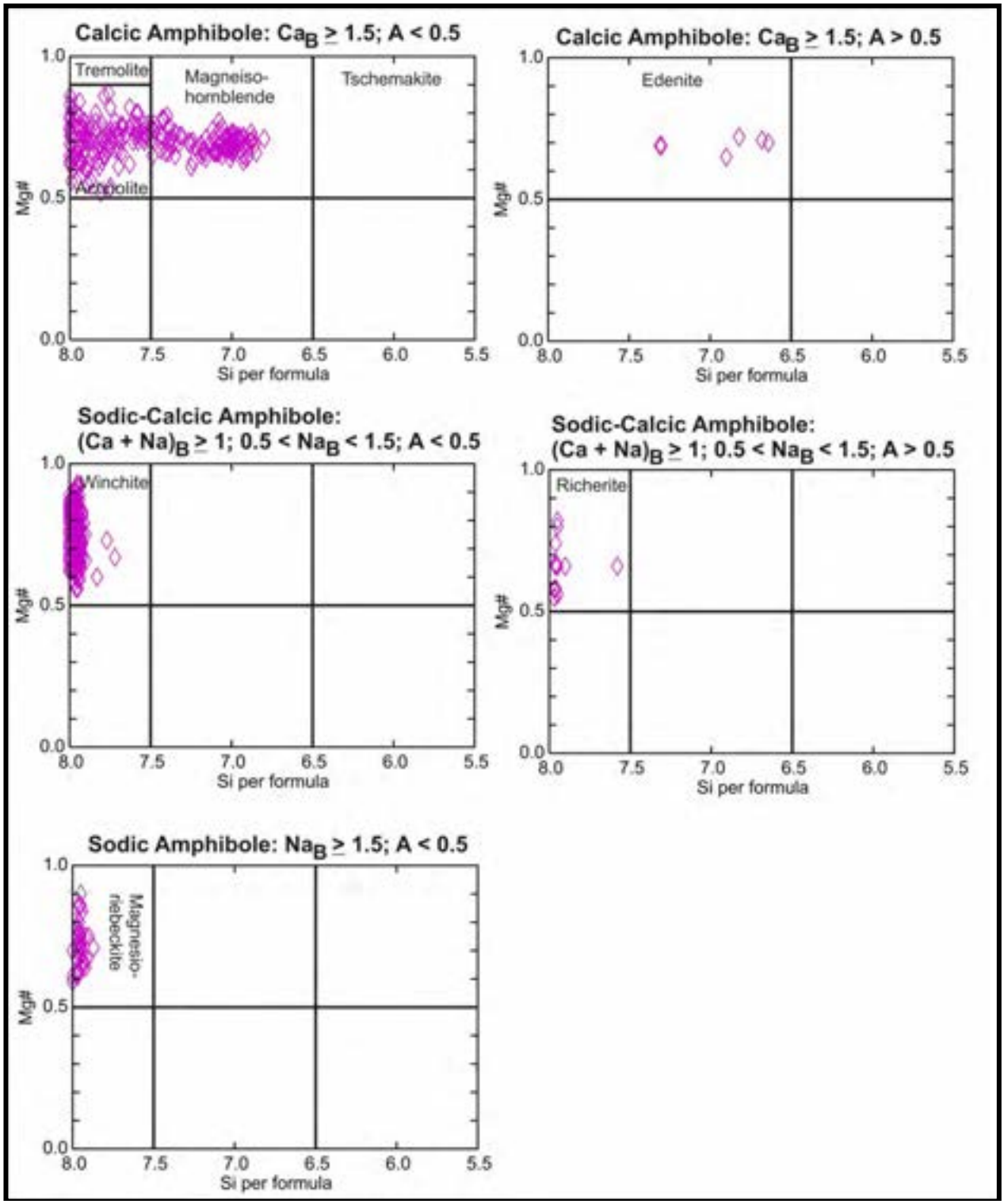

Figure 2-3. Amphibole classification diagrams (Leake et al., 1997) showing EPMA-WDS data set for altered rocks from Mohave County, Arizona (data from Metcalf and Buck, 2015, Pfau et al 2017, unpublished data)..

Amphibole analyses from unaltered portions of the Miocene Wilson Ridge pluton are shown in Figure 2-4; the data set includes 255 analyses from eight samples. These amphiboles are igneous in origin and grew as pluton magmas cooled and crystallized beneath the Earth's surface. As such these amphibole analyses reflect magmatic compositions prior to the hydrothermal alteration that produced amphibole NOA. The unaltered Wilson Ridge samples are calcic amphiboles dominated by magnesiohornblende (99 %) plus three analyses of actinolite (1%).

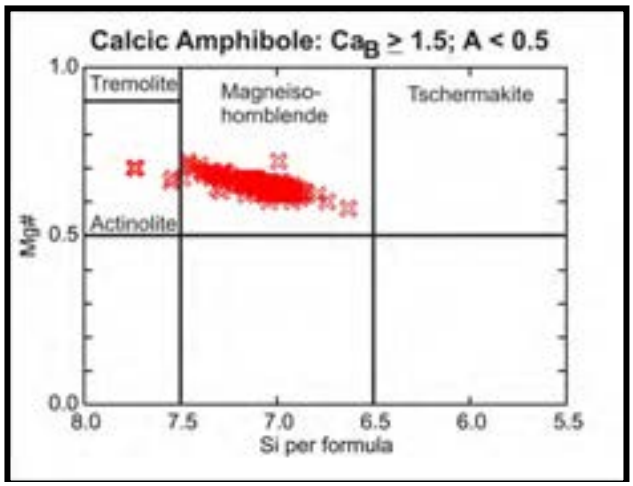

Figure 2-4. Amphibole classification diagrams (Leake et al., 1997) showing EPMA-WDS data set for igneous amphiboles from unaltered Miocene plutons in Mohave County, Arizona. (Metcalf, 2004).

Analyses of amphiboles from the Precambrian gneiss are shown in Figure 2-5; this data set includes 19 analyses from two samples. These samples formed during high temperature metamorphism and lack evidence of NOA growth. Amphiboles in the Precambrian gneiss are calcic amphiboles dominated by magnesiohornblende (99%) with one analysis yielding a tschermakite composition and one an edenite composition.

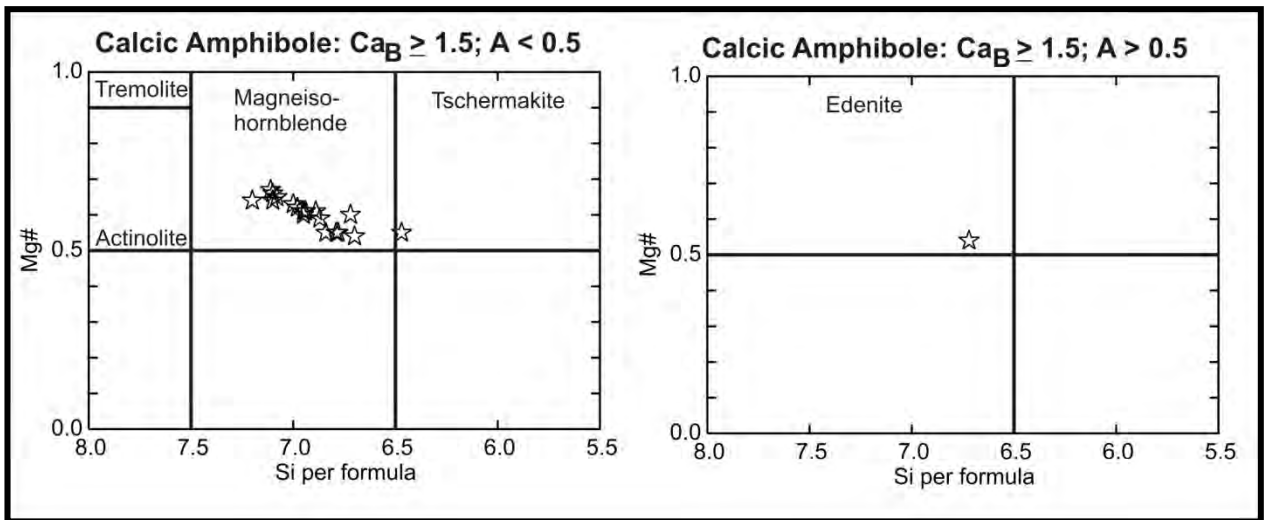

Figure 2-5. Amphibole classification diagrams (Leake et al., 1997) showing EPMA-WDS data for amphiboles in unaltered metamorphic Precambrian gneiss, Mohave County, Arizona. (Beshears, 2016).

Comparing the four data sets, all analyses, altered and unaltered, have Mg# (Mg/[Mg + Fe^{2+}]) above 0.5 (Figures 2-2 to 2-6). The greatest variation across these four data sets is found in the B-site cation occupy, reflecting the occurrence of calcic amphiboles, sodium amphiboles (including sodic-calcic & sodic), and Mg-Fe-Mn amphiboles; these compositional differences can be illustrated using a ternary (triangular) plot of Ca, Na and Fe on the amphibole B-site (Figure 2-6).

The unaltered igneous and metamorphic amphiboles exhibit a narrow range of composition centered on magnesiohornblende (Figures 2-4 to 2-6), with a clear covariance between Mg# and T-site Si (measure of Al substitution in T-site); such narrow, correlated compositional variations are typical of high temperature igneous and metamorphic amphiboles. In contrast, the *altered Nevada and Arizona data* sets show considerable composition variability in terms of Mg# and Si on T-site (Figures 2.2, 2.3) and significant variation in B-site occupancy (Figure 2-6). Calcic amphibole compositions dominate the *altered Nevada data set* but B-site substitution varies from Ca end member towards the Fe end member, with a small number of analyses showing Na exchange (Figure 2-6). Amphiboles in the *altered Arizona data set* show a continuous compositional variation between Ca and Na end members (calcic to sodic-calcic to calcic).

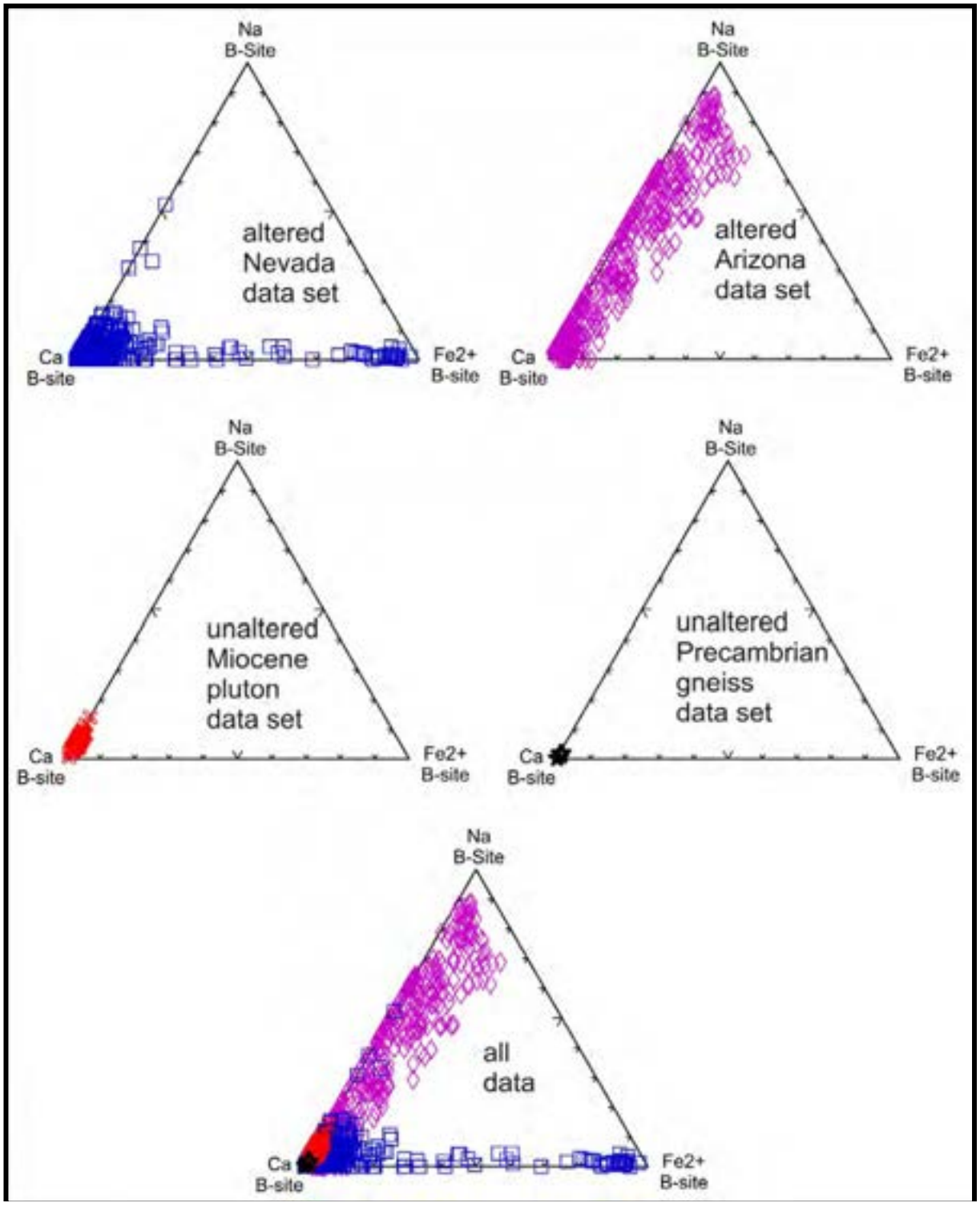

Figure 2-6. Amphibole B-site cation occupancy based on full 23-oxygen normalized structural formulae (including calculated Fe^{2+}-Fe^{3+}) using EPMA-WDS data sets

SEM-EDS Amphibole Particle Data Sets

We used the scanning electron microscope (SEM) with energy dispersive spectroscopy (EDS) to collected images and mineral chemical data on individual particles from rock and soil samples (see sample collection methods in Chapter 4). We used the mineral chemistry to evaluate whether or not a particle was an amphibole, and then to classify the amphibole. We only collected morphology measurements on particles that where confirmed as amphibole using mineral chemistry.

The SEM-EDS analysis is typically reported as a continuous spectra plot (x-ray energy peaks corresponding to elements and their relative abundances); interpreting such plots somewhat subjective and is time consuming for large data sets. The EDS data can also be reported as weight percent oxides, similar to that reported in EPMA-WDS analysis. Under ideal conditions, for example, long count times collected on polished thin-sections, SEM-EDS analyses are *semi-quantitative*. Collecting SEM-EDS data on individual micro-scale particles is less than ideal due to low x-ray count rates in the small, micron to sub-micron diameter particles being analyzed (an another related issue called mass absorption). Attempts to do full structural formula calculations that estimate Fe^{2+} and Fe^{3+} using SEM-EDS data on individual particles generally do not yield reasonable results so we followed the technique used by Meeker et al. (2003) of using a simpler calculation that treated all Fe as Fe^{2+}. Knowledge of Fe^{3+} is most important when dealing with Na-rich amphiboles (winchite) but it is still possible to properly classify those minerals without Fe^{3+} estimates (Meeker et al 2003); for samples low in Fe^{3+} (e.g. our calcic amphiboles) the all- Fe-as-Fe^{2+} calculation is essentially equivalent to the full Fe^{2+}- Fe^{3+} calculation and resulting classification.

We used SEM-EDS wt% oxide data to calculate an all-Fe-as-Fe^{2+} structural formulae on each particle examined. We then used the resulting structural formula to evaluate whether or not the particle was an amphibole (yes/no). This evaluation examined cation totals for each amphibole cation site; ideal stoichiometry is T-site sum ~8, C-site sum ~ 5, B-site sum ~ 2, A-site sum < 1, and total cations of 15-16. Based on close inspection of our first ~2000 SEM-EDS particles we set acceptable upper and lower limits for each of these totals, for a particle to be considered an amphibole, the analysis results had to pass all five cation-site tests. We then set up an Excel spreadsheet to calculate the all-Fe-as-Fe^{2+} structural formulae and apply the five cation-totals amphibole stoichiometry test; our particle morphology measurements and statistics were limited to particles that passed this amphibole stoichiometry test.

During the study we evaluated SEM-EDS data for more than 6000 particles, of those approximately 50% were excluded based on the amphibole stoichiometry test discussed above. Figure 2-7 shows the structural formula data for the nearly 3000 SEM-EDS particles that passed the amphibole stoichiometry test and compares those results with the altered Nevada and altered Arizona EPMA-WDS data sets discussed in the previous section. [Note: the EPMA-WDS data plotted in Figure 2-7 is based on the all-Fe-as-Fe^{2+} calculation allowing for a more direct comparison with the SEM-EDS results.]

As a whole the SEM-EDS data set collected from individual particles reveals remarkably similar patterns to that seen in the EPMA-WDS data set collected from polished thin-sections. The bulk of the SEM-EDS data set has Mg# and Si cations per formula values similar to the EPMA-WDS data sets (compare Figure 2-7 b and d). As with the EPMA-WDS data sets, in the SEM-EDS particle data sets are dominated by calcic amphibole compositions, show compositional trends from Ca towards more Na compositions (sodic-calcic and sodic), and show compositional trends from Ca towards Fe compositions with some analyses plotting near the Fe (cummingtonite) end-member corner.

More information on the distribution, occurrence, and particle morphologies associated with these different amphibole minerals can be found in Chapter 4.

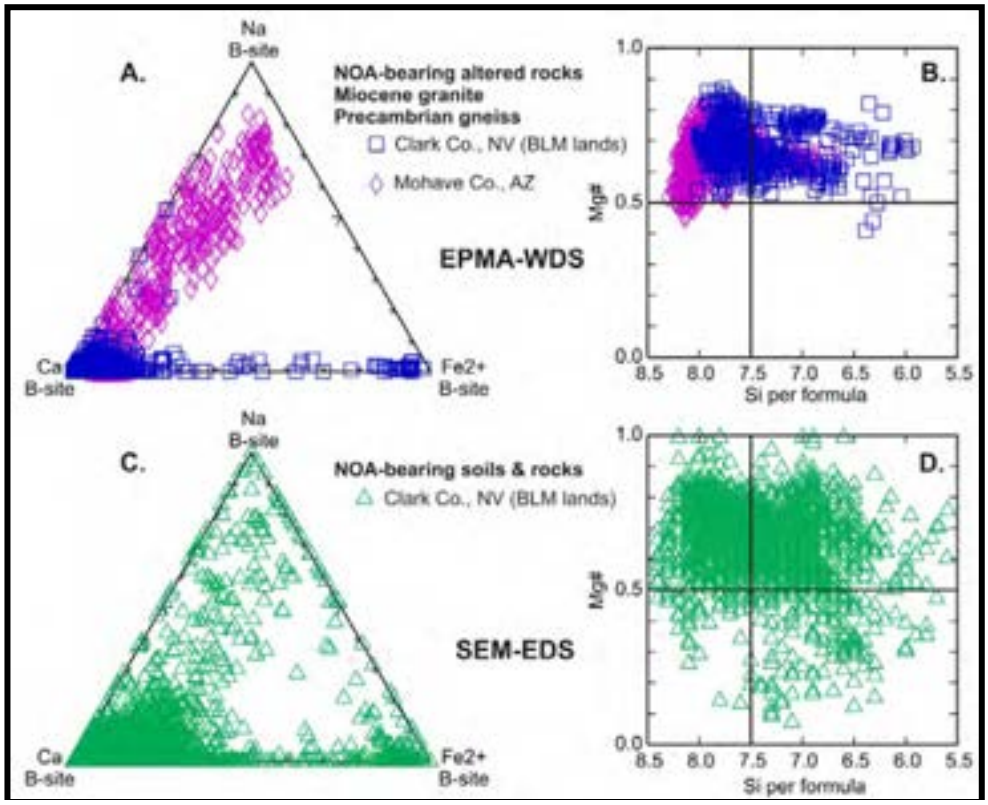

Figure 2-7. Comparision of structural formula calculations using EPMA-WDS on polished thin-sections with structural formula calculations using SEM-EDS on individual fibers from soils and rocks. Both sets of calculations treat all Fe as Fe^{2+}.

References

Beshears, M. (2016) Characterizing the Earliest Stages of Partial Melting: A Study of the Pyrometamorphic Aureole of Miocene Mt. Perkins Pluton, Northwest Arizona. UNLV M.S.Thesis, 224 pages.

Buck, B.J., Goossens, D. Metcalf, R.V., McLaurin, B., Ren, M., and Freudenberger, F., 2013, Naturally occurring asbestos: Potential for human exposure, southern Nevada USA, Soil Science Society of America Journal, 77:2192-2204. doi:10.2136/sssaj2013.05.0183

Metcalf, R.V., and Buck, B.J., 2015, Genesis and health risk implication of an unusual occurrence of NaFe3+-amphibole: Geology v. 43, p. 63-66, doi:10.1130/G36199.1

Leake, B.E., Woolley, A., Arps C., Birch, W. Gilbert, M. Grice, J. Hawthorne, F. Kato, H. Kasch, A., Krivovichev, V., Linthout, K., Laird, J. Mandarino, J., Maresch, W., Nichel, E., Rock, N., Schumacher, J., Smith, D., Stephenson, N., Ungaretti, L., Whittaker, E. and Youzhi, G., 1997, Nomenclature of the amphiboles: Report of the subcommittee on amphiboles of the International Mineralogical Association, Commission on New Minerals and Mineral Names: American Mineralogist, v. 82, p. 1019–1037.

Pfau, Jean C., Buck, Brenda J., Metcalf, Rodney V., Kaupish, Zoie, Stair, Caleb, Rodriguez, Maria, Keil, Deborah E. (2017) Comparative Health Effects in Mice of Libby Amphibole Asbestos and a Fibrous Amphibole from Arizona. Toxicology and Applied Pharmacology, v. 334, p. 24-34, doi.org/10.1016/j.taap.2017.08.022.

Chapter 3:

Petrogenesis of Amphibole Asbestos in Clark County, Nevada and Adjacent Areas

Rodney V. Metcalf[1]
Brenda J. Buck[1]
Tomoyo Austin[1]

[1]Department of Geoscience, University of Nevada Las Vegas, 4505 South Maryland Parkway, Las Vegas, Nevada 89119-4010

Introduction

An understanding of the processes forming, and geologic settings hosting, amphibole asbestos is necessary to mitigate environmental, non-occupational exposure to amphibole asbestos. This chapter deals with that part of the Life Cycle of Asbestos (Figure 1-1, Chapter 1) that links the **Protolith** to **Primary Asbestos Minerals**, specifically the hydrothermal, metamorphic and metasomatic processes that generates asbestos, in this case, amphibole asbestos, and the geologic settings where that might happen. Our first paper (Buck et al., 2013) reporting amphibole asbestos near Boulder City was a surprise to scientists, including asbestos experts, because of gaps in our knowledge of how and where amphibole asbestos forms. This chapter discusses our research efforts aimed at a better understand the genesis of amphibole asbestos.

Geologic Context of NOA in NV-AZ Study Area

Fibrous actinolite and winchite/Mg-riebeckite are found in faulted and hydrothermally altered Miocene age (17-13 million year) igneous plutons along the AZ-NV border parallel to the Colorado River. These plutons form a belt from near Hoover Dam in the north to near Laughlin in the south (Buck et al., 2013; Metcalf and Buck, 2015). The youngest and most altered of these plutons are near Hoover Dam and have reported ion probe U-Pb zircon crystallizations ages is 13.7 ±0.5 Ma (Wilson Ridge pluton, Metcalf and Buck 2015) and 13.96 ±0.25 Ma (Boulder City pluton, Felger et al. 2014).

These plutons were faulted, uplifted, eroded and shedding detritus containing amphibole asbestos with 2 million years of solidification (Felger et al., 2014; Metcalf and Buck, 2015). The onset of fibrous amphibole mineralization at Wilson Ridge is constrained between 13.7 and 11.7 Ma (Metcalf and Buck, 2015) and geologic constraints suggest similar timing of fibrous amphibole mineralization at Boulder City. Miocene plutons to the south are slightly older (17-15 Ma) but have a similar faulting and uplift history that began soon after solidification, and amphibole asbestos is also found associated with these southern plutons (see Chapter 4).

In the most altered rocks, fibrous minerals are found as veins in fractured hornblende-bearing plutonic rock in the proximity of faults responsible for pluton uplift. Individual veins are millimeters to centimeters wide; planar networks of veins and breccia up to several meters wide can be traced for hundreds of meters parallel to mapped faults. Fibrous amphiboles also are found disseminated within the plutonic rocks. Disseminated fibrous amphiboles are present as replacement of magmatic hornblende in rocks that contain veins. In addition, disseminated fibrous amphiboles are found in rocks that lack fibrous amphiboles as vein material, in these case it takes a trained eye, and or optical microscopy or electron microscopy, to confirm the presence of amphibole asbestos.

Fibrous amphiboles are associated with Miocene plutons in NV are dominantly calcic amphiboles (actinolite) with a minor amount of more sodic compositions (Figures 2-2, 2-6; Chapter 2). One sample of Precambrian gneiss in the Eldorado Range (NV) contains the fibrous cummingtonite, a Fe-Mg amphibole (Figures 2-2, 2-6; Chapter 2). Fibrous amphiboles in altered Wilson Ridge pluton, AZ are dominated by sodic-calcic and sodic amphiboles, winchite, magnesioriebeckite and richterite (Figure 2-3, 2-6; Chapter 2).

Methods

We used the polarizing petrographic light (optical) microscope fitted with a digital camera to examine polished-thin sections made from a suite of variably altered amphibole-bearing Miocene plutonic rocks and spatially associated Precambrian gneiss in Clark County and adjacent areas in Arizona. The petrographic microscope was used to evaluated, categorize, and photomicrograph images of the mineralogy and textures associated with hydrothermal alteration and amphibole asbestos. Mineral chemistry of amphibole and feldspar (plagioclase and K-feldspar) were analyzed in polished thin-section on an Electron Probe Micro-Analyzer (EPMA) using Wavelength Dispersive Spectrometers (WDS) x-ray detectors (JEOL 8900 Superprobe house at UNLV, see Buck et al., 2013 and Metcalf and Buck, 2015 for a discussion of analytical procedures).

Amphibole Mineral Chemistry

The full EPMA-WDS amphibole data sets were discussed in Chapter 2 but are reproduced here for convenience; please refer to Chapter 2 for figures related to amphibole chemistry.

The *altered Nevada data set* includes a total of 547 analyses collected from 11 individual samples, nine samples of NOA-bearing Miocene plutonic rocks and three samples of NOA-bearing Precambrian gneiss. Prior to collecting data on the EPMA, polished thin-sections were examined and photographed on the petrographic (optical) microscope and areas for EPMA analysis selected. Results for the altered Nevada data set are shown in Figure 2-2 (Chapter 2). The majority of the altered Nevada analyses yielded calcic amphibole formulas including actinolite (54%), magnesiohornblende (33%), edenite (2%), and pargasite (2%). One sample (a Precambrian gneiss) yielded Mg-Fe-Mn amphibole formulas for the mineral cummingtonite (67%). The remainder of

the *altered Nevada data set* also includes several analyses with sodic-calcic compositions (winchite, magnesiokatophorite, taramite).

The *altered Arizona data set* includes 507 analyses from 11 samples; all samples are from the Miocene Wilson Ridge pluton, Mohave County, Arizona. Results for the altered Arizona data set are plotted in Figure 2-3 (Chapter 2). Sodic-calcic and sodic compositions make up a large portion of the data set, including winchite (41%), magnesioriebeckite (8%) and richterite (3%). Calcic amphiboles, including actinolite (26%), magnesiohornblende (21%), and edenite (1%) make up the remainder of the *altered Arizona data set*.

Amphibole analyses from unaltered portions of the Miocene Wilson Ridge pluton are shown in Figure 2-4 (Chapter 2); the data set includes 255 analyses from eight samples. These amphiboles are igneous in origin and grew as pluton magmas cooled and crystallized beneath the Earth's surface. As such these amphibole analyses reflect magmatic compositions prior to the hydrothermal alteration that produced amphibole NOA. The unaltered Wilson Ridge samples are calcic amphiboles dominated by magnesiohornblende (99 %) plus three analyses of actinolite (1%).

Analyses of amphiboles from the Precambrian gneiss are shown in Figure 2-5 (Chapter 2); this data set includes 19 analyses from two samples. These samples formed during high temperature metamorphism and lack evidence of NOA growth. Amphiboles in the Precambrian gneiss are calcic amphiboles dominated by magnesiohornblende (99%) with one analysis yielding a tschermakite composition and one an edenite composition.

Comparing the four data sets, all analyses, altered and unaltered, have Mg# (Mg/[Mg + Fe^{2+}]) above 0.5 (Figures 2-2 to 2-6, Chapter 2). The greatest variation across these four data sets is found in the B-site cation occupy, reflecting the occurrence of calcic amphiboles, sodium amphiboles (including sodic-calcic & sodic), and Mg-Fe-Mn amphiboles; these compositional differences can be illustrated using a ternary (triangular) plot of Ca, Na and Fe on the amphibole B-site (Figure 2-6; Chapter 2).

The unaltered igneous and metamorphic amphiboles exhibit a narrow range of composition centered on magnesiohornblende (Figures 2-4 to 2-6; Chapter 2), with a clear covariance between Mg# and T-site Si (measure of Al substitution in T-site); such narrow, correlated compositional variations are typical of high temperature igneous and metamorphic amphiboles. In contrast, the *altered Nevada and Arizona data* sets show considerable composition variability in terms of Mg# and Si on T-site (Figures 2-2, 2-3; Chapter 2) and significant variation in B-site occupancy (Figure 2-6; Chapter 2). Calcic amphibole compositions dominate the *altered Nevada data set* but B-site substitution varies from Ca end member towards the Fe end member, with a small number of analyses showing Na exchange (Figure 2-6; Chapter 2). Amphiboles in the *altered Arizona data set* show a continuous compositional variation between Ca and Na end members (calcic to sodic-calcic to calcic).

Plagioclase Chemistry Results

Plagioclase feldspar is a Na-Ca solid solution series where compositions can vary continuously between two end members, albite (Ab = $NaAlSi_3O_8$) and anorthite (An = $CaAl_2Si_2O_8$); plagioclase can also have a minor of orthoclase (Or = $KAlSi_3O_8$) content. Plagioclase wt% oxide analyses were converted to plagioclase structural formula which report percent Ab-An-Or, and plagioclase compositions are typically reported as An% (An_{0-100}) and ranges of An are given names (ablite (An_{0-10}), oligoclase (An_{10-30}), andesine (An_{30-50}), labradorite (An_{50-70}), bytownite (An_{70-90}), and anorthite (An_{90-100})). Plagioclase results are shown in Figure 3-1 and included both altered and unaltered samples. Plagioclases from unaltered samples, and unaltered areas in weakly altered samples, have oligoclase to labradorite compositions (An_{23-70}) typical of such igneous plagioclase. Altered grains associated with amphibole asbestos have close to end-member albite compositions (An_{0-10}) which is typical of hydrothermal plagioclase.

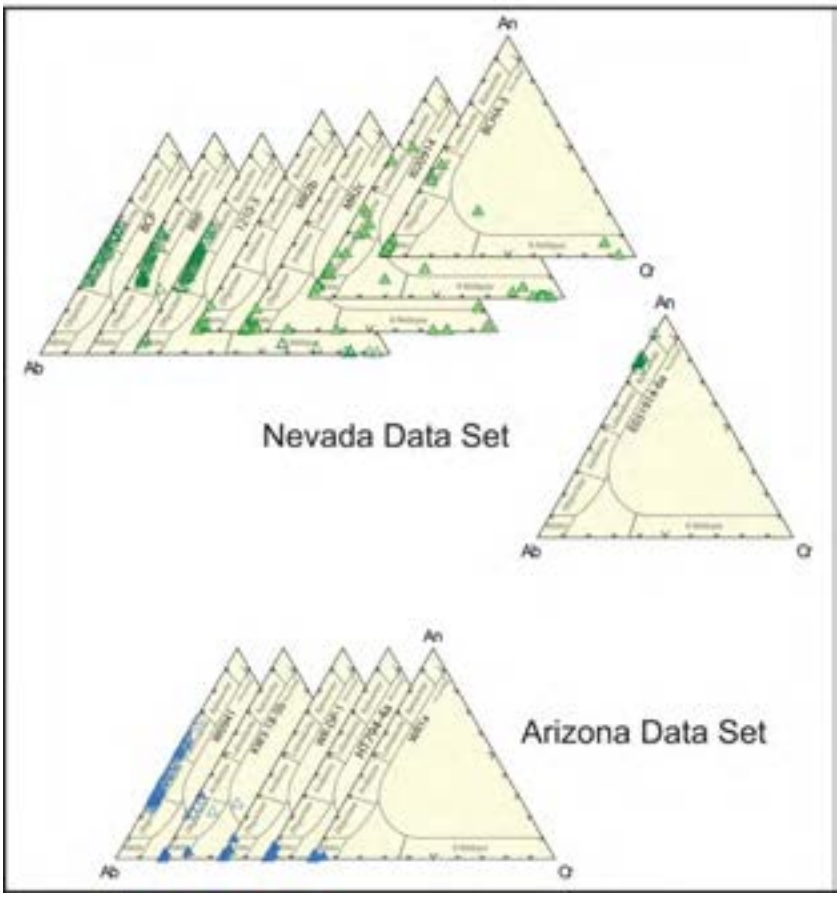

Figure 3-1. Plagioclase EPMA_WDS results, upper set from Nevada, lower set from Arizona. Nevada samples BCP (Boulder City pluton), RRP (Railroad Pass pluton), and 1210-3 are for unaltered pluton rocks in Nevada, samples MR2b and MR2c are heavy altered and contain actinolite asbestos, samples I020914 and BCHA-3 are moderately altered samples containing actinolite asbestos, sample E031914-6a is a moderately alter Precambrian gneiss with cummingtonite asbestos. Sample Wo841 is an unaltered sample of Wilson Ridge pluton in Arizona, the remaining samples in the Arizona data set are heavily altered samples with winchite-magnesioriebeckite asbestos.

Petrography

Protolith (unaltered) Mineralogy and Textures: Unaltered samples of Miocene plutonic rocks from NV and AZ both contain plagioclase, orthoclase, quartz, hornblende, and biotite and a minor amount of apatite, opaque oxides (magnetite), zircon, and titanite (Figure 3-2). Plagioclase (oligoclase to labradorite, An_{23}-An_{70}) is subhedral to euhedral, relatively unaltered (lacking significant sericite) and clear in plane light, and many grains exhibit euhedral optical growth zoning (Figure 3-2) and well-defined albite and Carlsbad twinning. Magmatic amphibole (magnesiohornblende) is subhedral to euhedral prismatic, moderately pleochroic dark green to light green and shows {110} cleavage intersecting at 56° and 124 ° for crystals cut perpendicular to the c-axis (Figure 3-2).

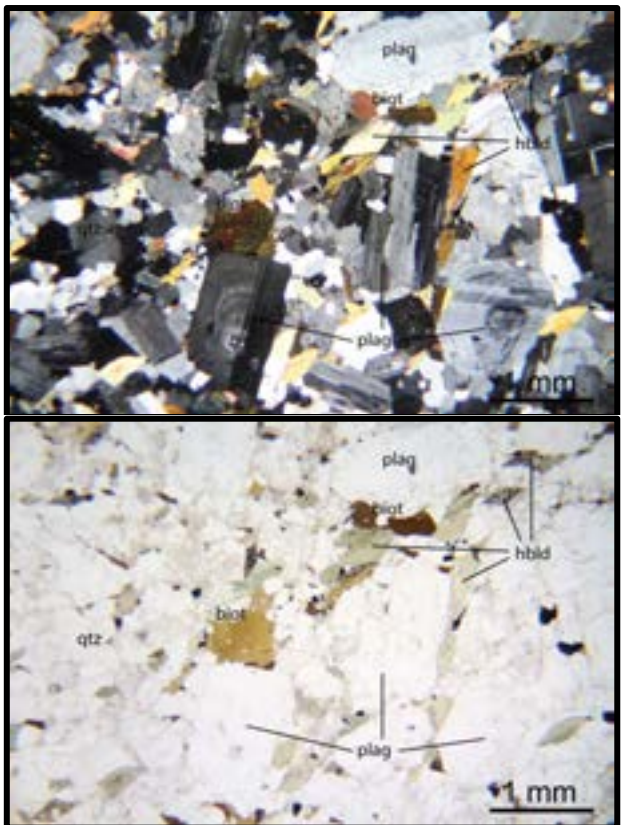

Figure 3-2. Photomicrograph of unaltered Miocene plutonic rock, top is under polarized light, bottom image under light. Images show unaltered magmatic plagioclase, magnesiohornblende, quartz, and biotite.

Altered Nevada Sample Set: Fibrous amphibole in the Nevada data set is dominantly actinolite, but includes minor winchite and cummingtonite. Fibrous amphibole in Nevada samples is present in as fracture fill material, and as pseudomorphic replacement of magmatic (protolith) magnesiohornblende. Additional alteration minerals associated with fibrous amphiboles include albite (Na end-member of the Na-Ca plagioclase feldspar solid solution series) as pseudomorphic replacement of magmatic plagioclase of

intermediate (oligoclase to labradorite) composition, ± K-feldspar (as veins), ± quartz (as veins) ± epidote (as veins and as replacement of magmatic plagioclase), ± hematite (alteration of magnetite or as veins), and more rarely chlorite (as replacement of magmatic magnesiohornblende). Late stage calcite ($CaCO_3$) veins are commonly observed cross-cutting fibrous amphibole.

Altered Arizona Sample Set: Fibrous amphibole in the Nevada samples is dominated by sodium-rich amphiboles (winchite, richterite and magnesio-riebeckite) but does include the calcic amphibole actinolite. As with the Nevada samples, fibrous amphibole in Arizona is present in as fracture fill material, and as pseudomorphic replacement of magmatic (protolith) magnesiohornblende. Additional alteration minerals associated with fibrous amphiboles include albite (Na end-member of the Na-Ca plagioclase feldspar solid solution series) as pseudomorphic replacement of magmatic plagioclase of intermediate (oligoclase to labradorite) composition, ± quartz, ± hematite (alteration of magnetite or as veins). Late stage calcite veins (post-dating fibrous amphibole) have been observed but are rare.

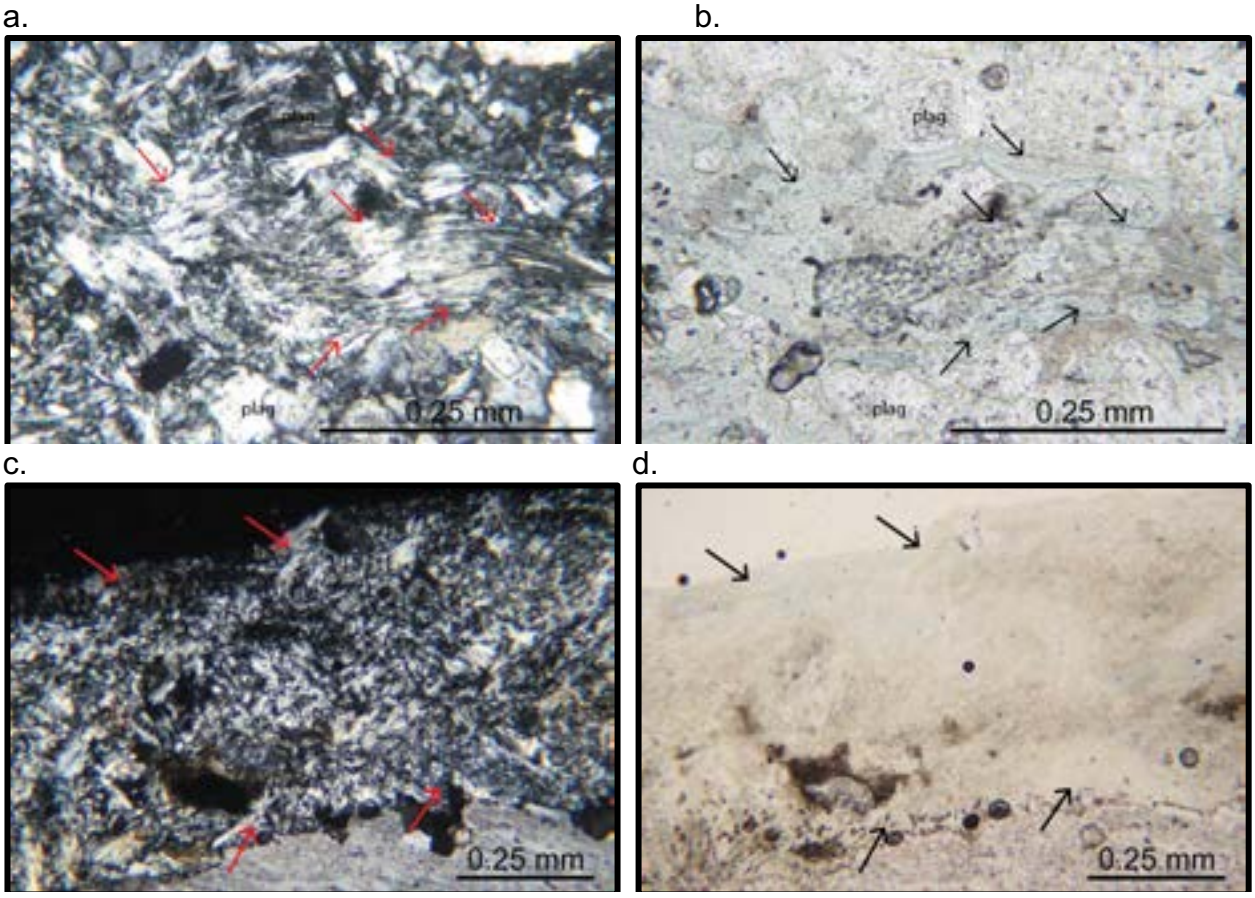

Figure 3-3. Photomicrographs of monomineralic veins of fibrous actinolite from Nevada (Type I). Sample MR2a under crossed-polars (a) and plain polarized light (b); images show fibrous actinolite vein (arrows) ~0.1 mm wide cutting altered plagioclase in granite. Fibers are parallel to vein margins, such fibers are called slip-fibers. Sample MR415-1 under crossed-polars (c) and plain polarized light (d); images show part of a fibrous actinolite vein (arrows) at the edge of the thin section, no preferred orientation of fibers is observed

Fibrous Amphibole Textures: We have observed three types of fibrous amphibole textures which are important to the petrogenesis of the fibrous amphiboles and have categorized them into textural Types I-III. Type I (fracture-fill) occur as mats of amphibole fibers infilling fractures in the host granitoid rock (Figure 3-3). Type I fiber mats, present in both NV and AZ samples, are typically mono-mineralic (containing only amphibole) and often occur as slip-fibers, defined as fibers parallel to fracture walls, suggesting growth during faulting. Type II fibrous amphibole (intergrowths) are present as splayed bundles intergrown within other minerals (Figure 3-4). Type II (winchite) fibers are found intergrown with clear albite and more rarely quartz in AZ samples. In NV samples Type II (actinolite) fibers have been found intergrown with clear albite, K-feldspar, quartz and epidote. Type III (Figure 3-5) is defined as the secondary pseudomorphic replacement of primary magmatic amphibole (magmatic magnesiohornblende) by fibrous amphibole. Pseudomorphic replacements are recognizable because the original shape and crystallographic order of the original grain is preserved and/or the replacement is incomplete.

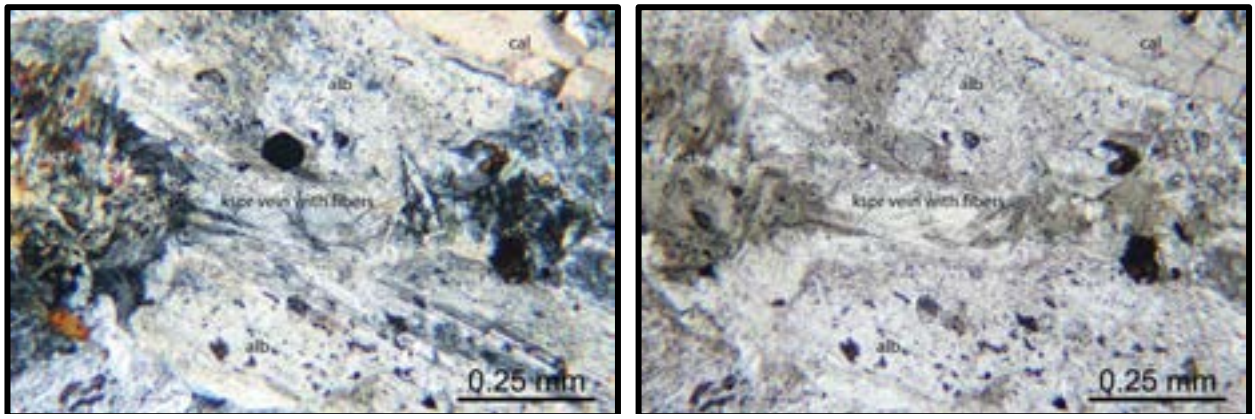

Figure 3-4 Photomicrographs of actinolite asbestos intergrown with other alteration minerals in NV sample. Sample MR2c under crossed-polars (left) and plain polarized light (right); clear orthoclase vein that contains actinolite asbestos fibers with irregular orientation within turbid albite.

Albite Textures: In both the Nevada and Arizona samples plagioclase grains near amphibole asbestos are altered to albite (An_{0-10}), extensively so in fractured and heavily altered samples. We have identified two generations of albite (Figure 3-6) which we call Ablite-1 (early) and Albite-2 (late). Albite-1 is accompanied by sericite alteration (microscopic K-rich mica that is common in altered plagioclase), which gives Albite-1 a cloudy or turbid appearance in plane light, making it easily recognizable in the petrographic microscope. Albite-2 is clear, lacks sericite alteration, and is found (1) along the edges of larger Albite-1 grains, (2) as micro-veins cutting Albite-1, and (3) in plagioclase fragments near/in fracture-fill veins (Type I amphibole asbestos). Albite-1 and Albite-2 are optically continuous, suggesting a replacement mechanism. Much of Albite-2 contains splayed bundles of fibrous amphibole (Type II amphibole asbestos). Our interpretation is that Albite-2 post-dates growth of Albite-1 (Figure 3-6).

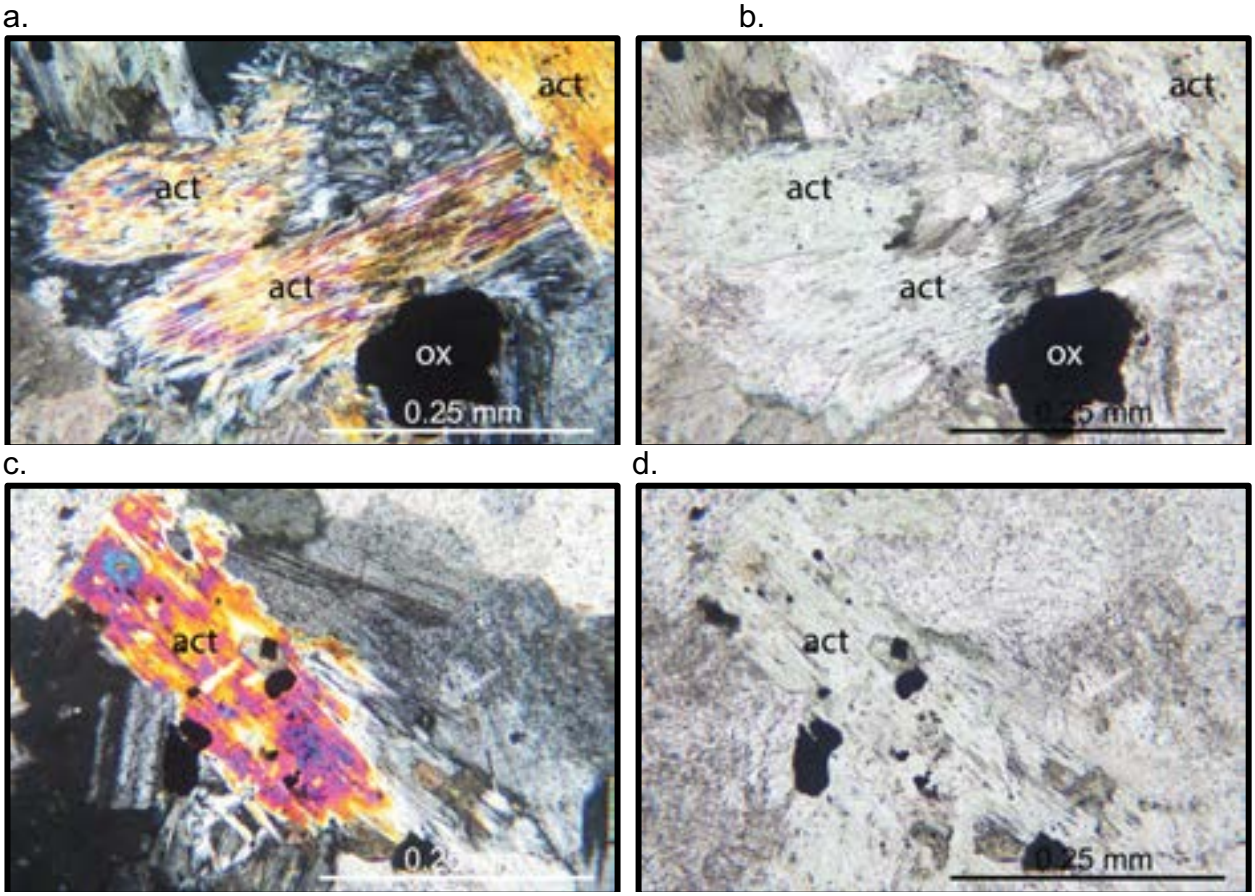

Figure 3-5. Photomicrographs of secondary replacement of prismatic magmatic amphibole in Nevada (Type III). Images show fibrous actinolite as pseudomorphic replacement of primary magmatic magnesiohornblende within altered granitic rock. Sample MR2c under crossed-polars (a) and plain polarized light (b); Sample MR2a under crossed-polars (c) and plain polarized light (d).

Discussion and Interpretations

Within two million years of Miocene pluton solidification (at 750-900°C) a hydrothermal system was established where circulation of aqueous solutions were channeled along active faults and fracture zones in the plutonic host rocks, and in places in adjacent Precambrian gneisses. Brittle fracturing of quartz and plagioclase feldspar, seen in outcrop and thin-section, suggests temperatures of ≤350ºC. The active Salton Sea geothermal field in southern California is good analog for NOA genesis via hydrothermal processes. Drilling in the Salton Sea field has recovered fibrous actinolite as part of a hydrothermal assemblage that includes albite, K-feldspar, epidote, and chlorite, nearly identical to the assemblages in our Nevada data set. Salton Sea fluid temperatures at the depth of actinolite asbestos recover are in the 310-330°C range (Yau et al., 1986). We believe that amphibole asbestos formation in southern Nevada because the timing of active faulting and uplift of the plutons provided fluid access pathways at the time that

the solidified plutons cooled from magmatic temperatures and passed through the ~300-350°C range.

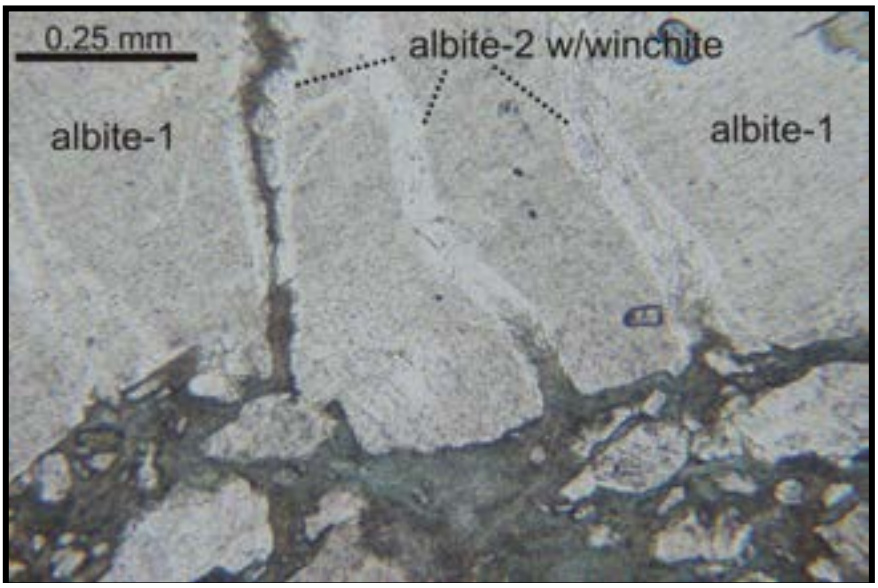

Figure 3-6. Photomicrograph illustrating the difference between turbid looking Albite-1 (with sericite alteration) and clear Albite-2 containing fibrous winchite asbestos. Sample KW3-18-5b from Wilson Ridge, Arizona.

Amphibole asbestos in fracture-fill veins (Type 1) precipitated directly from hydrothermal fluids, this type of growth is called *neocrystallization*, which refers to growth of new mineral structure, in this case from direct precipitation of fibrous amphibole from an aqueous solution into an open space (fluid filled fracture). Type II fibrous amphibole, i.e. intergrowths with albite and other minerals, is also a *neocrystallization* process (also results from growth of new mineral structure). Amphibole asbestos present as pseudomorphic replacements of magmatic amphibole (Type III) results from *recrystallization* of an existing mineral structure, in this case replacing non-fibrous magnesiohornblende within the host rock.

Alteration of protolith plagioclase to albite (An_{0-10}) is called albitization and is generally seen a clear record of hydrothermal alteration (Putnis and John, 2010). Based on both experimental studies and studies of natural samples, albitization is thought to progress as an atom-by-atom process of dissolution-reprecipitation, without the need for open space or the growth of new mineral structures (Putnis and John, 2010). We similarly interpret the Type III amphibole replacement textures in terms of a dissolution-reprecipitation processes, one in which grain-scale fluid-mineral interaction converts non-fibrous magnesiohornblende into fibrous amphibole. An important consequence of this process is that ion exchange between the fluid and the reacting minerals (process

called *metasomatism*) drives (buffers) the fluid composition towards equilibrium with the reaction product (in this case actinolite, winchite cummingtonite asbestos). Once such fluids have been generated they would be capable of precipitating these minerals directly from fluids.

In general terms we recognized three types of reactions that produced Type III (replacement) amphibole asbestos, in word-form these are:

Magnesiohornblende + ions in solution → Actinolite + ions in solution,
Magnesiohornblende + ions in solution → Winchite + ions in solution, and
Magnesiohornblende + ions in solution → Cummingtonite + ions in solution.

The ions gained and ions lost by both the amphibole and the fluid differ between each of these three general reactions. During our EMPA-WDS work we collected reactant-product pairs across reaction fronts in partial altered Type III amphibole grains. Each reactant-product pair could be used to calculate ions gained and ions lost by/to the fluid (or the mineral) during the reaction. Figure 3-7 illustrates the results for such calculations. Consistent ion exchanges for the Magnesiohornblende → Actinolite are gains in Si and Fe^{2+} by the mineral from the fluid, and losses of Al and Fe^{3+} from the mineral to the fluid; both gains and losses of Mg are recorded by this mineral. Consistent ion exchanges for the Magnesiohornblende → Winchite/Magnesioreibeckite reaction are gains in Na, Si, Fe^{3+} by the mineral and of Ca, Al, and typically Mg losses to the fluid. Consistent ion exchanges for the Magnesiohornblende → Cummingtonite reaction includes gains of Si and Mg (major gain) by the mineral and losses of Al, Fe^{2+}, Fe^{3+}, and Ca (major loss) to the fluid. We conclude that the composition of the infiltrating fluids, specifically ionic concentrations, controlled the composition of the resulting Type III amphibole asbestos.

The first order control on the composition of the fibrous amphibole (actinolite, winchite, or cummingtonite) is likely the relative concentrations of ions in the initial hydrothermal fluids, which drives hydrothermal fluid compositions towards equilibrium with the reaction products resulting in fluids capable of the direct precipitation of amphibole asbestos, i.e. the neocrystallization that produced both Type I and Type II amphibole asbestos we have observed. The two generations of albite may be recording such an evolution of the hydrothermal fluids, with Albite-1 lacking fibrous amphibole while later Albite-2 co-precipitated with fibrous amphibole from an evolved fluid, one that was in equilibrium with Type III fibrous amphibole. In support of this interpretation, we point out that the three general Type III amphibole reactions explain nearly all of the compositional variation we see in the large altered Nevada and altered Arizona data presented in Chapter 2 (see Figure 3-8), and the entire SEM-EDS data set presented in Chapter 2 and used to map the distribution of NOA in Clark County as discussed in Chapter 4.

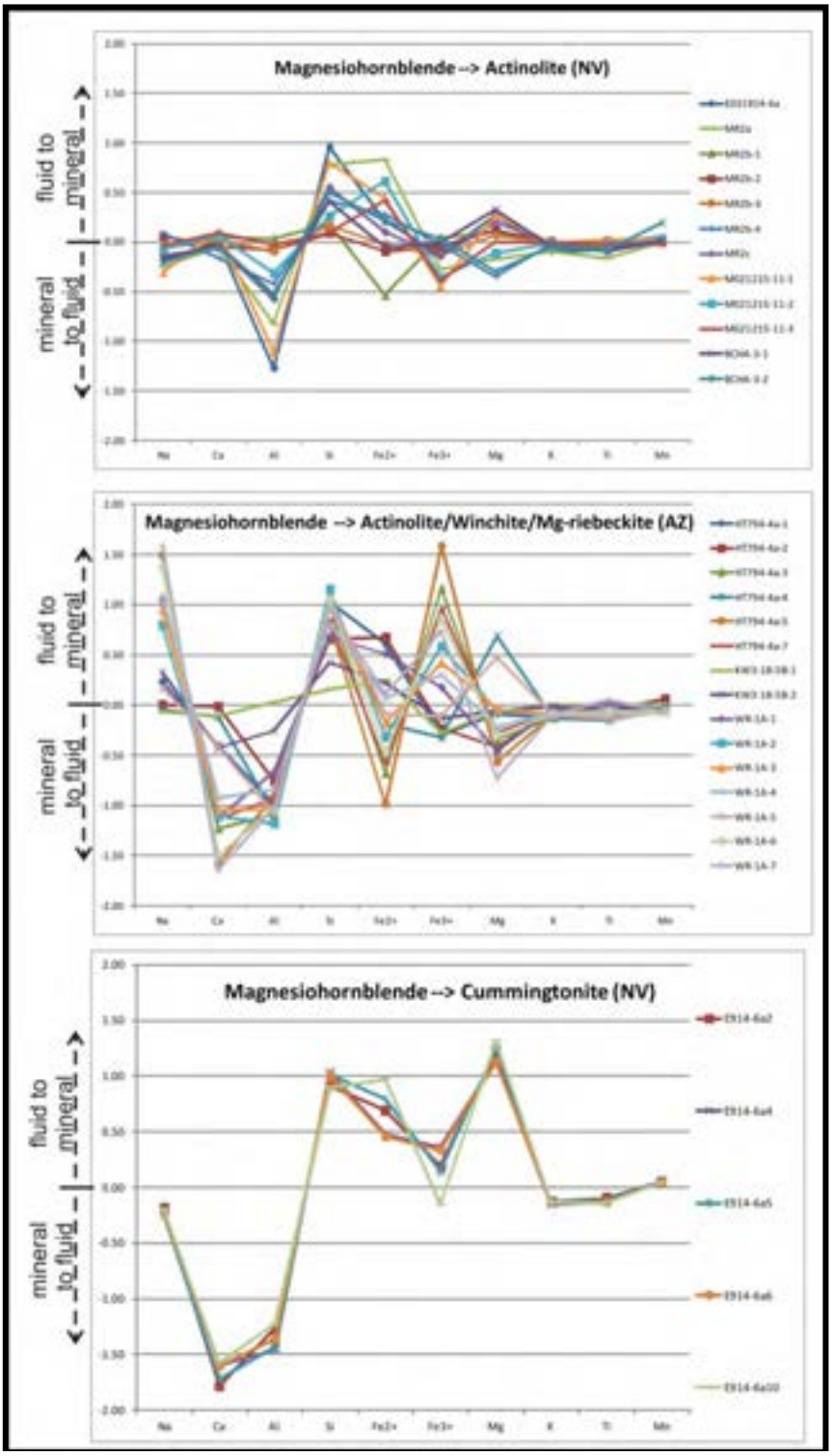

Figure 3.7. Plots illustrating ion exchange between reactant magnesio-hornblende (protolith) and hydrothermal fluid necessary to produce amphibole asbestos products; see text for full discussion.

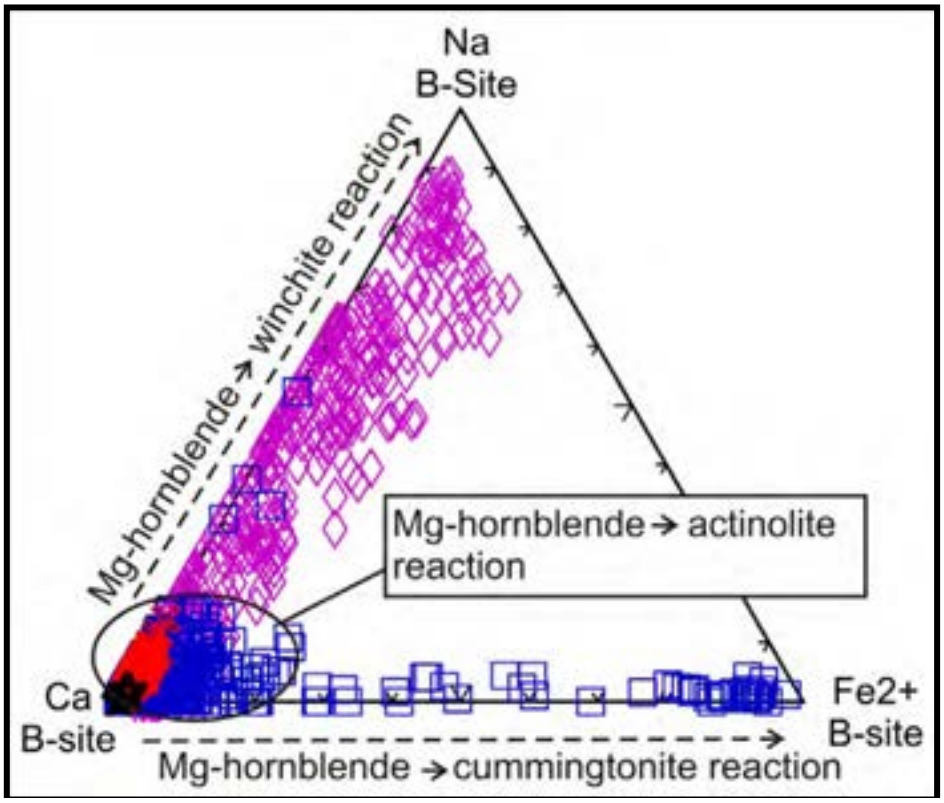

Figure 3-8. Amphibole composition diagram showing relationship between amphibole compositions and compositional changes produced by amphibole replacement reactions discussed in text.

Conclusions and Implications

We can draw several conclusions that have implications for our understanding of the genesis of amphibole asbestos and our attempts to understand its geologic distribution and predict its occurrence.

1. Hydrothermal alteration of rock types that contain non-fibrous amphibole have the potential to produce amphibole asbestos. Amphiboles are common rock-forming minerals that are found in varying concentrations in many common types of igneous and metamorphic rocks. Any geologic environment where amphibole-bearing rock types are accessible to hydrothermal fluid flow have the potential for the formation of amphibole asbestos.

2. The reactions that convert non-fibrous primary amphiboles to amphibole asbestos can generate fluids that are capable of direct precipitation of amphibole asbestos.

3. A vigorous hydrothermal system operating within amphibole-rich igneous or metamorphic rocks may be capable producing a significant amount of recrystallized amphibole asbestos as well as fluids capable of migration into fracture systems where amphibole asbestos could form through neocrystallization. Such fracture systems are would be a likely source of easily eroded amphibole asbestos.

4. Models of asbestos petrogenesis based solely on an understanding of commercial ore deposits are likely inadequate when trying to understand the distribution of naturally-occurring asbestos in the environment.

References

Buck, B.J., Goossens, D. Metcalf, R.V., McLaurin, B., Ren, M., and Freudenberger, F., 2013, Naturally occurring asbestos: Potential for human exposure, southern Nevada USA, Soil Science Society of America Journal, 77:2192-2204. doi:10.2136/sssaj2013.05.0183

Felger, T.J., Beard, L.S., Anderson, Z.W., Fleck, R.J., Wooden, J.L., Seixas, G.B., 2014, Preliminary geologic map of Black Canyon and surrounding areas, Nevada and Arizona. USGS Open File Report 2013-1267-A.

Metcalf, R.V., 2004, Volcanic-plutonic links, plutons as magma chambers and crust-mantle interaction: A lithospheric scale view of magma systems: Transactions of the Royal Society of Edinburgh – Earth Sciences, v. 95, p. 357-374.

Metcalf, R.V., and Buck, B.J., 2015, Genesis and health risk implication of an unusual occurrence of NaFe3+-amphibole: Geology v. 43, p. 63-66, doi:10.1130/G36199.1

Yau. Y-C, Peacor, D.R. & Essene, E. J., 1986, Occurrence of wide-chain Ca-pyriboles as primary crystals in the Salton Sea geothermal field, California USA: Contributions to Mineralogy and Petrology, v. 94, p. 127-134.

Chapter 4:

Distribution, Mineralogy, and Morphology of Naturally-Occurring Asbestos in Southern Nevada

Brenda J Buck[1]
Brett T. McLaurin[2]
Rodney V. Metcalf[1]

[1]Department of Geoscience, University of Nevada Las Vegas, 4505 South Maryland Parkway, Las Vegas, Nevada 89119-4010
[2]Department of Environmental, Geographical and Geological Sciences, Bloomsburg University of Pennsylvania, 400 East Second Street, Bloomsburg, Pennsylvania 17815, USA

Introduction

Previous research identified naturally-occurring asbestos (NOA) in and around Boulder City, Henderson and Lake Mead National Recreation Area in southern Nevada and northwestern Arizona (Buck et al., 2013, Metcalf and Buck, 2015). These papers were the first reported occurrence of amphibole NOA forming in a hydrothermally-altered pluton and therefore fundamentally changed scientific ideas on the distribution and occurrence of naturally-occurring amphibole asbestos. Buck et al. (2013) hypothesized that additional areas in southern Nevada would also be likely to contain NOA (Figure 4-1).

A later study, in collaboration with scientists from the US Environmental Protection Agency, found evidence for another highly carcinogenic mineral, erionite, to also be present in the Boulder City and Nellis Dunes areas (Buck et al., 2016). Erionite is a group 1 human carcinogen (IARC, 2012) and is most widely known from the epidemic of mesothelioma in Cappadocia, Turkey (Baris¸ et al. 1978; Artvinli and Baris¸ 1979; Baris¸ et al. 1987 ; Baris¸ and Grandjean 2006; Carbone et al. 2007, 2011). Studies suggest that erionite may be significantly more carcinogenic than the regulated asbestos minerals (Wagner et al., 1985; Hill et al., 1990; Coffin et al., 1992), and it also induces production of autoantibodies similar to amphibole fibers (Pfau et al., 2014; Zebedeo et al., 2014).

The sources of the possible erionite found in and around the Boulder City area and Nellis Dunes are unknown (Buck et al., 2016). Erionite is known to form in ash-flow tuffs, in vugs in hydrothermal- or groundwater-altered basalt, in diagenetically-altered silicic tuffs deposited into alkaline lakes (or less commonly, marine settings), and in other hydrothermally-altered rocks (Sheppard et al., 1965; Sheppard and Gude, 1973; Tschernich, 1992; Bargar and Keith, 1995; Sheppard, 1996; Hay and Sheppard, 2001; Langella et al., 2001). For these reasons, we analyzed the well-known altered tuffs present in the Bitter Spring Basin and other areas north of Lake Mead because they

seemed the most likely candidates for some of the source(s) of the possible erionite found in the Buck et al. (2016) study.

The goal of this research was to test the Buck et al., 2013 hypotheses (Figure 4-1) and produce hazard maps predicting where NOA is likely to occur based on current geological maps, well-known geological and surficial processes, and on sample testing. Sites were grouped into 11 regions based on geographic location and include: (in alphabetical order) El Dorado Mountains, Gold Butte, Highland Mountains, Ireteba Mountains, Jean-Primm, Las Vegas, Laughlin, Nellis Dunes, Nelson Road, Searchlight, and the Virgin Mountains.

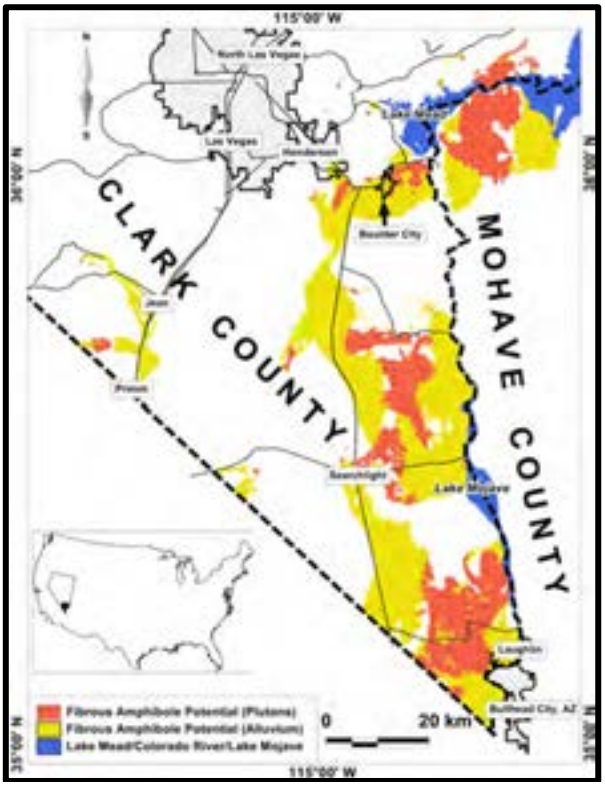

Figure 4-1. Predicted occurrence of NOA from Buck et al., 2013 – one of the hypotheses tested in this study.

Methods and Terminology

In this chapter, we present data on a total of 241 samples of soil and rock that were collected and analyzed for NOA. Field sampling was performed using safety gear including level 3 Tyvek suits, and respirators. Rock samples were collected by using a rock hammer to break fresh samples from exposed outcrops. Soil was collected using a new, clean trowel that was sealed in a ziplock bag to prevent any contamination prior to use, and unless otherwise described below, the uppermost < 1 cm loose soil from the surface was collected. All samples were contained in double-bagged and sealed plastic bags and stored in air-tight containers. Samples were only opened at UNLV after being

placed in special asbestos hoods. Of the 241 total samples analyzed for this study, 40 samples of previously-collected, altered tuffs were kindly provided by Drs. Lisa Lamb and Tom Hickson from University of St. Thomas, and were analyzed for erionite at EMSL laboratories using the method TEM EPA 600/R-93/116: Analysis of Bulk Material Utilizing Cryogenic Analytical Electron Microscopy (Section 2.5.5.2) with Milling Preparation.

Rock samples were examined using a binocular microscope inside a special asbestos hood and dental tools were used to pick off green and blue minerals suspected to be fibrous amphiboles. A total of approximately 0.01 to 0.02 g sample was then put into approximately 5 to 10 mL of deionized water.

Soil samples often contained fibrous carbonate particles which were removed to increase speed, accuracy, and efficiency of SEM/EDS analyses. Soil samples were first tested with 10% HCl to check effervescence for existence of carbonate minerals. If the soil reacted with the acid solution, then carbonate minerals were removed by placing approximately 5 g of soil and 25 mL of 5% HCl into a 50 ml centrifuge tube and left to react for 1 hr. The sample was then repeatedly centrifuged at 2000 RPM for 5 minutes followed by decanting of clear supernatant fluid, and the procedure was repeated until no more effervescence was observed. The sample was then washed and centrifuged three times with approximately 25 mL of pure water to remove any remaining HCl. A subsample of approximately 0.01 to 0.02 g sample was then put into approximately 10-20 mL of deionized water.

For all samples, a glass filtration apparatus was used to disperse these sub-samples in deionized water over 0.4-µm polycarbonate membrane filters (see Meeker et al., 2006). The filters were mounted to plastic disks using carbon tape. These filters were then coated with carbon and analyzed using a JEOL SEM (JSM5600) scanning electron microscope equipped with an Oxford EDS detector. Samples were scanned for fibrous particles.

Particle dimensions were measured by individually measuring SEM images using the scales provided with each image. Aspect ratios were calculated using the maximum length and mean width of each particle as was done in previous studies (Campbell et al., 1977; Meeker et al., 2003, 2006; Buck et al., 2013). EDS data were collected on each particle and used to estimate mineralogy.

We used SEM-EDS wt% oxide data to calculate an all-Fe-as-Fe^{2+} structural formulae on each particle examined. We then used the resulting structural formula to evaluate whether or not the particle was an amphibole (yes/no). This evaluation examined cation totals for each amphibole cation site; ideal stoichiometry is T-site sum ~8, C-site sum ~ 5, B-site sum ~ 2, A-site sum < 1, and total cations of 15-16. Based on close inspection of our first ~2000 SEM-EDS particles we set acceptable upper and lower limits for each of these totals, for a particle to be considered an amphibole, the analysis results had to pass all five cation-site tests. We then set up an Excel spreadsheet to calculate the all-Fe-as-Fe^{2+} structural formulae and apply the five cation-totals amphibole stoichiometry

test; our particle morphology measurements and statistics were limited to particles that passed this amphibole stoichiometry test (see Chapter 2 for more details). In this study WMMR refers to 'Libby-type' minerals, undivided: winchite, richterite, magnesio-riebeckite.

Assessment and mapping of potential bedrock and soils/alluvium utilized geospatial methods and compiled existing geologic maps, topographic and hydrological datasets, and aerial photography into a GIS database. A map for initial geological exploration was created using data from House et al. (2010a) and Felger and Beard (2010) to delineate areas in Clark County and northwestern Arizona that could potentially contain fibrous amphiboles. From the House et al. (2010a) map, these include granitoid plutons and metamorphic rocks along with areas of alluvial deposits eroded from them. The more detailed areas of fiber potential in soils and alluvium were developed by digitizing and integrating topography, hydrology, and aerial photography data sets (National Elevation Dataset, https://viewer.nationalmap.gov/advanced-viewer/; National Hydrology Dataset, https://www.usgs.gov/core-science-systems/ngp/national-hydrography; and the Geospatial Data Gateway, http:// datagateway.nrcs.usda.gov). These data were superimposed on the geologic map data compiled from multiple sources (Volborth, 1972; Bingler and Bonham, 1973; Anderson,1977; Hose, 1980; Smith, 1984, Capps, 1997; Faulds et al., 2002; Faulds et al., 2010; Felger and Beard, 2010; House et al., 2010a; Smith et al., 2010; Hinz et al., 2012a; Hinz et al., 2012b; Dee et al., 2016) to determine the intersection of these drainages with exposed plutonic and metamorphic rocks in the study area.

For this study, fibers were defined as amphibole particles $\leq$ 1µm wide and that have an aspect ratio of 3:1 or higher. Some of these particles will further split into thinner fibrils, and as such could be considered bundles. However, we combined all amphibole particles that are $\leq$ 1µm wide into the "fiber" classification. since accurately identifying such splitting requires finer resolution which can only be achieved by FE-SEM (Field Emission Scanning Electron Microscopy), or TEM (Transmission Electron Microscopy). Particles that were greater than 1 µm wide were classified as bundles if they have evidence showing that they are in the process of splitting into thinner fibers, and all other particles were classified as prismatic crystals.

Aspect ratio (length/width) is an important characteristic of asbestos fibers since many studies have found that greater aspect ratios correlate to increased toxicity (e.g. Aust et al., 2011). Legally, an aspect ratio of 3:1 or more is required for a particle to be defined as asbestos. This is in addition to other requirements such as mineralogy (e.g. see NIOSH, 2011). A recent study found that aspect ratios of 8:1 or greater was the best fit for a model fitting asbestos particle sizes to mesothelioma disease (Cook et al., 2016). Because of this, we have created additional maps to designate where amphibole particles with aspect ratios of 8:1 or greater occur, in addition to where amphibole particles with aspect ratios of 3:1 or more were measured.

Results and Discussion

The results will first be presented as the entire dataset, then followed by each region in alphabetical order.

Entire Project: All Areas Combined

In this study, a total of 241 samples collected over a broad area in southern Nevada were analyzed for NOA (Tables 4.1 to 4.3). Using those results as well as previously published studies and maps (as described in methods), we developed a NOA-predictive map for both bedrock and for soils where alluvium (e.g. water-transported sediment) has been eroded from bedrock-containing NOA (Figure 4-2). In order to better understand how natural processes erode, transport, and deposit NOA across the landscape, samples were additionally identified as bedrock (e.g. rock in Figures 4-3 and 4-4), alluvium (e.g. samples transported by water, which can include rock samples), and eolian (e.g. samples transported by wind, which for this study included wind-deposited silt in vesicular soil horizons and wind-blown sand in dunes).

Figure 4-2. Example of NOA-containing alluvium from Wilson Ridge region in Lake Mead National Recreation Area, northwestern Arizona. Sediments in the foreground (with road) are recent/late Holocene alluvium; whereas the hills in this photo are older Miocene/Pliocene alluvium (Black Mountain conglomerate).

In southern Nevada and northwestern Arizona, NOA occurs in hydrothermally-altered plutonic rocks (see also previous chapters), metamorphic rocks, and in sedimentary rocks and sediments that have formed from the erosion, transport, and deposition of these NOA-containing rocks (Figures 4-3 and 4-4). This study tested the hypothesis presented by Buck et al., 2013 (Figure 4.1), that all of the Tertiary plutons in southern Nevada would contain NOA. This study found that to be true (Figures 4-3 and 4-4). However, Buck et al. (2013) did not include metamorphic rocks in their predictions nor did they include older plutonic rocks, both of which were found to also contain NOA in this study. Therefore, the footprint of rock and alluvium (e.g. soils) that are predicted to contain NOA is significantly larger than Buck et al., 2013 predicted (Figures 4-3 and 4-4).

As a result of this study, we determined that more than 689,000 acres of alluvium in southern Nevada is predicted to contain NOA. In addition, more than 404,000 acres of bedrock in southern Nevada is also predicted to contain NOA. This is more than double the acreage predicted to contain NOAA in the Buck et al. (2013) study. Mapping from that study estimated more than 363,000 acres of potential NOA in alluvium and over 179,000 acres of potential NOA in bedrock. These figures do not include acres that may contain NOA as a result of eolian processes (e.g. vast areas of southern Nevada that contain vesicular horizons). Thus, just mapping bedrock and alluvium (water-transport), we predict over 1.09 million acres, which is approximately 20% of Clark County, contains NOA.

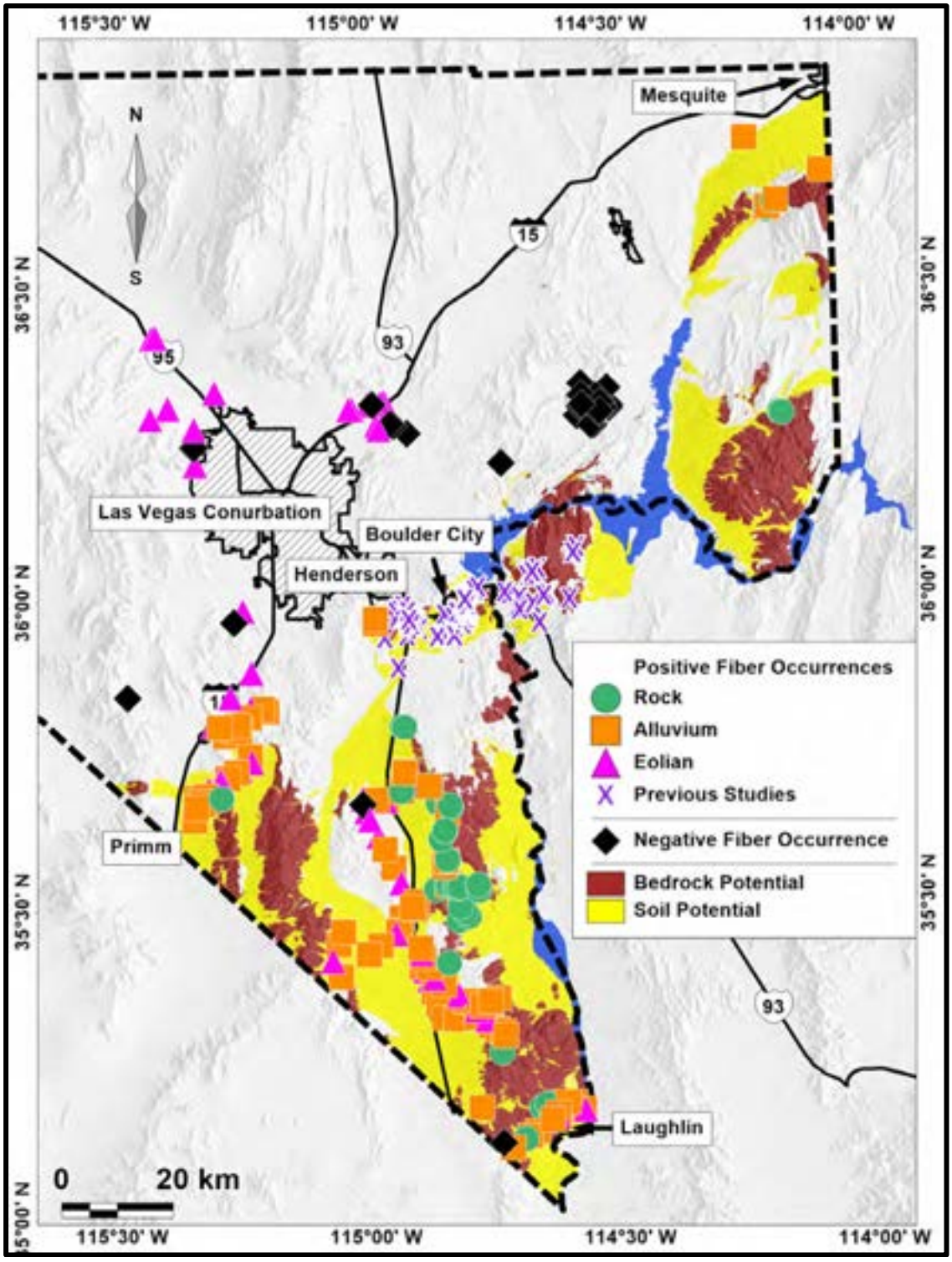

Figure 4-3. Map of sample locations with predicted occurrences of NOA based on alluvial (water-transport) processes that transport material from the source rock out into the basin. Bedrock potential represents areas of potential occurrence for amphibole asbestos in igneous and metamorphic rock exposures. Soil potential delineates areas where runoff could potentially distribute amphibole asbestos fibers downslope from bedrock areas. Positive occurrences are for amphibole asbestos with aspect ratios of 3:1 or greater.

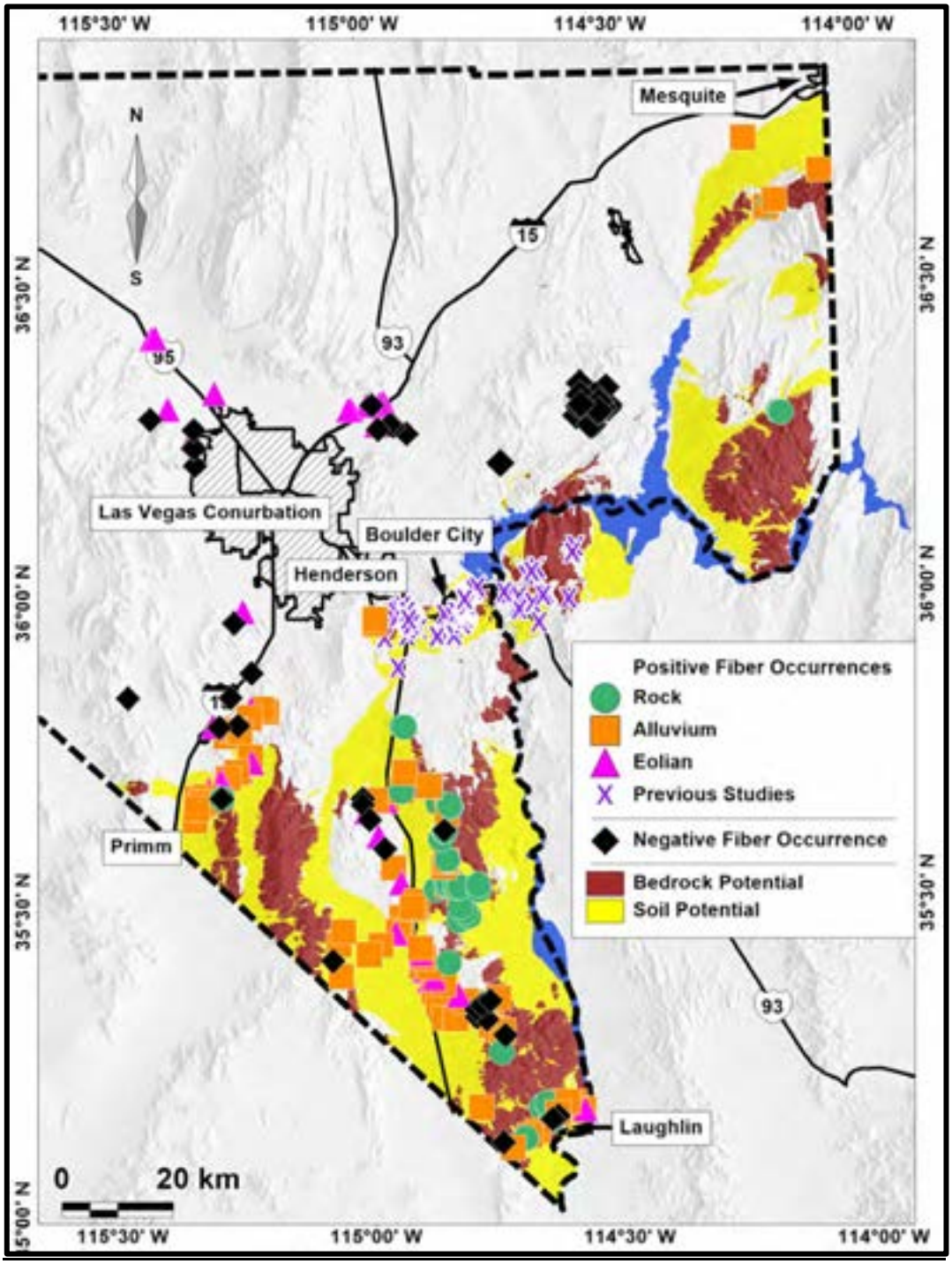

Figure 4-4. Map of sample locations with predicted occurrences of NOA based on alluvial (water-transport) processes that transport material from the source rock out into the basin. Bedrock potential represents areas of potential occurrence for amphibole asbestos in igneous and metamorphic rock exposures. Soil potential delineates areas where runoff could potentially distribute amphibole asbestos fibers downslope from bedrock areas. Positive occurrences are for amphibole asbestos with aspect ratios of 8:1 or greater.

Erionite

The 40 samples of altered tuff that were analyzed for erionite all occur north of Lake Mead (Figures 4-3 and 4-4) in the Horse Spring Formation (e.g. Lamb et al., 2010). All 40 samples tested negative for erionite. Many of these volcanic ash deposits (tuffs) were altered because either they were deposited in alkaline lakes or later groundwater had interacted with the volcanic ash. These samples were targeted because such depositional environments are excellent candidates for erionite to form (e.g. Sheppard et al., 1965; Sheppard and Gude, 1973; Tschernich, 1992, Bargar and Keith, 1995, Sheppard, 1996; Hay and Sheppard, 2001; Langella et al., 2001). Unfortunately, because of the negative results in this study, we still do not know the source(s) of the possible erionite that was found at Nellis Dunes, Boulder City, and the El Dorado dry lake (playa) reported by Buck et al. (2016).

Distribution via Water

Over geological time, significant erosion, transport, and deposition occurs through the processes of water running off and eroding bedrock. In this study, we have mapped the areas in which we predict water-transport has moved NOA from bedrock locations out into sediments/soils in the basins (see 'soil potential' in Figures 4-3 and 4-4). We tested several of these predictions by testing samples of alluvium for the presence of NOA (Figures 4-3 and 4-4). Only in a few cases did alluvial samples test positive when they were collected from areas outside of our predicted NOA occurrences. These were found in the Jean-Primm and Highland Mountains regions and are likely best explained by contamination from dust (see next section and individual regions for more explanation).

Distribution via Wind

In this study we also looked at the potential for wind-deposited sediment to contain NOA. We did this because, in the Mojave Desert, dust erosion, transport and deposition are important processes that modify landforms, affect soil composition and morphology, and have large impacts on ecosystems. The mean rate of dust deposition in southern Nevada and southeastern California ranges from less than 5 to more than 15 $g/m^2/yr$ (Reheis and Kihl, 1995). When deposited, much of this dust forms vesicular soil horizons underneath desert pavements (e.g., McFadden et al., 1987; Wells et al., 1995; McFadden et al., 1998; Turk and Graham 2011). It may also form vesicular horizons underneath biological soil crusts (e.g., Williams et al., 2012).

Once disturbed by geomorphic or human processes, these desert pavement or biologic soil crust surfaces are no longer stable and dust that contains NOA fibers can be released into the air during episodes of wind erosion or during human activities. NOA fibers can then become transported with the wind, most of them in suspension, and may again settle to the Earth's surface up to many tens of kilometers from the original source depending on their size and the wind regime. When falling back to the Earth's surface, they contaminate the local soil, transferring these areas into new, secondary sources for potential human fiber exposures. Contrary to fluvial processes, where transport and

deposition of fibers is limited to the hydrological catchment, wind can distribute fibers great distances across the landscape.

Buck et al., 2016 found a wide range of NOA structures in a vesicular horizon in the Nellis Dunes Recreation Area, which they interpreted to have been transported there by wind since vesicular horizons are eolian deposits (e.g., McFadden et al., 1987; Wells et al., 1995; McFadden et al., 1998; Turk and Graham 2011). The results of that study lead us to explore additional areas outside of our predicted NOA occurrences where wind deposition may have increased the potential footprint for NOA. In particular, we sampled various areas in and around the Las Vegas metropolitan area, where over 2 million people currently live (see the section on Las Vegas region, later in this chapter). We also sampled vesicular horizons in areas around the Highland Mountains and Jean-Primm regions (Figure 4-3; see later sections on these regions for more details). Only 5 of 52 eolian samples did not test positive for NOA at 3:1 aspect ratio. This supports the interpretation that NOA-distribution via wind, especially in arid and semi-arid environments, can be widespread and can occur great distances from the alluvial and bedrock sources of NOA (Figures 4-3 and 4-4).

We are currently unable to identify exactly where the NOA originated for each of the eolian samples that tested positive in this study (Figure 4-3 and 4-4). This is partly because current wind speeds and directions commonly vary diurnally, seasonally, yearly (e.g. El Niño-Southern Oscillation), and through geologic time (e.g. glacial vs. interglacial time periods), which depending on the age of the eolian deposit, must be taken into account. In addition, there are numerous currently-known bedrock sources of NOA in this region (described in this report) and including areas in Death Valley (Van Gosen et al., 2004) and Mountain Pass California (Van Gosen, 2007), which could have contributed to the NOA found in eolian deposits in this study.

Figure 4-5. An example of a dust storm entering the Las Vegas valley from the south, on October 19, 2009. This dust is extremely likely to contain NOA because of all the easily-erodible NOA-containing soils found south of Las Vegas (see Figure 3). View from UNLV facing south.

Figure 4-6. Another example of a dust storm entering the Las Vegas Valley from the south, on March 7, 2012. View from UNLV to the south.

Currently, the dominant wind directions in this region are from the south/southwest in the spring, and from the north/northeast during the winter, but any wind direction is possible, especially when frontal storms occur (e.g. Goossens et al., 2011). The most likely sources for the NOA found in eolian deposits in and around the Las Vegas Valley are NOA-containing sediments to the south and/or west. As shown on Figure 4-3 and 4-4, vast areas of southern Nevada contain NOA, this combined with strong southerly winds, particularly in the spring months, could easily bring NOA fibers into the Las Vegas region and deposit them in surrounding vesicular horizons. In addition, Death Valley and other areas in California are known to also contain NOA (Van Gosen, 2004; 2007), so westerly winds could also bring those sources into the Las Vegas region.

The Las Vegas metropolitan area commonly has dust storms that enter the city from the south (Figures 4-5 and 4-6), but dust storms are also known to occur from the west, north, and less frequently, the east (personal observations, B. Buck). A likely contributor to much of this dust is the El Dorado dry lake bed (playa) that contains high concentrations of amphibole NOA (see last chapter in this report), and contains erionite (Buck et al., 2013; 2016). This dry lake bed can be especially emissive from both human activities such as off-road-driving, as well as natural wind (Figures 4-7 and 4-8).

Figure 4-7. Dust emissions from the El Dorado dry lake bed (playa) on July 21, 2017. Wind is from the south, blowing this dust northward into the Las Vegas valley. Photo courtesy of Regine Trias (regine-trias.com).

Figure 4-8. An off-road-driving enthusiast at the El Dorado dry lake bed (playa) west of Boulder City. Notice the amount of dust generated even though the lake bed is wet (see standing water in the foreground). This dry lake bed contains NOA (Buck et al., 2013; 2016)

Morphology

The size/shape of asbestos particles is an important parameter for toxicity (Aust et al., 2011). Particles that have a higher aspect ratio (e.g. are longer and thinner) are considered more toxic (e.g. Aust et al., 2011). We analyzed over 6000 particles in this study, of which 2555 were identified as amphibole minerals (see Chapter 2 for more details). The mean aspect ratio of all the amphibole particles was 8.8 ± 0.1 (Table 4.1-4.4).

In this study, we divided southern Nevada into 11 regions: El Dorado Mountains, Gold Butte, Highland Mountains, Ireteba Mountains, Jean-Primm, Las Vegas, Laughlin, Nellis Dunes, Nelson Road, Searchlight, and the Virgin Mountains. The regions with the greatest mean aspect ratios, suggesting increased toxicity, include: El Dorado (12.5 ± 0.7), Searchlight (9.9 ± 0.4), and the Virgin Mountains Virgin (9.1 ± 0.1). Those with slightly lower mean aspect ratios include Jean-Primm region (8.6 ± 0.5), Gold Butte (8.4 ± 0.5), and the Highland (8.1 ± 0.5) and Ireteba (8.1 ± 0.3) mountains regions. These areas may be slightly less hydrothermally altered than the El Dorado, Searchlight and Virgin mountains regions. Similarly, the Nelson Road and Laughlin areas also had slightly lower mean aspect ratios: Nelson Road (7.6 ± 0.3); Laughlin (7.5 ± 0.3). The regions with comparably lower mean aspect ratios include those that are dominated by eolian processes and include: Las Vegas region (7.2 ± 0.3) and Nellis Dunes (5.7 ± 1.2).

Table 4.1. Particle sizes and group mineralogy results for all SEM/EDS data in project. Number of particles (N), standard error of the mean (S.E.)

ALL DATA													
Mineralogy	**N**	**Minimum Width (µm)**	**Maximum Width (µm)**	**Mean Width (µm)**	**S.E.**	**Minimum Length (µm)**	**Maximum Length (µm)**	**Mean Length (µm)**	**S.E.**	**Minimum Aspect Ratio**	**Maximum Aspect Ratio**	**Mean Aspect Ratio**	**S.E.**
Calcic group	1959	0.1	91.0	**1.7**	0.1	0.8	372.0	**12.7**	0.5	3.0	72.1	**8.2**	0.1
Sub-Calcic group	448	0.3	19.7	**1.2**	0.1	1.1	103.0	**10.2**	0.5	3.1	40.0	**8.9**	0.3
Sodic group	47	0.2	57.0	**2.9**	1.4	1.6	372.6	**33.3**	10.3	5.0	77.2	**21.0**	2.4
Sodic-Calcic group	89	0.1	16.2	**1.1**	0.2	1.3	172.2	**15.2**	2.3	3.3	68.3	**14.8**	1.0
Fe-Mg group	12	0.8	5.1	**1.7**	0.4	3.9	31.5	**13.3**	2.7	3.0	28.6	**9.7**	2.4
All particles	**2555**	**0.1**	**91.0**	**1.6**	**0.1**	**0.8**	**372.6**	**12.8**	**0.4**	**3.0**	**77.2**	**8.8**	**0.1**

Table 4.2. Particle sizes and individual mineralogy results for all SEM/EDS data in project. Number of particles (N), standard error of the mean (S.E.).

ALL DATA													
Mineralogy	**N**	**Minimum Width (µm)**	**Maximum Width (µm)**	**Mean Width (µm)**	**S.E.**	**Minimum Length (µm)**	**Maximum Length (µm)**	**Mean Length (µm)**	**S.E.**	**Minimum Aspect Ratio**	**Maximum Aspect Ratio**	**Mean Aspect Ratio**	**S.E.**
Actinolite	1075	0.1	91.0	1.6	0.1	0.8	372.0	13.5	0.7	3.0	65.7	8.7	0.2
Anthophyllte	10	1.0	2.7	1.5	0.2	4.5	17.5	10.3	1.2	3.0	11.0	7.4	0.8
Arfvedsonite	1	2.8	2.8	2.8	-	33.0	33.0	33.0	-	11.8	11.8	11.8	-
Barrosite	4	1.2	2.3	1.7	0.2	6.4	27.2	19.2	4.5	6.3	17.8	11.5	2.4
Edenite	72	0.3	7.4	1.5	0.1	1.8	95.3	11.8	1.6	3.1	16.8	7.6	0.4
Fe-hbld	2	0.9	1.1	1.0	0.1	3.9	5.3	4.6	0.7	3.5	5.9	4.7	1.2
Ferro-anthophyllite	1	2.8	2.8	2.8	-	40.5	40.5	40.5	-	14.5	14.5	14.5	-
Gedrite	12	0.5	2.1	1.0	0.1	1.8	9.4	5.4	0.7	3.1	13.4	5.6	0.9
Hornblende	3	1.2	8.0	3.7	2.1	3.7	58.2	23.7	17.3	3.1	7.3	5.0	1.2
Mg-rieb	23	0.2	57.0	4.9	2.7	1.6	372.6	47.5	20.5	5.0	58.0	17.4	3.0
Mg-hbld	803	0.2	44.9	1.7	0.1	1.1	201.0	11.7	0.6	3.0	72.1	7.5	0.2
Mg-katop	3	0.2	1.5	1.0	0.4	2.5	13.2	7.9	3.1	6.7	12.5	9.3	1.7
Pargasite	1	1.7	1.7	1.7	-	6.4	6.4	6.4	-	3.8	3.8	3.8	-
Richerite	3	1.1	2.7	1.6	0.5	9.5	14.8	11.8	1.6	5.5	10.2	8.1	1.4
Tremolite	1	4.0	4.0	4.0	-	12.4	12.4	12.4	-	3.1	3.1	3.1	-
Tschermakite	3	0.8	1.5	1.2	0.2	6.1	11.6	8.3	1.7	5.1	9.1	7.3	1.2
Winchite	45	0.1	16.2	1.4	0.4	1.3	172.2	17.8	4.1	3.3	47.6	13.9	1.4
WMRR	11	0.5	1.2	0.7	0.1	8.6	23.5	13.8	1.5	13.8	39.2	19.2	2.2
Unidentified	477	0.2	19.7	1.2	0.1	1.1	103.0	10.8	0.6	3.1	77.2	10.2	0.4
All Particles	**2555**	**0.1**	**91.0**	**1.6**	**0.1**	**0.8**	**372.6**	**12.8**	**0.4**	**3.0**	**77.2**	**8.8**	**0.1**

Table 4.3. Morphology classification for all SEM/EDS data in the project. Number of particles (N), standard error of the mean (S.E.)

ALL DATA													
Morphology	**N**	**Minimum Width (µm)**	**Maximum Width (µm)**	**Mean Width (µm)**	**S.E.**	**Minimum Length (µm)**	**Maximum Length (µm)**	**Mean Length (µm)**	**S.E.**	**Minimum Aspect Ratio**	**Maximum Aspect Ratio**	**Mean Aspect Ratio**	**S.E.**
Fiber	1179	0.1	1.0	0.7	0.0	0.8	49.7	6.7	0.1	3.0	77.2	9.5	0.2
Bundle	491	1.1	91.0	3.1	0.3	3.8	372.6	27.1	1.9	3.1	58.5	10.0	0.3
Prismatic Crystals	885	1.1	28.0	1.9	0.1	3.3	168.4	12.9	0.5	3.0	72.1	7.2	0.2
All	**2555**	**0.1**	**91.0**	**1.6**	**0.1**	**0.8**	**372.6**	**12.8**	**0.4**	**3.0**	**77.2**	**8.8**	**0.1**

Table 4.4. Particle sizes for different depositional processes and roads/not-roads for all SEM/EDS data in the project. Number of particles (N), standard error of the mean (S.E.)

ALL DATA													
Depositional Environment	**N**	**Minimum Width (µm)**	**Maximum Width (µm)**	**Mean Width (µm)**	**S.E.**	**Minimum Length (µm)**	**Maximum Length (µm)**	**Mean Length (µm)**	**S.E.**	**Minimum Aspect Ratio**	**Maximum Aspect Ratio**	**Mean Aspect Ratio**	**S.E.**
Rock (All)	1955	0.1	91.0	1.7	0.1	0.8	372.6	13.6	0.5	3.0	77.2	8.9	0.2
Soil (All)	599	0.2	22.0	1.2	0.0	1.8	85.5	9.9	0.3	3.0	68.3	8.5	0.2
Bedrock only	1505	0.1	91.0	1.8	0.1	0.8	372.6	14.4	0.7	3.0	72.1	8.7	0.2
Alluvium (rocks only)	450	0.2	19.7	1.3	0.1	1.3	115.3	11.1	0.5	3.1	77.2	9.5	0.3
Alluvium (soil only)	407	0.2	22.0	1.2	0.1	1.8	85.5	10.0	0.4	3.0	68.3	9.0	0.3
Alluvium (rock and soil)	857	0.2	22.0	1.3	0.0	1.3	115.3	10.6	0.3	3.0	77.2	9.3	0.2
Eolian	192	0.3	4.3	1.3	0.1	2.2	76.1	9.6	0.6	3.1	44.7	7.3	0.3
Road (including playas)	266	0.3	22.0	1.3	0.1	1.8	85.5	10.3	0.6	3.0	33.7	8.9	0.3
Road (not including playas)	250	0.4	22.0	1.3	0.1	1.8	85.5	10.4	0.6	3.0	33.7	8.7	0.3
Not Road/not playa	2289	0.1	91.0	1.6	0.1	0.8	372.6	13.0	0.5	3.0	77.2	8.8	0.1
Not road but includes playa	2332	0.1	91.0	1.6	0.1	0.8	372.6	13.0	0.5	3.0	77.2	8.8	0.1
All	**2555**	**0.1**	**91.0**	**1.6**	**0.1**	**0.8**	**372.6**	**12.8**	**0.4**	**3.0**	**77.2**	**8.8**	**0.1**

The amphibole particles can be divided into 5 large groups of amphibole mineralogy: (1) Calcic (2) Sub-calcic (3) Sodic (4) Sodic-Calcic and (5) Fe-Mg (Table 4.1) (see chapter 2 for more information). The vast majority of the amphiboles in southern Nevada are calcic composition, often further identified as actinolite or magnesiohornblende. The calcic group of amphiboles have a mean aspect ratio of 8.2 +/-0.1, which is the lowest mean aspect ratio of the 5 groups of amphiboles (Table 4.1). In contrast the sodic and sodic-calcic groups have significantly higher mean aspect ratios: 21.0 +/- 2.4, and 14.8 +/- 1.0 respectfully (Table 4.1).

An analysis of variance (ANOVA) identified statistically significant differences in mean aspect ratios for the amphibole mineralogy groups (p-value 0.000). Post-hoc Tukey's HSD tests (comparing the mean aspect ratios for these 5 groups of minerals) indicate calcic, sub-calcic and Fe-Mg were not statistically significant from each other at the 95% confidence level (p-value 0.196 for calcic/sub-calcic; and 0.926 for calcic/Fe-Mg) (Table 4.5). However, the mean aspect ratio for sodic particles is significantly different from the other 4 categories (p-value 0.000). Sodic-calcic group minerals also are significantly different from all but the Fe-Mg category in mean aspect ratio (p-value 0.000; and 0.072 for sodic-calcic/Fe-Mg) (Table 4.5).

Table 4.4 shows particle morphology results for different depositional processes. In particular, we wanted to better understand whether aspect ratios of asbestos fibers vary depending on the surficial processes that have eroded, transported, and deposited them across the landscape. Buck et al., 2013 found no difference between asbestos particles in rocks versus those moved by water or wind across the landscape. For this study, an ANOVA identified statistically significant differences in the mean aspect ratios among bedrock, alluvium and eolian deposits (p-value of 0.000). Post-hoc Tukey's HSD tests indicate the mean aspect ratios for these 3 groups of depositional processes at the 95% confidence level. The mean aspect ratios of eolian-deposited NOA particles are significantly different and lower than those deposited by alluvial processes or those found in bedrock (p-value 0.001 and 0.017, respectively; Table 4.6). However, there was no statistically significant difference between mean aspect ratios of bedrock and alluvium (Table 4.6).

Table 4.5. ANOVA results comparing the mean aspect ratio of each of the 5 mineral groups. Pairs that are significantly different from one another (p-value less than 0.05) are highlighted in blue.

Multiple Comparisons (Post-hoc Tukey HSD)		
Aspect Ratio (length/width)		
(I) Calcic (1) vs Sub-calcic (2) vs Sodic (3) vs Sodic-Calcic (4) vs Fe-Mg (5)	Calcic (1) vs Sub-calcic (2) vs Sodic (3) vs Sodic-Calcic (4) vs Fe-Mg (5)	p-value
Calcic	Sub-calcic	.196
	Sodic	.000*
	Sodic-Calcic	.000*
	Fe-Mg	.926
Sub-calcic	Calcic	.196
	Sodic	.000*
	Sodic-Calcic	.000*
	Fe-Mg	.994
Sodic	Calcic	.000*
	Sub-calcic	.000*
	Sodic-Calcic	.000*
	Fe-Mg	.000*
Sodic-Calcic	Calcic	.000*
	Sub-calcic	.000*
	Sodic	.000*
	Fe-Mg	.072
Fe-Mg	Calcic	.926
	Sub-calcic	.994
	Sodic	.000*
	Sodic-Calcic	.072

* The mean difference is significant at the 95% confidence level.

Table 4.6. ANOVA results comparing the mean aspect ratio of each of the 3 depositional processes groups. Pairs that are significantly different from one another (p-value less than 0.05) are highlighted in blue.

Multiple Comparisons (Post-hoc Tukey HSD)		
Aspect Ratio (length/width)		
Bedrock (1) vs Alluvium (2) vs Eolian (3)	Bedrock (1) vs Alluvium (2) vs Eolian (3)	p-value
Bedrock	Alluvium	.127
	Eolian	.017*
Alluvium	Bedrock	.127
	Eolian	.001*
Eolian	Bedrock	.017*
	Alluvium	.001*

* The mean difference is significant at the 95% confidence level.

This difference in eolian-deposited NOA particles from that of bedrock or alluvium may be explained by one or more processes: (1) The eolian samples in this study come from one or more different amphibole populations (e.g. some larger regional mixing of amphibole sources). (2) One or more processes are affecting the physical shape of the amphibole particles as they erode out of the bedrock and are transported across the landscape. The lower aspect ratios of eolian NOA particles may be the result of wind erosion, transport, and deposition processes that physically shortens the length of these particles such that they have lower aspect ratios than particles found in bedrock or alluvium, and (3) It could also be that wind processes do a better job of sorting amphibole particles so that eolian deposits contain more NOA particles that are shorter/wider than those found in bedrock and alluvium.

We also wanted to understand if there was a difference in mean aspect ratio of NOA particles in bedrock (mean 8.7 +/- 0.2) versus rock samples transported in alluvium (mean 9.5 +/- 0.3). An independent samples t-test indicated that the mean aspect ratio for NOA particles in bedrock is significantly different (p-value 0.036) from rock samples transported in alluvium. It may be that rocks transported in alluvium are slightly more weathered, such these particles may be more easily extracted from the rock with the use of dental tools, which may result in longer particles and therefore higher aspect ratios being measured. Similarly, it may require more force to extract less-weathered particles from fresh bedrock samples, which may result in breakage along the length of the particle and therefore shorter aspect ratios in bedrock samples. Lastly, there could be collection biases involved in which more-highly altered samples that contain fibers with greater aspect ratios, were unconsciously preferentially collected in alluvium as a

result of our desire to not miss important NOA deposits. Thus, more analyses are needed to explain these results.

Similarly, we examined the differences between mean aspect ratio of rock (8.9 +/- 0.2) versus soil samples (8.5 +/- 0.2). An independent samples t-test indicates that these values are not significantly different (p-value 0.131).

We also wanted to examine if there are any differences in mean aspect ratio between samples collected on roads versus those not on roads. An independent samples t-test indicates that these are not significantly different (p-value 0.847). Since dirt roads are built upon the underlying sediment, the fact that there is no difference between these groups is to be expected.

Distribution of NOA mineralogy

The amphibole particles measured in this study were grouped into 5 amphibole mineral categories: (1) Calcic, (2) Sub-Calcic, (3) Sodic, (4) Sodic-calcic and (5) Fe-Mg (see Chapters 2 and 3 for discussion on amphibole chemistry). Samples that tested positive for these mineral groups are shown on the following maps (Figures 4-9 to 4-13).

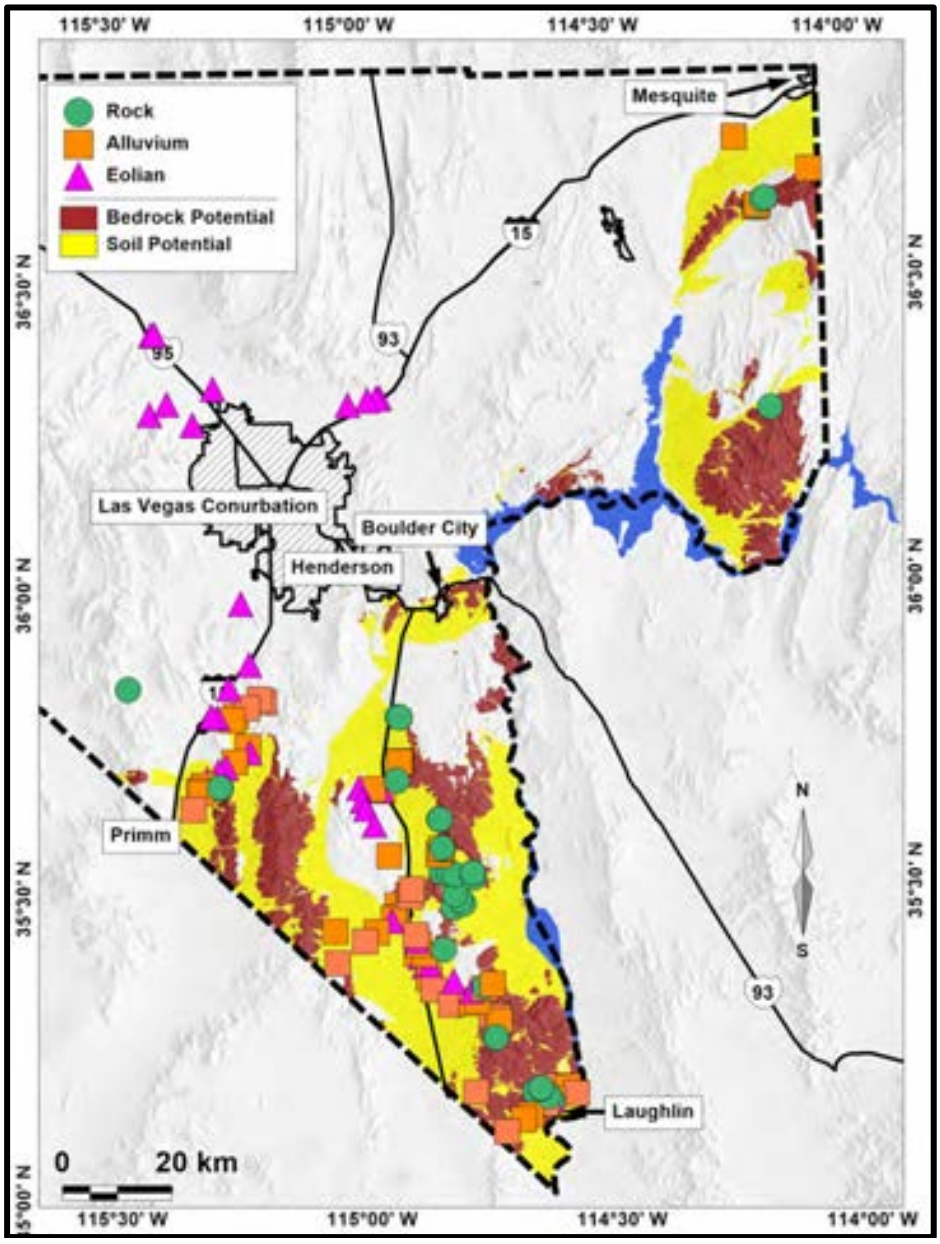

Figure 4-9. Map of southern Nevada showing predicted NOA-containing areas with samples indicated where calcic-group amphiboles were identified. This is the most common mineralogy group of amphibole NOA found in southern Nevada.

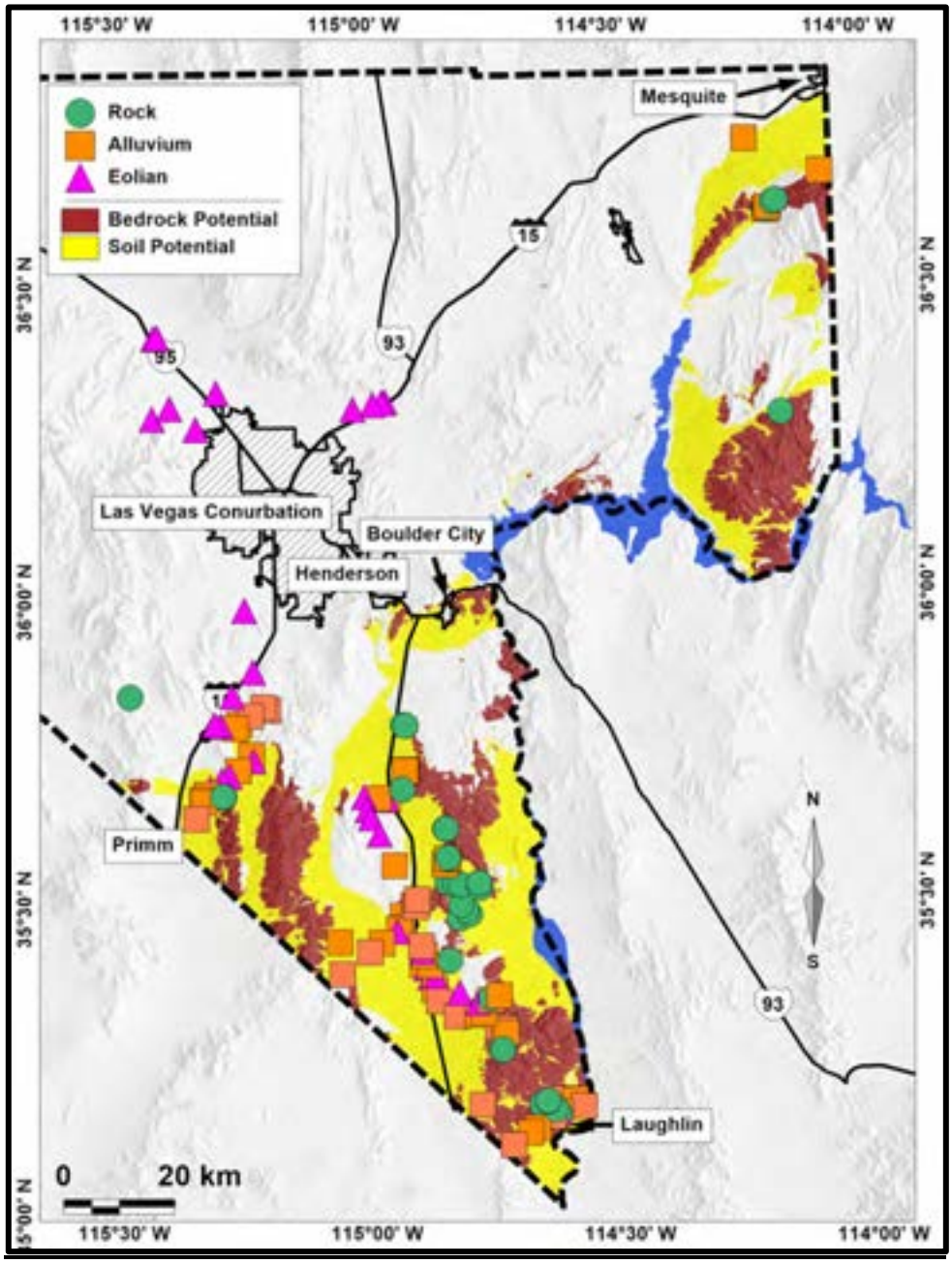

Figure 4-10. Map of southern Nevada showing predicted NOA-containing areas with samples indicated where sub-calcic-group amphiboles were identified. This is the second-most common mineralogy group of amphibole NOA found in southern Nevada.

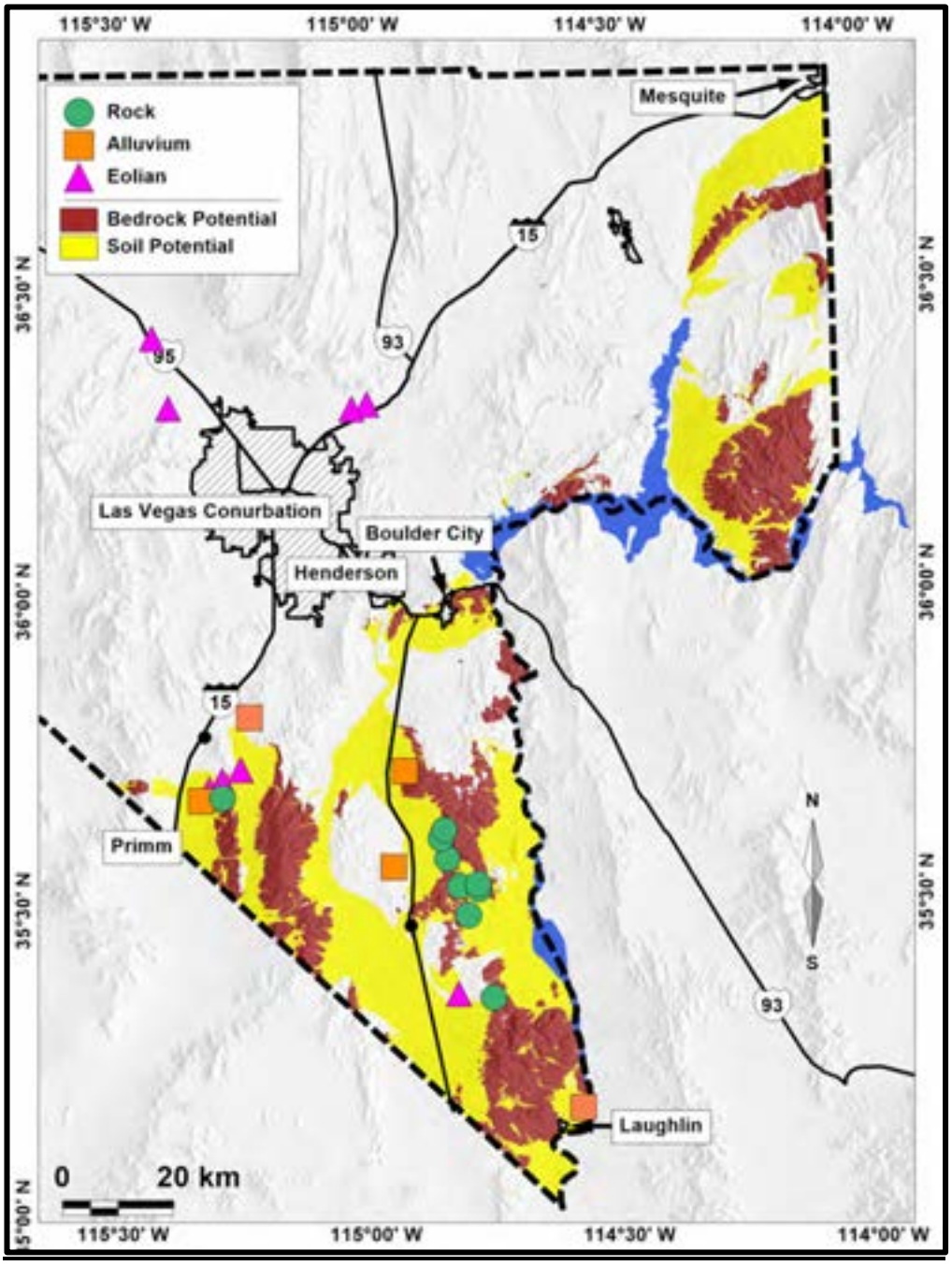

Figure 4-11. Map of southern Nevada showing predicted NOA-containing areas with samples indicated where sodic-group amphiboles were identified. This mineralogy group consistently has the longest and thinnest amphibole particles, which is a likely indication of increased toxicity, especially when compared to the calcic, and sub-calcic groups.

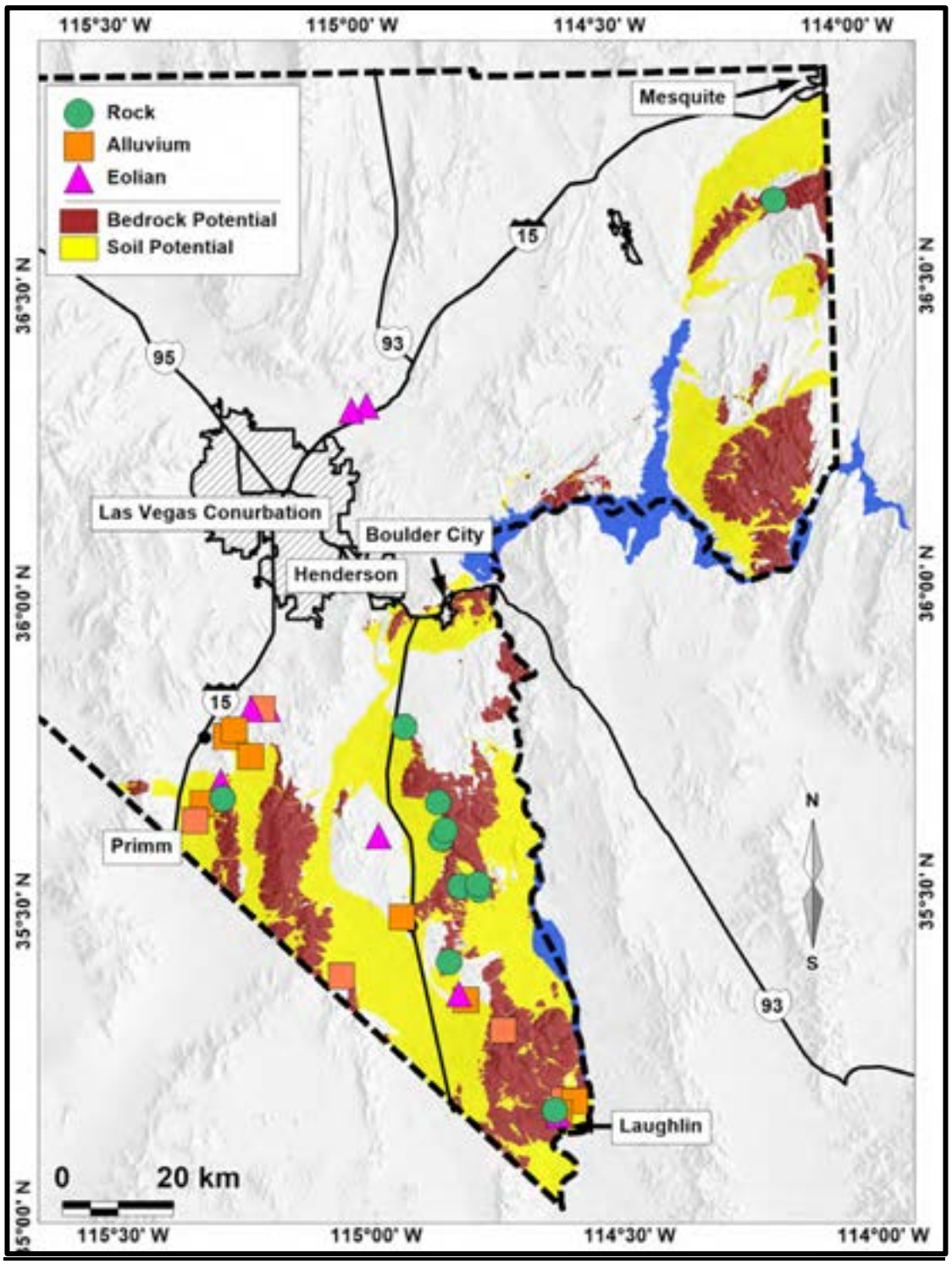

Figure 4-12. Map of southern Nevada showing predicted NOA-containing areas with samples indicated where sodic-calcic group amphiboles were identified. This mineralogy group, similarly to the sodic group minerals, consistently has longer and thinner amphibole particles, which is a likely indication of increased toxicity, especially when compared to the calcic, and sub-calcic groups.

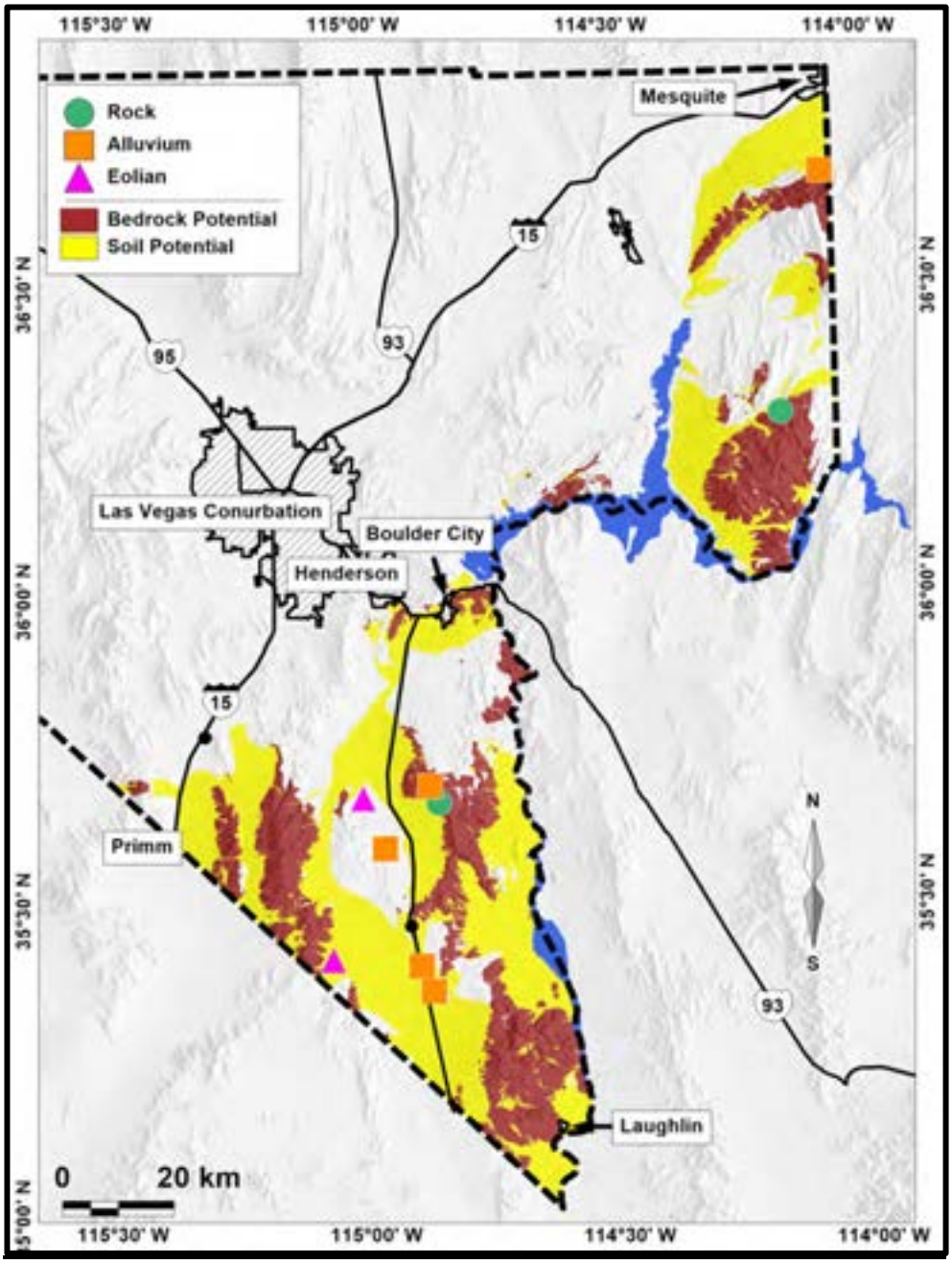

Figure 4-13. Map of southern Nevada showing predicted NOA-containing areas with samples indicated where Fe-Mg group amphiboles were identified.

El Dorado Mountains Region

The El Dorado Mountains region refers primarily to the area surrounding Keyhole Canyon south of Boulder City (Figures 4-14, 4-15). A total of 11 samples, 5 collected from alluvium and 6 collected from bedrock outcrops, were obtained and analyzed (Table 4.7; Figures 4-16, 4-17). All tested positive for amphibole asbestos with aspect ratio of 3:1, and for 8:1.

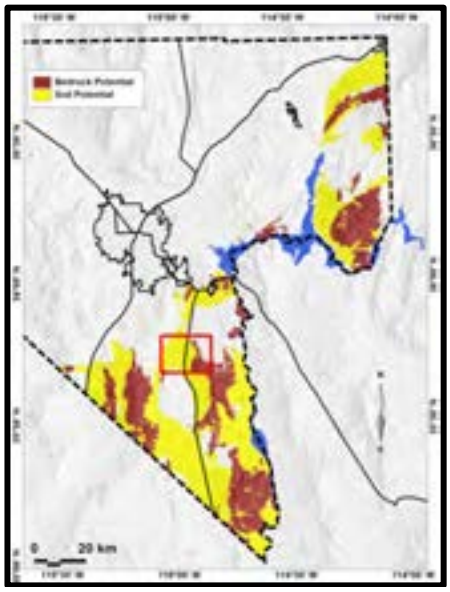

Figure 4-14. Map of southern Nevada showing predicted NOA-containing areas with the El Dorado region outlined in red box.

Figure 4-15. Photo of Keyhole Canyon looking up into the canyon towards the east from the parking area.

Figure 4-16. Map of El Dorado region sample locations. Positive occurrences are for amphibole asbestos with aspect ratios of both 3:1 or greater and 8:1 or greater. Samples are identified according to the geological process that deposited the material: bedrock (in place), alluvium (water-deposited), or eolian (wind-deposited)

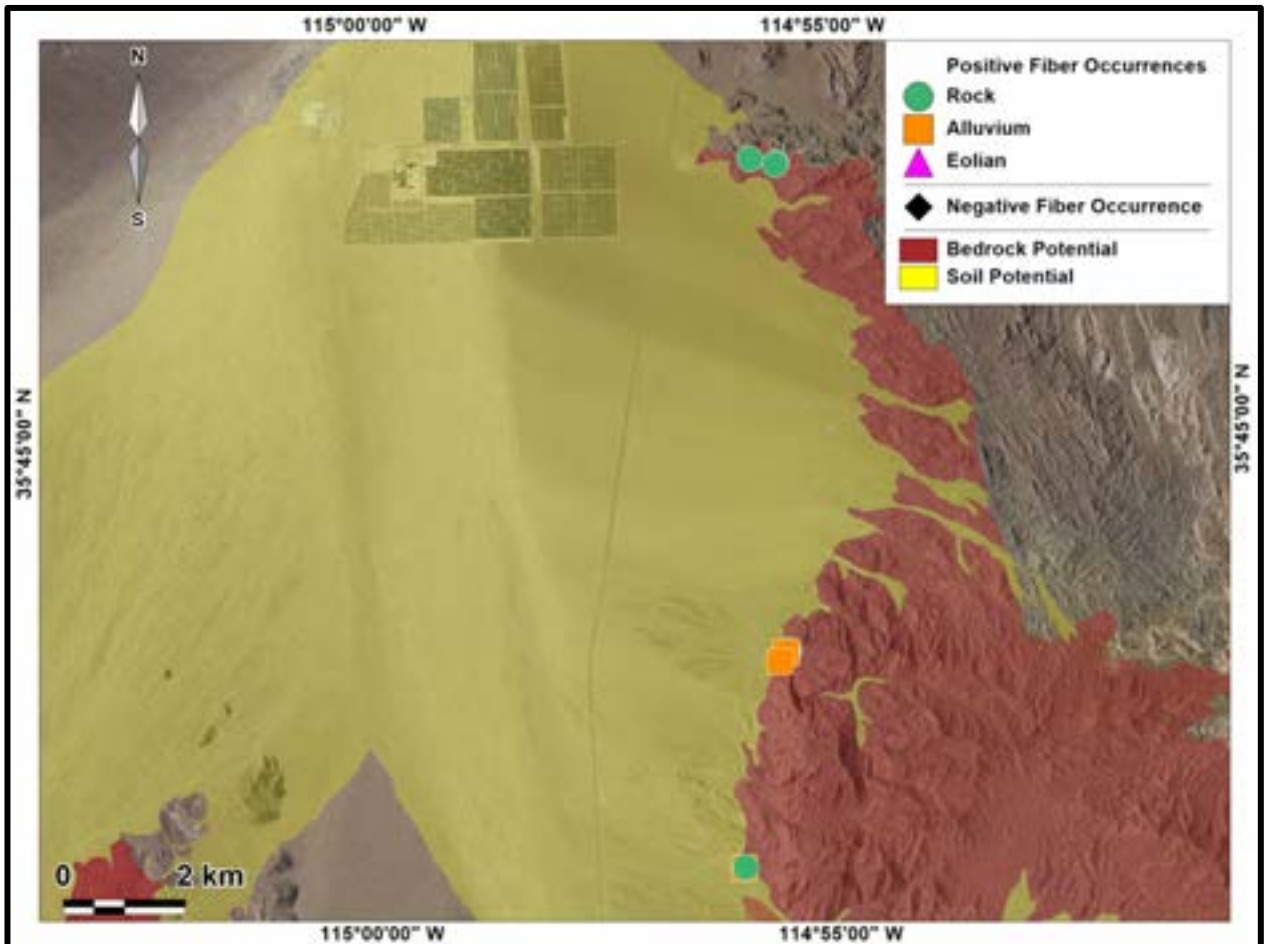

Figure 4-17. Map of sample locations in the El Dorado region with predicted occurrences of NOA based on alluvial (water-transport) surficial processes that transport material from the source rock out into the basin. Bedrock potential represents areas of potential occurrence for amphibole asbestos in igneous and metamorphic rock exposures. Soil potential delineates areas where runoff could potentially distribute amphibole asbestos fibers downslope from bedrock areas. Positive occurrences are for amphibole asbestos with aspect ratios of both 3:1 or greater and 8:1 or greater for samples in the El Dorado Region.

Table 4.7. Summary of sample type, depositional process, and mean and maximum aspect ratios for samples in the El Dorado Region.

EL DORADO							
Sample ID	**N**	**Mean Aspect Ratio**	**Maximum Aspect Ratio**	**Aspect Ratio Cutoff 8+**	**Aspect Ratio Cutoff 3+**	**Type**	**Depositional Process**
E031914-1	19	7.8	14.9	Positive	Positive	rock	rock
E031914-2	42	14.4	105.6	Positive	Positive	rock	rock
E031914-3	21	10.4	17.7	Positive	Positive	rock	rock
E031914-4	10	12.9	24.7	Positive	Positive	rock	rock
E031914-5	26	8.4	15.8	Positive	Positive	rock	rock
E031914-6a	15	12.4	30.1	Positive	Positive	rock	alluvium
E031914-6b	16	29.5	77.2	Positive	Positive	rock	alluvium
E031914-6c	26	12.8	26.8	Positive	Positive	rock	alluvium
E031914-7	25	12.0	18.0	Positive	Positive	rock	alluvium
E031914-8	22	10.9	16.7	Positive	Positive	rock	alluvium
E031914-9	23	9.2	17.1	Positive	Positive	rock	rock
TOTAL =	**245**	**12.5**	**105.6**				

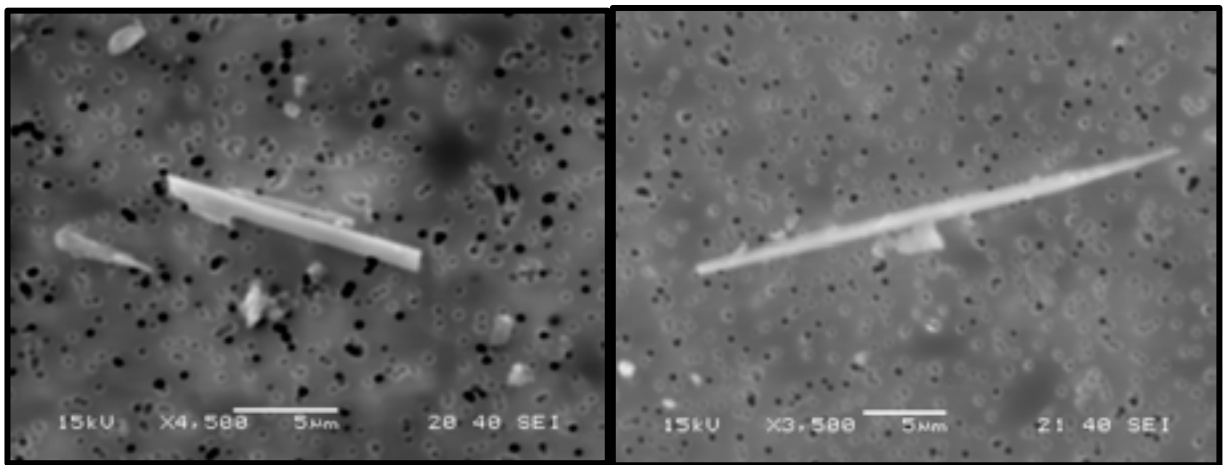

Figure 4-18. SEM image of actinolite amphibole from sample E031914-3 (left) and a sub-calcic amphibole from sample E031914-6c (right).

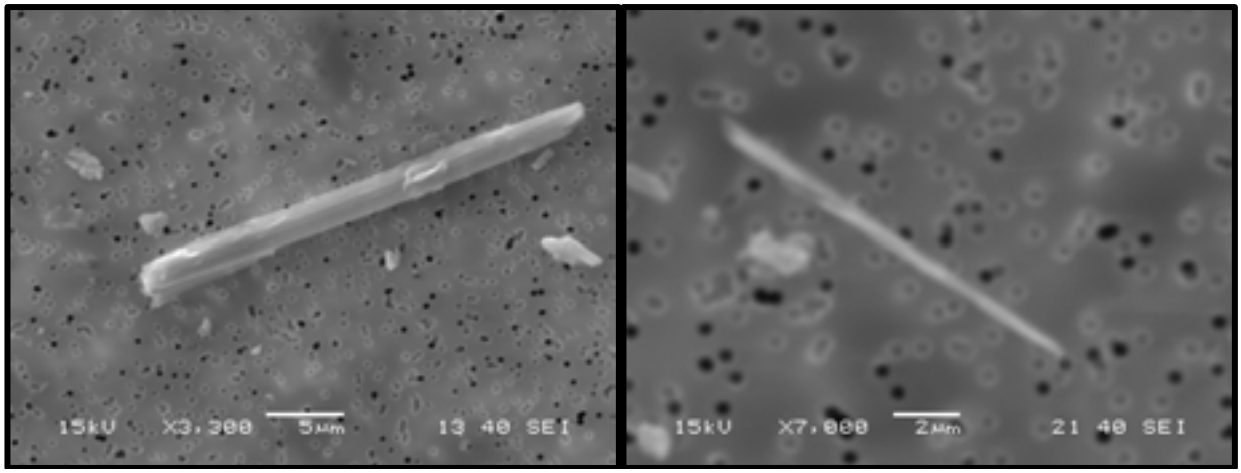

Figure 4-19. SEM image of magnesio-hornblende amphibole particle from sample E031914-3 (left) and actinolite amphibole from sample E031914-6c (right).

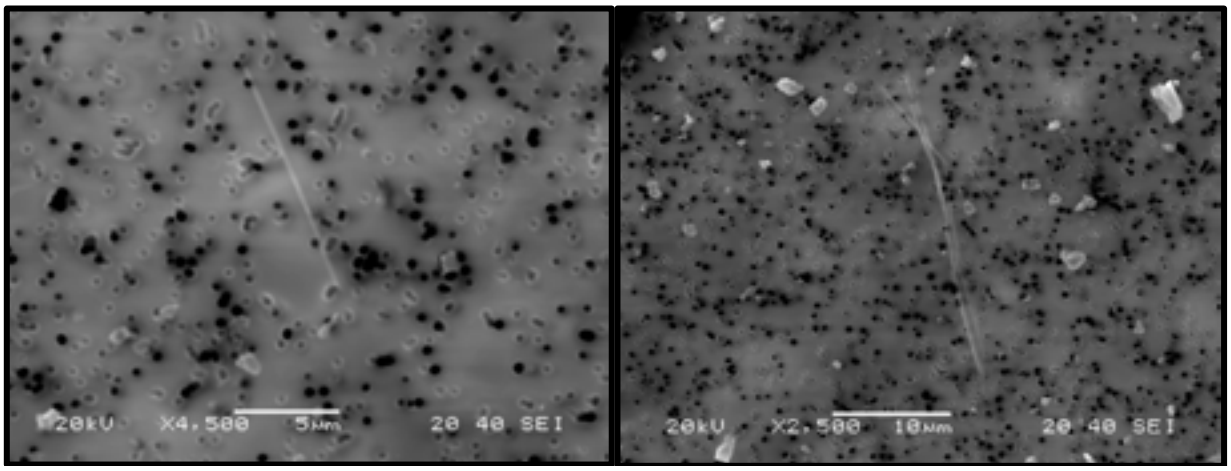

Figure 4-20. SEM image of sodic amphibole fibers from sample E031914-6b

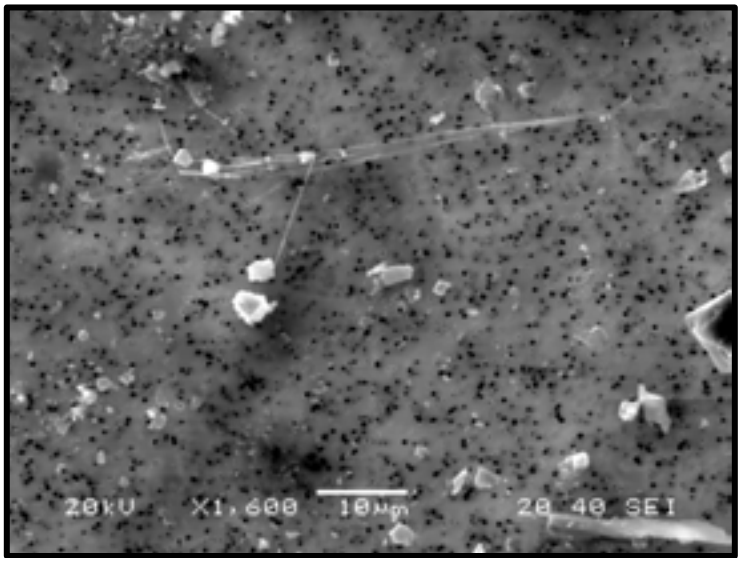

Figure 4-21. SEM image of sodic amphibole bundle from sample E031914-6b

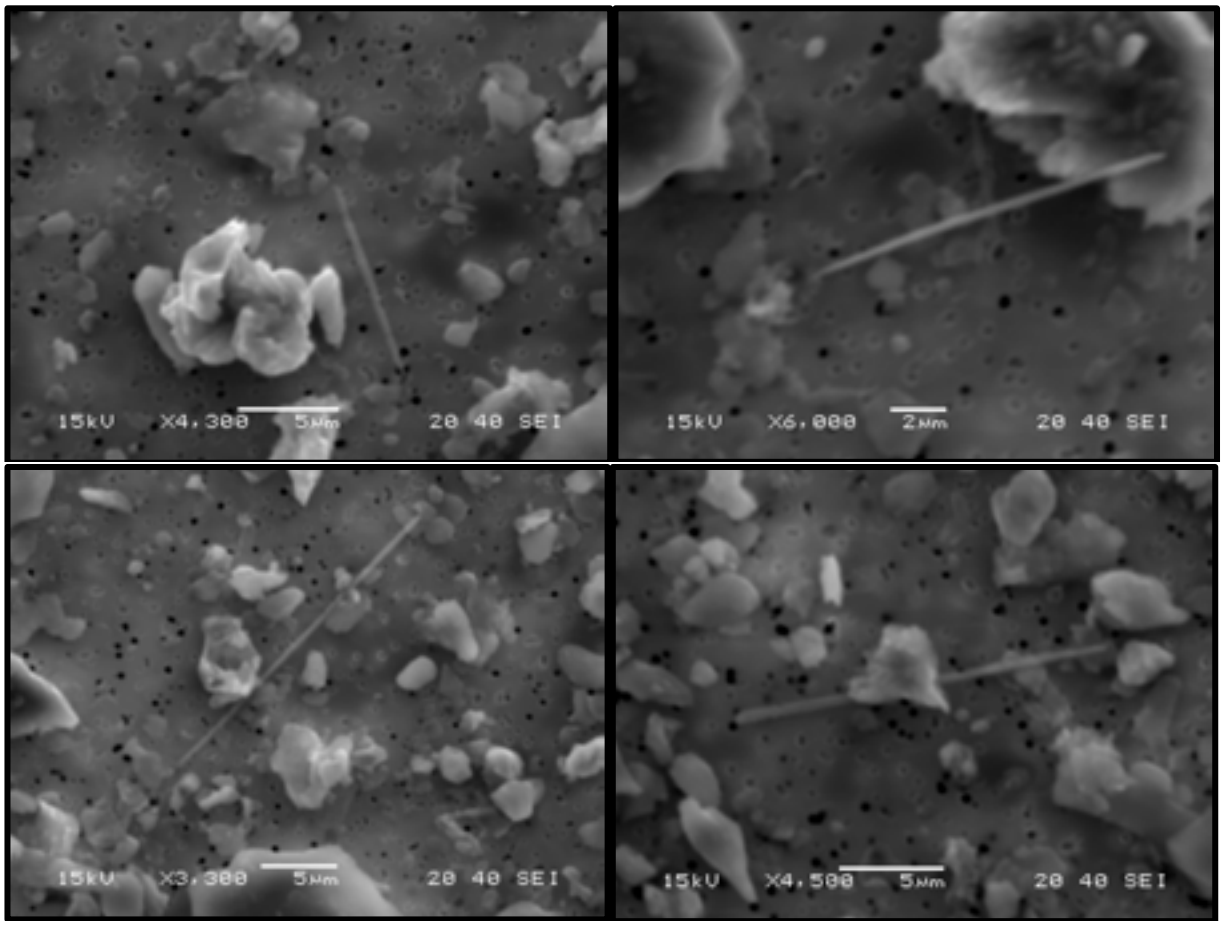

Figure 4-22. SEM images of actinolite fibers from sample E031914-2

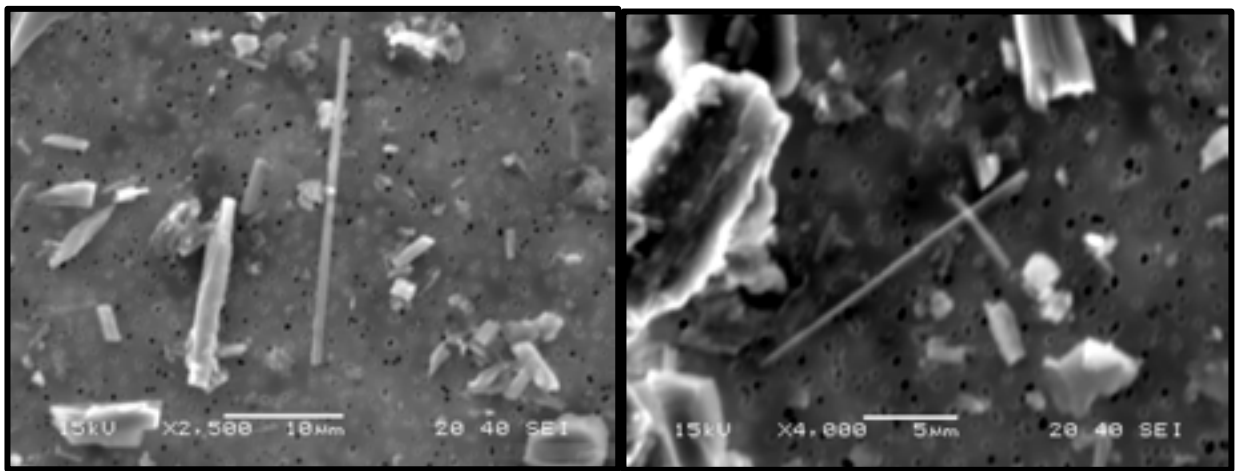

Figure 4-23. SEM images of sub-calcic fibers from sample E031914-6a

The amphibole samples collected in the El Dorado Region have a wide range of compositions including sub-calcic, calcic, sodic, and sodic-calcic (Table 4.8). Much more detailed work is needed in this area to understand their distributions and genesis (see Chapters 2 and 3). However, amphibole particles in this region tend to have high aspect ratios. The mean aspect ratio of fibers in this region was 12.5 ± 0.7 and the maximum aspect ratio was 105.6 (Table 4.8). SEM images of typical particles measured in this region are shown in Figures 4-18 to 4-23.

Significantly, amphibole particles with sodic, or sodic-calcic compositions are consistently found to have greater aspect ratios than those with a calcic or sub-calcic composition (Table 4.8).

Bundles, fibers and even prismatic crystals all had high mean aspect ratios in this region and suggests that the rocks in this area are highly altered (Table 4.9).

Table 4.8. Particle sizes and mineralogy results of amphibole particles in the El Dorado Region. Number of particles (N), standard error of the mean (S.E.)

El Dorado Region													
Mineralogy	**N**	**Minimum Width (µm)**	**Maximum Width (µm)**	**Mean Width (µm)**	**S.E.**	**Minimum Length (µm)**	**Maximum Length (µm)**	**Mean Length (µm)**	**S.E.**	**Minimum Aspect Ratio**	**Maximum Aspect Ratio**	**Mean Aspect Ratio**	**S.E.**
Actinolite	115	0.4	7.3	1.3	0.1	3.6	105.6	14.2	1.1	4.9	105.6	12.1	1.0
Edenite	5	0.8	6.7	3.9	1.0	8.3	57.2	35.5	9.2	6.5	10.4	9.2	0.7
Mg-hbld	47	0.3	36.6	3.1	0.8	1.7	134.7	23.0	3.9	3.7	17.1	9.5	0.4
Winchite	1	0.4	0.4	0.4	-	10.6	10.6	10.6	-	26.5	26.5	26.5	-
Sodic-calcic group	1	0.4	0.4	0.4	-	10.6	10.6	10.6	-	26.5	26.5	26.5	-
Sodic group	12	0.2	1.6	0.5	0.1	4.7	48.6	16.2	4.0	15.2	77.2	36.4	5.3
Sub-Calcic group	64	0.3	7.0	1.3	0.2	2.4	65.2	12.5	1.3	3.6	30.1	10.9	0.7
Calcic group	168	0.3	36.6	1.9	0.2	1.7	134.7	17.3	1.4	3.7	105.6	11.3	0.7
All Particles	**245**	**0.2**	**36.6**	**1.7**	**0.2**	**1.7**	**134.7**	**16.0**	**1.0**	**3.6**	**105.6**	**12.5**	**0.7**

Table 4.9. Morphology classification of particles analyzed in the El Dorado region. Number of particles (N), standard error of the mean (S.E.)

El Dorado Region													
Morphology	**N**	**Minimum Width (µm)**	**Maximum Width (µm)**	**Mean Width (µm)**	**S.E.**	**Minimum Length (µm)**	**Maximum Length (µm)**	**Mean Length (µm)**	**S.E.**	**Minimum Aspect Ratio**	**Maximum Aspect Ratio**	**Mean Aspect Ratio**	**S.E.**
Bundles	50	1.1	36.6	3.6	0.8	7.9	134.7	29.5	3.4	3.7	30.4	10.4	0.6
Fibers (≤1 µm)	126	0.2	1.0	0.7	0.0	1.7	105.6	10.0	0.9	5.4	105.6	15.0	1.2
Prismatic Crystals	69	1.1	9.2	1.9	0.2	5.6	81.2	17.2	1.5	3.6	26.8	9.4	0.5
All Particles	**245**	**0.2**	**36.6**	**1.7**	**0.2**	**1.7**	**134.7**	**16.0**	**1.0**	**3.6**	**105.6**	**12.5**	**0.7**

Gold Butte Region

Due to political circumstances, we were unable to do much fieldwork in the Gold Butte Region, north of Lake Mead and east of the Overton arm of Lake Mead (Figure 4-24). Three samples were obtained for analyses, and all tested positive for amphibole asbestos with aspect ratio of at least 3:1, and for 8:1 or higher (Table 4.10; Figures 4-25, 4-26). These samples were all collected in an area in which vermiculite occurs. Amphibole minerals are commonly found intergrown with vermiculite. The plutonic rocks in this region require more testing to determine the potential for NOA.

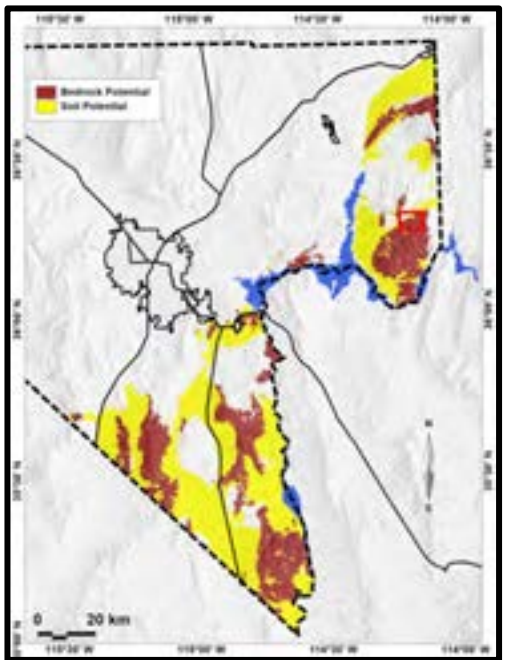

Figure 4-24. Map of southern Nevada showing predicted NOA-containing areas with the Gold Butte region where samples were obtained outlined in red box.

Figure 4-25. Map of Gold Butte region sample locations. Positive occurrences are for amphibole asbestos with aspect ratios of both 3:1 or greater and 8:1 or greater. Samples are identified according to the geological process that deposited the material: bedrock (in place), alluvium (water-deposited), or eolian (wind-deposited).

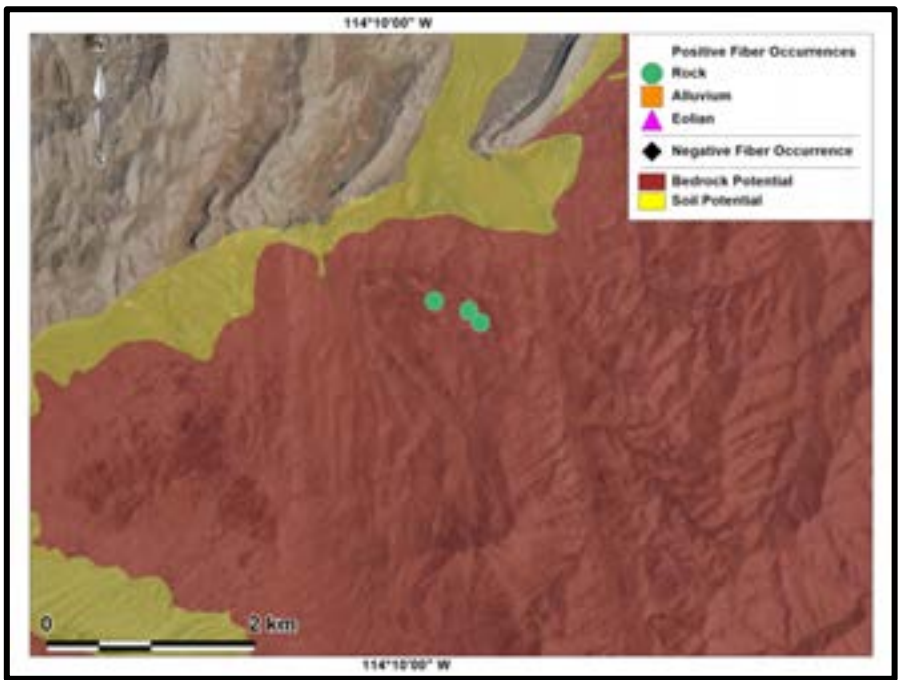

Figure 4-26. Map of sample locations in the Gold Butte region with predicted occurrences of NOA based on alluvial (water-transport) surficial processes that transport material from the source rock out into the basin. Bedrock potential represents areas of potential occurrence for amphibole asbestos in igneous and metamorphic rock exposures. Soil potential delineates areas where runoff could potentially distribute amphibole asbestos fibers downslope from bedrock areas. Positive occurrences are for amphibole asbestos with aspect ratios of both 3:1 or greater and 8:1 or greater for samples in the El Dorado Region.

Table 4.10. Summary of sample type, depositional process, and mean and maximum aspect ratios for samples in the Gold Butte Region

GOLD BUTTE							
Sample ID	**N**	**Mean Aspect Ratio**	**Maximum Aspect Ratio**	**Aspect Ratio Cutoff 8+**	**Aspect Ratio Cutoff 3+**	**Type**	**Depositional Process**
GB1	18	7.7	16.7	Positive	Positive	rock	rock
GB2	12	9.2	16.3	Positive	Positive	rock	rock
GB3	27	8.4	21.5	Positive	Positive	rock	rock
TOTAL =	**57**	**8.4**	**21.5**				

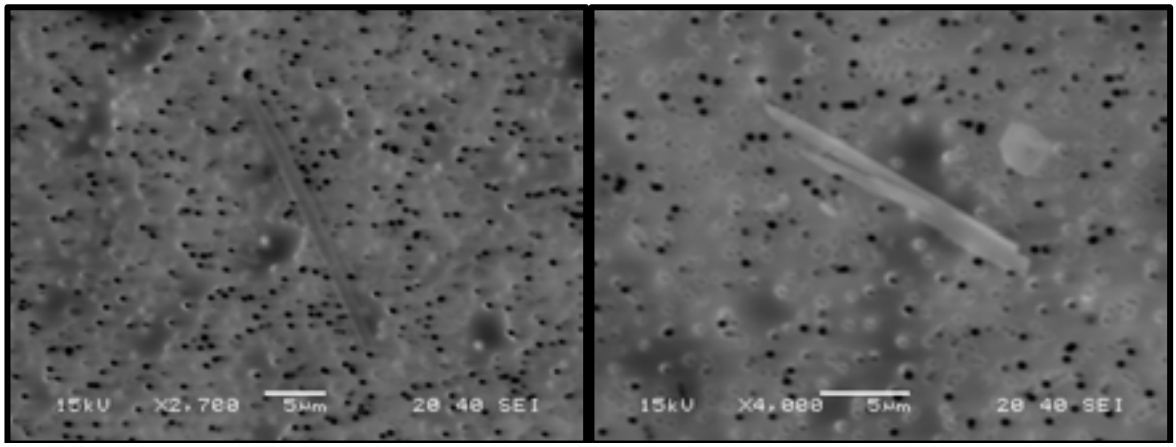

Figure 4-27. SEM images of magnesio-hornblende particles from sample GB1.

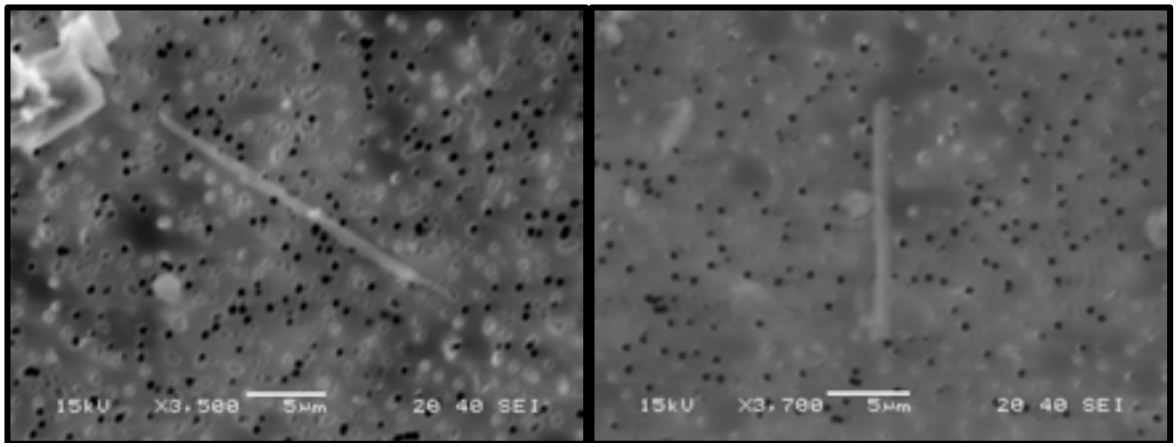

Figure 4-28. SEM images of magnesio-hornblende particles from sample GB3.

The amphibole samples collected in the Gold Butte region are calcic and sub-calcic in composition, but only reflect the results from these 3 samples which were collected all in one area (Table 4.11; Figure 4-26). More research in this region may find other compositions are also present. SEM images are shown in Figures 4-27 and 4-28.

The mean aspect ratio for these 3 samples was 8.4 ± 0.5 (Tables 4.11, 4.12), the maximum aspect ratio was 21.5 (Tables 4.11, 4.12).

Table 4.11. Particle sizes and mineralogy results of amphibole particles in the Gold Butte Region. Number of particles (N), standard error of the mean (S.E.)

Gold Butte Region													
Mineralogy	**N**	**Minimum Width (µm)**	**Maximum Width (µm)**	**Mean Width (µm)**	**S.E.**	**Minimum Length (µm)**	**Maximum Length (µm)**	**Mean Length (µm)**	**S.E.**	**Minimum Aspect Ratio**	**Maximum Aspect Ratio**	**Mean Aspect Ratio**	**S.E.**
Actinolite	1	1.4	1.4	1.4	-	17.9	17.9	17.9	-	12.8	12.8	12.8	-
Mg-hbld	49	0.6	9.3	1.6	0.2	2.7	58.5	12.4	1.4	3.0	21.5	8.2	0.6
Calcic group	50	0.6	9.3	1.6	0.2	2.7	58.5	12.5	1.4	3.0	21.5	8.3	0.6
Fe-Mg	2	0.8	1.6	1.2	0.4	3.9	9.0	6.5	2.6	4.9	5.6	5.3	0.4
Sub-Calcic group	5	2.3	5.2	3.8	0.6	17.6	84.5	42.8	12.1	6.5	16.3	10.6	1.6
All Particles	**57**	**0.6**	**9.3**	**1.8**	**0.2**	**2.7**	**84.5**	**14.9**	**1.9**	**3.0**	**21.5**	**8.4**	**0.5**

Table 4.12. Morphology classification of particles analyzed in the El Dorado region. Number of particles (N), standard error of the mean (S.E.)

Gold Butte Region													
Morphology	**N**	**Minimum Width (µm)**	**Maximum Width (µm)**	**Mean Width (µm)**	**S.E.**	**Minimum Length (µm)**	**Maximum Length (µm)**	**Mean Length (µm)**	**S.E.**	**Minimum Aspect Ratio**	**Maximum Aspect Ratio**	**Mean Aspect Ratio**	**S.E.**
Bundles	17	1.0	9.3	2.7	0.5	5.6	84.5	22.8	4.8	3.4	18.5	8.7	1.0
Fibers (≤1 µm)	16	0.6	1.0	0.8	0.0	2.7	21.5	6.7	1.1	3.0	21.5	7.8	1.1
Prismatic Crystals	24	1.0	5.1	1.7	0.2	4.9	58.5	14.9	2.5	3.8	16.7	8.5	0.7
All Particles	**57**	**0.6**	**9.3**	**1.8**	**0.2**	**2.7**	**84.5**	**14.9**	**1.9**	**3.0**	**21.5**	**8.3**	**0.5**

Highland Mountains Region

The Highland Mountains region refers primarily to the area west of Highway 93, south of the El Dorado Playa and north of the town of Searchlight (Figure 4-29). A total of 14 soil samples were obtained and analyzed (Table 4.13; Figures 4-30 to 4-34). Eight of the 14 samples were collected from eolian deposts (vesicular A horizons on desert pavements) and the remaining samples were collected in surface alluvium. All but one tested positive for amphibole asbestos with aspect ratio of 3:1 or greater, and 10 of 14 tested positive for aspect ratios of 8:1 or greater. For the region, the mean aspect ratio was 8.1 ± 0.5 and the maximum aspect ratio measured was 20.8 (Table 4.13).

The source of these amphiboles is thought to be both alluvial and eolian deposition from surrounding asbestos-bearing bedrock, especially in the El Dorado, Nelson and Ireteba Mountains regions (Figures 4-30 to 4-34).

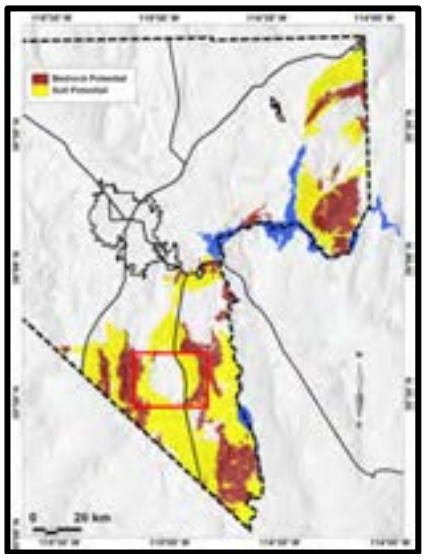

Figure 4-29. Map of southern Nevada showing predicted NOA-containing areas with the Highland Mountains region outlined in red box.

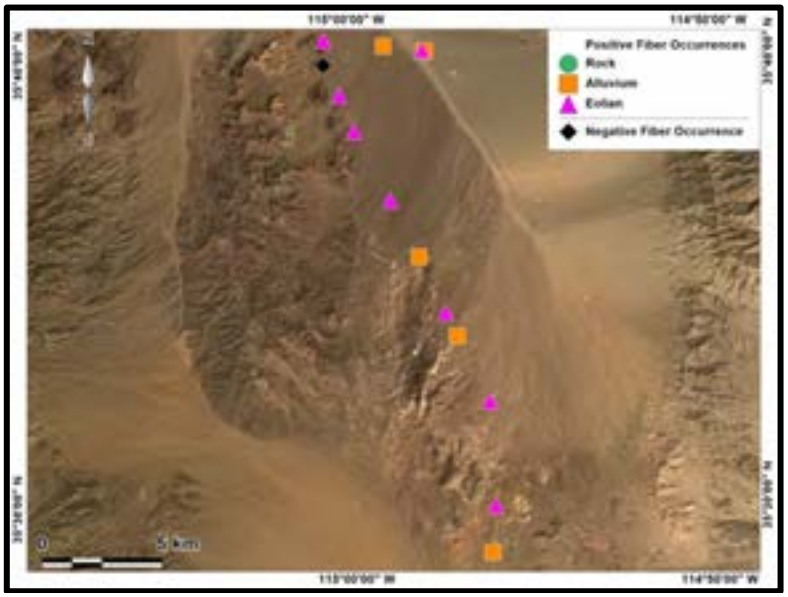

Figure 4-30. Map of Highland Mountains region sample locations. Positive occurrences are for amphibole asbestos with aspect ratios of 3:1 or greater. Samples are identified according to the geological process that deposited the material: bedrock (in place), alluvium (water-deposited), or eolian (wind-deposited).

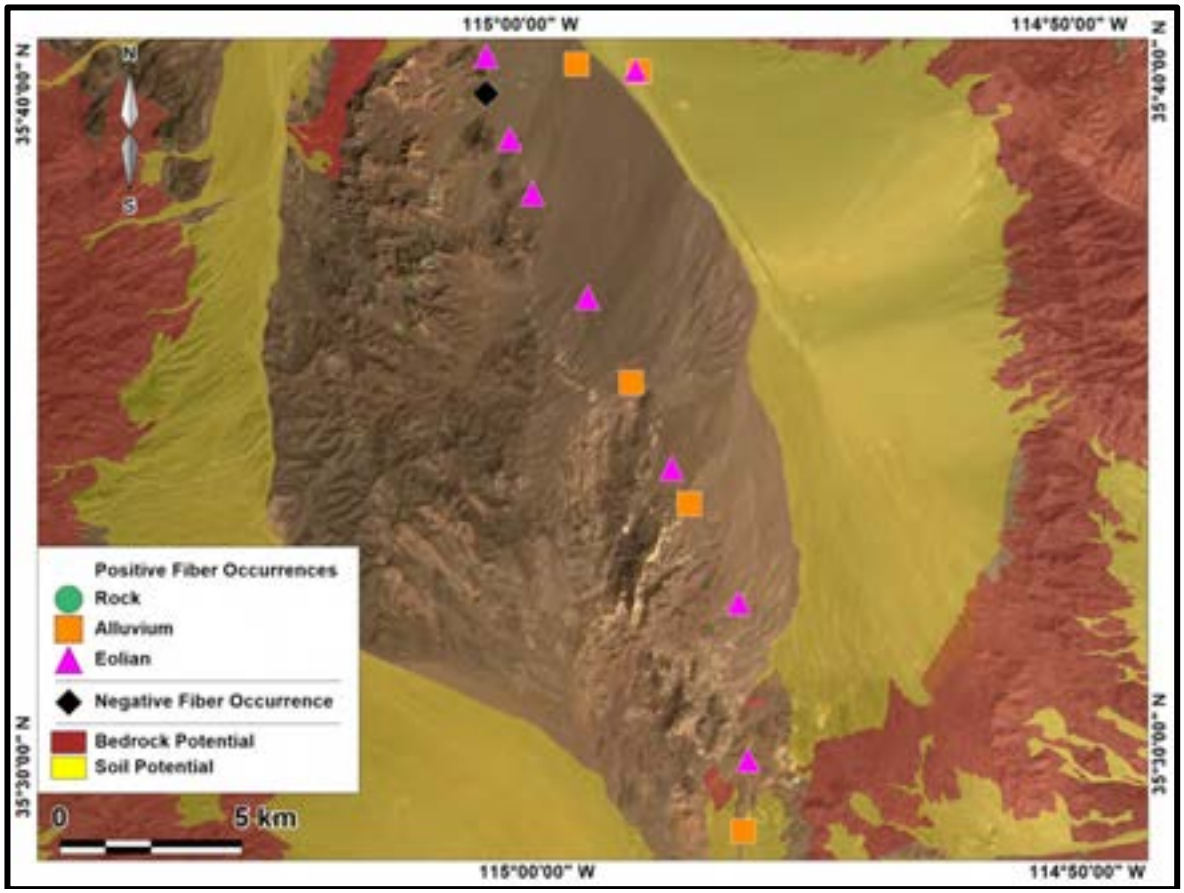

Figure 4-31. Map of sample locations in the Highland Mountains region with predicted occurrences of NOA based on alluvial (water-transported) surficial processes that transport material from the source rock out into the basin. Bedrock potential represents areas of potential occurrence for amphibole asbestos in igneous and metamorphic rock exposures. Soil potential delineates areas where runoff could potentially distribute amphibole asbestos fibers downslope from bedrock areas. Positive occurrences are for amphibole asbestos with aspect ratios of 3:1 or greater.

The positive eolian and alluvium samples that were found in the Highland Mountains region in areas *not* predicted to contain NOA, can be mostly explained by wind deposition of NOA-containing sediment. All of the eolian samples tested positive for NOA in this region (Table 4.13). Three of the four alluvial samples in this region tested positive for NOA, yet occur in areas where water-deposition from NOA-containing bedrock is not indicated. However, because dust is such an important process in the Mojave Desert, and one that never completely ceases, all alluvial samples in this region also contain some component of eolian particulates. These three alluvial sediments probably are contaminated with NOA-containing dust, especially since this entire region (see Figure 4.3) has vast areas of NOA-containing soils from which these particles could have been sources. It is also possible that weathering and erosion of Miocene conglomerate (Faulds et al., 2002) along the eastern edge of the mountains could be a

source of the NOA. In this scenario the conglomerate would contain clasts of igneous and/or metamorphic rocks that contain NOA. Weathering of fibers out of these clasts would allow erosion and transport of the fibers through the alluvial system. This would be similar to what Metcalf and Buck (2015) noted in the Wilson Ridge area of Arizona. There, they observed clasts of Wilson Ridge plutonic rocks containing NOA within the Miocene to Pliocene-age Black Mountain conglomerate. Another possible explanation involves the occurrence of NOA within trachyandesite and trachydacite volcanic rocks of the Highland Mountains. McKee (2016) observed hornblende as phenocrysts and within the groundmass of samples of volcanic rock. Although the hornblende is non-asbestiform, alteration of such amphiboles by hydrothermal alteration could result in the growth of NOA that could be weathered and eroded.

Figure 4-32. Photo from Highland Mountains on a rainy day.

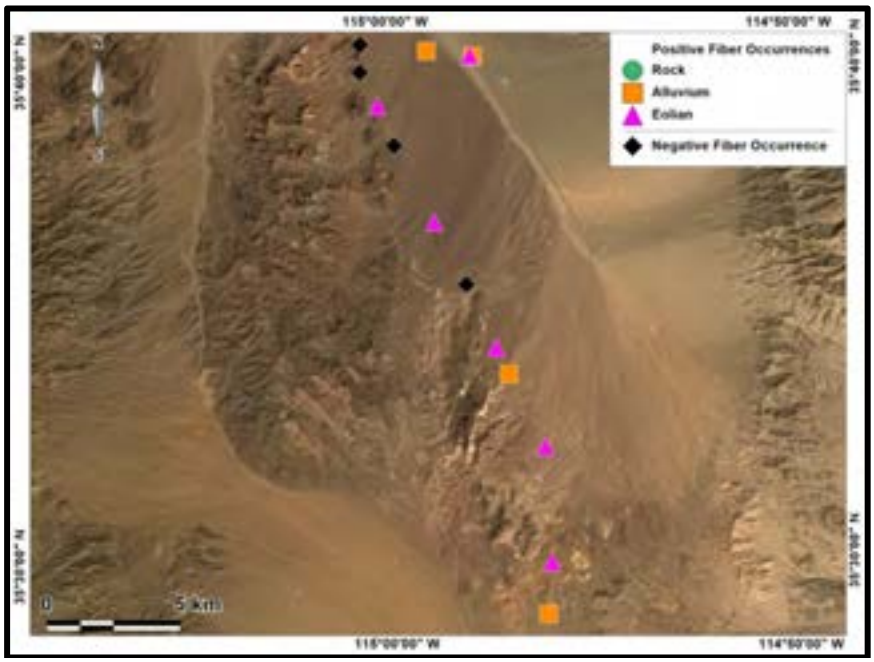

Figure 4-33. Map of Highland Mountains region sample locations. Positive occurrences are for amphibole asbestos with aspect ratios of 8:1 or greater. Samples are identified according to the geological process that deposited the material: bedrock (in place), alluvium (water-deposited), or eolian (wind-deposited).

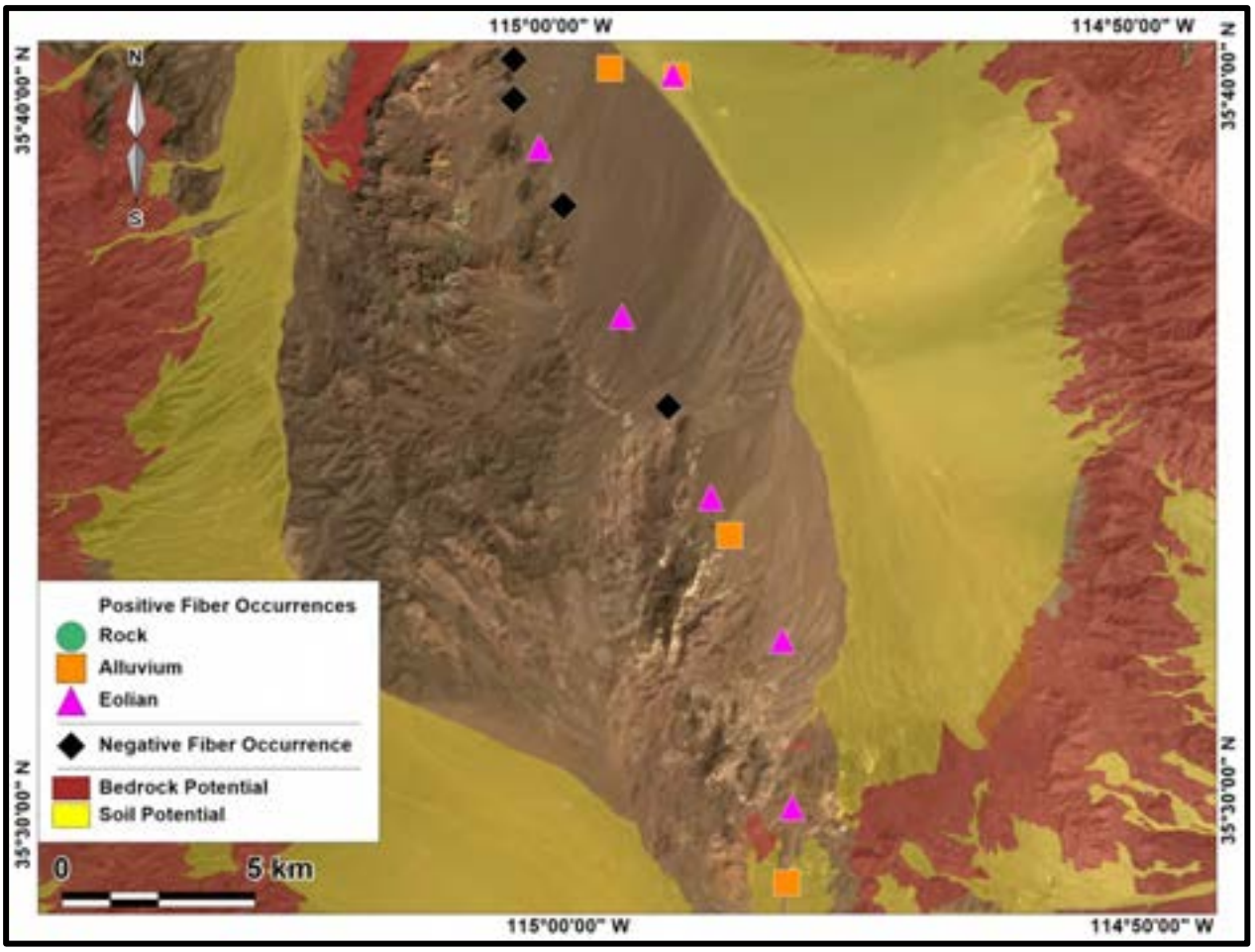

Figure 4-34. Map of sample locations in the Highland Mountains region with predicted occurrences of NOA based on alluvial (water-transported) surficial processes that transport material from the source rock out into the basin. Bedrock potential represents areas of potential occurrence for amphibole asbestos in igneous and metamorphic rock exposures. Soil potential delineates areas where runoff could potentially distribute amphibole asbestos fibers downslope from bedrock areas. Positive occurrences are for amphibole asbestos with aspect ratios of 8:1 or greater.

Table 4.13. Summary of sample type, depositional process, and mean and maximum aspect ratios for samples in the Highland Mountains Region.

HIGHLAND MOUNTAINS							
Sample ID	**N**	**Mean Aspect Ratio**	**Maximum Aspect Ratio**	**Aspect Ratio Cutoff 8+**	**Aspect Ratio Cutoff 3+**	**Type**	**Depositional Process**
H030115-1	10	11.9	20.8	Positive	Positive	soil	alluvium
H030115-2	6	6.2	12.5	Positive	Positive	soil	eolian
H030115-3	2	8.4	9.3	Positive	Positive	soil	alluvium
H030115-4	5	5.2	6.3	Negative	Positive	soil	eolian
H030115-5	0	NA	NA	Negative	Negative	soil	alluvium
H030115-6	4	7.4	9.4	Positive	Positive	soil	eolian
H030115-7	4	5.0	6.3	Negative	Positive	soil	eolian
H030115-8	5	7.4	19.5	Positive	Positive	soil	eolian
H030115-9	1	3.0	3.0	Negative	Positive	soil	alluvium
H030115-10	3	9.2	15.0	Positive	Positive	soil	eolian
H030115-11	5	10.7	15.1	Positive	Positive	soil	alluvium
H030115-12	5	8.7	12.0	Positive	Positive	soil	eolian
H030115-13	5	6.6	10.3	Positive	Positive	soil	eolian
H030115-14	5	7.2	11.1	Positive	Positive	soil	alluvium
TOTAL =	**60**	**8.1**	**20.8**				

The amphibole samples collected in the Highland Mountains Region have a wide range of compositions including sub-calcic, calcic, sodic, Fe-Mg, and sodic-calcic (Table 4.14). The mean aspect ratio for the 14 samples in the Highland Mountains region was 8.1 ± 0.5 (Table 4.14), the maximum aspect ratio was 20.8 (Table 4.14).

Amphibole particles with sodic, or sodic-calcic compositions are consistently found to have greater aspect ratios than those with a calcic, sub-calcic or Fe-Mg composition (Table 4.14). Fibers have a greater aspect ratio as compared to bundles or prismatic crystals (Table 4.15). SEM images are shown in Figures 4-35 to 4-37.

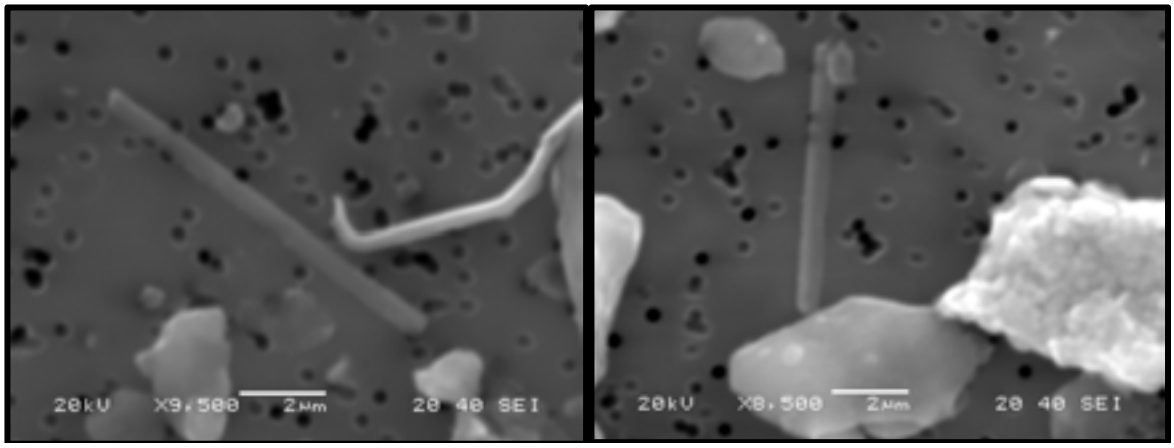

Figure 4-35. SEM images of sub-calcic amphibole fibers from sample H030115-1.

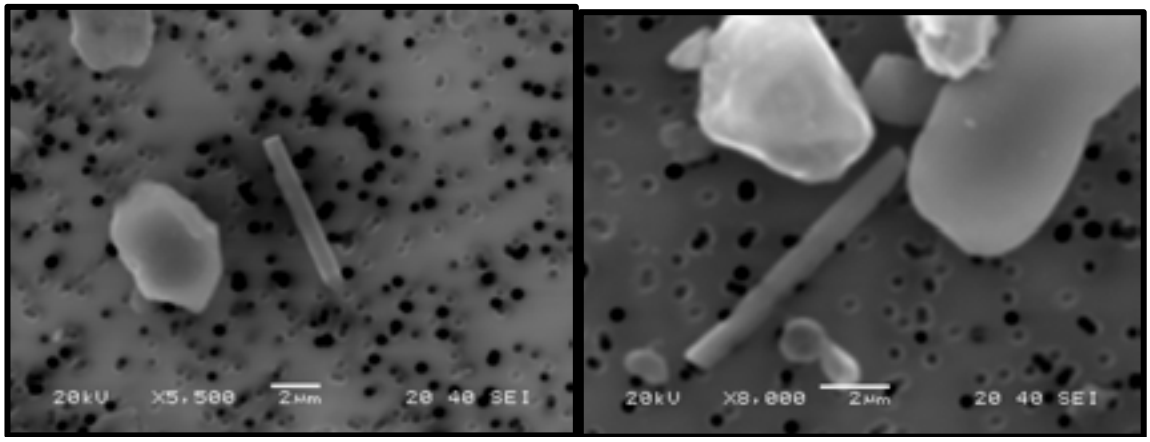

Figure 4-36. SEM images of sub-calcic amphibole fibers from sample H030115-3 (left), and H030115-6 (right).

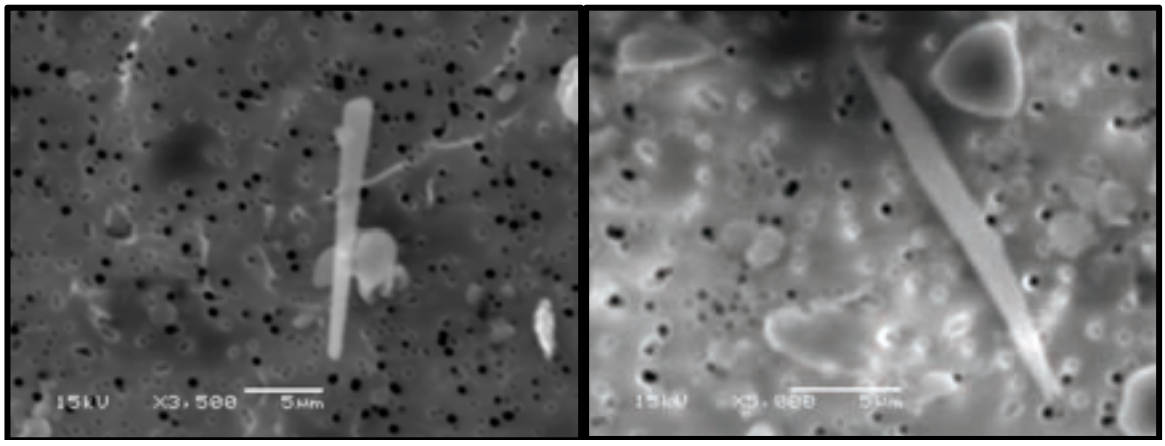

Figure 4-37. SEM image of magnesio-hornblende amphibole particle from sample H030115-14 (left), and edenite amphibole particle from sample H030115-12.

Table 4.14. Particle sizes and mineralogy results of amphibole particles in the Highland Mountains Region. Number of particles (N), standard error of the mean (S.E.)

Highland Mountains Region													
Mineralogy	**N**	**Minimum Width (µm)**	**Maximum Width (µm)**	**Mean Width (µm)**	**S.E.**	**Minimum Length (µm)**	**Maximum Length (µm)**	**Mean Length (µm)**	**S.E.**	**Minimum Aspect Ratio**	**Maximum Aspect Ratio**	**Mean Aspect Ratio**	**S.E.**
Actinolite	13	0.5	2.6	1.4	0.2	3.0	21.1	10.3	1.4	4.4	20.8	8.4	1.3
Edenite	3	0.9	3.8	2.1	0.9	13.6	22.6	18.1	2.6	5.9	15.1	11.0	2.7
Mg-hbld	10	0.6	1.7	1.2	0.1	3.2	16.7	7.5	1.5	3.5	11.1	6.1	0.9
Anthophyllite	1	2.5	2.5	2.5	-	7.4	7.4	7.4	-	3.0	3.0	3.0	-
Mag-rieb	1	0.8	0.8	0.8	-	9.2	9.2	9.2	-	11.5	11.5	11.5	-
Winchite	1	1.8	1.8	1.8	-	13.6	13.6	13.6	-	7.6	7.6	7.6	-
Calcic group	27	0.5	3.8	1.4	0.1	3.0	22.6	10.0	1.1	3.5	20.8	7.7	0.8
Sodic group	1	0.8	0.8	0.8	-	9.2	9.2	9.2	-	11.5	11.5	11.5	-
Sodic-Calcic group	2	1.8	3.9	2.9	1.1	13.6	76.1	44.9	31.3	7.6	19.5	13.5	6.0
Sub-Calcic group	28	0.4	2.2	1.1	0.1	4.0	13.7	7.9	0.5	3.4	15.2	8.2	0.6
Fe-Mg group	2	1.2	2.5	1.9	0.7	6.3	7.4	6.9	0.6	3.0	5.3	4.1	1.1
All Particles	**60**	**0.4**	**3.9**	**1.3**	**0.1**	**3.0**	**76.1**	**10.1**	**1.3**	**3.0**	**20.8**	**8.1**	**0.5**

Table 4.15. Morphology classification of particles analyzed in the Highland Mountains region. Number of particles (N), standard error of the mean (S.E.)

Highland Mountains Region													
Morphology	**N**	**Minimum Width (µm)**	**Maximum Width (µm)**	**Mean Width (µm)**	**S.E.**	**Minimum Length (µm)**	**Maximum Length (µm)**	**Mean Length (µm)**	**S.E.**	**Minimum Aspect Ratio**	**Maximum Aspect Ratio**	**Mean Aspect Ratio**	**S.E.**
Bundles	6	1.1	2.1	1.7	0.2	7.6	18.0	12.0	1.7	3.8	12.0	7.5	1.2
Fibers (≤1 µm)	23	0.4	1.0	0.7	0.0	3.0	13.6	7.3	0.6	4.4	20.8	10.2	0.8
Prismatic Crystals	31	1.1	3.9	1.7	0.1	4.7	76.1	11.8	2.3	3.0	19.5	6.5	0.6
All Particles	**60**	**0.4**	**3.9**	**1.3**	**0.1**	**3.0**	**76.1**	**10.1**	**1.3**	**3.0**	**20.8**	**8.1**	**0.5**

Ireteba Mountains Region

In this report, the Ireteba Mountains region refers primarily to samples collected from bedrock outcrops in the Ireteba Mountains area north and northeast of Searchlight NV (Figure 4-38). A total of 27 samples were obtained and analyzed (Table 4.16; Figures 4-39 to 4-45). All tested positive for amphibole asbestos with aspect ratio of 3:1, and all but one sample tested positive for NOA with aspect ratio of 8:1 (Table 4.16).

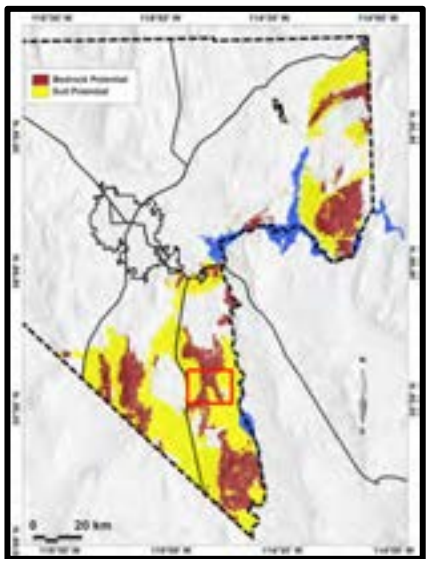

Figure 4-38. Map of southern Nevada showing predicted NOA-containing areas with the Ireteba Mountains region outlined in red box.

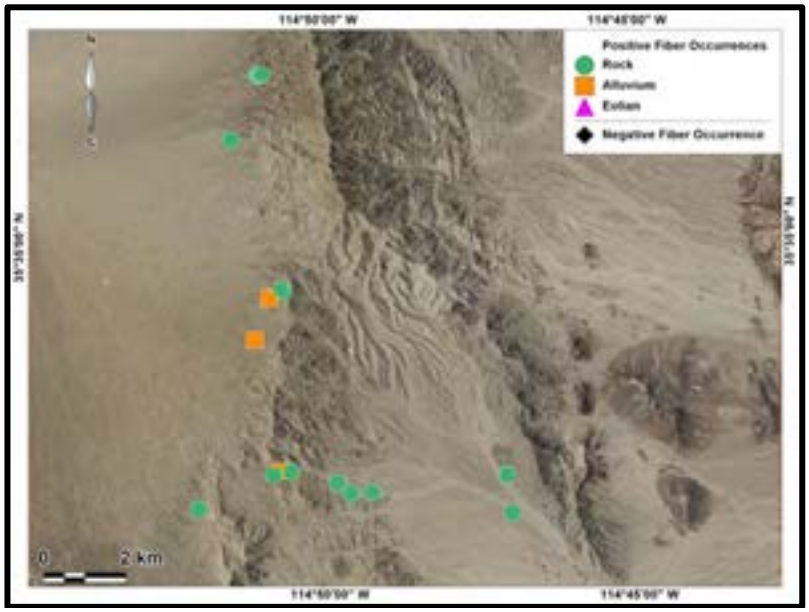

Figure 4-39. Map of Ireteba region sample locations. Positive occurrences are for amphibole asbestos with aspect ratios of 3:1 or greater. Samples are identified according to the geological process that deposited the material: bedrock (in place), alluvium (water-deposited), or eolian (wind-deposited).

Figure 4-40. Example of green amphibole (NOA) on fracture surface of rock in the Ireteba Mountains.

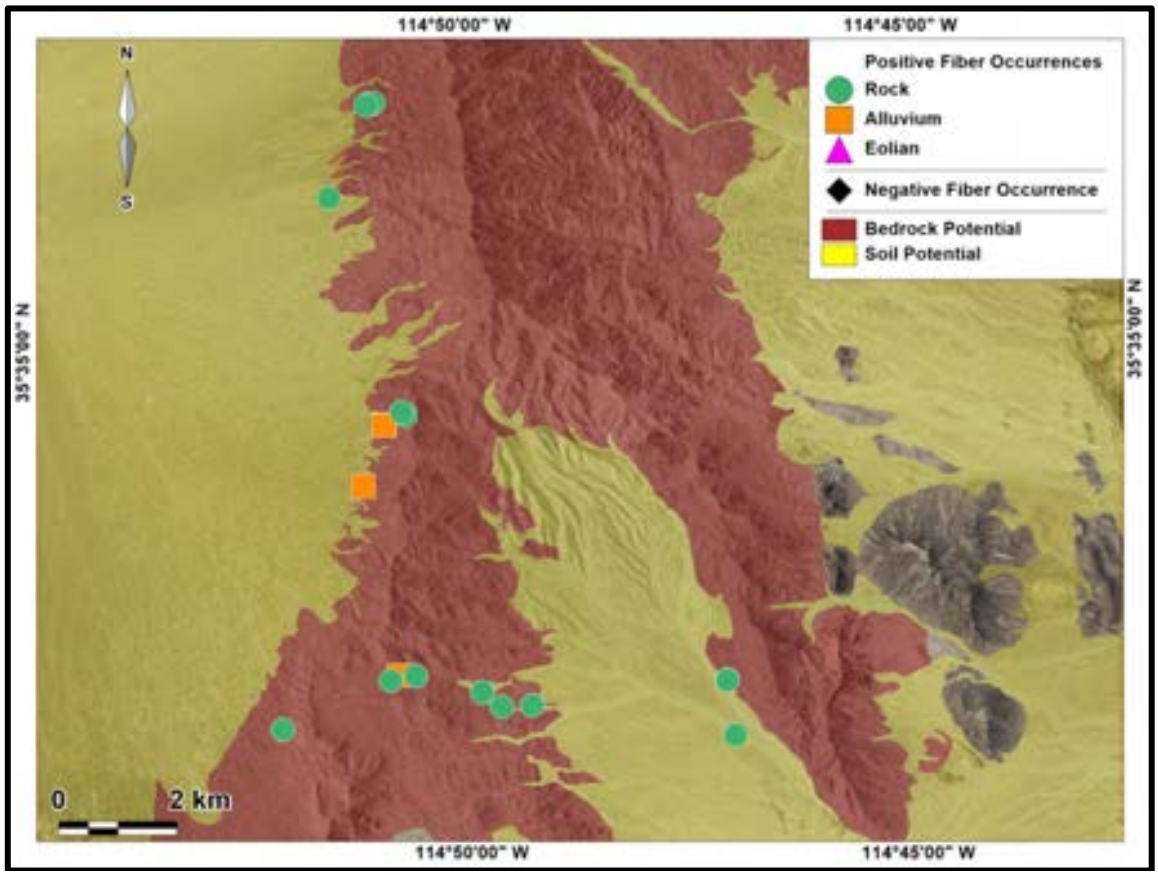

Figure 4-41. Map of sample locations in the Ireteba Mountains region with predicted occurrences of NOA based on alluvial (water-transported) surficial processes that transport material from the source rock out into the basin. Bedrock potential represents areas of potential occurrence for amphibole asbestos in igneous and metamorphic rock exposures. Soil potential delineates areas where runoff could potentially distribute amphibole asbestos fibers downslope from bedrock areas. Positive occurrences are for amphibole asbestos with aspect ratios of 3:1 or greater.

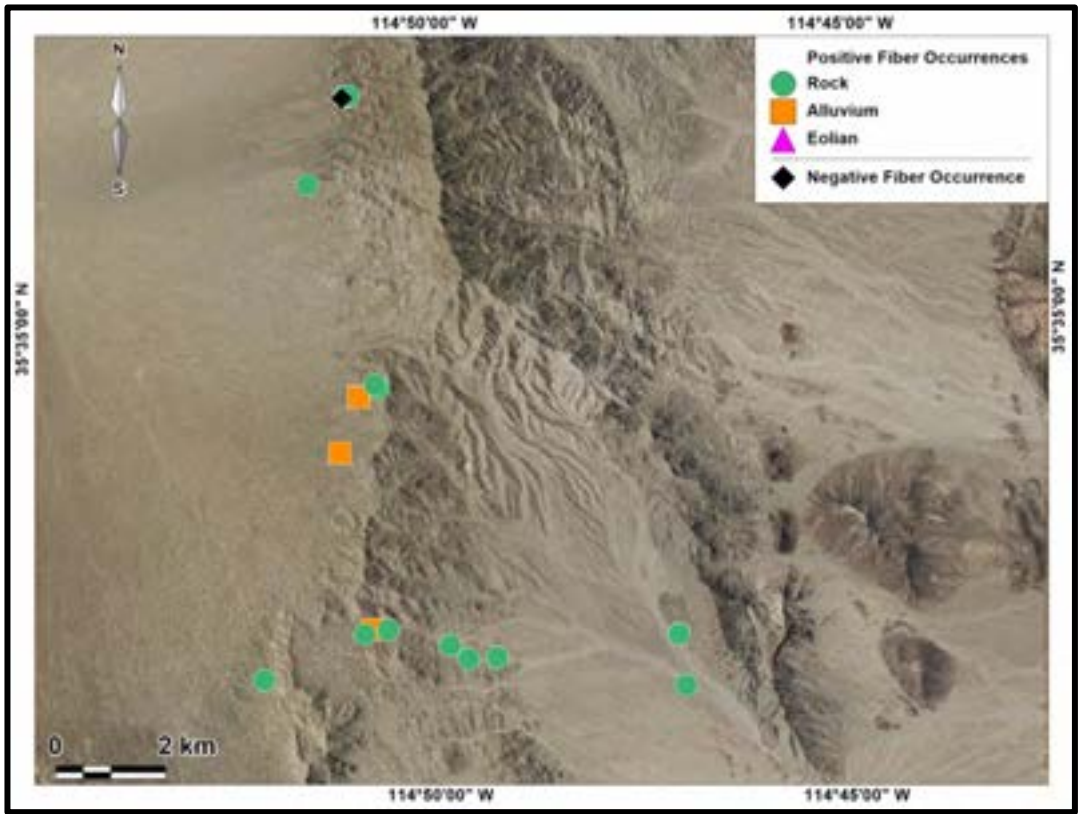

Figure 4-42. Map of Ireteba Mountains region sample locations. Positive occurrences are for amphibole asbestos with aspect ratios of 8:1 or greater. Samples are identified according to the geological process that deposited the material: bedrock (in place), alluvium (water-deposited), or eolian (wind-deposited).

Figure 4-43. Typical NOA-containing plutonic rock in the Ireteba Mountains Region.

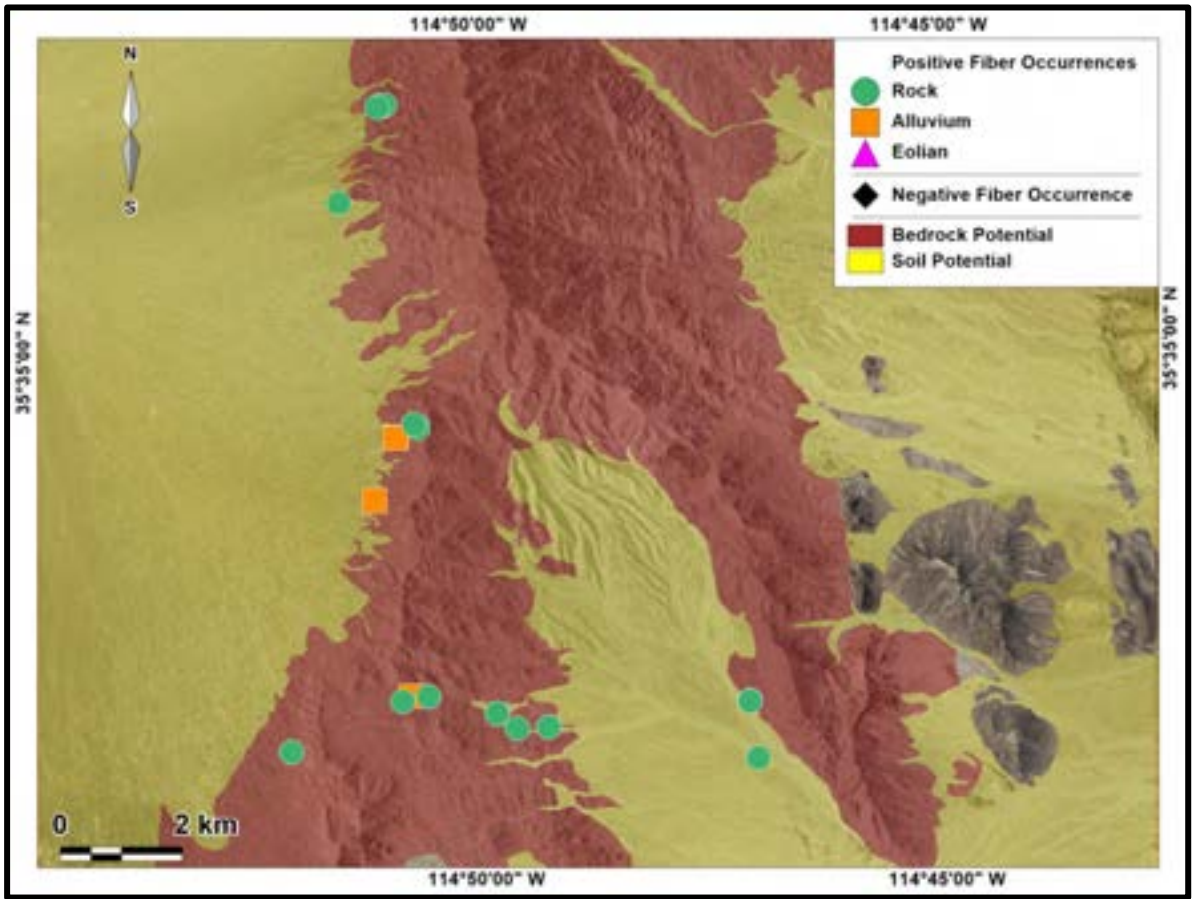

Figure 4-44. Map of sample locations in the Ireteba Mountains region with predicted occurrences of NOA based on alluvial (water-transported) surficial processes that transport material from the source rock out into the basin. Bedrock potential represents areas of potential occurrence for amphibole asbestos in igneous and metamorphic rock exposures. Soil potential delineates areas where runoff could potentially distribute amphibole asbestos fibers downslope from bedrock areas. Positive occurrences are for amphibole asbestos with aspect ratios of 8:1 or greater.

Figure 4-45. Typical NOA-containing metamorphic rocks in the Ireteba Mountains region

Table 4.16. Summary of sample type, depositional process, and mean and maximum aspect ratios for samples in the Ireteba Mountains Region.

IRETEBA MOUNTAINS							
Sample ID	**N**	**Mean Aspect Ratio**	**Maximum Aspect Ratio**	**Aspect Ratio Cutoff 8+**	**Aspect Ratio Cutoff 3+**	**Type**	**Depositional Process**
I020914-1	21	6.5	18.3	Positive	Positive	rock	rock
I020914-2	18	5.1	12.0	Positive	Positive	rock	rock
I020914-3	26	6.0	18.1	Positive	Positive	rock	alluvium
I020914-4	15	6.5	23.9	Positive	Positive	rock	rock
I020914-5	24	6.3	14.9	Positive	Positive	rock	rock
I020914-6	28	6.3	21.5	Positive	Positive	rock	rock
I020914-7	3	7.1	10.6	Positive	Positive	rock	rock
I020914-8	16	6.2	9.0	Positive	Positive	rock	rock
I020914-9	5	14.6	30.5	Positive	Positive	rock	rock
I020914-10	17	4.8	8.0	Positive	Positive	rock	rock
I020914-11	12	4.9	8.2	Positive	Positive	rock	rock
I020914-12	7	8.7	14.5	Positive	Positive	rock	rock
I020914-13	25	9.5	65.7	Positive	Positive	rock	rock
I020914-14	47	12.9	58.0	Positive	Positive	rock	rock
I020914-15	20	6.1	20.4	Positive	Positive	rock	rock
I-030114-11	9	7.0	9.6	Positive	Positive	soil	alluvium
I-030114-12	16	5.7	15.7	Positive	Positive	rock	alluvium
I-030114-13	38	5.3	11.1	Positive	Positive	rock	alluvium
I-030114-14	18	6.0	12.8	Positive	Positive	rock	rock
I-030114-15	1	9.1	9.1	Positive	Positive	rock	rock
I-030114-16	34	8.8	36.3	Positive	Positive	rock	rock
I-030114-17	29	7.4	26.1	Positive	Positive	rock	rock

Table 4.16 (continued). Summary of sample type, depositional process, and mean and maximum aspect ratios for samples in the Ireteba Mountains Region.

IRETEBA MOUNTAINS (continued)							
Sample ID	**N**	**Mean Aspect Ratio**	**Maximum Aspect Ratio**	**Aspect Ratio Cutoff 8+**	**Aspect Ratio Cutoff 3+**	**Type**	**Depositional Process**
I-030114-18	3	3.9	5.1	Negative	Positive	rock	rock
I-030114-19	54	7.3	22.0	Positive	Positive	rock	rock
I-030114-20	127	11.1	58.5	Positive	Positive	rock	rock
I-030114-21	71	8.8	38.9	Positive	Positive	rock	rock
I-030114-22	17	5.4	11.2	Positive	Positive	rock	rock
TOTAL =	**701**	**8.1**	**65.7**				

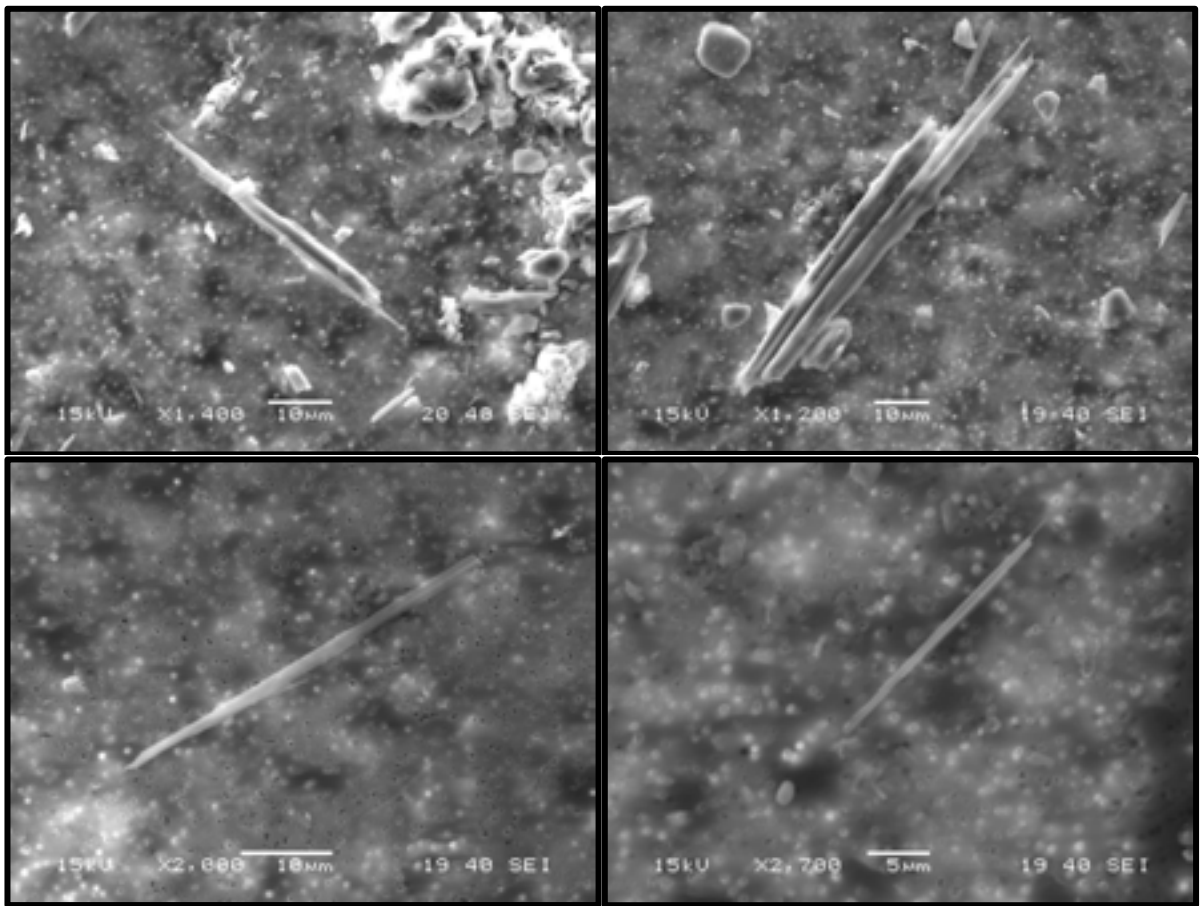

Figure 4-46. SEM images of actinolite amphibole bundles from sample I030114-20.

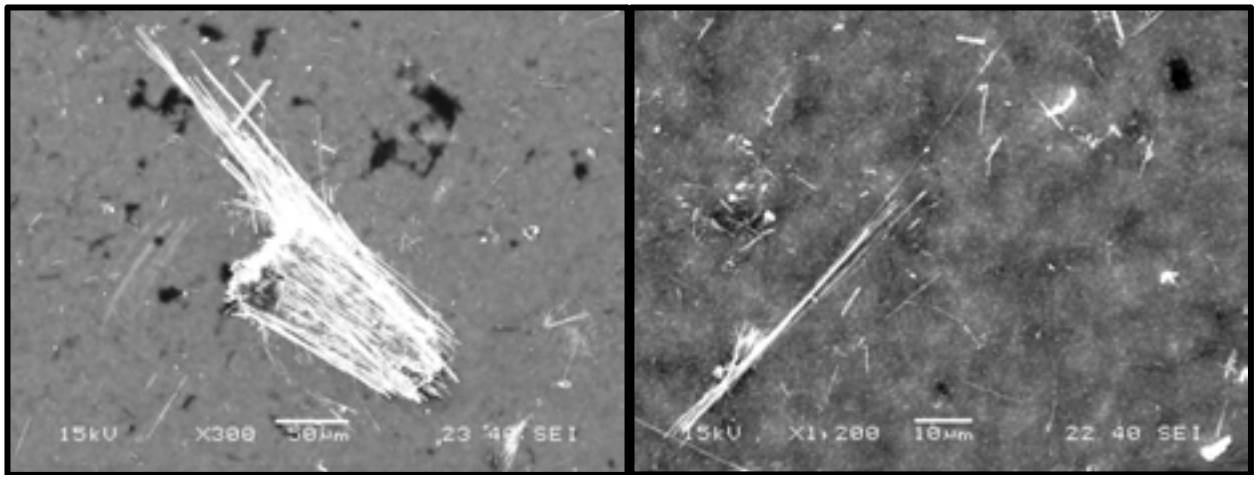

Figure 4-47. SEM images of numerous amphibole fibers and bundles from sample I030114-14.

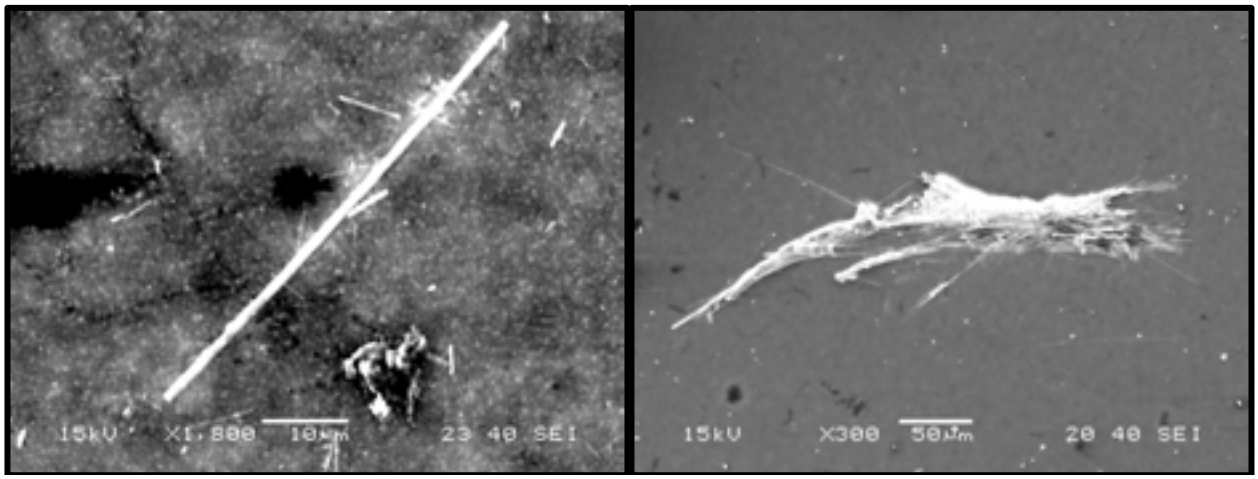

Figure 4-48. SEM image of magnesio-hornblende amphibole fibers from sample I030114-14 (left) and magnesio-riebeckite amphibole bundle from sample I020914-9 (right).

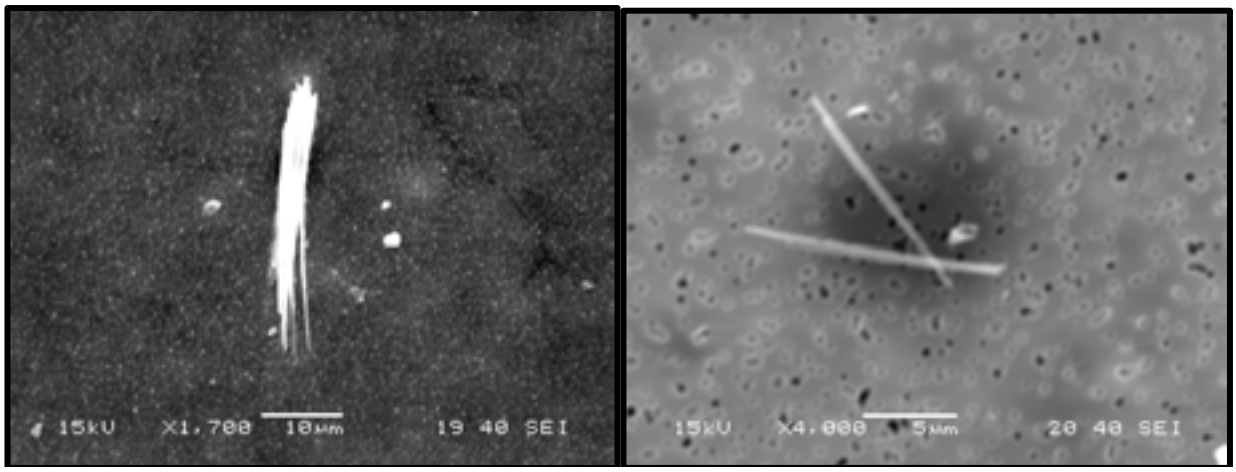

Figure 4-49. SEM image of winchite amphibole bundle from sample I020914-9 (left) and two winchite amphibole fibers from sample I030114-16 (right).

Figure 4-50. SEM image of actinolite amphibole particle from sample I030114-16 (left) and upper horizontal particle on right is a winchite amphibole bundle from sample I030114-16.

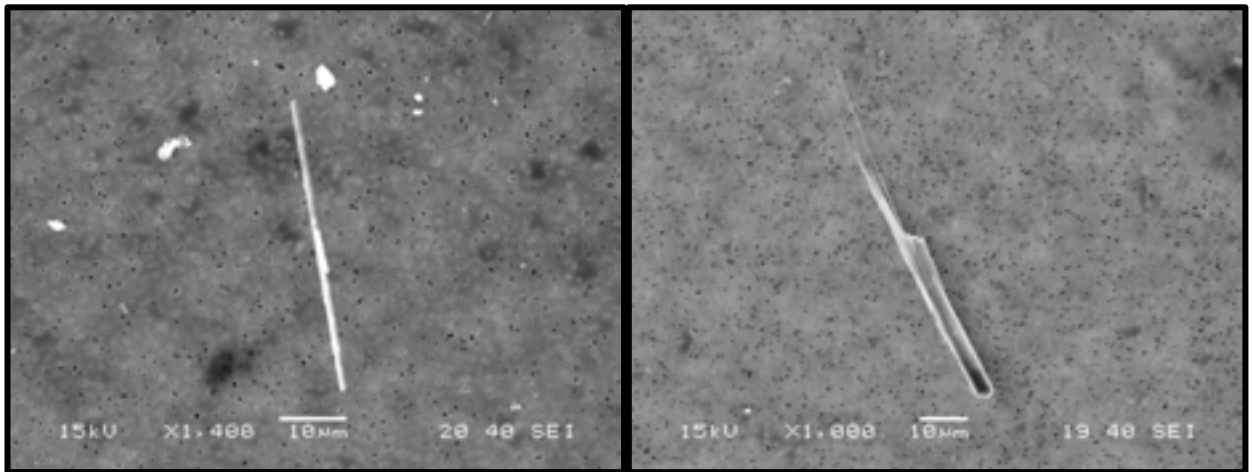

Figure 4-51. SEM image of winchite amphibole particle from sample I030114-16 (left) and sodic amphibole bundle from sample I030114-17 (right).

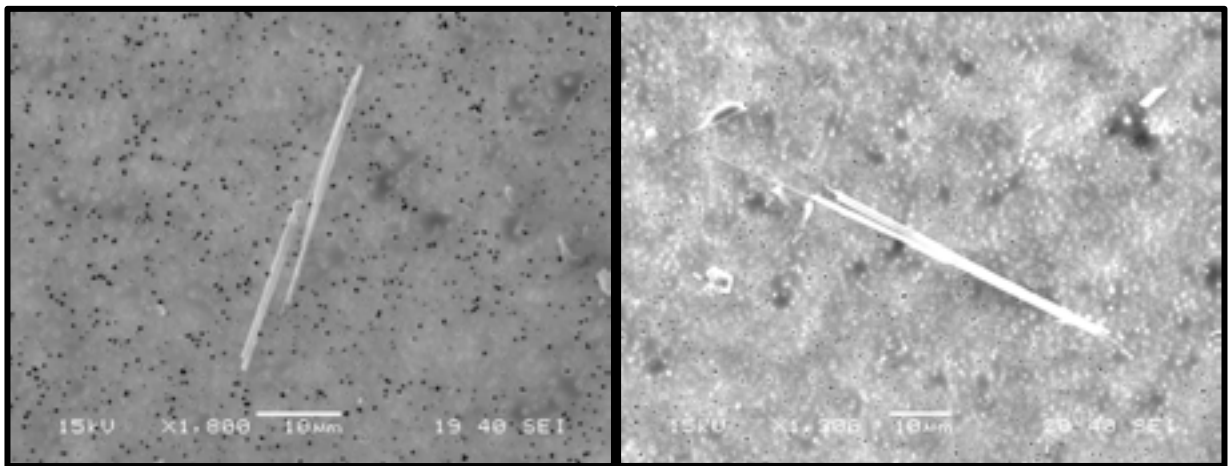

Figure 4-52. SEM image of sodic-calcic amphibole bundles from sample I030114-17 (left) and actinolite amphibole bundle from sample I030114-20 (right).

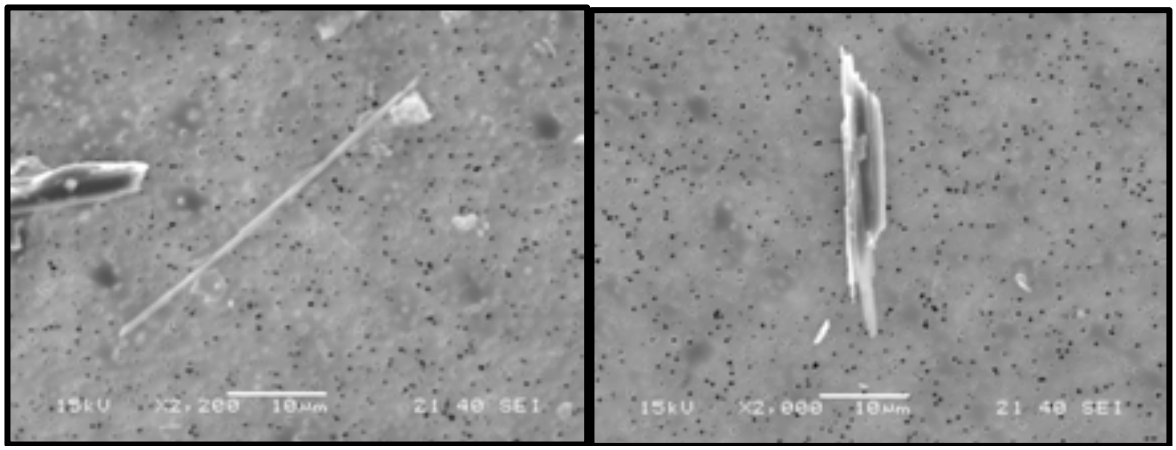

Figure 4-53. SEM image of actinolite amphibole fiber from sample I020914-13 (left) and actinolite amphibole bundle from sample I030114-13 (right).

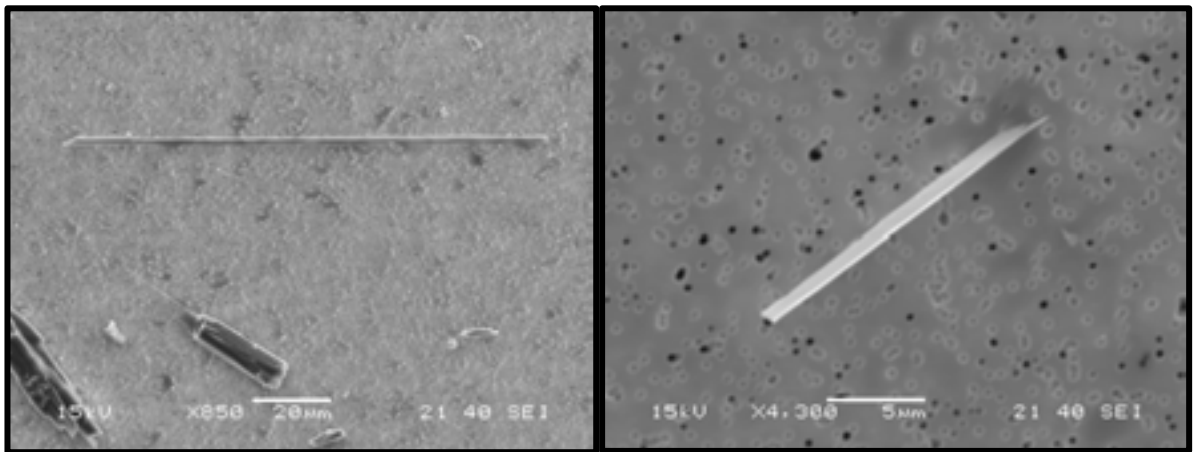

Figure 4-54. SEM image of several actinolite amphibole particles from sample I030114-20 (left) and actinolite amphibole fiber from sample I030114-19 (right).

The amphibole samples collected in the Ireteba Mountains Region have a wide range of compositions including sub-calcic, calcic, sodic, and sodic-calcic (Table 4.17). Consistent with other data in this study, amphibole particles with sodic, or sodic-calcic compositions are found to have greater aspect ratios than those with a calcic or sub-calcic composition (Table 4.17). As discussed in Metcalf and Buck (2015), the composition of the amphibole minerals depends upon the processes operating at the time these crystals formed or were hydrothermally altered. Much more detailed work is needed in this area to understand their distribution and genesis (see Chapter 3).

The mean aspect ratio for the 27 samples in the Ireteba Mountains region was 8.1 ± 0.3 (Table 4.17), the maximum aspect ratio was 65.7 (Table 4.17). Bundles had a greater aspect ratio as compared to fibers and prismatic crystals given the definition of fibers used in this study (Table 4.18). SEM images are shown in Figures 4-46 to 4-54. Additional field photos shown in Figures 4-55, 4-56.

Table 4.17. Particle sizes and mineralogy results of amphibole particles in the Ireteba Mountains Region. Number of particles (N), standard error of the mean (S.E.)

Ireteba Mountains Region													
Mineralogy	**N**	**Minimum Width (µm)**	**Maximum Width (µm)**	**Mean Width (µm)**	**S.E.**	**Minimum Length (µm)**	**Maximum Length (µm)**	**Mean Length (µm)**	**S.E.**	**Minimum Aspect Ratio**	**Maximum Aspect Ratio**	**Mean Aspect Ratio**	**S.E.**
Actinolite	372	0.1	19.7	1.7	0.1	0.8	312.3	14.9	1.5	3.0	65.7	8.1	0.4
Edenite	2	1.5	1.8	1.7	0.2	5.4	12.5	9.0	3.6	3.6	6.9	5.3	1.7
Mg-hbld	220	0.2	13.2	1.4	0.1	1.1	49.1	7.7	0.4	3.0	20.2	6.1	0.2
Pargasite	1	1.7	1.7	1.7	-	6.4	6.4	6.4	-	3.8	3.8	3.8	-
Tschermakite	2	0.8	1.2	1.0	0.2	6.1	7.3	6.7	0.6	5.1	9.1	7.1	2.0
Mag-rieb	15	0.2	57.0	6.9	4.1	1.6	372.6	66.0	30.6	5.9	58.0	20.9	4.3
Winchite	30	0.1	16.2	1.7	0.5	1.3	172.2	21.8	6.1	3.3	47.6	15.0	1.9
Ferro-anthophyllite	1	2.8	2.8	2.8	-	40.5	40.5	40.5	-	14.5	14.5	14.5	-
Calcic group	599	0.1	19.7	1.6	0.1	0.8	312.3	12.3	1.0	3.0	65.7	7.3	0.3
Sodic group	17	0.2	57.0	6.5	3.7	1.6	372.6	66.8	26.9	5.9	58.0	21.2	3.8
Sodic-Calcic group	25	0.1	16.2	1.8	0.6	1.3	172.2	22.6	7.2	3.3	47.6	13.9	2.0
Sub-Calcic group	60	0.3	4.5	1.0	0.1	1.1	88.9	10.9	2.0	3.1	36.3	9.6	1.0
All Particles	**701**	**0.1**	**57.0**	**1.7**	**0.1**	**0.8**	**372.6**	**13.8**	**1.1**	**3.0**	**65.7**	**8.1**	**0.3**

Table 4.18. Morphology classification of particles analyzed in the Ireteba Mountains region. Number of particles (N), standard error of the mean (S.E.)

Ireteba Mountains Region													
Morphology	**N**	**Minimum Width (µm)**	**Maximum Width (µm)**	**Mean Width (µm)**	**S.E.**	**Minimum Length (µm)**	**Maximum Length (µm)**	**Mean Length (µm)**	**S.E.**	**Minimum Aspect Ratio**	**Maximum Aspect Ratio**	**Mean Aspect Ratio**	**S.E.**
Bundles	155	1.1	57.0	3.3	0.5	3.8	372.6	35.9	4.4	3.1	58.5	11.7	0.7
Fibers (≤1 µm)	337	0.1	1.0	0.6	0.0	0.8	39.4	4.9	0.2	3.0	65.7	7.9	0.4
Prismatic Crystals	209	1.1	17.3	2.1	0.1	3.4	157.7	11.9	1.0	3.0	49.0	5.8	0.4
All Particles	**701**	**0.1**	**57.0**	**1.7**	**0.1**	**0.8**	**372.6**	**13.8**	**1.1**	**3.0**	**65.7**	**8.1**	**0.3**

Figure 4-55. Photo of outcrop of sample I030114-19 showing very typical NOA-containing plutonic rock.

Figure 4-56. Green asbestos crystals from sample I030114-21 as seen in the field, with large sharpie pen for scale.

Jean-Primm Region

The Jean-Primm region refers primarily to the Ivanpah valley west of the McCullough Range and south of Las Vegas to the Nevada/California border (Figure 4-57). A total of 28 samples, primarily from soil or road/playa surfaces were obtained and analyzed (Table 4.19; Figures 4-58 to 4-64). Of these 28 samples, all tested positive for amphibole asbestos with aspect ratios greater than 3:1 except one sample near Goodsprings (G021715-3); and all tested positive for amphibole asbestos with an aspect ratio of 8:1 or higher except for 7 samples including one near Goodsprings, (G021715-3) and two at the north end of this region (J021715-1, and J021715-2) (Figures 4-59 to 4-65).

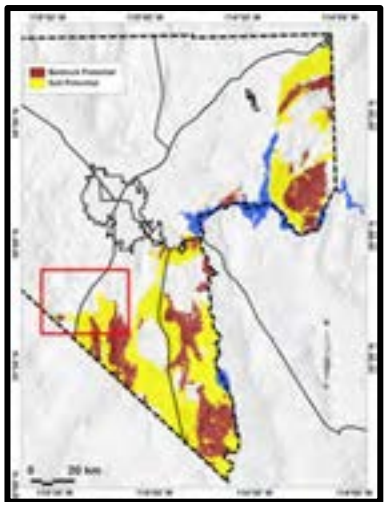

Figure 4-57. Map of southern Nevada showing predicted NOA-containing areas with the Jean-Primm region outlined in red box.

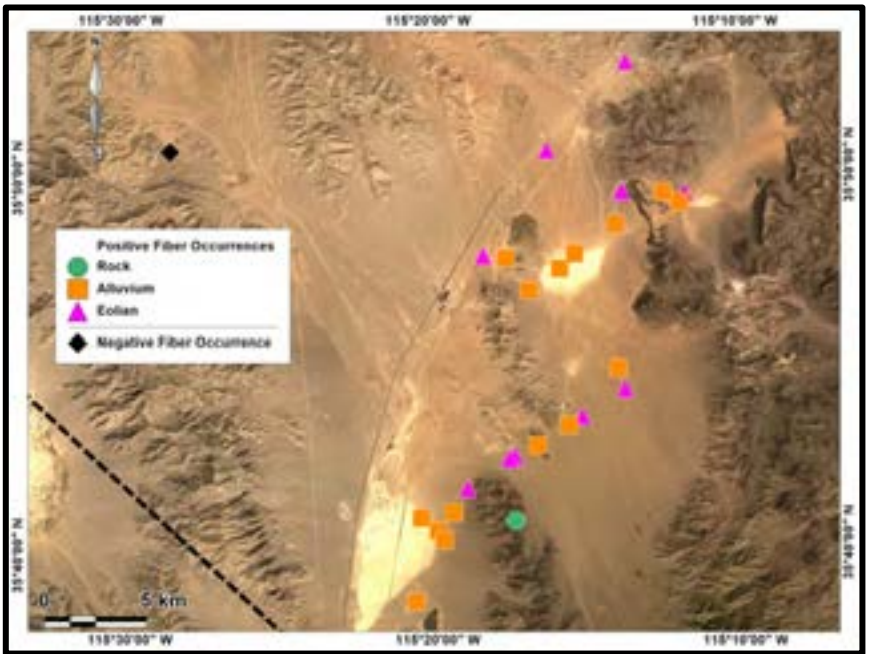

Figure 4-58. Map of Jean-Primm region sample locations. Positive occurrences are for amphibole asbestos with aspect ratios of 3:1 or greater. Samples are identified according to the geological process that deposited the material: bedrock (in place), alluvium (water-deposited), or eolian (wind-deposited).

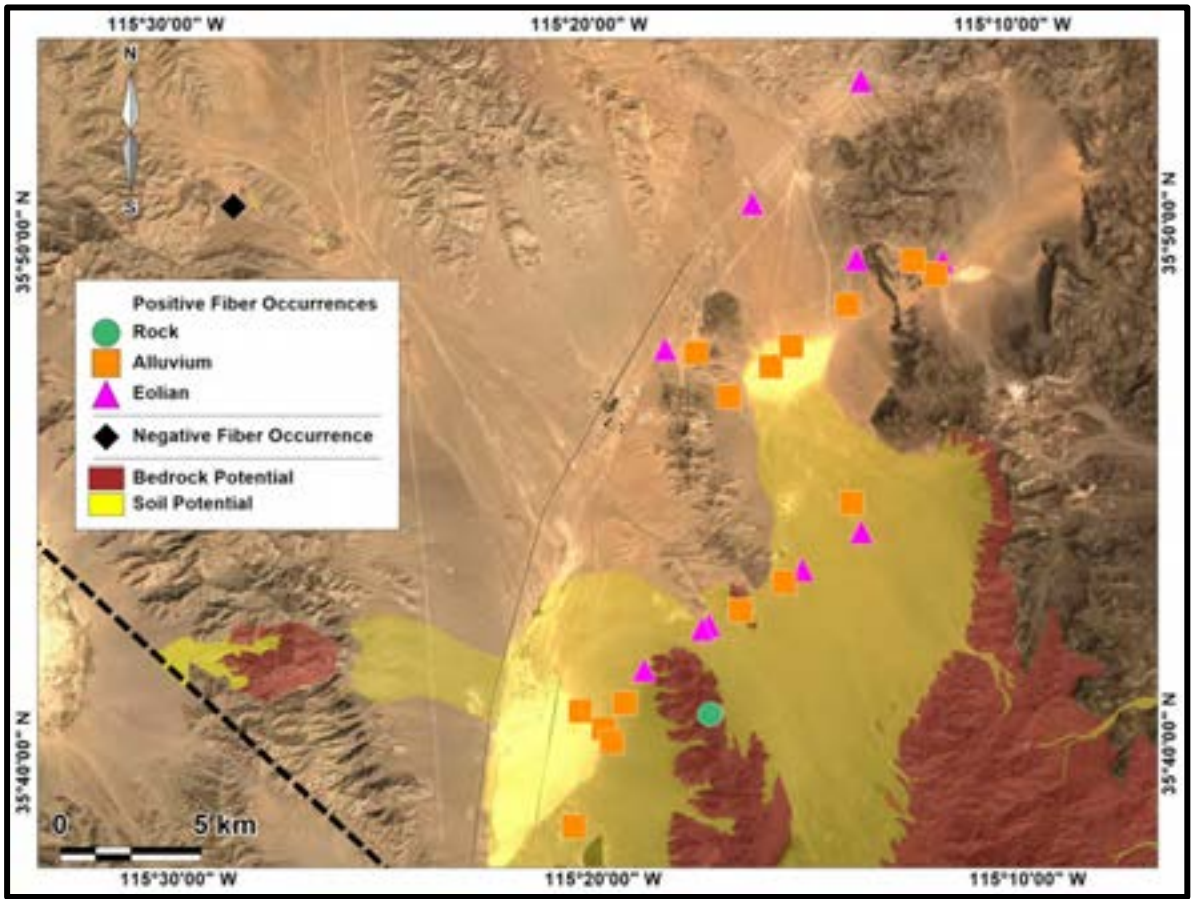

Figure 4-59. Map of sample locations in the Jean-Primm region with predicted occurrences of NOA based on alluvial (water-transported) surficial processes that transport material from the source rock out into the basin. Bedrock potential represents areas of potential occurrence for amphibole asbestos in igneous and metamorphic rock exposures. Soil potential delineates areas where runoff could potentially distribute amphibole asbestos fibers downslope from bedrock areas. Positive occurrences are for amphibole asbestos with aspect ratios of 3:1 or greater.

Figure 4-60. Anthropogenically disturbed area near site of Gayle 2, south of Jean Playa. View to the northwest with the Jean dry lake (playa) in the background.

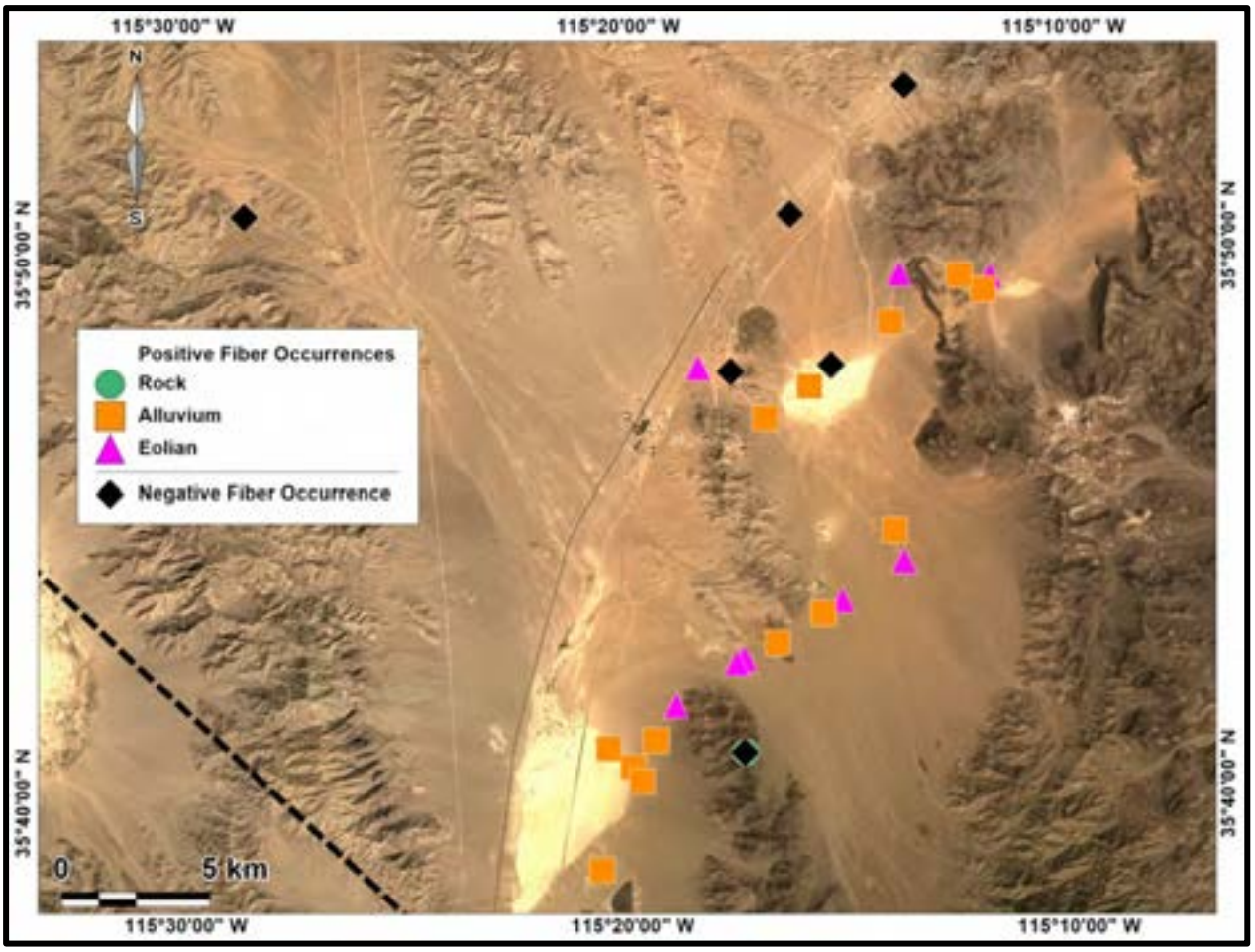

Figure 4-61. Map of Jean-Primm region sample locations. Positive occurrences are for amphibole asbestos with aspect ratios of 8:1 or greater. Samples are identified according to the geological process that deposited the material: bedrock (in place), alluvium (water-deposited), or eolian (wind-deposited).

Figure 4-62. Photo of Jean dry lake bed (playa), view to the north.

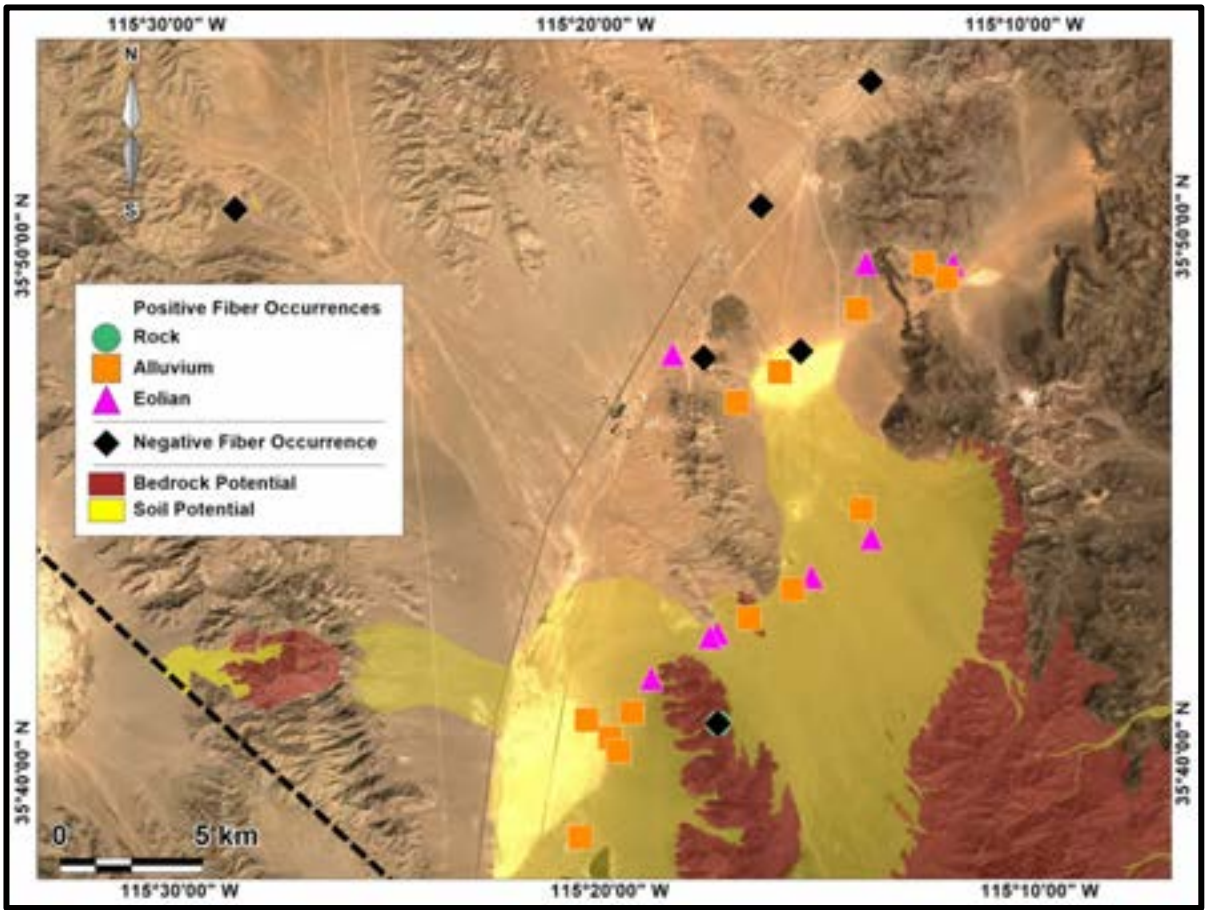

Figure 4-63. Map of sample locations in the Jean-Primm region with predicted occurrences of NOA based on alluvial (water-transported) surficial processes that transport material from the source rock out into the basin. Bedrock potential represents areas of potential occurrence for amphibole asbestos in igneous and metamorphic rock exposures. Soil potential delineates areas where runoff could potentially distribute amphibole asbestos fibers downslope from bedrock areas. Positive occurrences are for amphibole asbestos with aspect ratios of 8:1 or greater.

Figure 4-64. Photo of biologic soil crusts in Jean-Primm region. Biologic soil crusts trap dust, but when disturbed, the underlying dust (in vesicular horizons) can be released. If the dust contains asbestos fibers, people can become exposed through inhalation.

Table 4.19. Summary of sample type, depositional process, and mean and maximum aspect ratios for samples in the Jean-Primm Region.

JEAN-PRIMM							
Sample ID	**N**	**Mean Aspect Ratio**	**Maximum Aspect Ratio**	**Aspect Ratio Cutoff 8+**	**Aspect Ratio Cutoff 3+**	**Type**	**Depositional Process**
Gayle 1	4	12.0	21.0	Positive	Positive	soil	alluvium
Gayle 2	4	15.0	31.4	Positive	Positive	soil	alluvium
Gayle 3	3	7.7	8.7	Positive	Positive	soil	eolian
Gayle 4	1	7.4	7.4	Negative	Positive	soil	alluvium
Gayle 5	2	28.0	33.3	Positive	Positive	soil	alluvium
J020615-1	3	5.3	6.8	Negative	Positive	soil	eolian
J020615-3	4	9.2	13.6	Positive	Positive	soil	road (alluvium)
J020615-4	4	6.9	14.8	Positive	Positive	soil	road (alluvium)
J020615-5	3	20.9	44.7	Positive	Positive	soil	eolian
J020615-6	2	7.1	9.8	Positive	Positive	soil	road (alluvium)
J020615-7	4	8.6	13.2	Positive	Positive	soil	alluvium
J020615-8	3	6.4	8.5	Positive	Positive	soil	eolian
J020615-9	6	4.9	10.2	Positive	Positive	soil	eolian
J020615-10	10	5.1	8.3	Positive	Positive	soil	alluvium
J020615-11	5	14.7	22.4	Positive	Positive	soil	alluvium
J020615-12	2	10.5	12.7	Positive	Positive	soil	eolian

Table 4.19 (continued). Summary of sample type, depositional process, and mean and maximum aspect ratios for samples in the Jean-Primm Region.

JEAN-PRIMM (continued)							
Sample ID	**N**	**Mean Aspect Ratio**	**Maximum Aspect Ratio**	**Aspect Ratio Cutoff 8+**	**Aspect Ratio Cutoff 3+**	**Type**	**Depositional Process**
J020615-13	7	7.8	18.7	Positive	Positive	soil	eolian
J020615-14	3	7.4	9.5	Positive	Positive	soil	eolian
J020615-15	5	7.6	9.0	Positive	Positive	soil	alluvium
J020615-16	9	8.8	12.9	Positive	Positive	soil	alluvium
J020615-17	5	12.2	21.2	Positive	Positive	soil	alluvium
J020615-18	9	15.1	25.3	Positive	Positive	soil	road (alluvium)
J021715-1	4	5.5	7.3	Negative	Positive	soil	eolian
J021715-2	2	5.0	5.4	Negative	Positive	soil	alluvium
J021715-3	8	6.3	9.7	Positive	Positive	soil	eolian
G021715-3	0	NA	NA	Negative	Negative	rock	rock
L1	9	9.0	15.2	Positive	Positive	rock	rock
L2	21	4.4	7.7	Negative	Positive	rock	rock
TOTAL =	**142**	**8.6**	**44.7**				

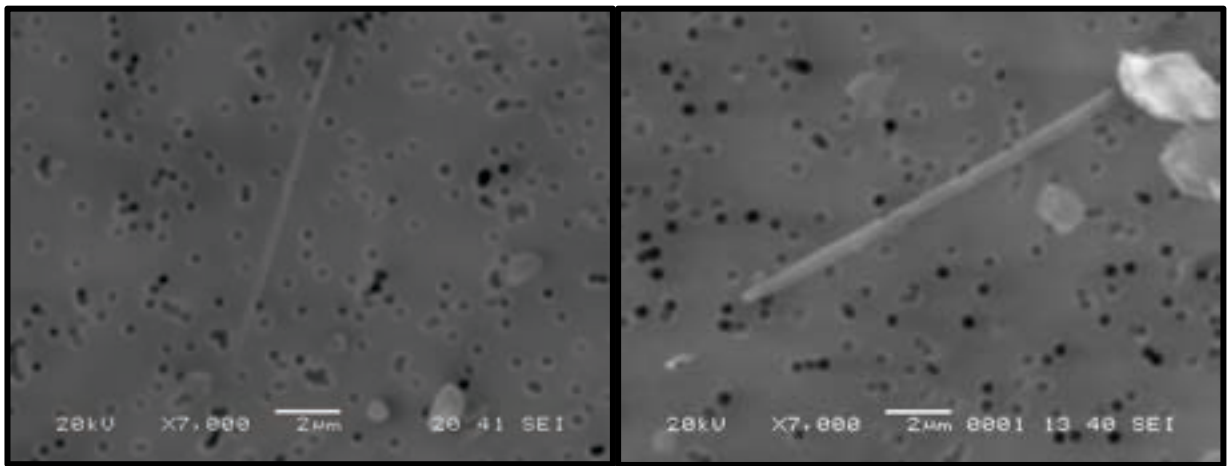

Figure 4-65. SEM image of sodic-calcic group amphibole fiber from sample Gayle #5 (Roach Playa, north of Primm, left), and sodic-calcic amphibole fiber from sample J020615-17 (right).

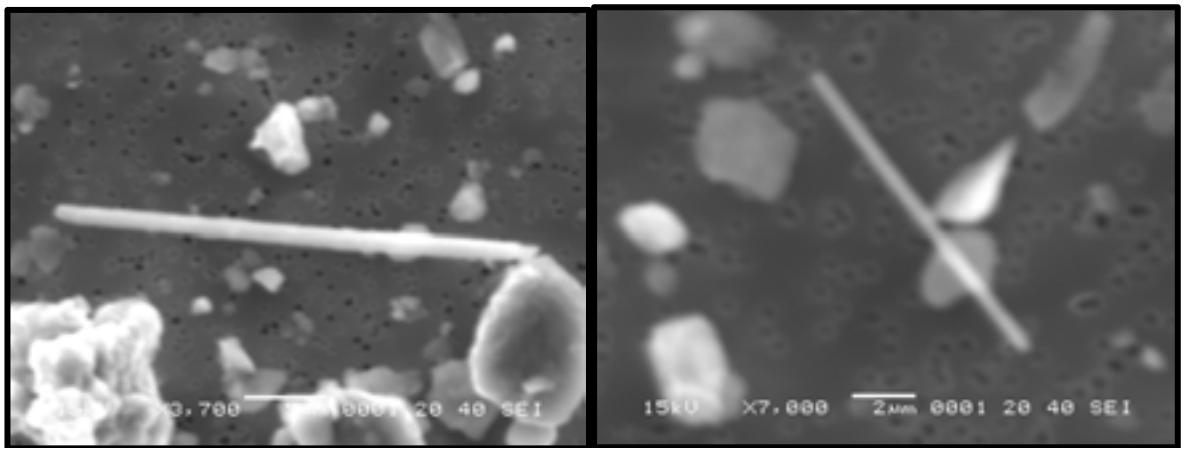

Figure 4-66. SEM image of magnesio-hornblende fibers from sample J020615-11.

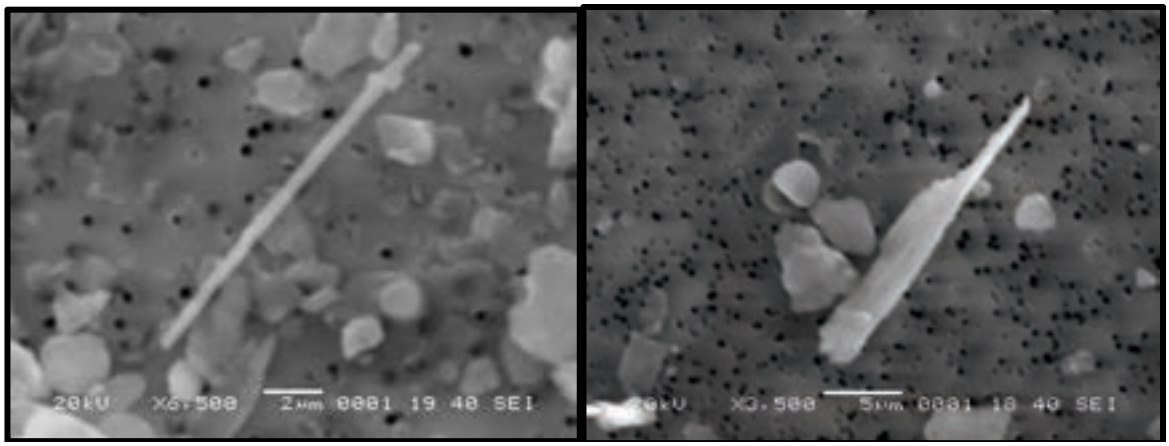

Figure 4-67. SEM image of sodic-calcic amphibole fiber from sample J020615-18 (left) and a sub-calcic amphibole bundle from sample J020615-15 (right).

The amphibole samples collected in the Jean-Primm Region have a wide range of compositions including sub-calcic, calcic, sodic, and sodic-calcic (Table 4.20). Consistent with other data in this study, amphibole particles with sodic, or sodic-calcic compositions are consistently found to have greater aspect ratios than those with a calcic or sub-calcic composition (Table 4.20). The mean aspect ratio for the 28 samples in the Jean-Primm region was 8.6 ± 0.5 (Table 4.20), the maximum aspect ratio was 44.7 (Table 4.20). Fibers have a greater aspect ratio as compared to the other morphologies (Table 4.21). SEM images shown in Figures 4-65 to 4-67. Field images are shown in Figures 4-68 to 4-72.

Much of the NOA in this region is likely derived through a combination of processes including alluvial processes that erode/transport/deposit the NOA from their bedrock sources in the Lucy Gray Mountains and the McCullough Range, as well as eolian processes that transport NOA through dust erosion/deposition. Wind directions in this

region can vary greatly, and can occur from any direction (Goossens et al., 2011). Therefore, especially through eolian deposition, the original source(s) of the NOA particles analyzed in these samples could have originated in numerous different areas and could even be from quite distant sources. The closest known sources would include the NOA found in this study in southern Nevada (Buck et al., 2013; Metcalf and Buck, 2015), the Mountain Pass area of southern California (Castor, 2008), and Death Valley, California (Van Gosen et al., 2004). Other, more distant, known asbestos sources are documented in Van Gosen 2008, and Van Gosen and Clinkenbeard (2011).

Dust contamination probably best explains the 4 alluvial sites which tested positive for NOA yet lie outside of our mapped soil potential footprint (Figure 4-59 and 4-63). This is especially likely for this region because of the numerous playas that are present and this area is heavily used for off-road vehicle recreation, which also increased eolian erosion.

Figure 4-68. Photo of major dirt roads used in off-road vehicle racing and by local recreationists in this area. Sample J020615-6 was collected from this road.

Figure 4-69. Photo of early Holocene to latest Pleistocene geomorphic surface from which sample J021715-1 was collected (unit Qay_1 from House et al., 2010b). The sample is from the vesicular horizon that directly underlies the single-layer of stones at the surface, called a desert pavement. The vesicular horizon is an eolian (wind-blown) deposit.

Table 4.20. Particle sizes and mineralogy results of amphibole particles in the Jean-Primm Region. Number of particles (N), standard error of the mean (S.E.)

Jean-Primm Region													
Mineralogy	**N**	**Minimum Width (µm)**	**Maximum Width (µm)**	**Mean Width (µm)**	**S.E.**	**Minimum Length (µm)**	**Maximum Length (µm)**	**Mean Length (µm)**	**S.E.**	**Minimum Aspect Ratio**	**Maximum Aspect Ratio**	**Mean Aspect Ratio**	**S.E.**
Actinolite	22	0.2	2.7	1.2	0.1	2.3	18.3	9.2	0.8	3.2	16.6	8.0	0.7
Mg-hbld	53	0.4	14.0	2.0	0.3	2.2	108.2	12.3	2.2	3.1	44.7	7.1	0.9
Mg-rieb	2	1.6	1.7	1.7	0.0	17.9	20.6	19.3	1.4	10.5	12.9	11.7	1.2
Richterite	1	1.1	1.1	1.1	-	11.2	11.2	11.2	-	10.2	10.2	10.2	-
Winchite	2	0.5	1.2	0.9	0.4	5.6	13.8	9.7	4.1	11.2	11.5	11.4	0.2
Sodic group	6	0.5	1.7	1.2	0.2	4.9	20.6	12.9	2.5	9.5	12.9	10.9	0.6
Sodic-Calcic group	20	0.3	2.3	0.9	0.1	3.5	32.9	11.9	1.8	4.7	33.3	14.4	1.7
Sub-Calcic group	41	0.4	2.3	1.1	0.1	2.2	20.8	7.7	0.7	3.3	31.4	7.7	0.7
Calcic group	75	0.2	14.0	1.8	0.2	2.2	108.2	11.4	1.6	3.1	44.7	7.4	0.7
Barrosite	2	1.7	2.3	2.0	0.3	10.7	27.2	19.0	8.3	6.3	11.8	9.1	2.8
All Particles	**142**	**0.2**	**14.0**	**1.4**	**0.1**	**2.2**	**108.2**	**10.5**	**0.9**	**3.1**	**44.7**	**8.6**	**0.5**

Table 4.21. Morphology classification of particles analyzed in the Jean-Primm region. Number of particles (N), standard error of the mean (S.E.)

Jean-Primm Region													
Morphology	**N**	**Minimum Width (µm)**	**Maximum Width (µm)**	**Mean Width (µm)**	**S.E.**	**Minimum Length (µm)**	**Maximum Length (µm)**	**Mean Length (µm)**	**S.E.**	**Minimum Aspect Ratio**	**Maximum Aspect Ratio**	**Mean Aspect Ratio**	**S.E.**
Bundles	13	1.3	8.8	2.2	0.6	7.8	42.2	15.2	2.8	4.6	15.8	7.4	0.8
Fibers (≤1 µm)	62	0.2	1.0	0.7	0.0	2.2	31.3	6.8	0.6	3.6	44.7	10.2	1.0
Prismatic Crystals	67	1.1	14.0	1.9	0.2	3.6	108.2	12.9	1.7	3.1	25.3	7.4	0.6
All Particles	**142**	**0.2**	**14.0**	**1.4**	**0.1**	**2.2**	**108.2**	**10.5**	**0.9**	**3.1**	**44.7**	**8.6**	**0.5**

Figure 4-70. Sample J020615-5, vesicular horizon (eolian deposit) collected from this desert pavement.

Figure 4-71. Dust generated through natural wind from the surface of the Primm dry lake bed (Roach Playa). View to the southwest.

Figure 4-72. Area near the site of Gayle 3, showing one vehicle driving on dirt road, with associated dust emissions.

Las Vegas Region

The Las Vegas region refers primarily to the Las Vegas valley region (Figure 4-73). A total of 19 samples, primarily from surficial vesicular soil horizons were obtained and analyzed (Table 4.22). Of these 19 samples, all tested positive for amphibole asbestos with aspect ratio of 3:1 except 4 samples, and more than half tested positive for amphibole asbestos with an aspect ratio of 8:1 or higher (Table 4.22; Figures 4-74 to 4-80).

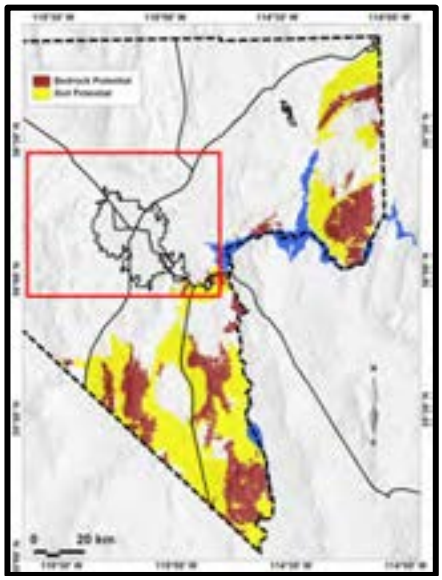

Figure 4-73. Map of southern Nevada showing predicted NOA-containing areas with the Las Vegas region outlined in red box.

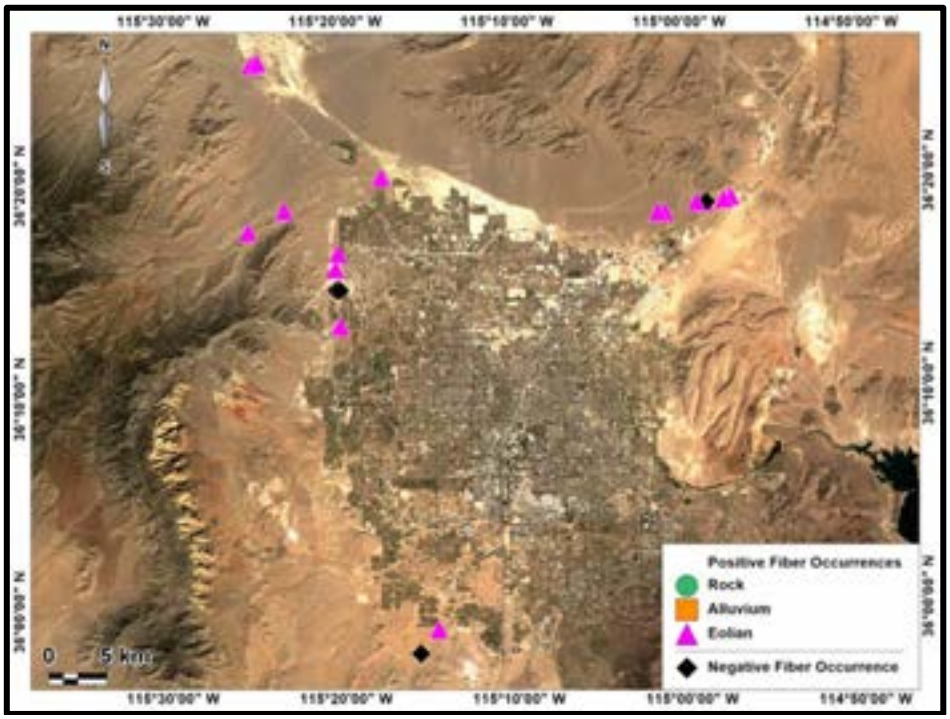

Figure 4-74. Map of Las Vegas region sample locations. Positive occurrences are for amphibole asbestos with aspect ratios of 3:1 or greater. Samples are identified according to the geological process that deposited the material: bedrock (in place), alluvium (water-deposited), or eolian (wind-deposited).

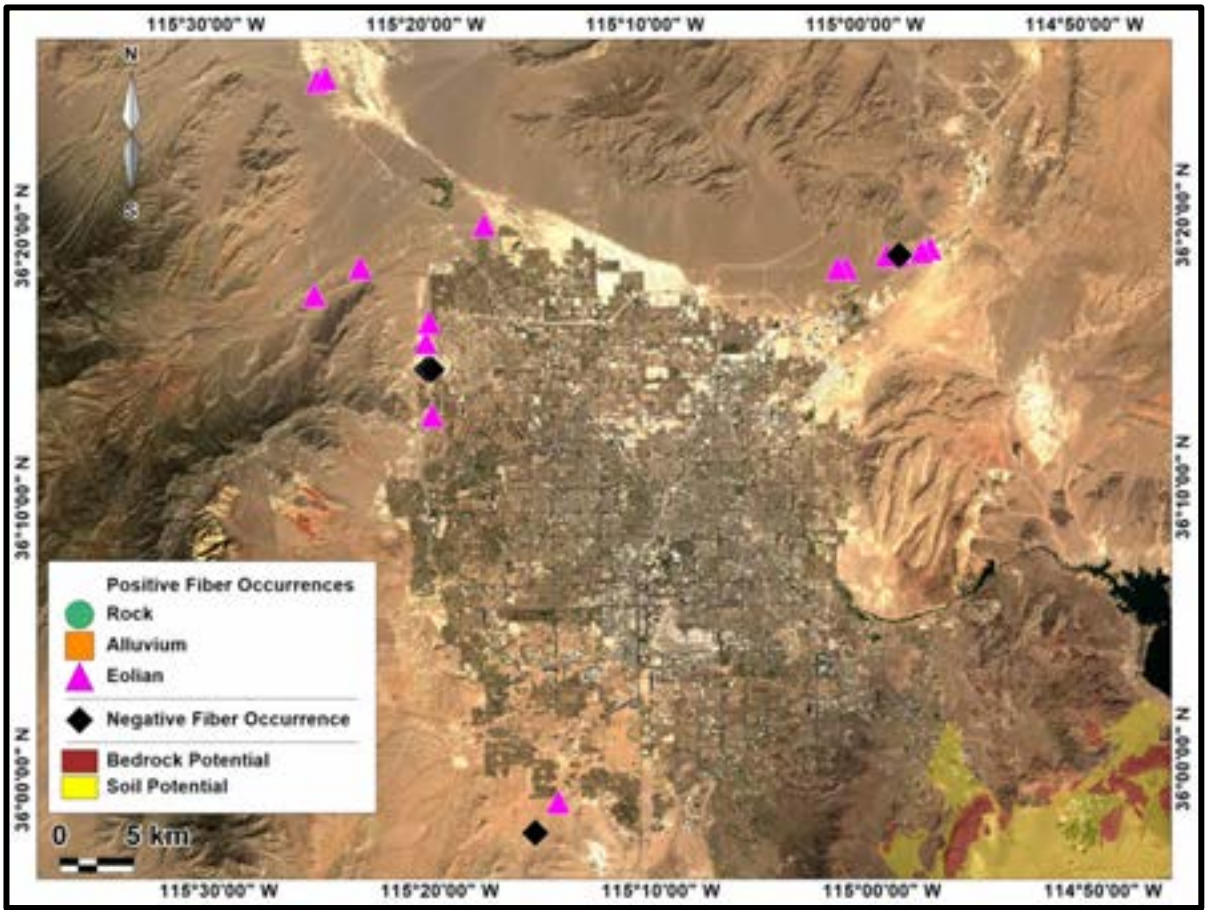

Figure 4-75. Map of sample locations in the Las Vegas region with predicted occurrences of NOA based on alluvial (water-transported) surficial processes that transport material from the source rock out into the basin. Bedrock potential represents areas of potential occurrence for amphibole asbestos in igneous and metamorphic rock exposures. Soil potential delineates areas where runoff could potentially distribute amphibole asbestos fibers downslope from bedrock areas. Positive occurrences are for amphibole asbestos with aspect ratios of 3:1 or greater.

Figure 4-76. Desert pavement from which the underlying vesicular horizon (eolian) was sampled for LV021615-10.

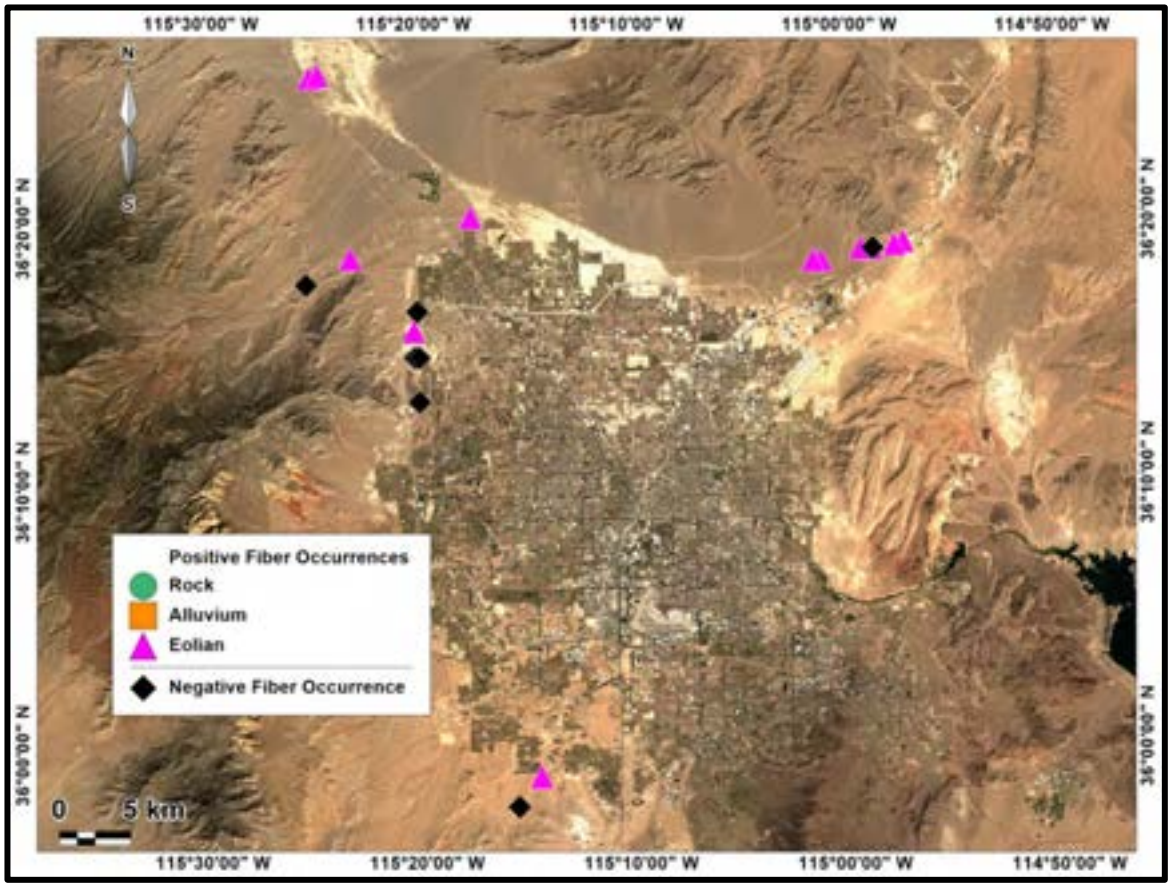

Figure 4-77. Map of Las Vegas region sample locations. Positive occurrences are for amphibole asbestos with aspect ratios of 8:1 or greater. Samples are identified according to the geological process that deposited the material: bedrock (in place), alluvium (water-deposited), or eolian (wind-deposited).

Figure 4-78. Photo of area and desert pavement from which sample LV021615-11, vesicular horizon (eolian), was collected.

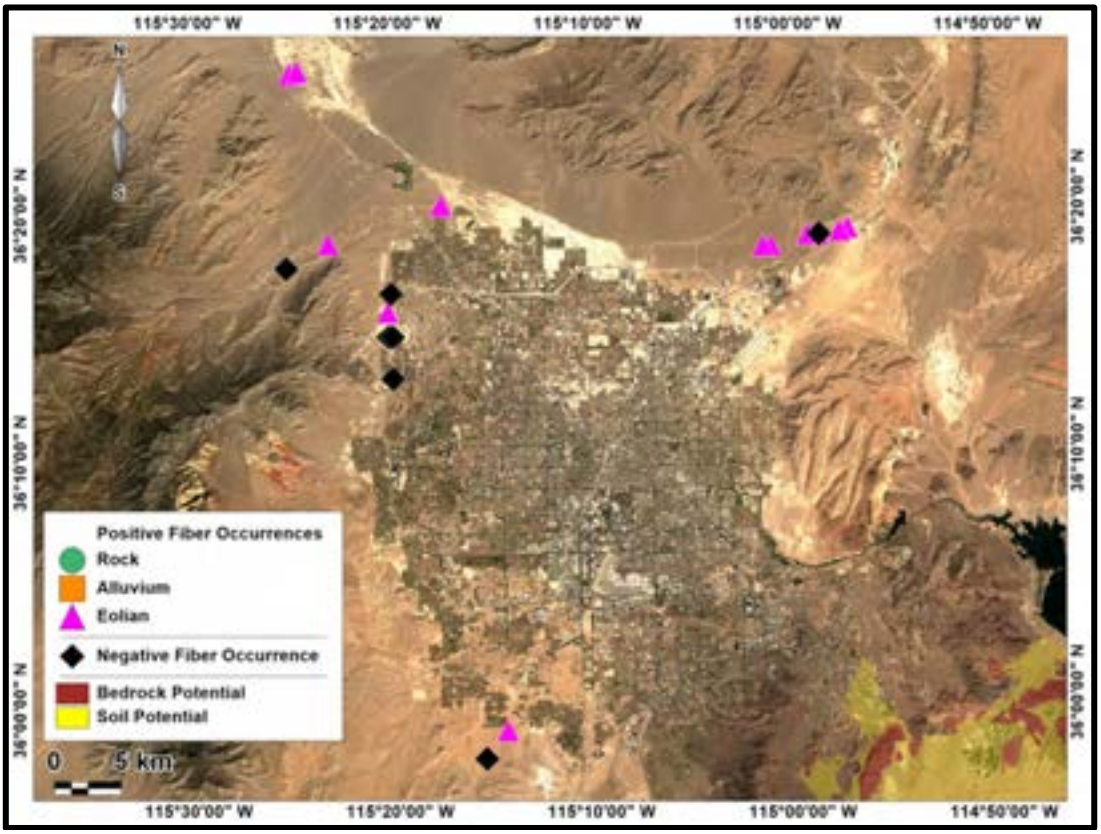

Figure 4-79. Map of sample locations in the Las Vegas region with predicted occurrences of NOA based on alluvial (water-transported) surficial processes that transport material from the source rock out into the basin. Bedrock potential represents areas of potential occurrence for amphibole asbestos in igneous and metamorphic rock exposures. Soil potential delineates areas where runoff could potentially distribute amphibole asbestos fibers downslope from bedrock areas. Positive occurrences are for amphibole asbestos with aspect ratios of 8:1 or greater.

Figure 4-80. View of area from which sample LV021615-7 was collected (vesicular horizon, eolian deposit).

Table 4.22. Summary of sample type, depositional process, and mean and maximum aspect ratios for samples in the Las Vegas Region.

LAS VEGAS							
Sample ID	**N**	**Mean Aspect Ratio**	**Maximum Aspect Ratio**	**Aspect Ratio Cutoff 8+**	**Aspect Ratio Cutoff 3+**	**Type**	**Depositional Process**
LV021615-1	2	7.1	7.8	Negative	Positive	Soil	eolian
LV021615-2	0	NA	NA	Negative	Negative	Soil	eolian
LV021615-3	0	NA	NA	Negative	Negative	Soil	eolian
LV021615-4	2	9.1	10.6	Positive	Positive	Soil	eolian
LV021615-5	2	6.6	7.4	Negative	Positive	Soil	eolian
LV021615-6	2	6.1	7.0	Negative	Positive	Soil	eolian
LV021615-7	5	5.6	9.4	Positive	Positive	Soil	eolian
LV021615-9	8	7.9	9.9	Postive	Positive	Soil	eolian
LV021615-10	10	5.9	8.5	Positive	Positive	Soil	eolian
LV021615-11	4	6.1	9.1	Postitive	Positive	Soil	eolian
LV022715-12	2	7.3	10.3	Postitive	Positive	Soil	eolian
LV022715-13	3	7.3	8.0	Positive	Positive	Soil	eolian
LV022715-14	2	8.7	10.5	Positive	Positive	Soil	eolian
LV022715-15	0	NA	NA	Negative	Negative	rock	rock
LV022715-16	6	6.9	8.4	Positive	Positive	Soil	eolian
LV022715-17	9	8.2	16.9	Positive	Positive	Soil	eolian
LV022715-18	2	9.0	12.0	Positive	Positive	Soil	eolian
LV040315-1	3	8.6	11.0	Positive	Positive	Soil	eolian
LV040315-2	0	NA	NA	Negative	Negative	Soil	eolian
TOTAL =	**62**	**7.2**	**16.9**				

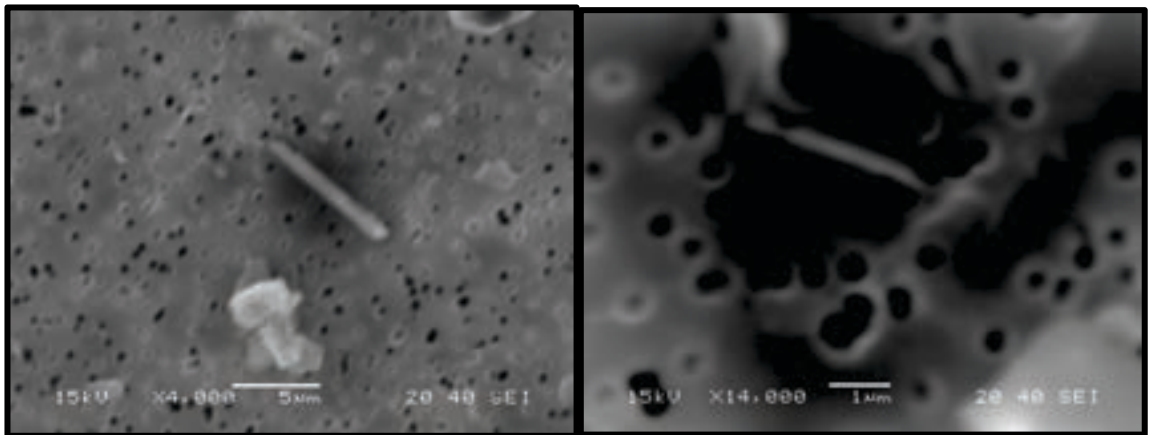

Figure 4-81. SEM image of actinolite fiber from sample LV021615_6 (left) and sub-calcic fiber from sample LV022715-12 (right)

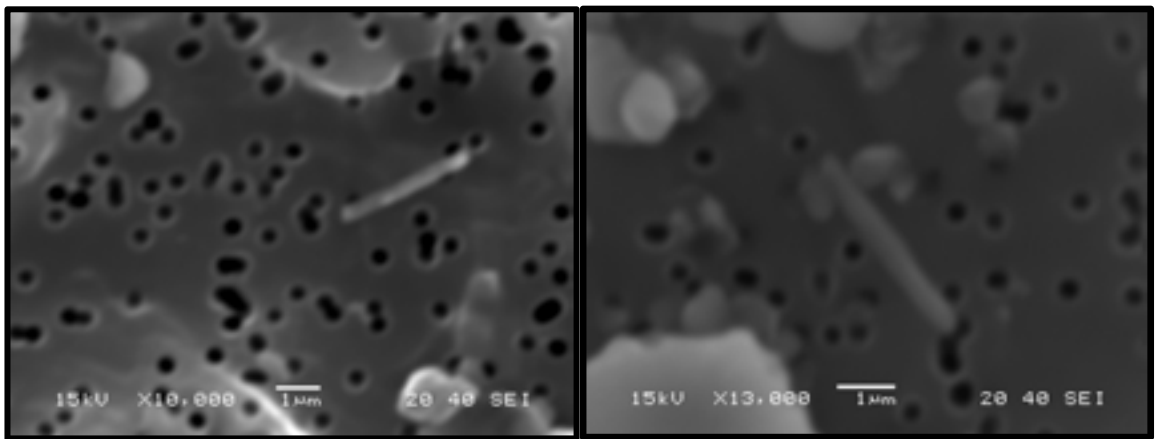

Figure 4-82. SEM image of magnesio-hornblende fiber from sample LV021615_7 (left) and sub-calcic fiber from sample LV021615_5 (right).

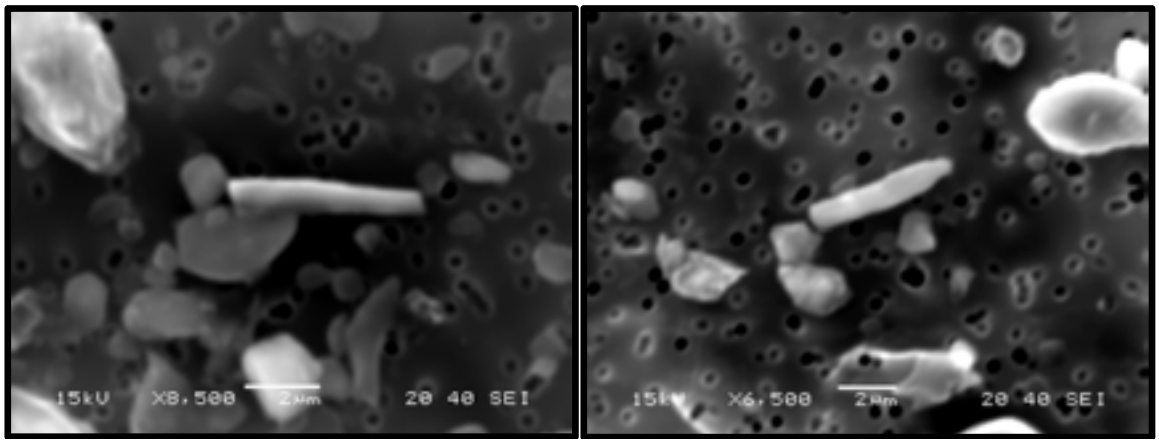

Figure 4-83. SEM image of sub-calcic fibers from sample LV021615_5 (left), and from sample LV021615_10 (right)

The amphibole samples collected in the Las Vegas Region have a wide range of compositions including sub-calcic, calcic, sodic, and sodic-calcic (Table 4.23; Figures 4-81 to 4-83).

Most of the samples collected in this region were collected from surface vesicular soil horizons which are deposits of wind-derived dust (e.g., McFadden et al., 1987; Wells et al., 1995; McFadden et al., 1998; Turk and Graham 2011). Wind directions in this region can vary greatly, and can occur from any direction (Goossens et al., 2011). Therefore, through eolian deposition, the original source(s) of the NOA particles analyzed in these samples could have originated in numerous different areas and could even be from quite distant sources. The closest known sources would include the NOA found in this study in southern Nevada (Figure 4-3) (Buck et al., 2013; Metcalf and Buck, 2015), the Mountain Pass area of southern California (Van Gosen, 2007), and Death Valley, California (Van Gosen et al., 2004). Other, more distant, known asbestos sources are documented in Van Gosen 2008, and Van Gosen and Clinkenbeard (2011).

The mean aspect ratio for the 19 samples in the Las Vegas region was 7.2 ± 0.3 (Table 4.23), the maximum aspect ratio was 16.9 (Table 4.23). Bundles were found to have the greatest mean aspect ratio (Table 4.24).

Table 4.23. Particle sizes and mineralogy results of amphibole particles in the Las Vegas Region. Number of particles (N), standard error of the mean (S.E.)

Las Vegas Region													
Mineralogy	**N**	**Minimum Width (µm)**	**Maximum Width (µm)**	**Mean Width (µm)**	**S.E.**	**Minimum Length (µm)**	**Maximum Length (µm)**	**Mean Length (µm)**	**S.E.**	**Minimum Aspect Ratio**	**Maximum Aspect Ratio**	**Mean Aspect Ratio**	**S.E.**
Arfvedsonite	1	2.8	2.8	2.8	-	33.0	33.0	33.0	-	11.8	11.8	11.8	-
Actinolite	15	0.7	3.5	1.7	0.2	2.3	23.7	10.9	1.4	3.3	10.5	6.4	0.5
Mg-hbld	11	0.4	3.4	1.6	0.3	2.8	20.3	11.8	1.7	4.6	12.0	7.5	0.7
Mg-rieb	2	0.6	0.7	0.7	0.1	3.0	6.4	4.7	1.7	5.0	9.1	7.1	2.1
Winchite	2	0.8	0.9	0.9	0.1	5.1	13.5	9.3	4.2	5.7	16.9	11.3	5.6
Sodic goup	6	0.6	2.8	1.6	0.4	3.0	33.0	13.1	4.4	5.0	11.8	7.8	1.1
Sodic-Calcic group	2	0.8	0.9	0.9	0.1	5.1	13.5	9.3	4.2	5.7	16.9	11.3	5.6
Sub-Calcic group	25	0.3	2.7	1.0	0.1	2.3	17.7	7.1	0.9	3.8	11.0	6.9	0.4
Calcic group	29	0.4	3.5	1.6	0.1	2.3	23.7	11.1	1.0	3.3	12.0	7.0	0.4
Anthophyllite	5	1.0	2.7	1.5	0.3	9.2	17.5	12.3	1.5	6.5	11.0	8.7	0.7
Mg-Katophorite	2	1.2	1.5	1.4	0.1	8.0	13.2	10.6	2.6	6.7	8.8	7.7	1.1
Richerite	1	2.7	2.7	2.7	-	14.8	14.8	14.8	-	5.5	5.5	5.5	-
Edenite	3	0.8	1.8	1.3	0.3	7.9	10.8	9.8	0.9	6.0	9.9	7.8	1.1
All Particles	**62**	**0.3**	**3.5**	**1.3**	**0.1**	**2.3**	**33.0**	**9.6**	**0.2**	**3.3**	**16.9**	**7.2**	**0.3**

Table 4.24. Morphology classification of particles analyzed in the Las Vegas region. Number of particles (N), standard error of the mean (S.E.)

Las Vegas Region													
Morphology	**N**	**Minimum Width (µm)**	**Maximum Width (µm)**	**Mean Width (µm)**	**S.E.**	**Minimum Length (µm)**	**Maximum Length (µm)**	**Mean Length (µm)**	**S.E.**	**Minimum Aspect Ratio**	**Maximum Aspect Ratio**	**Mean Aspect Ratio**	**S.E.**
Bundle	3	1.1	1.5	1.2	0.1	9.2	13.2	11.3	1.2	8.4	10.5	9.2	0.6
Fibers (≤1 µm)	25	0.3	1.0	0.7	0.0	2.3	13.5	4.7	0.5	3.3	16.9	6.8	0.6
Prismatic Crystals	34	1.1	3.5	1.8	0.1	5.0	33.0	13.1	0.9	3.6	12.0	7.3	0.3
All Particles	**62**	**0.3**	**3.5**	**1.3**	**0.1**	**2.3**	**33.0**	**9.6**	**0.8**	**3.3**	**16.9**	**7.2**	**0.3**

Laughlin Region

The Laughlin region refers primarily to the area on the Nevada side of the Colorado River near Laughlin (Figure 4-84). A total of 24 samples, collected from a mixture of surface soil horizons and bedrock, were obtained and analyzed (Table 4.25). Of these 24 samples, all tested positive for amphibole asbestos with aspect ratio of 3:1 except 1 sample (M021215-13) (Figures 4-85 to 4-86), and all but 3 tested positive for amphibole asbestos with an aspect ratio of 8:1 or higher (Figures 4-88, 4-90). Field photos shown in Figures 4-88, 4-89, 4-91.

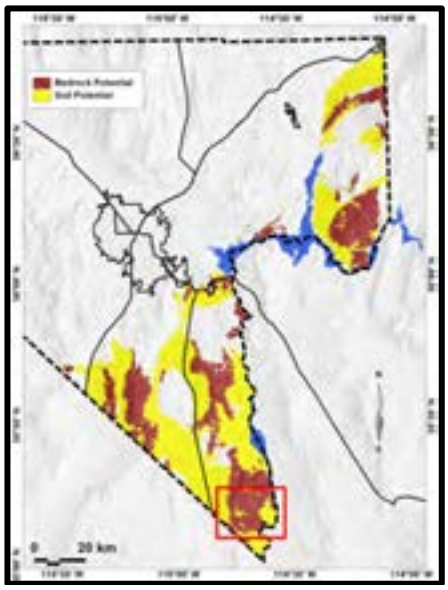

Figure 4-84. Map of southern Nevada showing predicted NOA-containing areas with the Laughlin region outlined in red box.

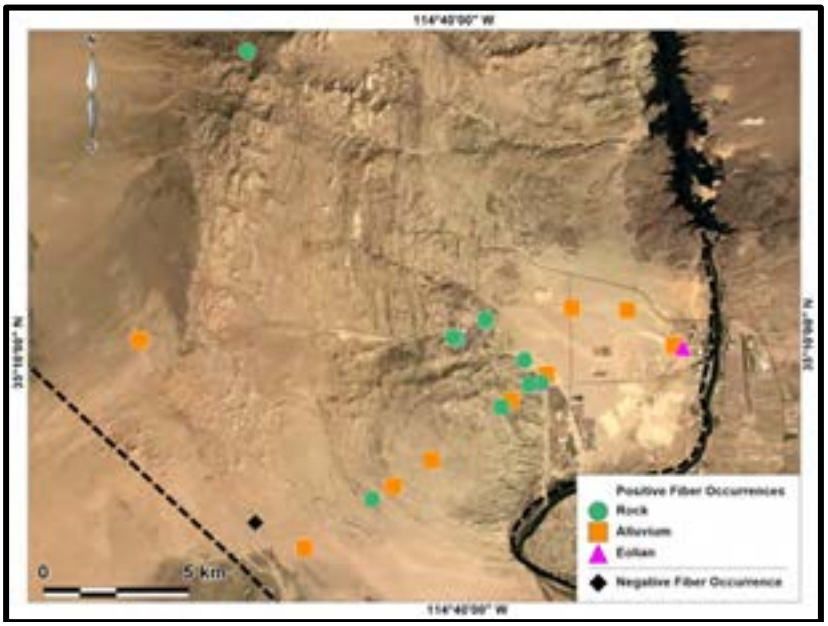

Figure 4-85. Map of Laughlin region sample locations. Positive occurrences are for amphibole asbestos with aspect ratios of 3:1 or greater. Samples are identified according to the geological process that deposited the material: bedrock (in place), alluvium (water-deposited), or eolian (wind-deposited).

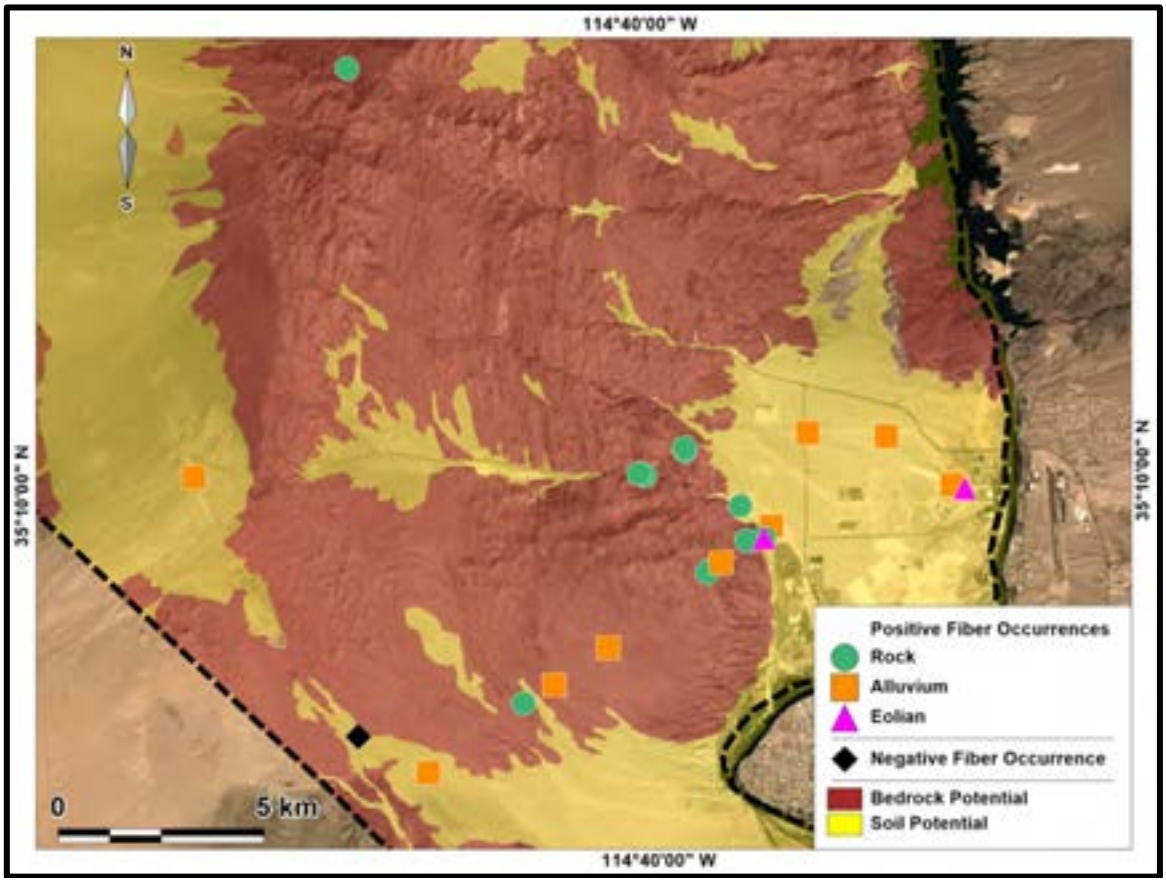

Figure 4-86. Map of sample locations in the Laughlin region with predicted occurrences of NOA based on alluvial (water-transported) surficial processes that transport material from the source rock out into the basin. Bedrock potential represents areas of potential occurrence for amphibole asbestos in igneous and metamorphic rock exposures. Soil potential delineates areas where runoff could potentially distribute amphibole asbestos fibers downslope from bedrock areas. Positive occurrences are for amphibole asbestos with aspect ratios of 3:1 or greater.

Figure 4-87. Plutonic rocks in the Laughlin region containing NOA.

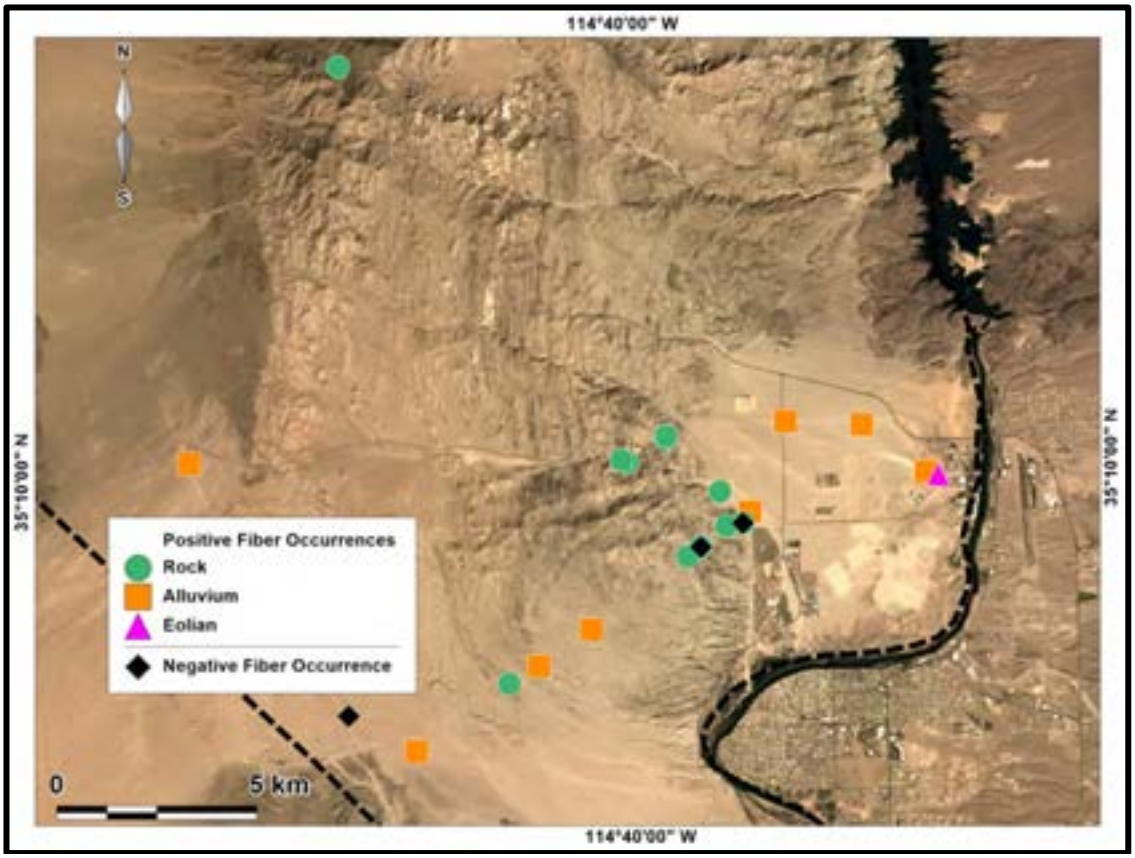

Figure 4-88. Map of Laughlin region sample locations. Positive occurrences are for amphibole asbestos with aspect ratios of 8:1 or greater. Samples are identified according to the geological process that deposited the material: bedrock (in place), alluvium (water-deposited), or eolian (wind-deposited).

Figure 4-89. Numerous dirt roads occur in areas containing NOA in the Laughlin region. Photo is a view to the south in the area near sample site for Gayle Laughlin 1.

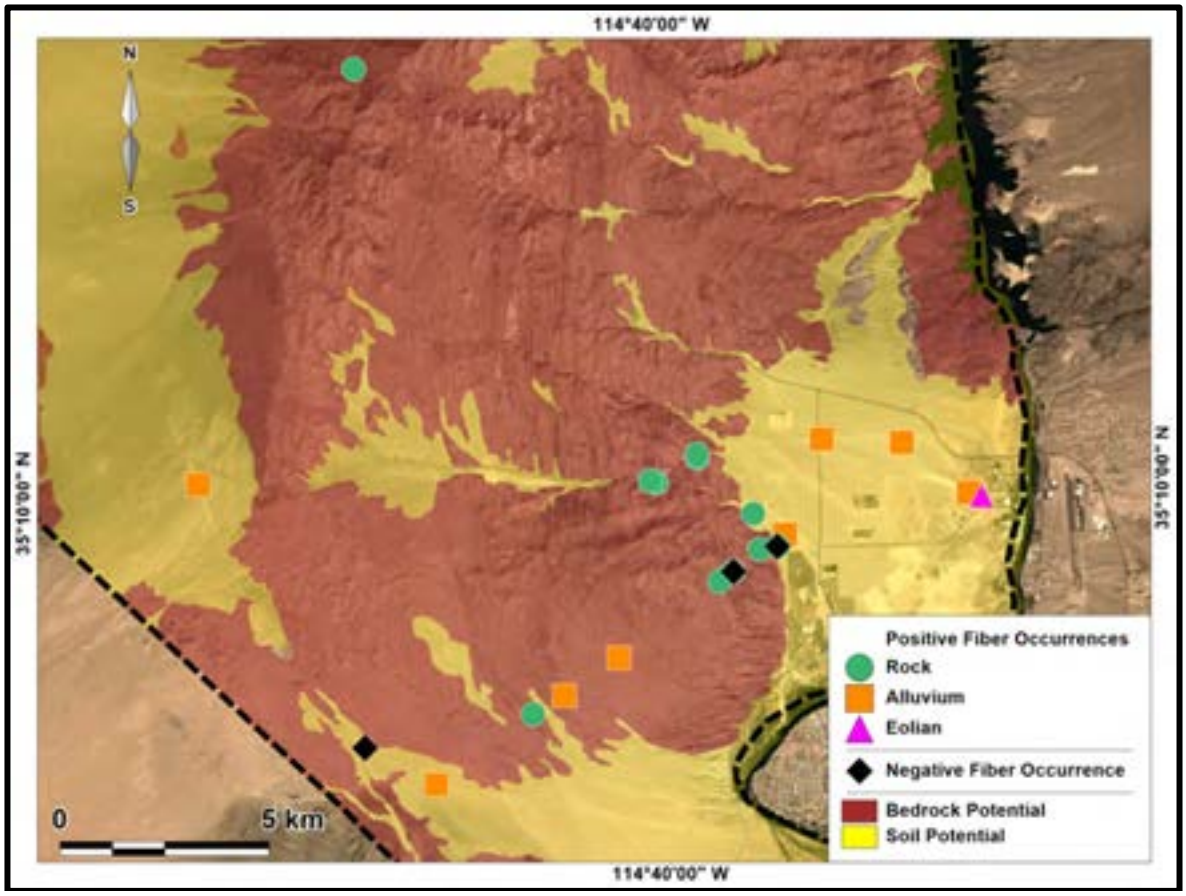

Figure 4-90. Map of sample locations in the Laughlin region with predicted occurrences of NOA based on alluvial (water-transported) surficial processes that transport material from the source rock out into the basin. Bedrock potential represents areas of potential occurrence for amphibole asbestos in igneous and metamorphic rock exposures. Soil potential delineates areas where runoff could potentially distribute amphibole asbestos fibers downslope from bedrock areas. Positive occurrences are for amphibole asbestos with aspect ratios of 8:1 or greater.

Figure 4-91. Typical mafic plutonic rocks containing NOA in Laughlin region.

Table 4.25. Summary of sample type, depositional process, and mean and maximum aspect ratios for samples in the Laughlin Region.

LAUGHLIN REGION							
Sample ID	**N**	**Mean Aspect Ratio**	**Maximum Aspect Ratio**	**Aspect Ratio Cutoff 8+**	**Aspect Ratio Cutoff 3+**	**Type**	**Depositional Process**
SM021714-1	19	4.8	9.8	Positive	Positive	rock	rock
SM021714-2	18	5.1	9.0	Positive	Positive	rock	rock
SM021714-3	19	4.5	9.6	Positive	Positive	rock	rock
SM021714-4	16	6.0	15.1	Positive	Positive	rock	rock
M021215-1	9	8.9	32.5	Positive	Positive	soil	road (alluvium)
BOR sample (BOR2)	8	11.6	20.8	Positive	Positive	soil	alluvium
Gayle Laughlin 2	6	9.5	17.7	Positive	Positive	soil	road (alluvium)
M021215-2	2	6.5	9.4	Positive	Positive	soil	eolian
Gayle Laughlin 1	11	17.0	68.3	Positive	Positive	soil	alluvium
M021215-3	5	4.4	6.3	Negative	Positive	soil	eolian
M021215-4	25	5.2	11.6	Positive	Positive	rock	rock
M021215-5	18	5.4	13.3	Positive	Positive	rock	rock
M021215-6	8	11.3	15.3	Positive	Positive	rock	rock
M021215-7	28	6.8	16.4	Negative	Positive	soil	road (alluvium)
M021215-8	29	6.4	14.6	Positive	Positive	rock	rock
M021215-9	3	8.1	9.0	Positive	Positive	soil	alluvium
M021215-10	6	9.3	13.6	Positive	Positive	soil	alluvium
M021215-11	11	10.9	14.7	Positive	Positive	rock	rock

Table 4.25 (continued). Summary of sample type, depositional process, and mean and maximum aspect ratios for samples in the Laughlin Region.

LAUGHLIN REGION (continued)							
Sample ID	**N**	**Mean Aspect Ratio**	**Maximum Aspect Ratio**	**Aspect Ratio Cutoff 8+**	**Aspect Ratio Cutoff 3+**	**Type**	**Depositional Process**
M021215-12	21	8.1	20.9	Positive	Positive	soil	road (alluvium)
M021215-13	0	NA	NA	Negative	Negative	soil	road (alluvium)
M021215-14	7	6.4	12.4	Positive	Positive	soil	road (alluvium)
L030117_1	24	10.3	32.6	Positive	Positive	rock	rock
L030117_2	22	7.5	12.4	Positive	Positive	rock	rock
L030117_3	4	10.3	17.1	Positive	Positive	rock	rock
TOTAL =	**319**	**7.4**	**68.3**				

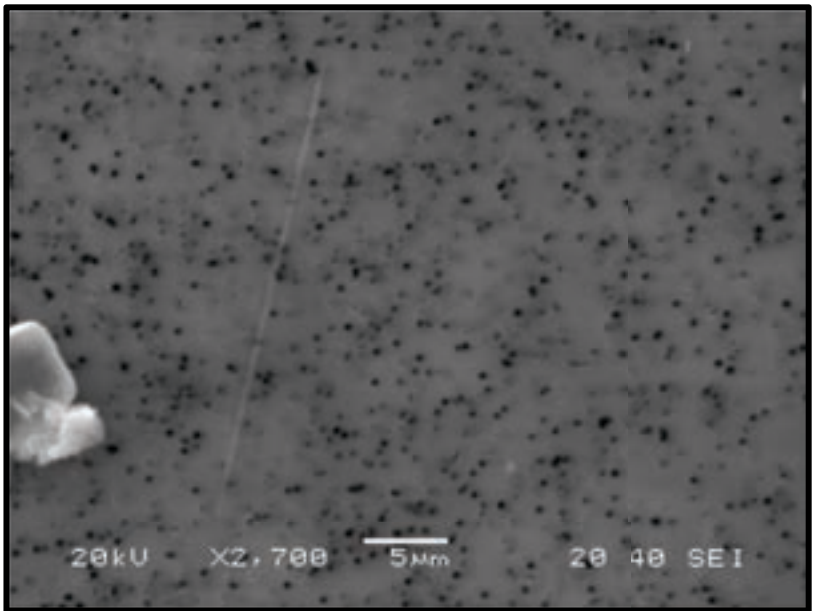

Figure 4-92. SEM image of sodic-calcic amphibole fiber from Gayle Laughlin 1 (similar to Libby, Montana asbestos).

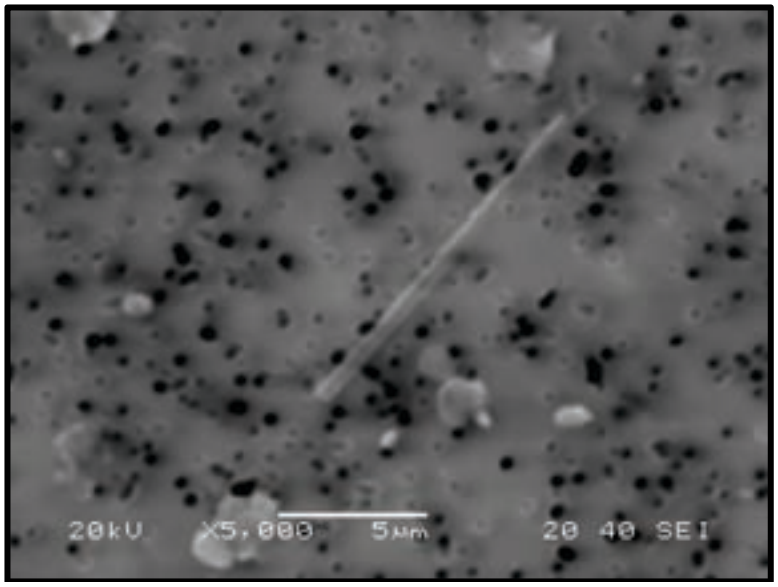

Figure 4-93. SEM image of sodic-calcic amphibole from Gayle Laughlin 2, mineralogy is similar to asbestos found in Libby Montana.

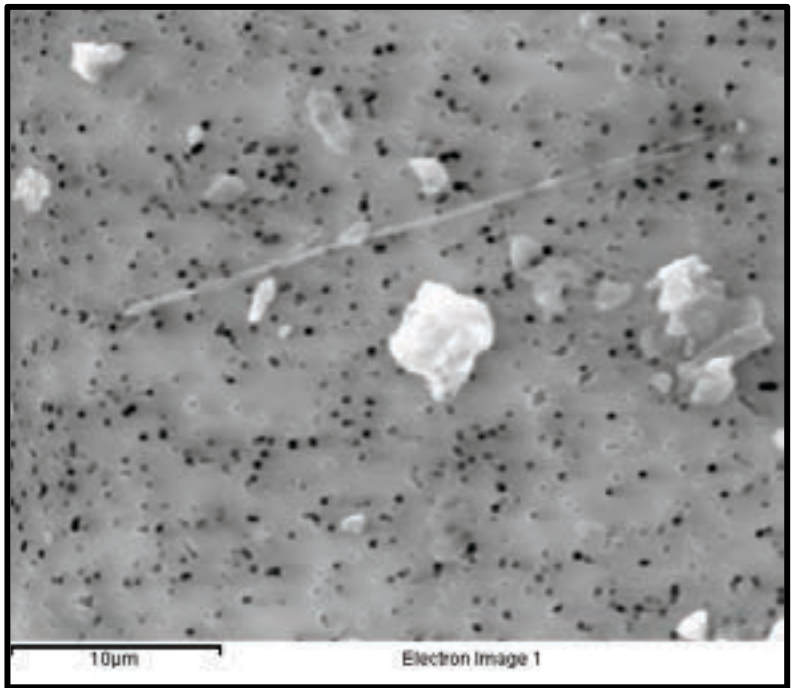

Figure 4-94. SEM image of sodic-calcic amphibole from Gayle Laughlin 2, mineralogy is similar to asbestos found in Libby Montana.

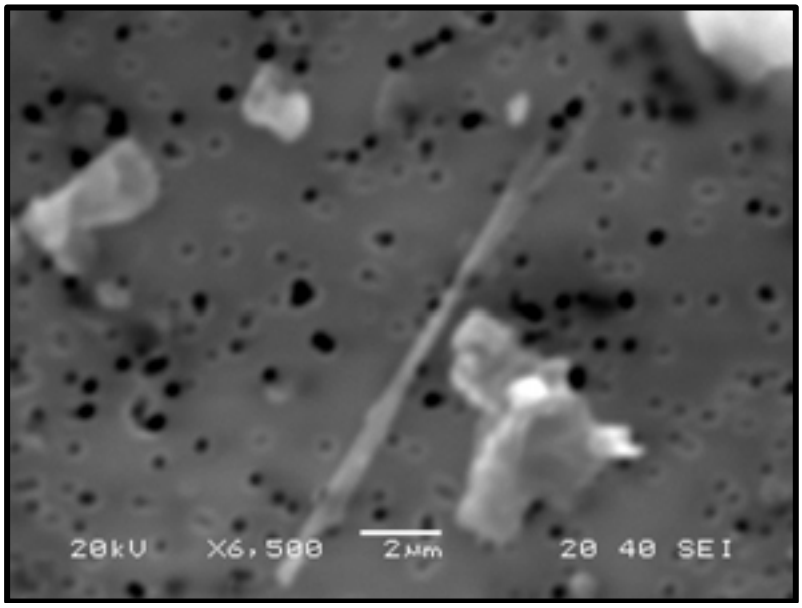

Figure 4-95. SEM image of sodic-calcic amphibole bundle from sample BOR2, mineralogy is similar to asbestos found in Libby Montana.

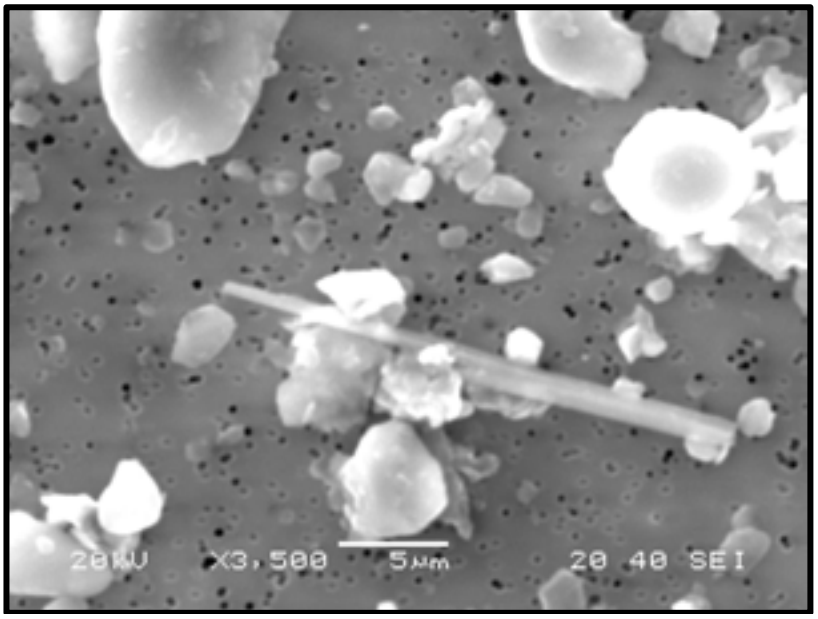

Figure 4-96. SEM image of sub-calcic amphibole particle from sample BOR2.

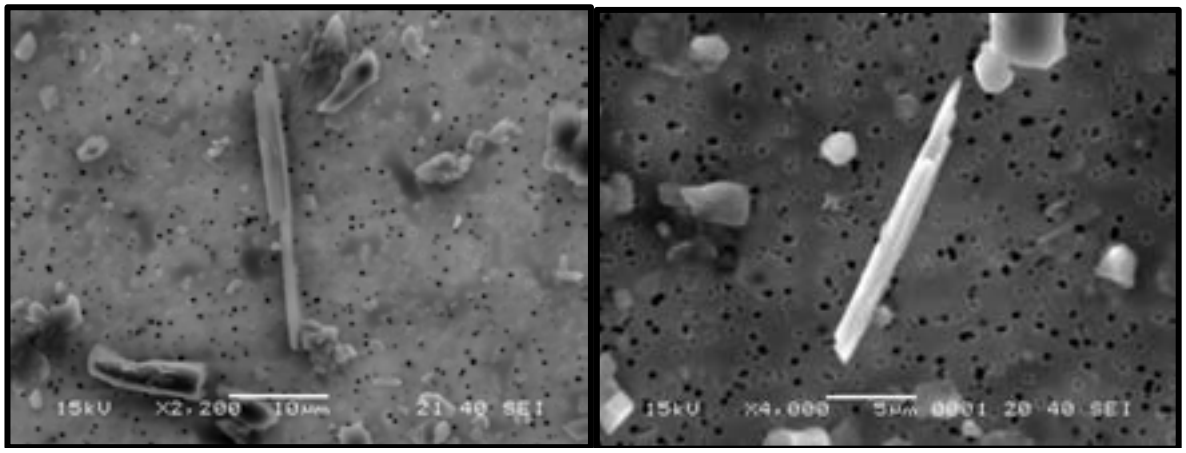

Figure 4-97. SEM image of actinolite amphibole particles from sample M021215-8 (left) and M021215-12 (right).

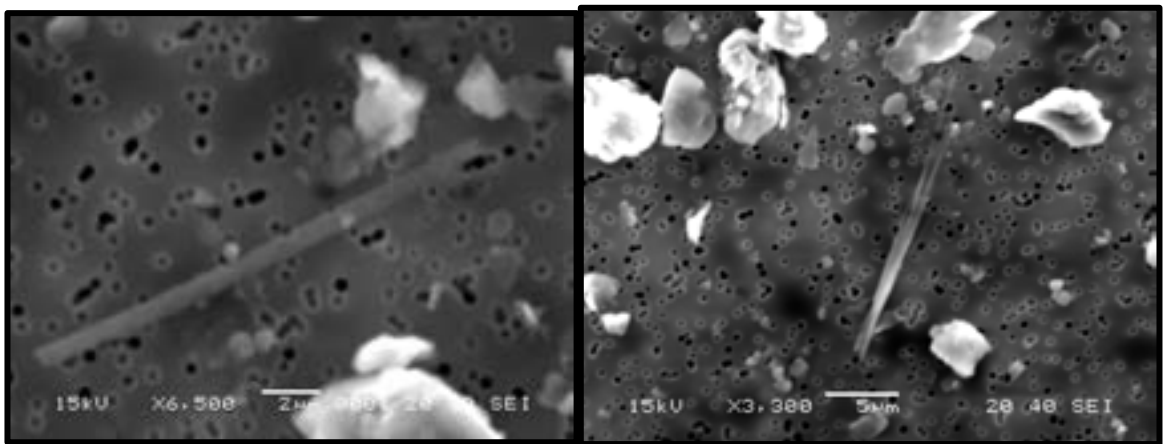

Figure 4-98. SEM image of actinolite amphibole particles from sample M021215-12.

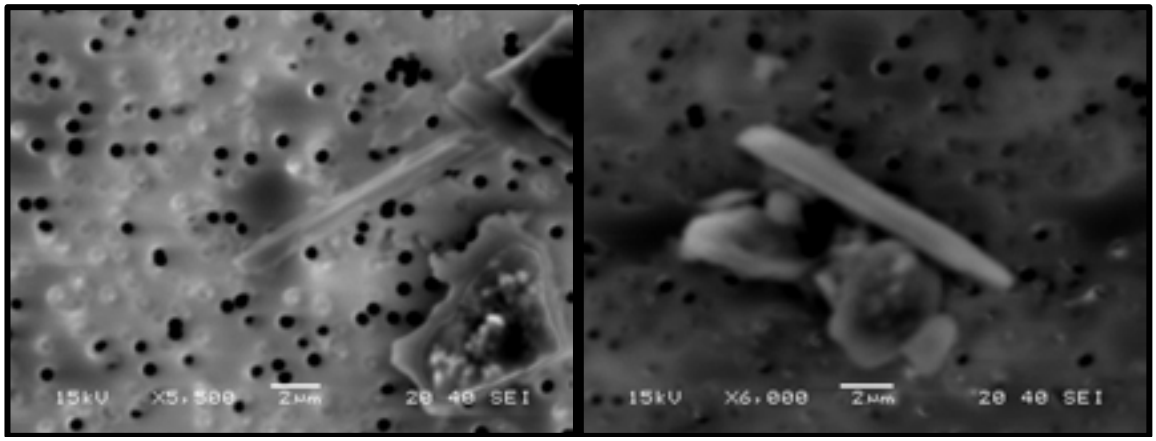

Figure 4-99. SEM image of magnesio-hornblende amphibole particle from sample SM021714-2 (left), and sub-calcic amphibole particle from sample SM021714-4 (right).

The amphibole samples collected in the Laughlin Region have a wide range of compositions including sub-calcic, calcic, sodic, and sodic-calcic (Table 4.26). Consistent with other data in this study, amphibole particles with sodic, or sodic-calcic compositions are consistently found to have greater aspect ratios than those with a calcic or sub-calcic composition (Table 4.26). As discussed in Metcalf and Buck (2015), the composition of the amphibole minerals depends upon the processes operating at the time these crystals formed or were hydrothermally altered. The soil and alluvial samples most likely derive their NOA from erosion and transportation from surrounding NOA-containing bedrock. Wind transport and deposition can also occur from great distances so some NOA in the soils and alluvium may be transported from more distant NOA sources. Much of this region is land managed by the US Bureau of Reclamation and more work and sampling are needed in those regions to better understand the distribution of NOA in this region.

The mean aspect ratio for the 24 samples in the Laughlin region was 7.5 ± 0.3, the maximum aspect ratio was 68.3 (Table 4.26). Bundles had the greatest mean aspect ratio of the 3 morphologic types (Table 4.27). SEM images are shown in Figures 4-92 to 4-99.

Table 4.26. Particle sizes and mineralogy results of amphibole particles in the Laughlin Region. Number of particles (N), standard error of the mean (S.E.)

Laughlin Region													
Mineralogy	**N**	**Minimum Width (µm)**	**Maximum Width (µm)**	**Mean Width (µm)**	**S.E.**	**Minimum Length (µm)**	**Maximum Length (µm)**	**Mean Length (µm)**	**S.E.**	**Minimum Aspect Ratio**	**Maximum Aspect Ratio**	**Mean Aspect Ratio**	**S.E.**
Actinolite	83	0.4	24.6	1.7	0.3	2.0	372.0	13.5	4.5	3.0	22.1	7.4	0.5
Edinite	22	0.3	1.6	1.0	0.1	1.8	13.0	5.6	0.7	3.1	11.8	5.7	0.5
Mg-hbld	129	0.4	36.3	2.1	0.4	1.8	201.0	11.7	2.1	3.0	14.7	6.1	0.3
Mg-Katophorite	1	0.2	0.2	0.2	-	2.5	2.5	2.5	-	12.5	12.5	12.5	-
Hornblende	2	1.2	8.0	4.6	3.4	3.7	58.2	31.0	27.3	3.1	7.3	5.2	2.1
Winchite	1	0.6	0.6	0.6	-	4.7	4.7	4.7	-	7.8	7.8	7.8	-
Sodic group	1	0.7	0.7	0.7	-	12.4	12.4	12.4	-	17.7	17.7	17.7	-
Sodic-Calcic group	11	0.2	0.7	0.5	0.0	2.5	27.3	7.9	2.1	6.3	68.3	17.3	5.4
Sub-Calcic group	74	0.3	8.0	1.2	0.1	2.4	58.2	9.7	1.0	3.1	32.6	8.8	0.6
Calcic group	233	0.3	36.3	1.8	0.2	1.8	372.0	11.8	2.0	3.0	22.1	6.5	0.2
All Particles	**319**	**0.2**	**36.3**	**1.6**	**0.2**	**1.8**	**372.0**	**11.2**	**1.5**	**3.0**	**68.3**	**7.5**	**0.3**

Table 4.27. Morphology classification of particles analyzed in the Laughlin region. Number of particles (N), standard error of the mean (S.E.)

Laughlin Region													
Morphology	**N**	**Minimum Width (µm)**	**Maximum Width (µm)**	**Mean Width (µm)**	**S.E.**	**Minimum Length (µm)**	**Maximum Length (µm)**	**Mean Length (µm)**	**S.E.**	**Minimum Aspect Ratio**	**Maximum Aspect Ratio**	**Mean Aspect Ratio**	**S.E.**
Bundles	52	1.1	36.3	3.3	0.8	4.0	372.0	28.6	7.8	3.4	19.9	9.3	0.5
Fibers (≤1 µm)	166	0.2	1.0	0.7	0.0	1.8	27.3	5.7	0.3	3.0	68.3	8.2	0.5
Prismatic Crystals	101	1.1	28.0	2.3	0.3	3.3	168.4	11.2	1.8	3.0	12.4	5.3	0.2
Total	**319**	**0.2**	**36.3**	**1.6**	**0.2**	**1.8**	**372.0**	**11.2**	**1.5**	**3.0**	**68.3**	**7.5**	**0.3**

Nellis Dunes Region

The Nellis Dunes Recreation Area (NDRA) is a special off-road recreation area managed by the Bureau of Land Management, where over 300,000 people per year drive various different quads, 3-wheelers, motorcycles, dune buggies and other off-road vehicles (Goossens et al., 2012). The NDRA is treated as a separate region in this study because of the special land use that occurs there (off-road vehicle recreation), although it is only 8 km northeast of Las Vegas (Figure 4-100). A total of 5 samples, primarily from surficial vesicular soil horizons were obtained and analyzed (Table 4.28). Of these 5 samples, 2 tested positive for amphibole asbestos with aspect ratio of 3:1 and only 1 sample tested positive for amphibole asbestos with an aspect ratio of 8:1 or higher (Figures 4-101 to 4-102).

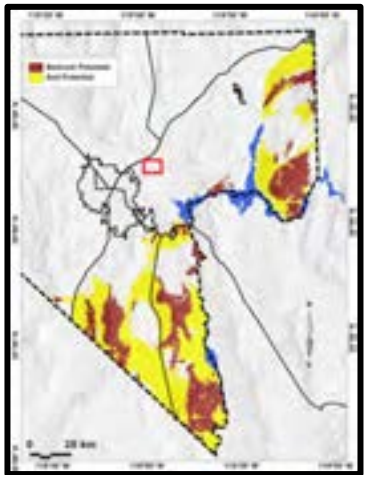

Figure 4-100. Map of southern Nevada showing predicted NOA-containing areas with the Nellis Dunes region outlined in red box.

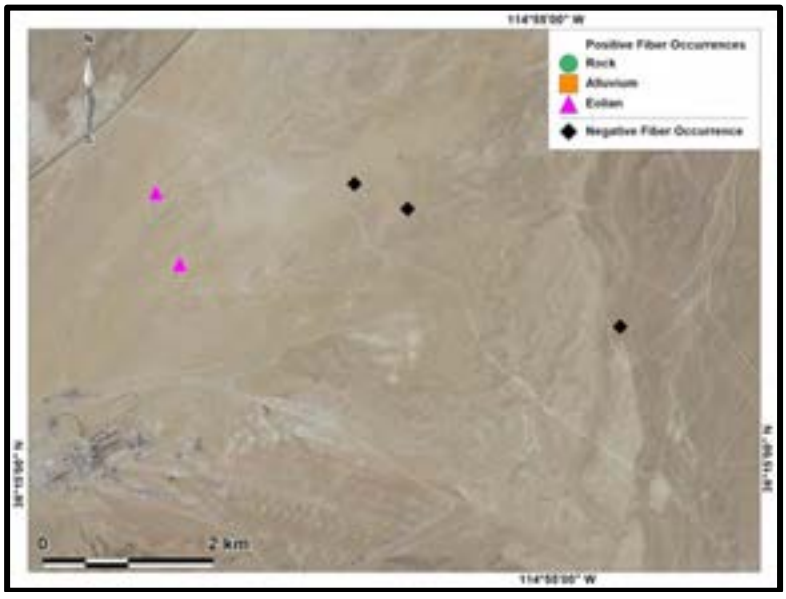

Figure 4-101. Map of Nellis Dunes region sample locations. Positive occurrences are for amphibole asbestos with aspect ratios of 3:1 or greater. Samples are identified according to the geological process that deposited the material: bedrock (in place), alluvium (water-deposited), or eolian (wind-deposited).

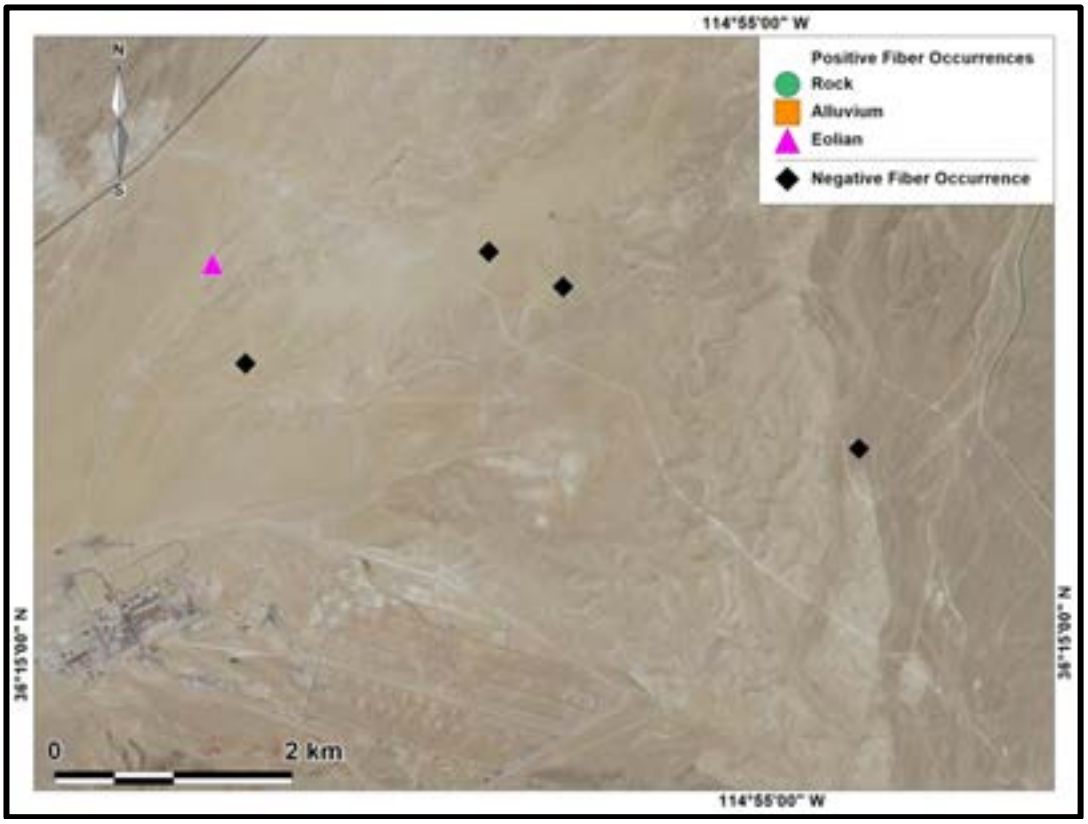

Figure 4-102. Map of Nellis Dunes region sample locations. Positive occurrences are for amphibole asbestos with aspect ratios of 8:1 or greater. Samples are identified according to the geological process that deposited the material: bedrock (in place), alluvium (water-deposited), or eolian (wind-deposited).

Figure 4-103. View towards Las Vegas from Nellis Dunes Recreation Area.

Table 4.28. Summary of sample type, depositional process, and mean and maximum aspect ratios for samples in the Nellis Dunes Recreation Area.

NELLIS DUNES							
Sample ID	**N**	**Mean Aspect Ratio**	**Maximum Aspect Ratio**	**Aspect Ratio Cutoff 8+**	**Aspect Ratio Cutoff 3+**	**Type**	**Depositional Process**
NSP-27	0	NA	NA	Negative	Negative	soil	eolian
NSP 171	0	NA	NA	Negative	Negative	soil	rock (muddy creek)
NSP 176	0	NA	NA	Negative	Negative	soil	eolian
DS1_60_052511	3	6.3	9.7	Positive	Positive	soil	eolian
DS9_60_052511	2	4.8	6.5	Negative	Positive	soil	eolian
TOTAL =	**5**	**5.6**	**9.7**				

Figure 4-104. SEM image of magnesio-hornblende amphibole bundle from sample DS9_60_052511 (left), and actinolite amphibole bundle from sample DS1_60_052511

Only calcic amphibole particles were found in NDRA in this study (Table 4.29).

Much of the NOA in this region is likely derived through a combination of processes, but primarily through wind erosion/deposition including nearby NOA localities in Lake Mead National Recreation Area AZ, and Boulder City NV. Wind directions in this region can vary greatly, and can occur from any direction (Goossens et al., 2011). Additionally, wind-derived NOA may be brought to this area from more distant sources (Van Gosen 2008, Van Gosen and Clinkenbeard (2011).

The mean aspect ratio for the samples in the NDRA was 5.7 ± 1.2, the maximum aspect ratio was 9.7 (Table 4.29). Particle morphology data are shown in Table 4.30. SEM images shown in Figure 4-104.

Table 4.29. Particle sizes and mineralogy results of amphibole particles in the Nellis Dunes Region. Number of particles (N), standard error of the mean (S.E.)

Nellis Dunes Region													
Mineralogy	**N**	**Minimum Width (µm)**	**Maximum Width (µm)**	**Mean Width (µm)**	**S.E.**	**Minimum Length (µm)**	**Maximum Length (µm)**	**Mean Length (µm)**	**S.E.**	**Minimum Aspect Ratio**	**Maximum Aspect Ratio**	**Mean Aspect Ratio**	**S.E.**
Actinolite	2	0.9	4.3	2.6	1.7	3.8	41.9	22.9	19.1	4.2	9.7	7.0	2.8
Mg-hbld	2	0.5	2.2	1.4	0.9	2.4	14.2	8.3	5.9	4.8	6.5	5.6	0.8
Tremolite	1	4.0	4.0	4.0	-	12.4	12.4	12.4	-	3.1	3.1	3.1	-
Calcic group	5	0.5	4.3	2.4	0.8	2.4	41.9	14.9	7.1	3.1	9.7	5.7	1.2
All Particles	**5**	**0.5**	**4.3**	**2.4**	**0.8**	**2.4**	**41.9**	**14.9**	**7.1**	**3.1**	**9.7**	**5.7**	**1.2**

Table 4.30. Morphology classification of particles analyzed in the Nellis Dunes Recreation Area. Number of particles (N), standard error of the mean (S.E.)

Nellis Dunes Region													
Morphology	**N**	**Minimum Width (µm)**	**Maximum Width (µm)**	**Mean Width (µm)**	**S.E.**	**Minimum Length (µm)**	**Maximum Length (µm)**	**Mean Length (µm)**	**S.E.**	**Minimum Aspect Ratio**	**Maximum Aspect Ratio**	**Mean Aspect Ratio**	**S.E.**
Bundle	3	2.2	4.3	3.5	0.7	12.4	41.9	22.8	9.5	3.1	9.7	6.4	1.9
Fibers (≤1 µm)	2	0.5	0.9	0.7	0.2	2.4	3.8	3.1	0.7	4.2	4.8	4.5	0.3
All particles	**5**	**0.5**	**4.3**	**2.4**	**0.8**	**2.4**	**41.9**	**14.9**	**7.1**	**3.1**	**9.7**	**5.7**	**1.2**

Nelson Road Region

The Nelson Road refers primarily to the dirt road that connects the town of Nelson to Highway 93 and other dirt roads that can be taken to reach Searchlight (Figure. 4-105). A total of 10 samples, 2 collected from alluvium and 8 collected from bedrock outcrops, were obtained and analyzed (Table 4.31). All tested positive for amphibole asbestos with an aspect ratio of greater than 3:1, and greater than 8:1 (Figures 4-106 and 4-107).

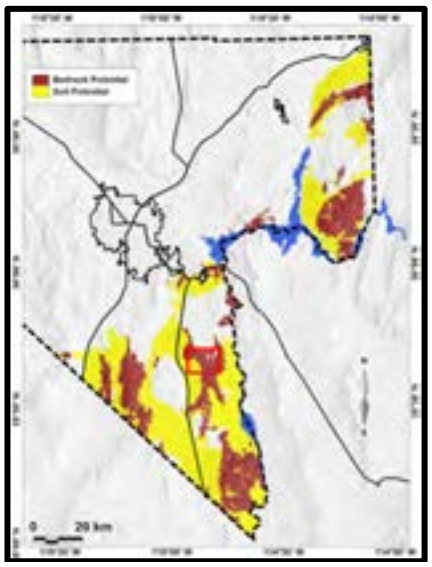

Figure 4-105. Map of southern Nevada showing predicted NOA-containing areas with the Nelson Road region outlined in red box.

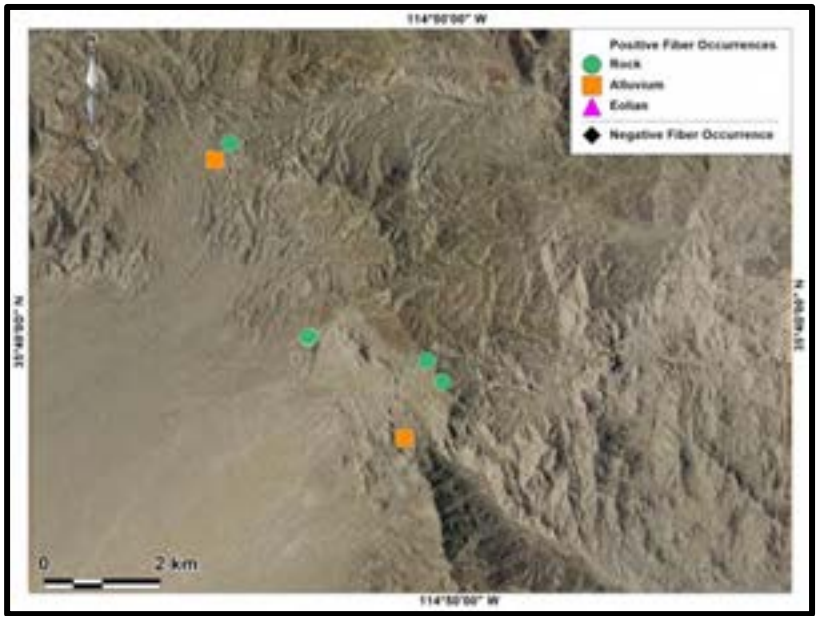

Figure 4-106. Map of Nelson Road region sample locations. Positive occurrences are for amphibole asbestos with aspect ratios of both 3:1 and 8:1 or greater. Samples are identified according to the geological process that deposited the material: bedrock (in place), alluvium (water-deposited), or eolian (wind-deposited).

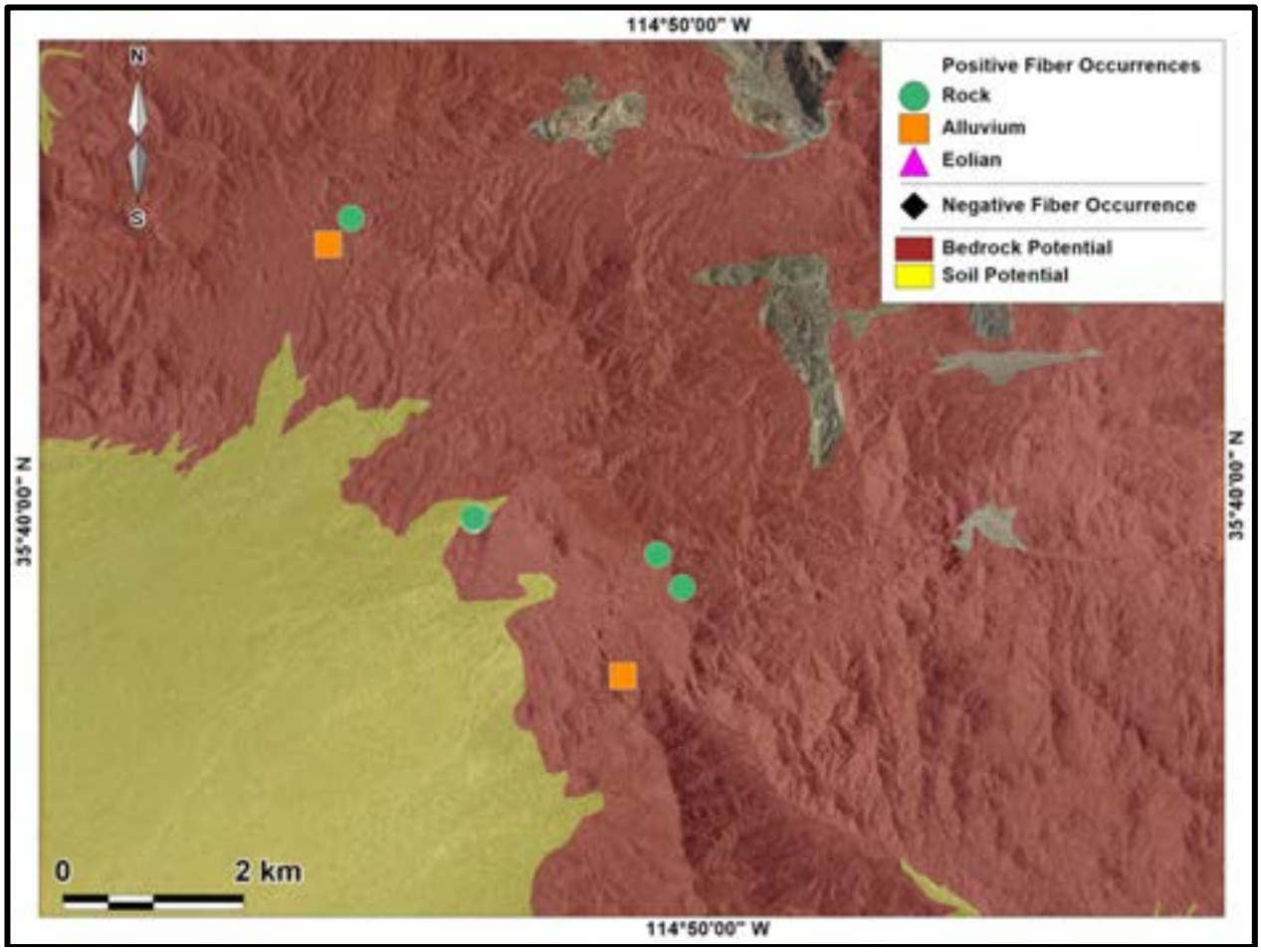

Figure 4-107. Map of sample locations in the Nelson Road region with predicted occurrences of NOA based on alluvial (water-transported) surficial processes that transport material from the source rock out into the basin. Bedrock potential represents areas of potential occurrence for amphibole asbestos in igneous and metamorphic rock exposures. Soil potential delineates areas where runoff could potentially distribute amphibole asbestos fibers downslope from bedrock areas. Positive occurrences are for amphibole asbestos with aspect ratios of both 3:1 and 8:1 or greater.

Table 4.31. Summary of sample type, depositional process, and mean and maximum aspect ratios for samples in the Nelson Road region.

NELSON ROAD REGION							
Sample ID	**N**	**Mean Aspect Ratio**	**Maximum Aspect Ratio**	**Aspect Ratio Cutoff 8+**	**Aspect Ratio Cutoff 3+**	**Type**	**Depositional Process**
N013015-1	24	5.4	13.7	Positive	Positive	rock	rock
N013015-2	24	5.9	11.2	Positive	Positive	rock	rock
N013015-3	25	4.7	9.5	Positive	Positive	rock	rock
N013015-4	6	6.3	10.0	Positive	Positive	rock	rock
N013015-5	22	5.1	11.2	Positive	Positive	rock	rock
N013015-6	9	11.7	25.9	Positive	Positive	soil	alluvium
N013015-7	31	6.0	15.5	Positive	Positive	rock	rock
N013015-8	28	6.7	9.5	Positive	Positive	rock	rock
N013015-9	20	16.2	33.7	Positive	Positive	soil	road (alluvium)
N013015-10	29	10.6	21.1	Positive	Positive	rock	rock
TOTAL =	**218**	**7.5**	**33.7**				

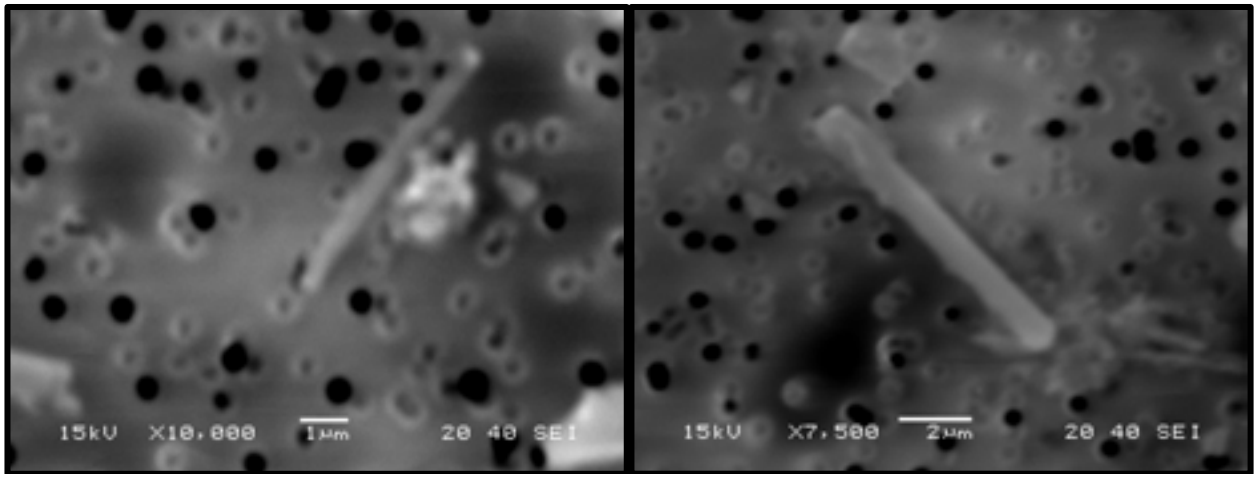

Figure 4-108. SEM image of actinolite amphibole fiber from sample N013015-1 (left), and actinolite amphibole from sample N013015-3 (right).

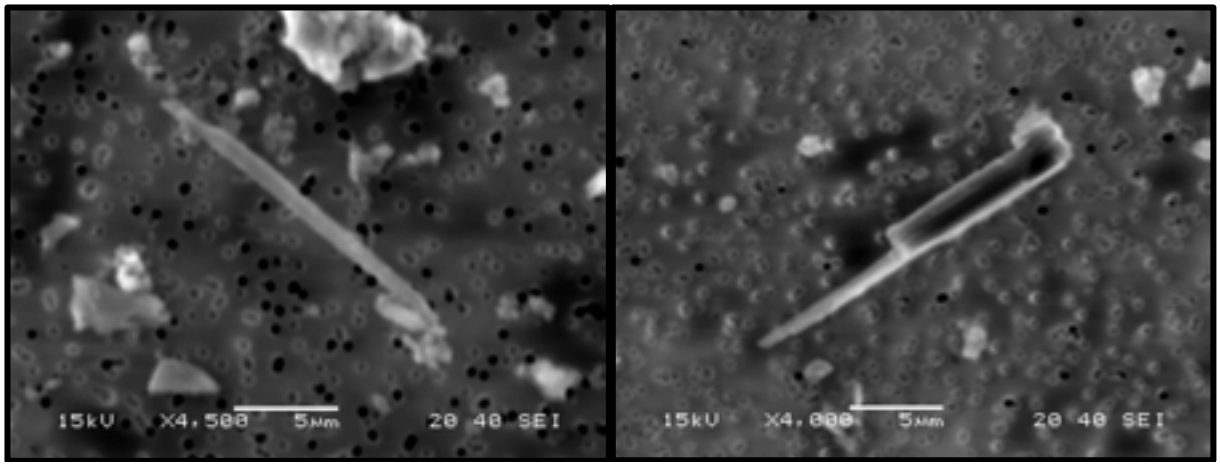

Figure 4-109. SEM image of actinolite amphibole particle from sample N013015-7 (left), and from sample N013015-5 (right).

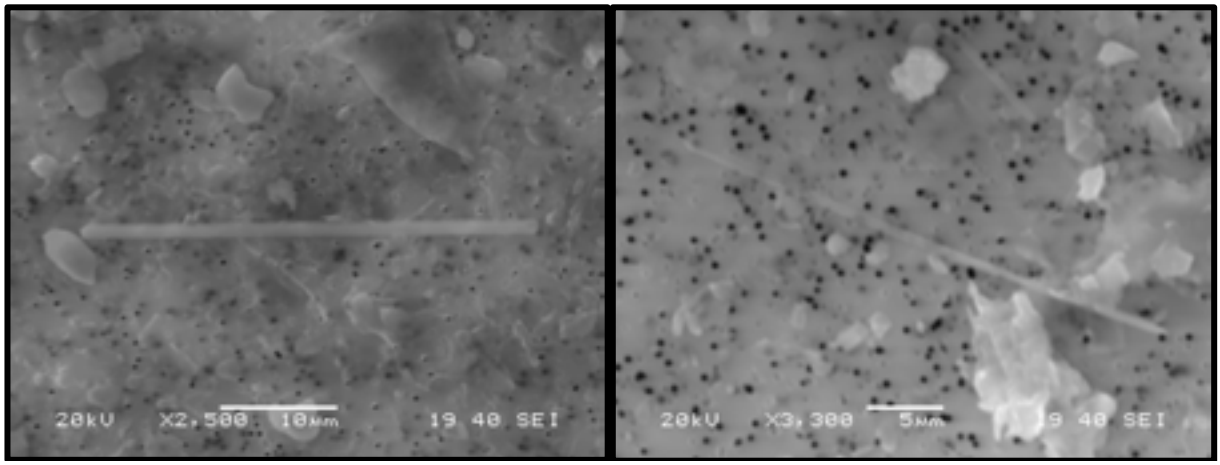

Figure 4-110. SEM image of actinolite amphibole particles from sample N013015-6 (left), and from sample N013015-9 (right).

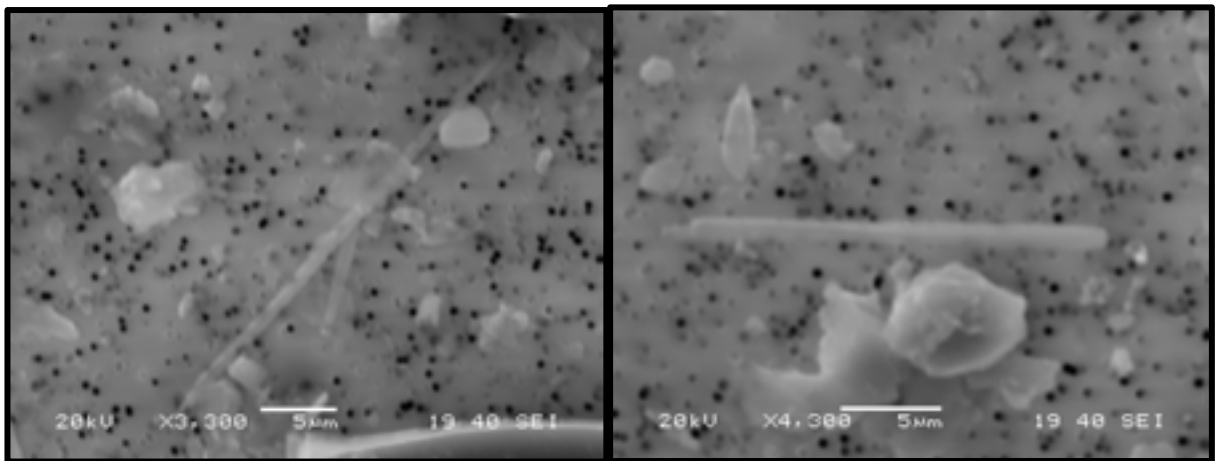

Figure 4-111. SEM image of Fe-Mg group amphibole particles (left) and actinolite amphibole (right) from sample N013015-9.

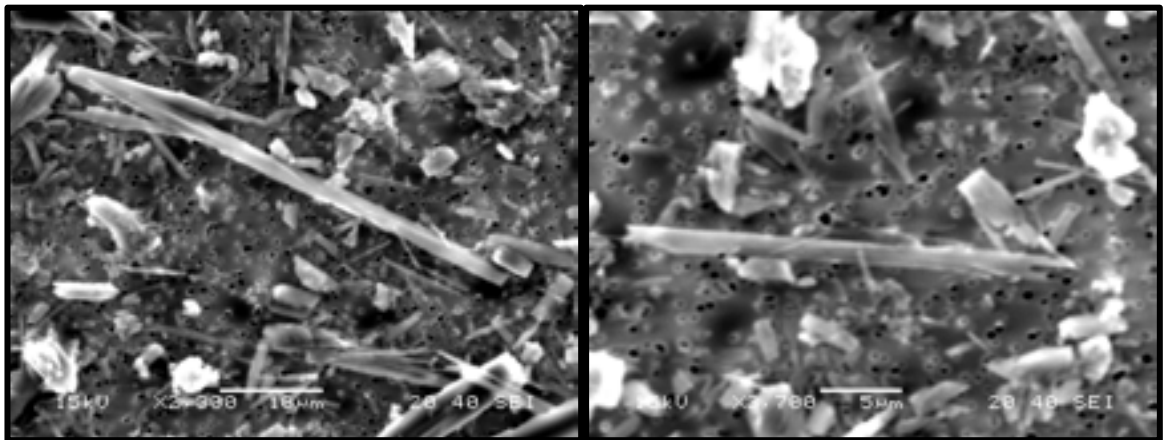

Figure 4-112. SEM images of actinolite amphibole fibers from sample N013015-10.

The amphibole samples collected in the Nelson Road region have a wide range of compositions including calcic, Fe-Mg, and sodic-calcic (Table 4.32). Much more detailed work is needed in this area to understand their distributions and genesis (see Chapter 3). Amphibole particles with Fe-Mg compositions have higher mean aspect ratios than compared to the other compositions in this area (Table 4.32).

The mean aspect ratio for the 10 samples in the Nelson Road region was 7.6 ± 0.3, the maximum aspect ratio was 33.7 (Table 4.32). Bundles had the greatest mean aspect ratio as compared to fibers or prismatic crystals (Table 4.33). SEM images shown in Figures 4-108 to 4-112.

Table 4.32. Particle sizes and mineralogy results of amphibole particles in the Nelson Road Region. Number of particles (N), standard error of the mean (S.E.)

Nelson Road Region													
Mineralogy	**N**	**Minimum Width (µm)**	**Maximum Width (µm)**	**Mean Width (µm)**	**S.E.**	**Minimum Length (µm)**	**Maximum Length (µm)**	**Mean Length (µm)**	**S.E.**	**Minimum Aspect Ratio**	**Maximum Aspect Ratio**	**Mean Aspect Ratio**	**S.E.**
Actinolite	190	0.5	7.6	1.5	0.1	2.4	58.1	11.2	0.6	3.0	33.7	7.7	0.3
Mg-hbld	24	0.6	2.4	1.3	0.1	2.1	15.6	7.0	0.8	3.0	10.0	5.4	0.4
Fe-Mg group	3	1.1	5.1	2.6	1.3	15.6	31.5	25.4	5.0	3.1	28.6	17.1	7.5
Sodic-Calcic group	1	0.9	0.9	0.9	-	3.3	3.3	3.3	-	3.7	3.7	3.7	-
Calcic group	214	0.5	7.6	1.5	0.1	2.1	58.1	10.7	0.5	3.0	33.7	7.4	0.3
All Particles	**218**	**0.5**	**7.6**	**1.5**	**0.1**	**2.1**	**58.1**	**10.9**	**0.5**	**3.0**	**33.7**	**7.6**	**0.3**

Table 4.33. Morphology classification of particles analyzed in the Nelson Road region. Number of particles (N), standard error of the mean (S.E.)

Nelson Road Region													
Morphology	**N**	**Minimum Width (µm)**	**Maximum Width (µm)**	**Mean Width (µm)**	**S.E.**	**Minimum Length (µm)**	**Maximum Length (µm)**	**Mean Length (µm)**	**S.E.**	**Minimum Aspect Ratio**	**Maximum Aspect Ratio**	**Mean Aspect Ratio**	**S.E.**
Bundles	69	1.1	5.1	1.8	0.1	4.2	46.5	14.8	1.0	3.1	21.1	8.6	0.5
Fibers (≤1 µm)	64	0.5	1.0	0.9	0.0	2.1	33.7	6.9	0.7	3.1	33.7	7.8	0.7
Prismatic Crystals	85	1.1	7.6	1.8	0.1	4.2	58.1	10.7	0.9	3.0	28.6	6.5	0.5
Total	**218**	**0.5**	**7.6**	**1.5**	**0.1**	**2.1**	**58.1**	**10.9**	**0.5**	**3.0**	**33.7**	**7.6**	**0.3**

Searchlight Region

The Searchlight Region refers primarily to the areas south, east, and west of Searchlight (Figure 4-113). A total of 47 samples were obtained and analyzed (Table 4.34). All tested positive for amphibole asbestos with aspect ratio of 3:1 or higher, and all but 7 samples for aspect ratios of 8:1 or higher (Figures 4-114 to 4-119).

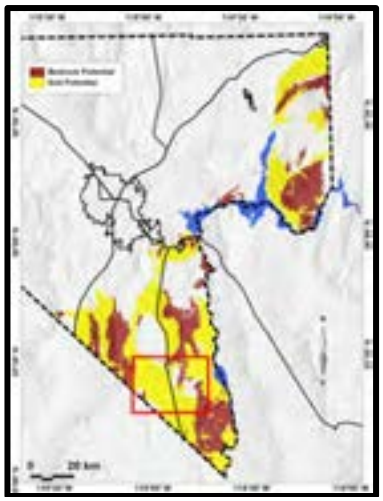

Figure 4-113. Map of southern Nevada showing predicted NOA-containing areas with the Searchlight region outlined in red box.

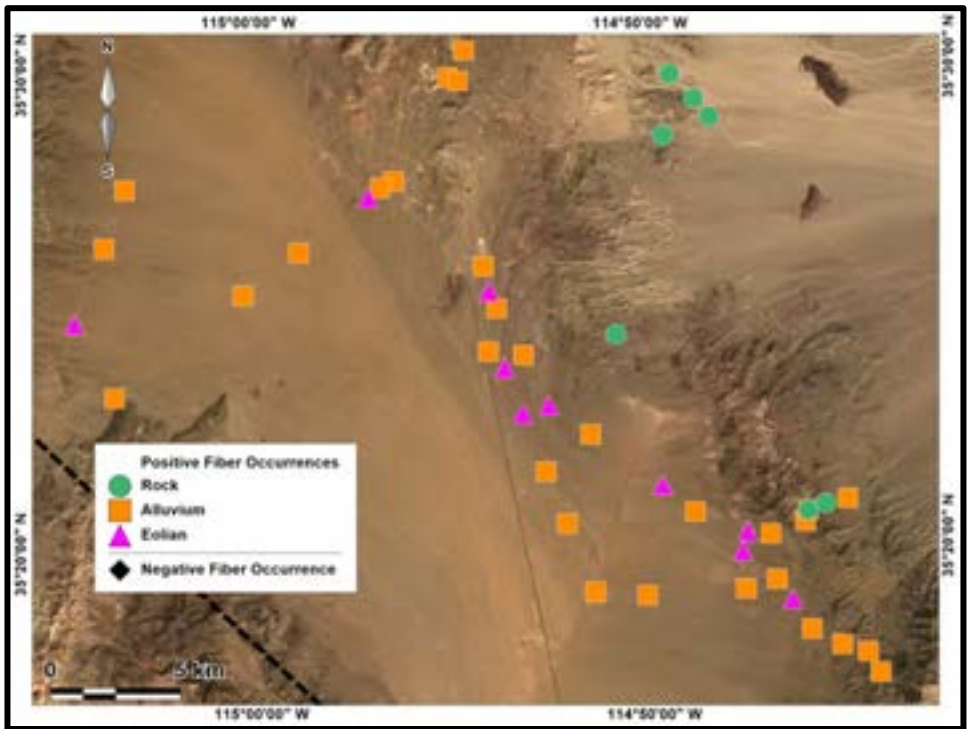

Figure 4-114. Map of Searchlight region sample locations. Positive occurrences are for amphibole asbestos with aspect ratios of 3:1 or greater. Samples are identified according to the geological process that deposited the material: bedrock (in place), alluvium (water-deposited), or eolian (wind-deposited).

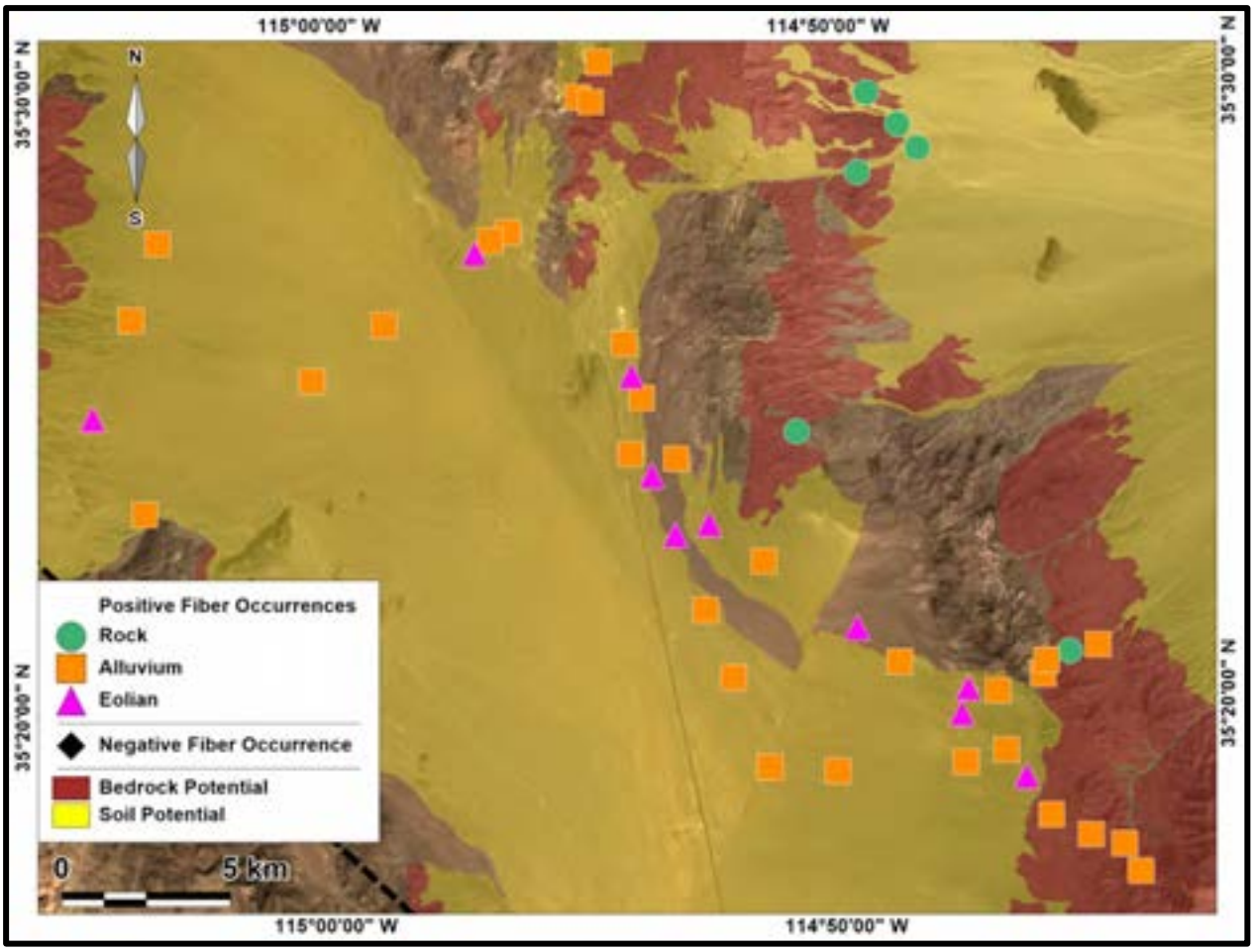

Figure 4-115. Map of sample locations in the Searchlight region with predicted occurrences of NOA based on alluvial (water-transported) surficial processes that transport material from the source rock out into the basin. Bedrock potential represents areas of potential occurrence for amphibole asbestos in igneous and metamorphic rock exposures. Soil potential delineates areas where runoff could potentially distribute amphibole asbestos fibers downslope from bedrock areas. Positive occurrences are for amphibole asbestos with aspect ratios of 3:1 or greater.

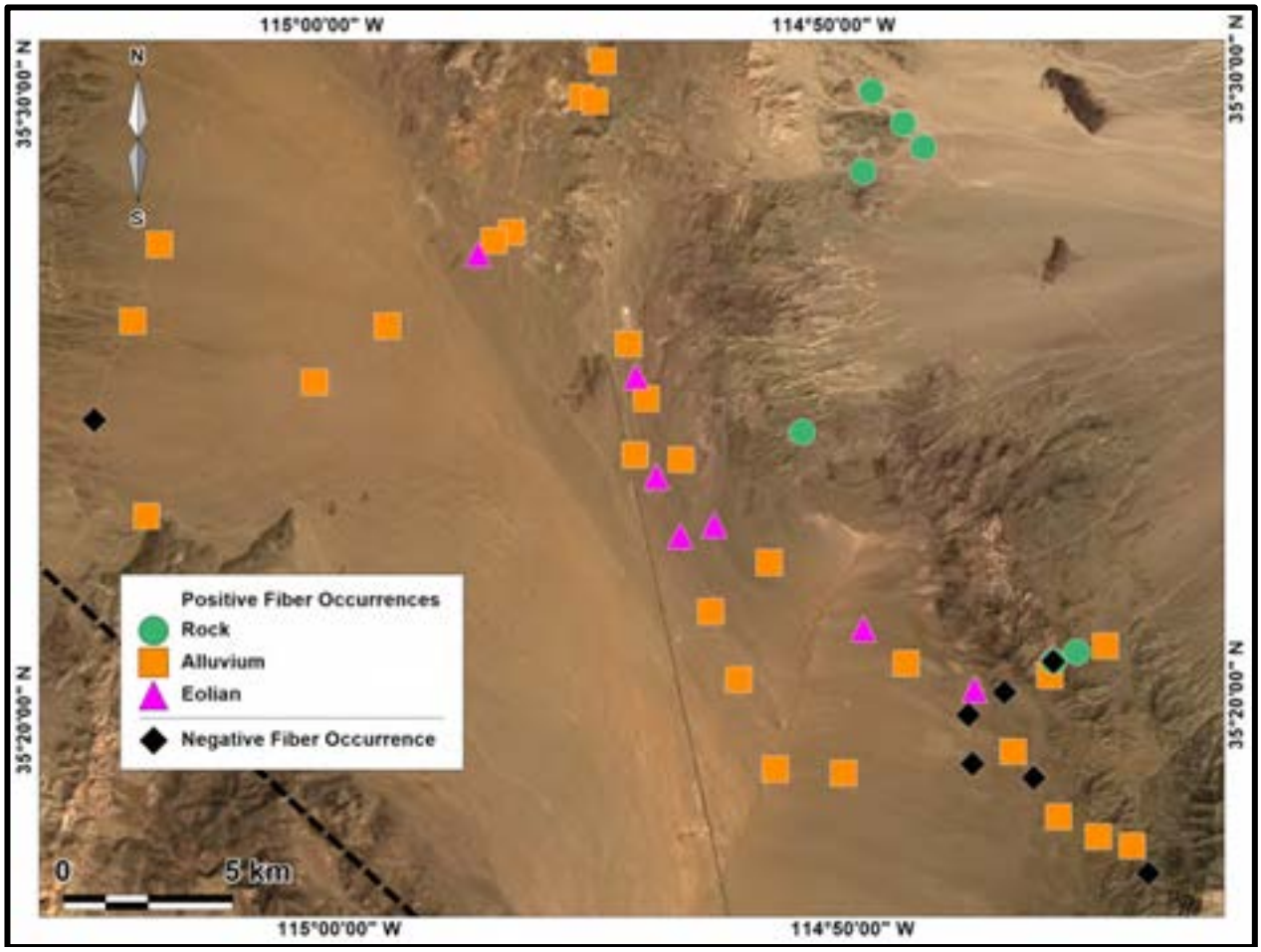

Figure 4-116. Map of Searchlight region sample locations. Positive occurrences are for amphibole asbestos with aspect ratios of 8:1 or greater. Samples are identified according to the geological process that deposited the material: bedrock (in place), alluvium (water-deposited), or eolian (wind-deposited).

Figure 4-117. NOA-containing metamorphic rock, site of sample S-5

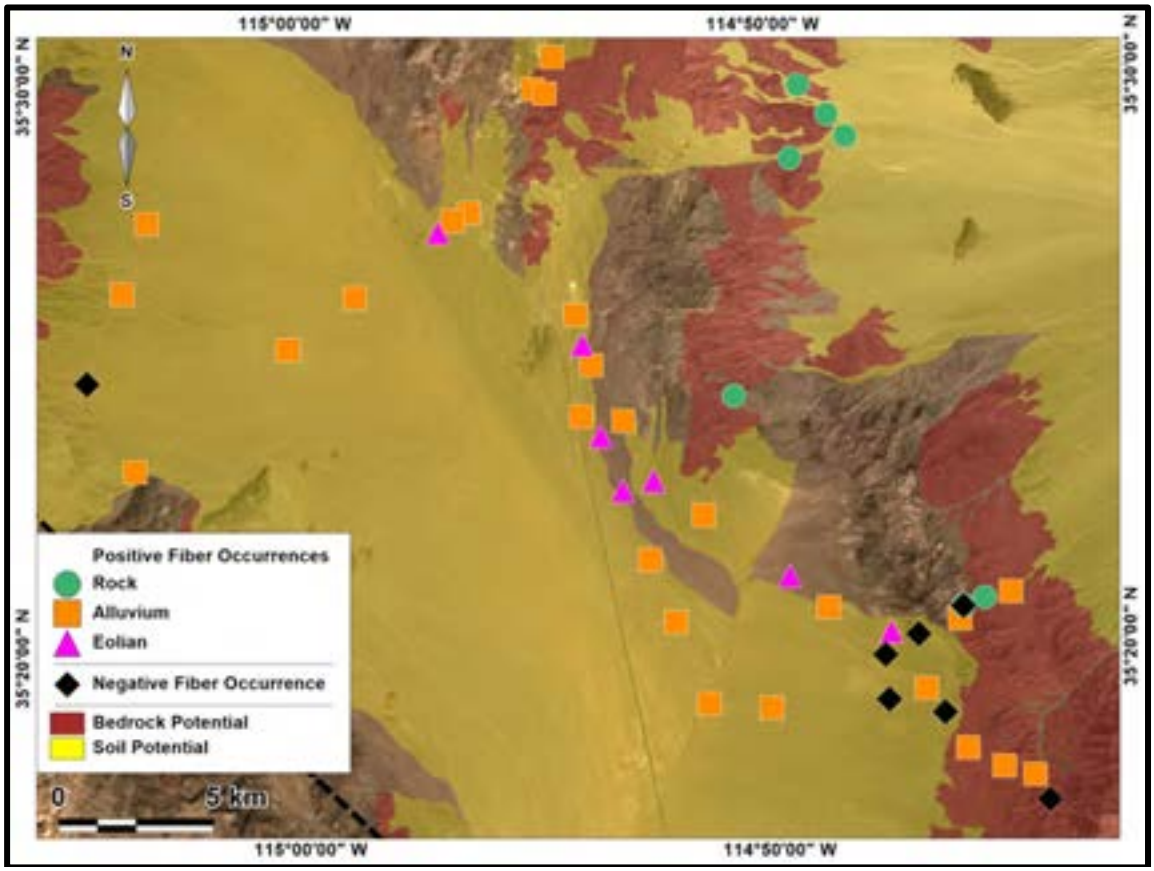

Figure 4-118. Map of sample locations in the Searchlight region with predicted occurrences of NOA based on alluvial (water-transported) surficial processes that transport material from the source rock out into the basin. Bedrock potential represents areas of potential occurrence for amphibole asbestos in igneous and metamorphic rock exposures. Soil potential delineates areas where runoff could potentially distribute amphibole asbestos fibers downslope from bedrock areas. Positive occurrences are for amphibole asbestos with aspect ratios of 8:1 or greater.

Figure 4-119. NOA-containing plutonic rock, east of Searchlight, sample S1.

Table 4.34. Summary of sample type, depositional process, and mean and maximum aspect ratios for samples in the Searchlight Region.

SEARCHLIGHT REGION							
Sample ID	**N**	**Mean Aspect Ratio**	**Maximum Aspect Ratio**	**Aspect Ratio Cutoff 8+**	**Aspect Ratio Cutoff 3+**	**Type**	**Depositional Process**
S030115-1	6	7.7	17.5	Positive	Positive	soil	road (alluvium)
S030115-2	6	8.1	17.9	Positive	Positive	soil	alluvium
S030115-3	2	6.6	9.0	Positive	Positive	soil	eolian
S030115-4	4	6.0	9.0	Positive	Positive	soil	alluvium
S030115-5	7	6.6	16.8	Positive	Positive	soil	road (alluvium)
S030115-6	7	7.4	13.4	Positive	Positive	soil	road (alluvium)
S030115-7	1	5.9	5.9	Negative	Positive	soil	eolian
S030115-8	3	5.6	8.2	Positive	Positive	soil	alluvium
S030115-9	1	12.4	12.4	Positive	Positive	soil	alluvium
S030115-10	8	10.8	23.8	Positive	Positive	soil	alluvium
S030115-11	6	7.2	9.5	Positive	Positive	soil	eolian
S030115-12	1	10.2	10.2	Positive	Positive	soil	eolian
S030115-13	8	5.1	8.0	Positive	Positive	soil	alluvium
S030115-14	3	5.1	8.0	Positive	Positive	soil	road (alluvium)
S030115-15	2	8.4	9.0	Positive	Positive	soil	alluvium
S030115-16	9	5.9	10.6	Positive	Positive	soil	road (alluvium)
S030115-17	5	5.0	6.7	Negative	Positive	soil	alluvium
S030115-18	2	7.2	7.9	Negative	Positive	soil	eolian
S030115-19	2	6.7	8.9	Positive	Positive	soil	road (alluvium)

Table 4.34 (continued). Summary of sample type, depositional process, and mean and maximum aspect ratios for samples in the Searchlight Region.

SEARCHLIGHT REGION (continued)							
Sample ID	**N**	**Mean Aspect Ratio**	**Maximum Aspect Ratio**	**Aspect Ratio Cutoff 8+**	**Aspect Ratio Cutoff 3+**	**Type**	**Depositional Process**
S030115-20	5	6.1	11.5	Positive	Positive	soil	road (alluvium)
S030115-21	6	9.4	17.8	Positive	Positive	soil	road (alluvium)
S030115-22	5	5.1	7.2	Negative	Positive	soil	alluvium
S030115-23	4	5.4	8.3	Positive	Positive	soil	alluvium
S030115-24	3	5.0	6.0	Negative	Positive	soil	eolian
S030115-25	6	8.3	11.9	Positive	Positive	soil	eolian
S030115-26	1	7.7	7.7	Negative	Positive	soil	alluvium
S030115-27	2	9.9	13.4	Positive	Positive	soil	road (alluvium)
S030115-28	1	4.9	4.9	Negative	Positive	soil	road (alluvium)
S030115-29	4	9.5	20.9	Positive	Positive	rock	rock
S030115-30	1	8.6	8.6	Positive	Positive	rock	rock
S030115-31	6	7.5	21.8	Positive	Positive	soil	alluvium
S030115-32	4	11.0	28.6	Positive	Positive	soil	alluvium
S030115-33	8	7.5	9.6	Positive	Positive	soil	eolian
S030115-34	4	6.2	8.9	Positive	Positive	soil	road (alluvium)
S030115-35	3	18.3	40.0	Positive	Positive	soil	eolian
S030115-36	6	7.8	14.7	Positive	Positive	soil	alluvium

Table 4.34 (continued). Summary of sample type, depositional process, and mean and maximum aspect ratios for samples in the Searchlight Region.

SEARCHLIGHT REGION (continued)							
Sample ID	**N**	**Mean Aspect Ratio**	**Maximum Aspect Ratio**	**Aspect Ratio Cutoff 8+**	**Aspect Ratio Cutoff 3+**	**Type**	**Depositional Process**
S030115-37	8	6.1	9.5	Positive	Positive	soil	alluvium
S030115-38	7	7.4	13.6	Positive	Positive	soil	eolian
S030115-39	6	8.3	17.0	Positive	Positive	soil	road (alluvium)
S030115-40	11	9.3	24.8	Positive	Positive	soil	road (alluvium)
S030115-41	19	7.9	18.7	Positive	Positive	soil	road (alluvium)
S030115-42	18	7.8	15.0	Positive	Positive	soil	road (alluvium)
S1	28	9.7	27.5	Positive	Positive	rock	rock
S2	5	15.1	40.3	Positive	Positive	rock	rock
S3	37	10.9	49.7	Positive	Positive	rock	rock
S4	10	10.4	27.1	Positive	Positive	rock	rock
S5	44	20.3	42.1	Positive	Positive	rock	rock
TOTAL =	**345**	**9.9**	**49.7**				

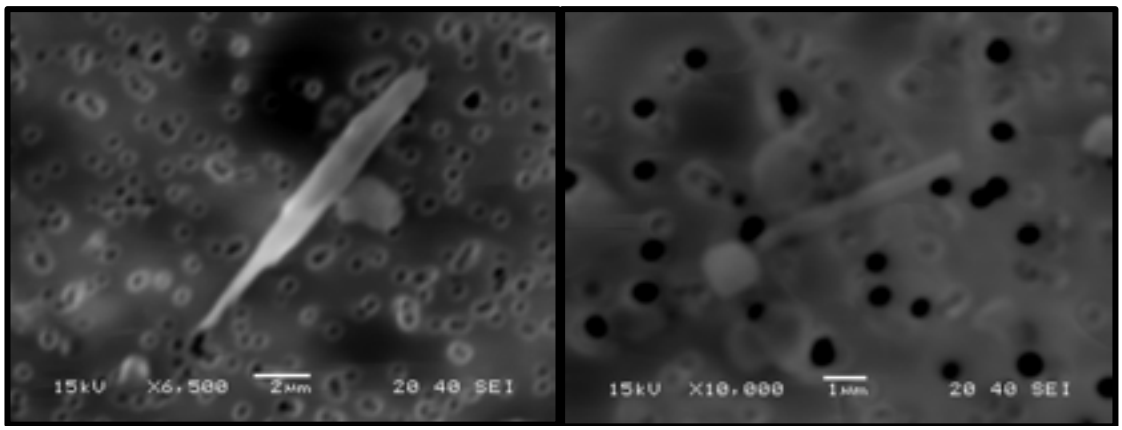

Figure 4-120. SEM image of magnesio-hornblende particle from sample S030115-9 (left) and sub-calcic amphibole fiber from sample S030115-12 (right).

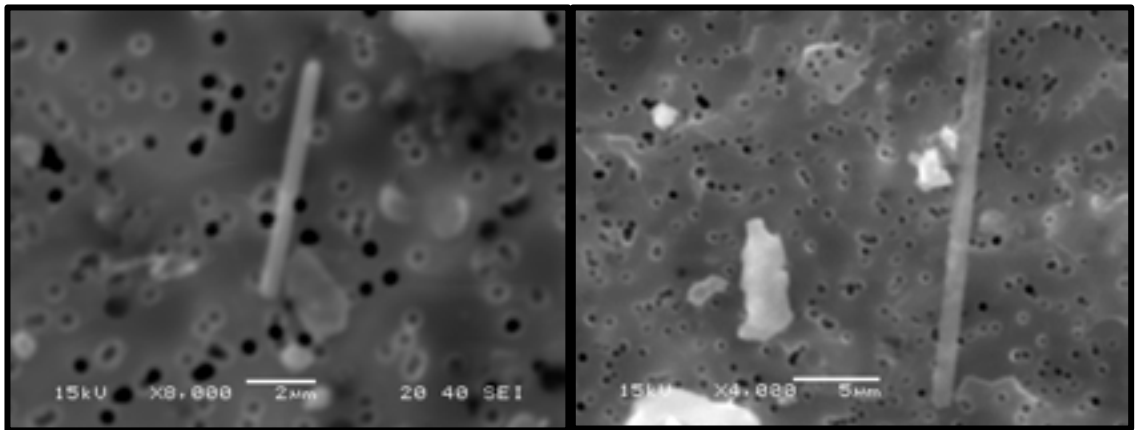

Figure 4-121. SEM image of magnesio-hornblende particle from sample S030115-20 (left) and edenite bundle form sample S030115-5 (right)

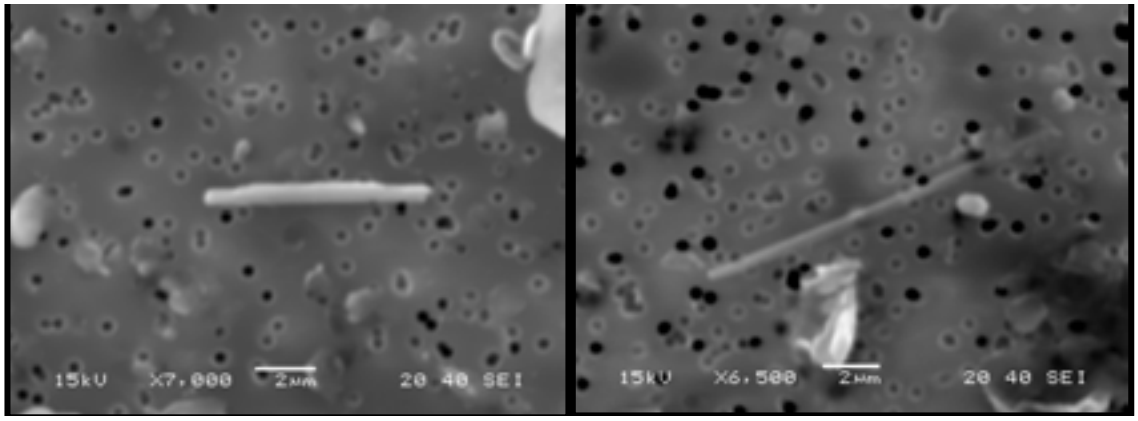

Figure 4-122. SEM image of actinolite amphibole fiber from sample S0301115-16 (left), and sub-calcic amphibole fiber from sample S030115-31 (right).

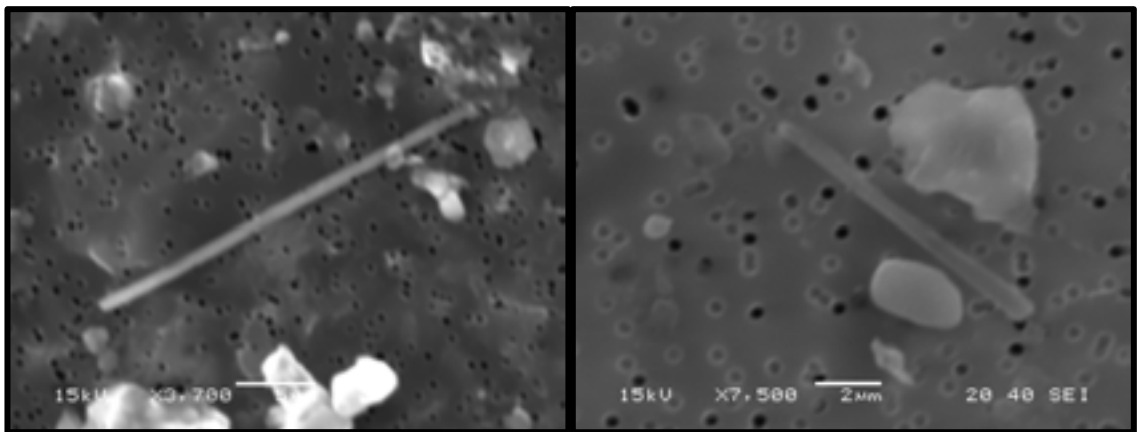

Figure 4-123. SEM image of actinolite amphibole fiber from sample S0301115-10 (left), and gedrite amphibole fiber from sample S030115-27 (right)

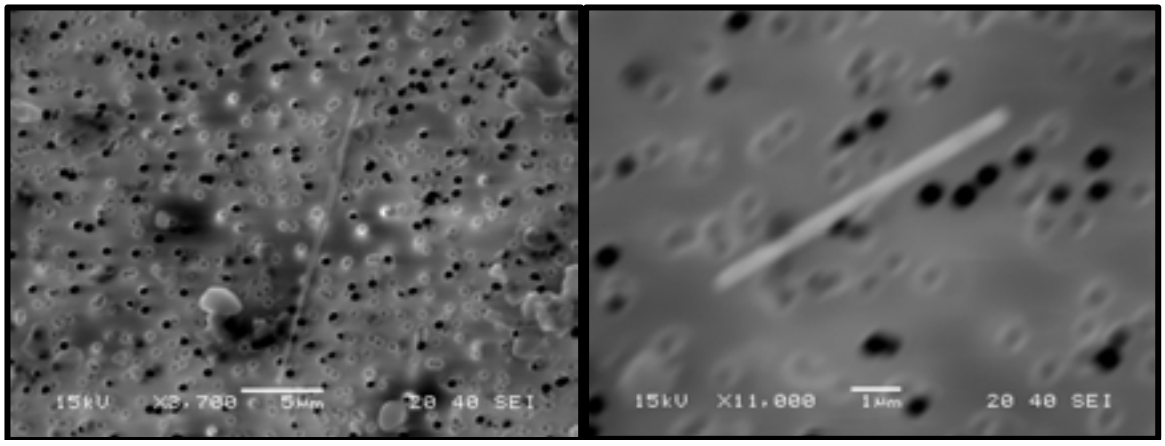

Figure 4-124. SEM image of sub-calcic amphibole fiber from sample S0301115-35 (left), and sub-calcic amphibole fiber from sample S030115-39 (right).

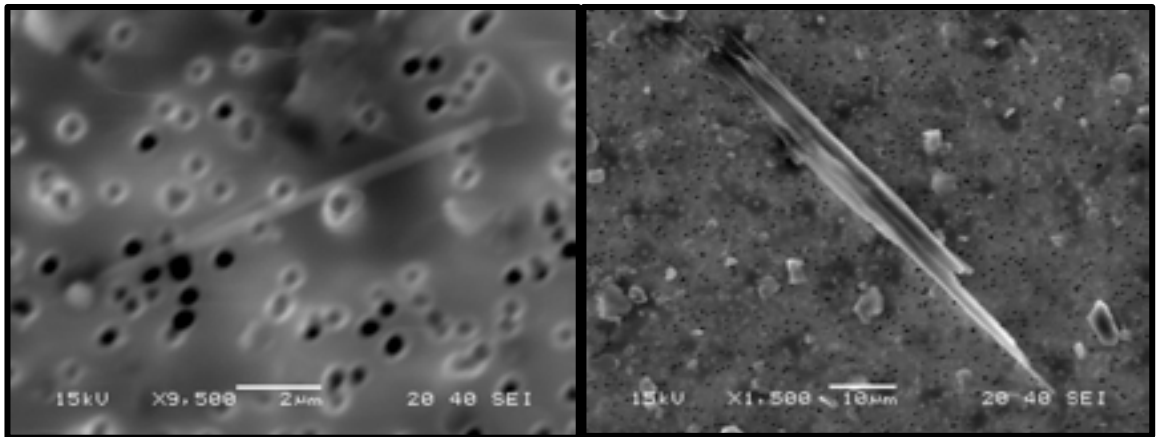

Figure 4-125. SEM image of actinolite amphibole fiber from sample S0301115-40 (left), and actinolite amphibole bundle from sample S030115-41 (right).

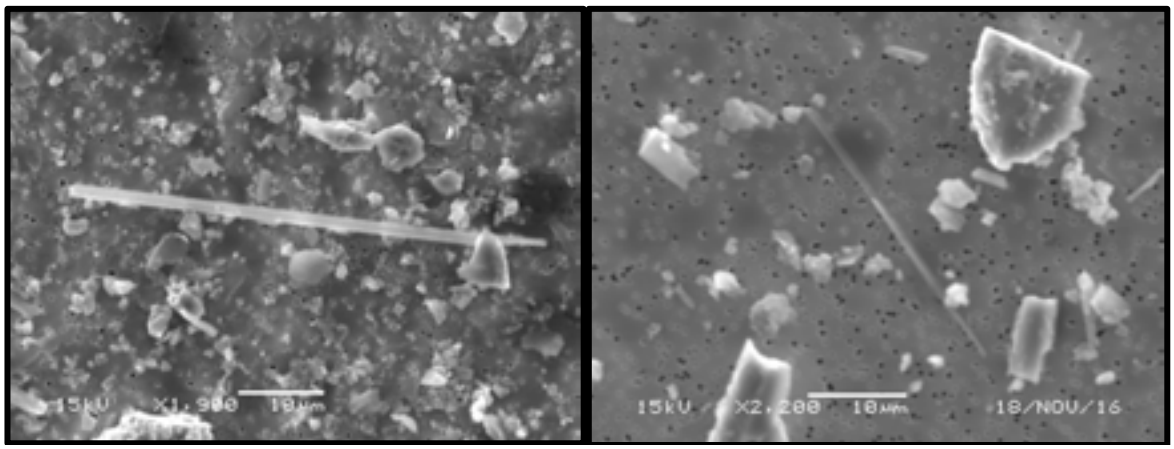

Figure 4-126. SEM image of actinolite amphibole (left) and magnesio-hornblende (right) from sample S5.

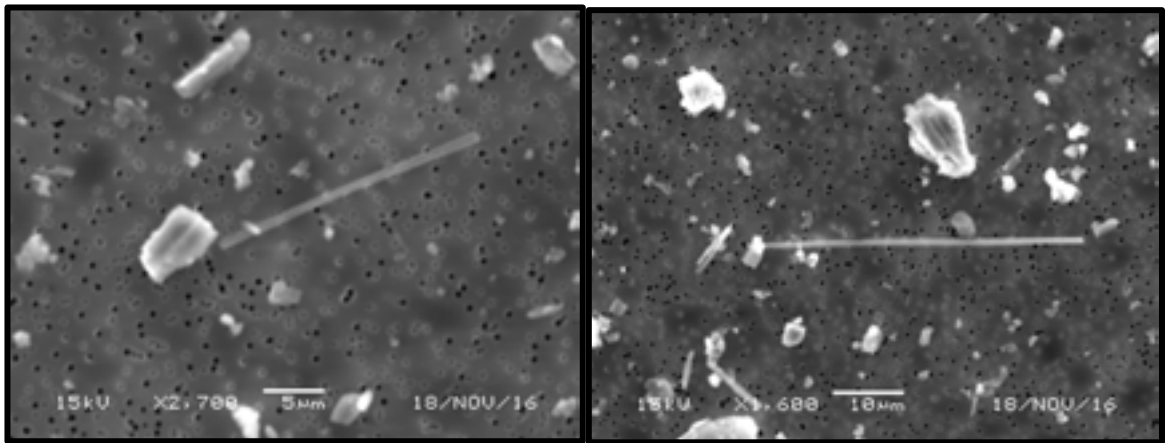

Figure 4-127. SEM image of sub-calcic amphibole (left) and actinolite (right) from sample S5.

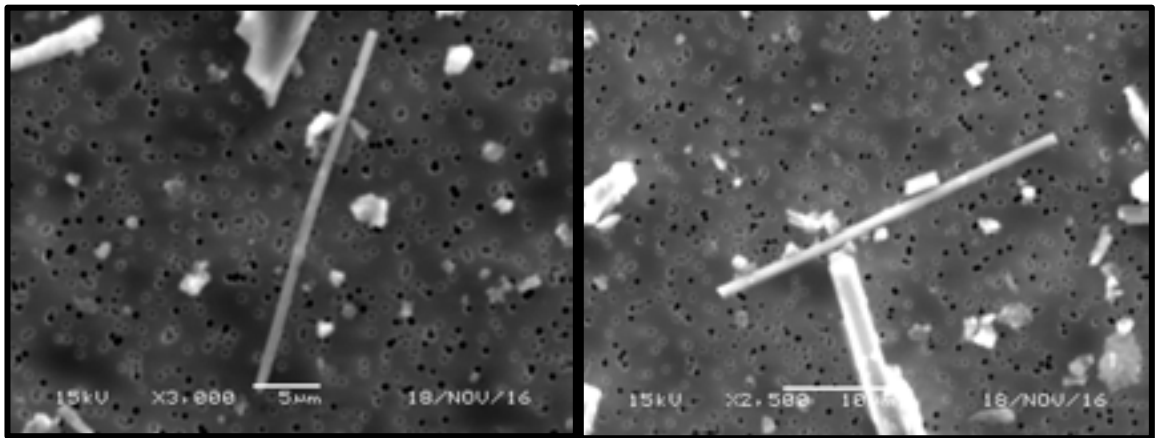

Figure 4-128. SEM images of actinolite amphibole fibers from sample S5.

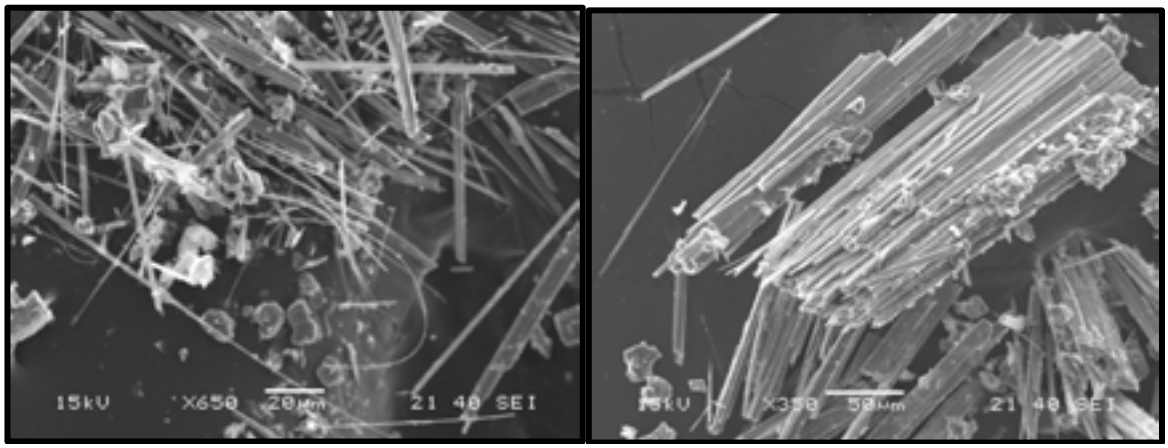

Figure 4-129. SEM images of amphibole fibers from sample S5. Notice bending of fibers on the left.

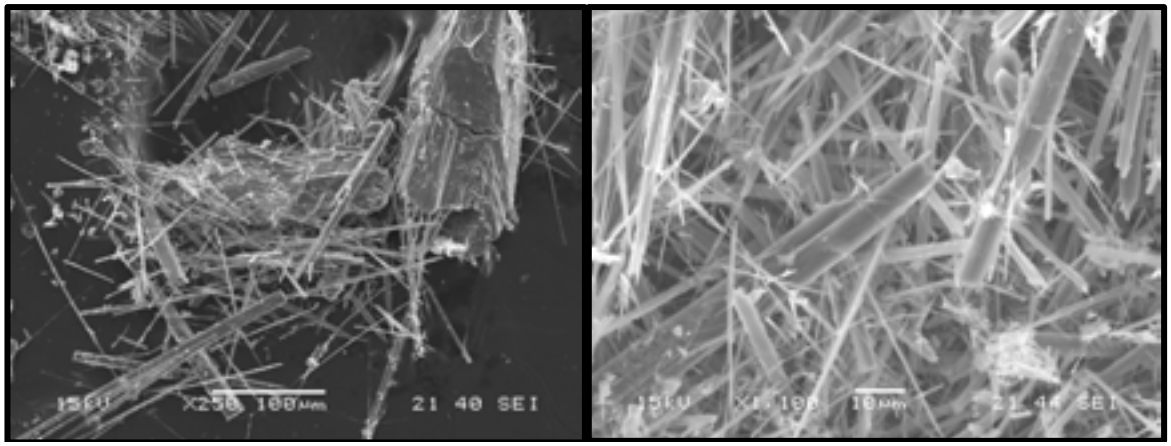

Figure 4-130. SEM images of amphibole fibers from sample S5.

The amphibole samples collected in the Searchlight region have a wide range of compositions including calcic, sub-calcic, Fe-Mg, sodic, and sodic-calcic groups (Table 4.35). Much more detailed work is needed in this area to understand their distributions and genesis (see Chapter 3). In contrast to other areas described in this report, in this group of data, the sodic and sodic-calcic groups did not have significantly greater aspect ratios as compared to the calcic group (Table 4.35).

The mean aspect ratio for the 47 samples in the Searchlight region was 9.9 ± 0.4, the maximum aspect ratio was 49.7 (Table 4.35). Bundles and fibers have greater mean aspect ratios as compared to prismatic crystals (Table 4.36). SEM images shown in Figures 4-120 to 4-130.

Figure 4-131. Photo of NOA-containing sediment draining east towards the Colorado River, from eroding plutonic rocks near the site of sample S1.

Table 4.35. Particle sizes and mineralogy results of amphibole particles in the El Dorado Region. Number of particles (N), standard error of the mean (S.E.)

Searchlight Region													
Mineralogy	**N**	**Minimum Width (µm)**	**Maximum Width (µm)**	**Mean Width (µm)**	**S.E.**	**Minimum Length (µm)**	**Maximum Length (µm)**	**Mean Length (µm)**	**S.E.**	**Minimum Aspect Ratio**	**Maximum Aspect Ratio**	**Mean Aspect Ratio**	**S.E.**
Edenite	10	0.7	2.8	1.5	0.2	5.9	21.8	12.0	1.8	4.3	16.8	8.6	1.2
Fe-hbld	1	0.9	0.9	0.9	-	5.3	5.3	5.3	-	5.9	5.9	5.9	-
Mg-hbld	73	0.6	22.0	1.8	0.3	2.9	85.5	14.4	1.6	3.0	49.7	9.5	0.9
Tschermakite	1	1.5	1.5	1.5	-	11.6	11.6	11.6	-	7.7	7.7	7.7	-
Actinolite	165	0.4	91.0	2.0	0.6	1.9	288.3	16.5	2.0	3.0	42.1	10.9	0.6
Gedrite	12	0.5	2.1	1.0	0.1	1.8	9.4	5.4	0.7	3.1	13.4	5.6	0.9
Anthophyllite	1	1.8	1.8	1.8	-	13.0	13.0	13.0	-	7.2	7.2	7.2	-
Mg-rieb	2	1.4	1.5	1.5	0.1	14.4	17.3	15.9	1.5	9.6	12.4	11.0	1.4
Richterite	1	1.1	1.1	1.1	-	9.5	9.5	9.5	-	8.6	8.6	8.6	-
Barrosite	1	1.5	1.5	1.5	-	26.7	26.7	26.7	-	17.8	17.8	17.8	-
Winchite	5	0.8	2.1	1.1	0.2	4.1	17.9	9.6	2.5	4.1	13.4	8.7	1.6
Calcic group	249	0.4	91.0	1.9	0.4	1.9	288.3	15.7	1.4	3.0	49.7	10.4	0.5
Sub-Calcic group	84	0.4	4.5	1.1	0.1	1.8	28.4	8.7	0.6	3.1	40.0	8.7	0.6
Fe-Mg group	3	1.0	2.7	1.6	0.6	5.9	15.3	10.5	2.7	5.7	10.3	7.3	1.5
Sodic group	3	1.1	1.5	1.3	0.1	9.5	17.3	13.7	2.3	8.6	12.4	10.2	1.1
Sodic-Calcic group	6	0.8	2.1	1.2	0.2	4.1	26.7	12.4	3.5	4.1	17.8	10.2	2.0
All Particles	**345**	**0.4**	**91.0**	**1.7**	**0.3**	**1.8**	**288.3**	**13.9**	**1.0**	**3.0**	**49.7**	**9.9**	**0.4**

Table 4.36. Morphology classification of particles analyzed in the Searchlight Region. Number of particles (N), standard error of the mean (S.E.)

Searchlight Region													
Morphology	**N**	**Minimum Width (µm)**	**Maximum Width (µm)**	**Mean Width (µm)**	**S.E.**	**Minimum Length (µm)**	**Maximum Length (µm)**	**Mean Length (µm)**	**S.E.**	**Minimum Aspect Ratio**	**Maximum Aspect Ratio**	**Mean Aspect Ratio**	**S.E.**
Bundles	58	1.1	91.0	4.4	1.6	5.4	288.3	28.2	5.2	3.2	31.6	10.3	0.9
Fibers (≤1 µm)	163	0.4	1.0	0.8	0.0	1.8	49.7	8.3	0.6	3.0	49.7	10.7	0.6
Prismatic Crystals	124	1.1	9.1	1.7	0.1	3.6	73.8	14.5	1.0	3.0	42.1	8.7	0.6
Total	**345**	**0.4**	**91.0**	**1.7**	**0.3**	**1.8**	**288.3**	**13.9**	**1.0**	**3.0**	**49.7**	**9.9**	**0.4**

Virgin Mountains Region

The Virgin Mountains Region refers primarily to an area in the Virgin Mountains, south of Mesquite NV, where previous mining had indicated that some of these rocks have undergone hydrothermal alteration (Figure 4-132). A total of 13 samples, 9 collected from alluvium and 4 collected from bedrock outcrops, were obtained and analyzed (Table 4.37). All tested positive for amphibole asbestos with aspect ratio of 3:1 or greater, and also for aspect ratios of 8:1 or greater (Figures 4-133 to 4-135).

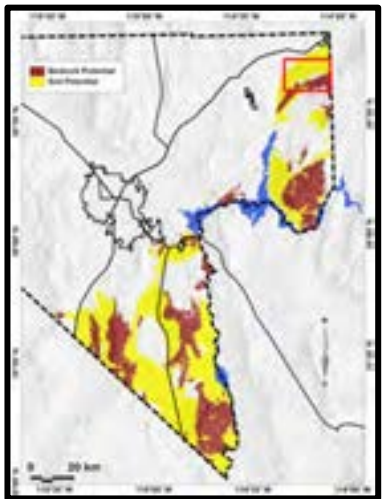

Figure 4-132. Map of southern Nevada showing predicted NOA-containing areas with the Virgin Mountains region outlined in red box.

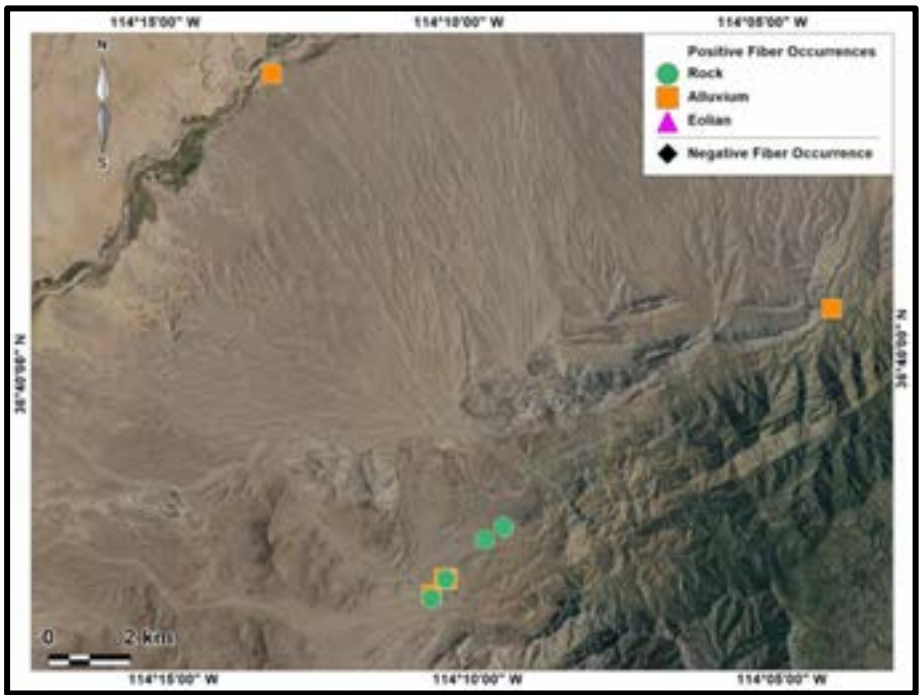

Figure 4-133. Map of Virgin Mountains region sample locations. Positive occurrences are for amphibole asbestos with aspect ratios of both 3:1 and 8:1 or greater. Samples are identified according to the geological process that deposited the material: bedrock (in place), alluvium (water-deposited), or eolian (wind-deposited).

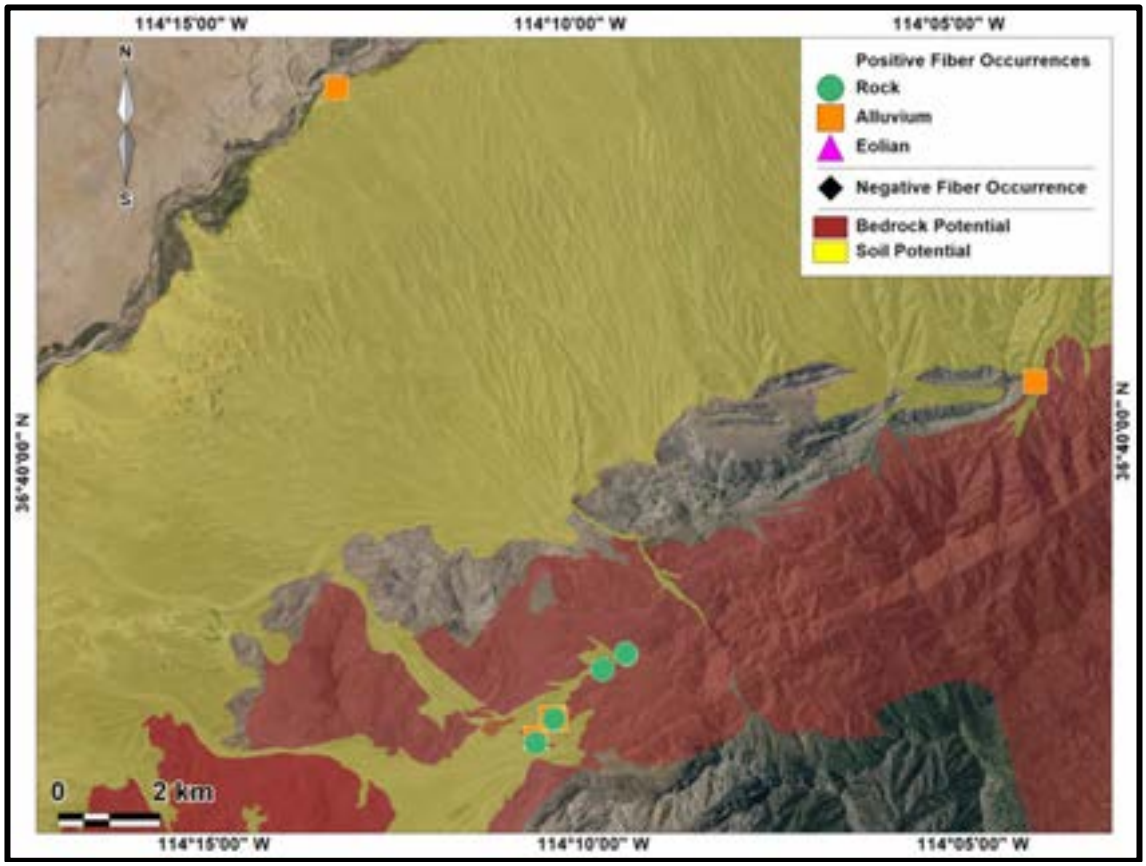

Figure 4-134. Map of sample locations in the Virgin Mountains region with predicted occurrences of NOA based on alluvial (water-transported) surficial processes that transport material from the source rock out into the basin. Bedrock potential represents areas of potential occurrence for amphibole asbestos in igneous and metamorphic rock exposures. Soil potential delineates areas where runoff could potentially distribute amphibole asbestos fibers downslope from bedrock areas. Positive occurrences are for amphibole asbestos with aspect ratios of both 3:1 and 8:1 or greater.

Figure 4-135. Highly weathered, NOA-containing amphibolite in Virgin Mountains, site of sample V042316-5.

Table 4.37. Summary of sample type, depositional process, and mean and maximum aspect ratios for samples in the Virgin Mountains region.

VIRGIN MOUNTAINS							
Sample ID	**N**	**Mean Aspect Ratio**	**Maximum Aspect Ratio**	**Aspect Ratio Cutoff 8+**	**Aspect Ratio Cutoff 3+**	**Type**	**Depositional Process**
V1	46	9.8	31.3	Positive	Positive	rock	alluvium
V2	25	15.6	39.2	Positive	Positive	rock	rock
V3	34	8.2	15.8	Positive	Positive	rock	alluvium
V-042315-1	21	6.4	22.7	Positive	Positive	rock	alluvium
V-042315-2	32	10.2	29.5	Positive	Positive	rock	rock
V-042315-3	30	7.1	19.2	Positive	Positive	rock	alluvium
V-042315-4	14	8.1	20.5	Positive	Positive	rock	alluvium
V-042315-5	17	6.3	13.8	Positive	Positive	rock	rock
V-042315-6	54	9.9	28.8	Positive	Positive	rock	alluvium
V-042315-7	23	6.6	14.0	Positive	Positive	rock	alluvium
V-042315-8	44	9.6	18.4	Positive	Positive	rock	alluvium
V-042315-9	39	9.7	17.2	Positive	Positive	rock	rock
V-042315-10	22	6.9	11.7	Positive	Positive	rock	rock
TOTAL =	**401**	**9.1**	**39.2**				

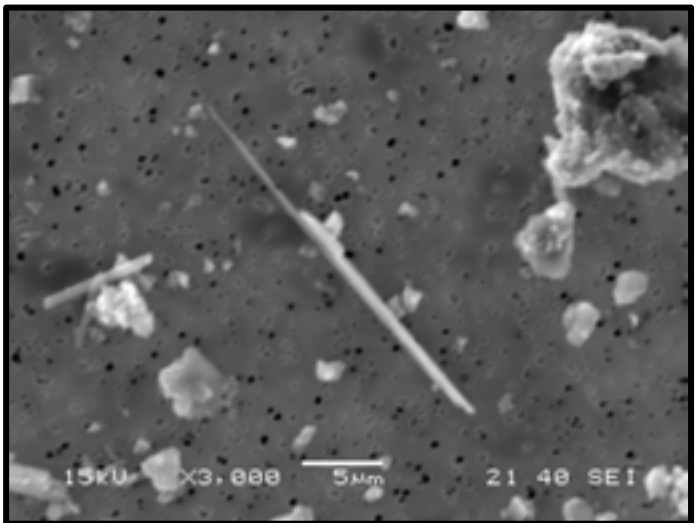

Figure 4-136. SEM image of actinolite amphibole from sample V1.

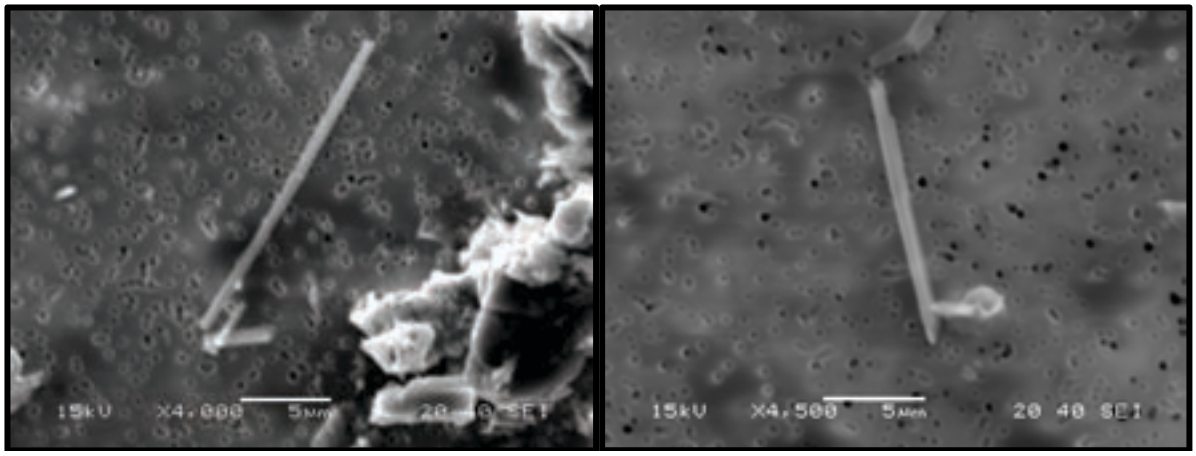

Figure 4-137. SEM image of sodic-calcic amphibole fibers from sample V2, similar mineralogy as asbestos from Libby Montana.

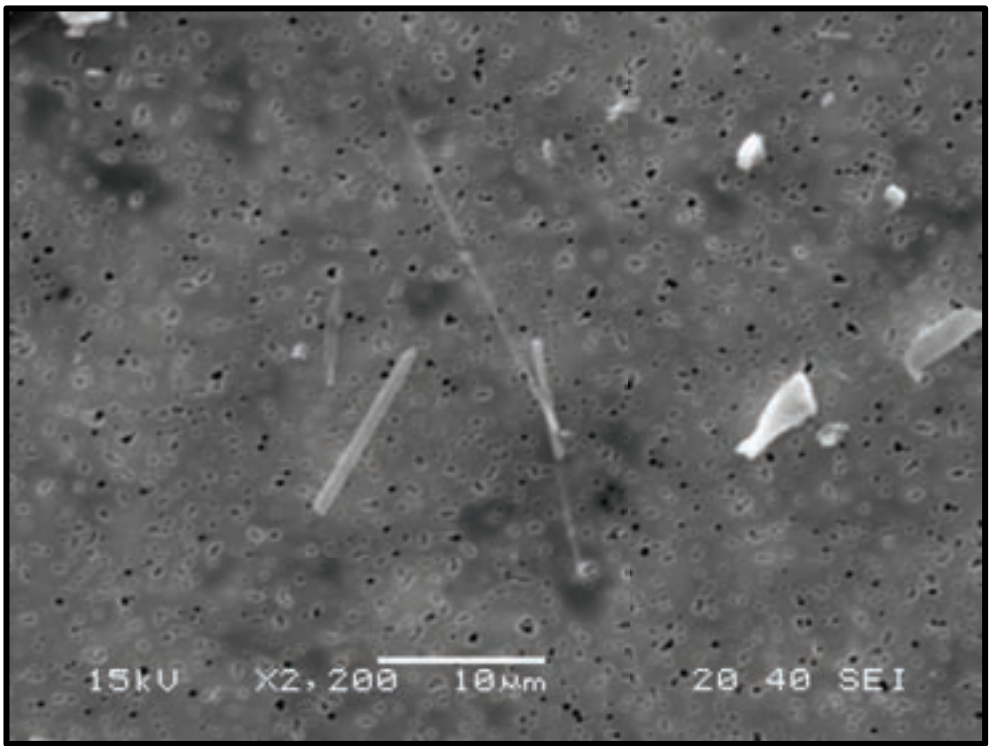

Figure 4-138. SEM image of numerous amphibole fibers from sample V2.

The amphibole samples collected in the Virgin Mountains region have a wide range of compositions including calcic, sub-calcic, Fe-Mg, and sodic-calcic groups (Table 4.38). Amphibole particles with Fe-Mg and sodic-calcic compositions have higher mean aspect ratios than compared to the other compositions in this area (Table 4.38).

The mean aspect ratio for the 13 samples in the Virgin Mountains region was 9.1 ± 0.2, the maximum aspect ratio was 39.2 (Table 4.38). Fibers have a greater mean aspect ratio as compared to bundles and prismatic crystals (Table 4.39). SEM images shown in Figures 4-136 to 4-138.

Figure 4-139. Photos of weathered NOA-containing biotite schist grading into amphibolite w/quartz veins. Sample V042316-10

Table 4.38. Particle sizes and mineralogy results of amphibole particles in the Virgin Mountains Region. Number of particles (N), standard error of the mean (S.E.)

Virgin Mountains Region													
Mineralogy	**N**	**Minimum Width (µm)**	**Maximum Width (µm)**	**Mean Width (µm)**	**S.E.**	**Minimum Length (µm)**	**Maximum Length (µm)**	**Mean Length (µm)**	**S.E.**	**Minimum Aspect Ratio**	**Maximum Aspect Ratio**	**Mean Aspect Ratio**	**S.E.**
Actinolite	98	0.4	3.3	1.2	0.1	2.9	34.4	9.7	0.6	3.1	31.3	8.3	0.4
Edenite	28	0.7	7.4	1.4	0.2	3.3	95.3	12.3	3.2	3.7	14.9	8.4	0.6
Fe-hornblende	1	1.1	1.1	1.1	-	3.9	3.9	3.9	-	3.5	3.5	3.5	-
Mg-hblnd	184	0.4	44.9	1.7	0.3	2.7	145.9	12.7	1.1	3.2	29.5	9.0	0.4
Anthophylite	1	1.0	1.0	1.0	-	4.5	4.5	4.5	-	4.5	4.5	4.5	-
WMRR	16	0.5	1.2	0.7	0.1	4.4	23.5	12.1	1.3	8.8	39.2	16.9	1.7
Winchite	3	0.6	0.8	1.4	0.1	5.5	15.3	10.8	2.9	6.9	19.2	15.1	4.1
Calcic group	311	0.4	44.9	1.5	0.2	2.7	145.9	11.7	0.7	3.1	31.3	8.7	0.3
Sub-Calcic group	68	0.3	19.7	1.5	0.3	2.0	103.0	10.7	1.8	3.3	22.7	8.5	0.4
Fe-Mg group	2	1.0	1.0	1.0	0.0	4.5	20.1	12.3	7.8	4.5	20.1	12.3	7.8
Sodic-Calcic group	20	0.5	1.2	0.8	0.0	4.4	23.5	12.5	1.1	8.8	39.2	16.8	1.4
All Particles	**401**	**0.3**	**44.9**	**1.5**	**0.1**	**2.0**	**145.9**	**11.6**	**0.7**	**3.1**	**39.2**	**9.1**	**0.2**

Table 4.39. Morphology classification of particles analyzed in the Virgin Mountains Region. Number of particles (N), standard error of the mean (S.E.)

Virgin Mountains Region													
Morphology	**N**	**Minimum Width (µm)**	**Maximum Width (µm)**	**Mean Width (µm)**	**S.E.**	**Minimum Length (µm)**	**Maximum Length (µm)**	**Mean Length (µm)**	**S.E.**	**Minimum Aspect Ratio**	**Maximum Aspect Ratio**	**Mean Aspect Ratio**	**S.E.**
Bundles	66	1.1	44.9	3.1	0.7	4.7	145.9	20.9	2.8	3.2	29.5	9.0	0.6
Fibers (≤1 µm)	193	0.3	1.0	0.8	0.0	2.0	25.0	7.7	0.3	3.4	39.2	10.3	0.4
Prismatic Crystals	142	1.1	8.3	1.6	0.1	3.5	115.3	12.5	1.1	3.1	28.8	7.6	0.4
Total	**401**	**0.3**	**44.9**	**1.5**	**0.1**	**2.0**	**145.9**	**11.6**	**0.7**	**3.1**	**39.2**	**9.1**	**0.1**

Summary

In southern Nevada and northwestern Arizona, NOA occurs in hydrothermally-altered plutonic rocks, metamorphic rocks, and in sedimentary rocks and sediments that have formed from the erosion, transport, and deposition of these NOA-containing rocks. In this study, we produced hazard maps predicting bedrock and alluvium (e.g. soil) that contain NOA. Our results mapped 1,093,000 acres in southern Nevada predicted to contain NOA. The majority of these acres are alluvium, 689,000 acres, compared to approximately 404,000 acres of bedrock. This is approximately 20% of Clark County. These numbers DO NOT include acres that may contain NOA as a result of eolian processes (e.g. vast areas in southern Nevada that containing vesicular horizons see Figures 4-3 and 4-4 for areas that tested positive for eolian samples).

In response to a UNLV-EPA joint study (Buck et al., 2016) that found evidence for the carcinogenic mineral erionite present in Boulder City, the El Dorado dry lake bed (playa) and Nellis Dunes, we tested 40 samples of altered volcanic ash and found no evidence of erionite in any of our samples. The potential source(s) for the erionite in the Buck et al., 2016 study are still unknown.

The size/shape of asbestos particles is an important parameter for toxicity (Aust et al., 2011). Particles that have a higher aspect ratio (e.g. are longer and thinner) are considered more toxic (e.g. Aust et al., 2011). We analyzed over 6000 particles in this study, of which 2555 were identified as amphibole minerals (see Chapter 2). The mean aspect ratio of all the amphibole particles was 8.8 ± 0.1 (Table 4.1-4.4). These can be divided into 5 groups of amphiboles: (1) calcic (2) sub-calcic (3) sodic (4) sodic-calcic and (5) Fe-Mg (Table 4.1). The vast majority of the amphiboles in southern Nevada are calcic composition, commonly actinolite or magnesiohornblende. The calcic group of amphiboles have a mean aspect ratio of 8.2 ± 0.1, which is the lowest mean aspect ratio of the 5 groups of amphiboles (Table 4.1). In contrast, the sodic and sodic-calcic groups have significantly higher mean aspect ratios: 21.0 ± 2.4, and 14.8 ± 1.0 respectfully (Table 4.1). Similarly, when we compare individual amphibole mineralogy and mean aspect ratio (Table 4.2), the sodic and sodic-calcic groups consistently have greater mean aspect ratios. This suggests that the sodic and sodic-calcic amphibole compositions may be more toxic than the calcic and sub-calcic compositions, however toxicity is complicated and is affected by more factors than aspect ratio (e.g. Aust et al., 2011).

In this study, we divided southern Nevada into 11 regions: El Dorado Mountains, Gold Butte, Highland Mountains, Ireteba Mountains, Jean-Primm, Las Vegas, Laughlin, Nellis Dunes, Nelson Road, Searchlight, and the Virgin Mountains. The regions with the greatest mean aspect ratios, suggesting increased toxicity, include: El Dorado (12.5 ± 0.7), Searchlight (9.9 ± 0.4), and the Virgin Mountains Virgin (9.1 ± 0.1). Those with slightly lower mean aspect ratios include Jean-Primm region (8.6 ± 0.5), Gold Butte (8.4 ± 0.5), and the Highland (8.1 ± 0.5) and Ireteba (8.1 ± 0.3) mountains regions. These areas may be slightly less hydrothermally altered than the El Dorado, Searchlight and Virgin mountains regions therefore resulting in slightly lower aspect ratios. Similarly, the

Nelson Road and Laughlin areas also had slightly lower mean aspect ratios: Nelson Road (7.6 ± 0.3); Laughlin (7.5 ± 0.3). The regions with comparably lower mean aspect ratios include those that are dominated by eolian processes and include: Las Vegas region (7.2 ± 0.3) and Nellis Dunes (5.7 ± 1.2).

This study found that erosion, transport, and deposition by wind can play a large role in increasing the footprint of the NOA hazard in southern Nevada. Of a total of 52 eolian samples tested in this study, only 5 did not test positive for NOA at aspect ratios of 3:1 or greater. This supports the interpretation that NOA-distribution via wind, especially in arid and semi-arid environments, can be widespread and can occur great distances from the alluvial and bedrock sources of NOA (Figures 4-3 and 4-4). This is not surprising, since eolian processes are extremely important in the Mojave Desert and vast areas of our landscape contain vesicular horizons. It has long been known that disturbance of desert pavements and biological soil crusts with associated underlying vesicular horizons can lead to significantly increased dust emissions. This study indicates that many of these areas may hold an additional hazard: NOA. Therefore, the results of this study indicate that the potential for NOA to be present should be considered when making land use decisions that will disrupt soils containing vesicular horizons.

In a previous study, Buck et al., 2013 found no difference between asbestos particles in rocks versus those moved by water or wind across the landscape. In this study, we found that the mean aspect ratios of eolian-deposited NOA particles are significantly different and lower than those deposited by alluvial processes or those found in bedrock (Table 4.6). However, there was no statistical difference between mean aspect ratios of bedrock and alluvium (Table 4.6). This suggests that one or more processes are affecting the physical shape of the amphibole particles as they erode out of the bedrock and are transported across the landscape. The lower aspect ratios of eolian NOA particles may be the result of wind erosion, transport, and deposition processes that physically break these particles resulting in lower aspect ratios than particles found in bedrock or alluvium. On the other hand, it could also be that wind processes do a better job of sorting amphibole particles so that eolian deposits contain more NOA particles that are shorter/wider than those found in bedrock and alluvium. More work is needed to understand how geological processes affect the distribution and morphology (and therefore toxicity) of NOA particles across the landscape.

The presence of NOA in southern Nevada is a hazard because even small amounts of NOA carry some finite level of risk. The level of risk may be higher in arid and semi-arid climates because of the increased potential for dust emissions. In areas that contain NOA, natural wind and/or anthropogenic activities that generate dust emissions from those surfaces will increase asbestos concentrations in air. Although we did not measure airborne concentrations of asbestos, a previous study did do this for the northern portion of the El Dorado Basin as part of a study to develop a mitigation plan for building the Boulder City Bypass, a portion of Interstate 11 (Tetra Tech, 2014).

In this study, ambient air was measured during the summer of 2014 (May 8-August 9) in the Railroad Pass area between Boulder City and Henderson (Tetra Tech, 2014). The mean for those months was 0.00021 f/cc. To understand how this value compares to health risk, we can compare this to the inhalation reference concentration (RfC) (non-cancer disease) for exposure to "Libby-type" amphiboles (U.S. EPA, 2014). This is expressed in terms of lifetime exposure (assumed to be 70 yrs): fibers per cubic centimeter of air (f/cc). The RfC value is 0.00009 f/cc. This information indicates how exceedingly low airborne concentrations can cause human disease. Due to their extremely small size, these fibers are invisible in air and therefore people are commonly not aware of their exposures. This means that if a person inhales this value or less everyday over their lifetime, they will not have an increased risk for disease. However, the results of the Tetra Tech (2014) study for the Boulder City area was 2.3 times higher than the RfC. This suggests that ambient air in this region contains 2.3 times more fibers than is considered safe for non-cancer disease. It is important to note however, that these data represent only one summer of research which also saw unusually high rain events, which decreased dust emissions (Figure 4-140). In addition, it is not yet known if all amphibole minerals behave similarly in the human body and this RfC value is based on the Libby-type minerals only. As discussed previously, southern Nevada contains primarily calcic group amphiboles, commonly actinolite and magnesio-hornblende, and contains fewer occurrences of the Libby-type minerals. However, the Libby-type minerals dominate some areas in this region, and are particularly common in the Lake Mead area of Wilson Ridge in northwestern Arizona (see also Figures 4-11 and 4-12).

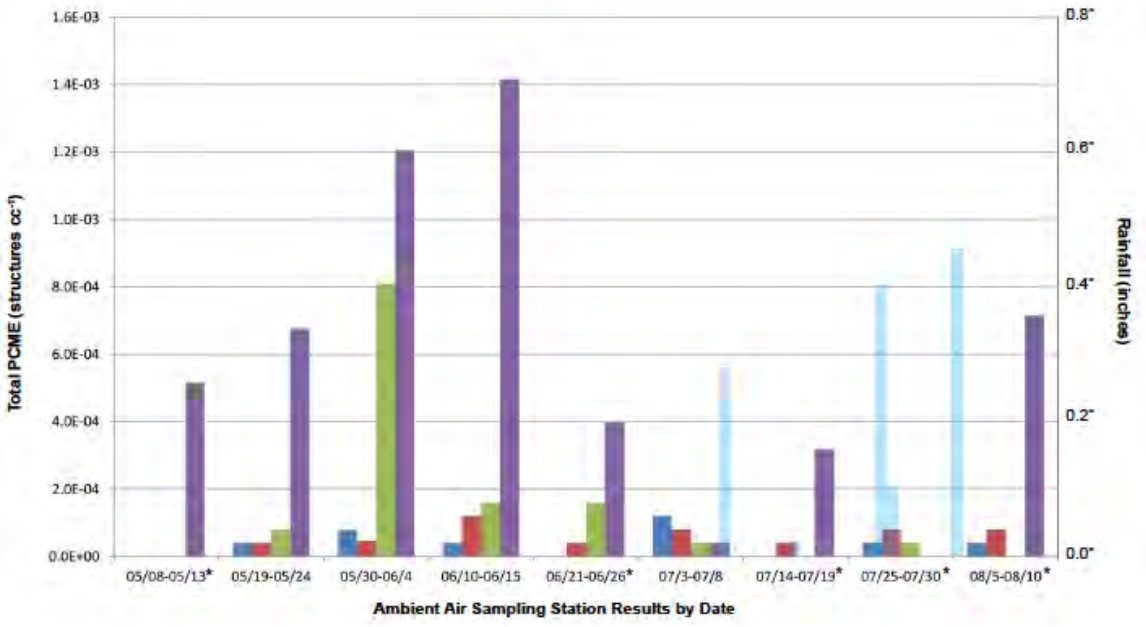

Figure 4-140. From Tetra Tech, Report to NDOT, 2014. The colors represent different stations (a total of 4). The light blue bars show rainfall in inches.

Many more airborne concentrations of NOA need to be collected in order to better understand risk to human populations, but these values do suggest that some combination of aridity and human activities are able to generate concentrations of airborne asbestos that may be of concern in southern Nevada.

Possible land-management solutions to lower asbestos emissions would include any mechanism that lessens human activities on surfaces known or predicted to contain NOA. Dust suppression techniques such as applying water, dust suppressants, or other mitigation techniques could also be utilized to decrease exposures. Additionally, several organizations in the USA Federal Government have recommendations on how to decrease exposures to NOA. **These are attached as appendices to this report.**

The State of Nevada currently does not have regulations pertaining to naturally occurring asbestos. However, regulations for occupational exposure may be applicable for some situations, and for those one should consult the Occupational Safety and Health Administration regulations for asbestos.

References

Anderson, R. E., 1977, Geologic map of the Boulder City 15-minute quadrangle, Clark County, Nevada: U.S. Geological Survey Map GQ-1395, scale 1:62500.

Artvinli, M. M., and Baris¸, Y. I., 1979. Malignant mesotheliomas in a small village in the Anatolian region of Turkey—an epidemiologic study. *Journal of the National Cancer Institute*, 63(1), 17–22.

Aust, A., P. Cook, and R. Dodson. 2011. Morphological and chemical mechanisms of elongated particle toxicities. *J. Toxicol. Environ. Health*, Part B 14:40–75. doi:10.1080/10937404.2011.556046

Bargar, K.E. and Keith, T.E.C. (1995) Calcium zeolites in rhyolitic drill cores from Yellowstone National Park. *In*: Ming, D.W. and Mumpton, F.S. (eds.) *Natural Zeolites '93*, International Committee on Natural Zeolites, Brockport, New York, 69-86.

Baris¸, Y. I., Sahin, A. A., Ozesmi, M. M., Kerse, I. I., Ozen, E. E., Kolcan, B. B., et al. (1978). An outbreak of pleural mesothelioma and chronic fibrosing pleurisy in the village of Karain/Urgu¨p in Anatolia. *Thorax*, 33(2), 181–192.

Baris¸, I., Simonato, L., Artvinli, M., Pooley, F., Saracci, R., Skidmore, J., et al. (1987). Epidemiological and environmental evidence of the health effects of exposure to erionite fibers—a four-year study in the Cappadocian region of Turkey. *International Journal of Cancer*, 39(1), 10–17.

Baris¸, Y. I., & Grandjean, P. P. (2006). Prospective study of mesothelioma mortality in Turkish villages with exposure to fibrous zeolite. Journal of the National Cancer Institute, 98(6), 414–417.

Bingler, E. C., and Bonham, H. F. J., 1973, Reconnaissance geologic map of the McCullough Range and adjacent areas, Clark County, Nevada: Nevada Bureau of Mines and Geology Map 45, scale 1:125,000.

Buck, B.J., Goossens, D. Metcalf, R.V., McLaurin, B., Ren, M., and Freudenberger*, F., 2013, Naturally occurring asbestos: Potential for human exposure, southern Nevada USA, *Soil Science Society of America Journal,* 77:2192-2204. doi:10.2136/sssaj2013.05.0183

Buck, B.J., Metcalf, R.V., Berry, D., McLaurin, B., Kent, D., Goossens, D., Januch, J., 2016. Naturally occurring asbestos in soils, southern Nevada: Interpretations for wind distribution and human exposure. Geological Society of America Abstracts with Programs. Vol. 48, No. 7 doi: 10.1130/abs/2016AM-278831

Campbell, W., R. Blake, L. Brown, E. Cather, and J. Sjoberg. 1977. Selected silicate minerals and their asbestiform varieties: Mineralogical definitions and identification-characterization. Inf. Circ. 8751. U.S. Bureau of Mines, Washington, DC.

Capps, R. C., 1997, Geologic map of the Castle Mountains, San Bernardino County, California and Clark County, Nevada: Nevada Bureau of Mines and Geology Map 108, scale 1:24000.

Carbone, M., Emri, S., Dogan, U., Steele, I., Tuncer, M., Pass, H. I., et al. (2007). A mesothelioma epidemic in Cappadocia—scientific developments and unexpected social outcomes. *Nature Reviews Cancer*, 7, 147–154.

Carbone, M., Baris¸, Y. I., Bertino, P., Brass, B., Comertpay, S., Dogan, A. U., et al. (2011). Erionite exposure in North Dakota and Turkish villages with mesothelioma. *Proceedings of the National Academy of Sciences of the United States of America,* 108(33), 13618–13623.

Castor, S.B., 2008, The Mountain Pass rare-earth carbonatite and associated ultrapotassic rocks, California: Canadian Mineralogist, v. 46, p. 779–806, doi:10.3749/canmin.46.4.779

Coffin DL, Cook PM, Creason JP (1992) Relative mesothelioma induction in rats by mineral fibers: Comparison with residual pulmonary mineral fiber number and epidemiology. *Inhal Toxicol* 4:273–300.

Cook, P.M., Swintek, J., Dawson, T., Chapman, D., Etterson, M., and Hoff, D., 2016. Quantitative structure-mesothelioma potency model optimization for complex mixtures of elongated particles I rat pleura: A retrospective study. *Journal of Toxicology and Environmental Health*, Part B, 19:5-6, 266-288, DOI: 10.1080/10937404.2016.1195326

Dee, S., Hinz, N. H., Anderson, R. E., and Johnsen, R., 2016, Preliminary geologic map of the Boulder City quadrangle, Clark County, Nevada: Nevada Bureau of Mines and Geology Open-File Report 2016-04, scale 1:24000.

Faulds, J. E., Bell, J. W., and Olson, E. L., 2002, Geologic map of the Nelson SW quadrangle, Clark County, Nevada Nevada Bureau of Mines and Geology Map 134, scale 1:24000.

Faulds, J. E., Ramelli, A. R., and Castor, S. B., 2010, Preliminary geologic map of the Searchlight quadrangle, Clark County, Nevada Nevada Bureau of Mines and Geology Open-File Report 2010-13 scale 1:24000.

Felger, T.J., and L.S. Beard. 2010. Geologic map of Lake Mead and surrounding regions, southern Nevada, southwest Utah, and northwestern Arizona, in, Umhoefer et al., editors, Miocene tectonics of the Lake Mead region, Central Basin and Range: Geological Society of America Special Paper 463, p. 29–38.

Hinz, N. H., Faulds, J. E., and Ramelli, A. R., 2012a, Preliminary geologic map of the north half of the Fourth of July Mountain quadrangle, Clark County, Nevada: Nevada Bureau of Mines and Geology Open-File Report 2012-08, scale 1:24000.

Hinz, N. H., Faulds, J.E., Ramelli, A.R., and Green, H.L., 2012b, Preliminary geologic map of the Ireteba Peaks quadrangle, Clark County, Nevada: Nevada Bureau of Mines and Geology Open File Report 2012-09, scale 1:24000.

Goossens, D. and Buck, B., 2011, Effects Of Wind Erosion, Off-Road Vehicular Activity, Atmospheric Conditions And The Proximity Of A Metropolitan Area On PM10 Characteristics In A Recreational Site. *Atmospheric Environment.* 45:94-107

Goossens, D., Buck, B., and McLaurin, B., 2012, Contributions to atmospheric dust production of natural and anthropogenic emissions in a recreational area designated for off-road vehicular activity (Nellis Dunes, Nevada, USA): Journal of Arid Environments, v. 78, p. 80-99.

Hay, R.L., & Sheppard, R.A. (2001). Occurrence of zeolites in sedimentary rocks—an overview. D.L. Bish, & D.W. Ming (Eds.), Natural zeolites—Occurrence, properties, applications (pp. 217–234).Washington,DC: The Mineralogical Society of America, Reviews in Mineralogy and Geochemistry, 45.

Hill RJ, Edwards RE, Carthew P (1990) Early changes in the pleural mesothelium following intrapleural inoculation of the mineral fibre erionite and the subsequent development of mesotheliomas. *J Exp Pathol* (Oxford) 71:105–118.

Hose, R. K., 1980, Geologic map of the Virgin Mountains Instant Study Area, Clark County, Nevada: U.S. Geological Survey Miscellaneous Field Studies Map 1204-A, scale 1:62500.

House, P.K., H. Green, and A. Grimmer, and Nevada Digital Dirt Mapping Team. 2010a. Preliminary surficial geologic map of Clark County, Nevada: Nevada Bureau of Mines and Geology Open-File Rep. 2010-7, scale 1:150,000.

House, P.K., Buck, B.J., and Ramelli, A.R., 2010b, Geologic assessment of piedmont and playa flood hazards in the Ivanpah Valley area, Clark County, Nevada (online only): Nevada Bureau of Mines and Geology Report 53.
http://www.nbmg.unr.edu/Pubs/r/r53/index.html

International Agency for Research on Cancer (IARC), 2012. Agents classified by the IARC Monographs, Volumes 1–105.
http://monographs.iarc.fr/ENG/Classification/index.php.

Kleinfelder, 2014. Interstate 11 – Boulder City Bypass Phase 2 Design Build Project Geologic Evaluation, Sampling and Testing for naturally-occurring asbestos, Boulder

City, Clark County, Nevada (Accessed Nov. 17, 2018) http://www.rtcsnv.com/wp-content/uploads/2012/07/LAS14R02679-Final-Text-thru-Appendix-A.pdf.

Lamb, M. A., Martin, K. L., Hickson, T. A., Umhoefer, P. J., and Eaton, L., 2010, Stratigraphy and age of the Lower Horse Spring Formation in the Longwell Ridges area, southern Nevada: Implications for tectonic interpretations, in Umhoefer, P. J., Beard, L. S., and Lamb, M. A., eds., Miocene Tectonics of the Lake Mead Region, Central Basin and Range: Geological Society of America Special Paper 463, p. 171-212.

Langella, A., Cappelletti, P., & de´ Gennaro, M. (2001). Zeolites in closed hydrologic systems. In D.L. Bish, & D.W. Ming (Eds.), Natural zeolites—Occurrence, properties, applications (pp. 235–260). Washington, D.C.: The Mineralogical Society of America, Reviews in Mineralogy and Geochemistry, 45.

McFadden, L.D., E.V. McDonald, S.G. Wells, K. Anderson, J. Quade, and S.L. Forman. 1998. The vesicular layer and carbonate collars of desert soils and pavements: Formation, age and relation to climate change. *Geomorphology* 24:101–145.

McFadden, L.D., S.G. Wells, and M.J. Jercinovich. 1987. Influences of eolian and pedogenic processes on the origin and evolution of desert pavements. *Geology* 15:504–508. doi:10.1130/0091-7613(1987)15<504:IOEAPP>2.0.CO;2

McKee, R.A., 2016, Structure and volcanic evolution of the northern Highland Range, Colorado River Extensional Corridor, Clark County, Nevada [M.S. thesis]: San Jose, San Jose State University, 129 p.

Meeker, G., A. Bern, I. Brownfield, H. Lowers, S. Sutley, T. Hoefen, and J. Vance, 2003. The composition and morphology of amphiboles from the Rainy Creek Complex near Libby, Montana. *Am. Mineral.* 88:1955–1969.

Meeker, G., H. Lowers, G. Swayze, B. Van Gosen, S. Sutley, and I. Brownfield. 2006. Mineralogy and morphology of amphiboles observed in soils and rocks in El Dorado Hills, California. USGS Open-File Rep. 2006-1362. USGS, Reston, VA.

Metcalf, R.V., and Buck, B.J., 2015, Genesis and health risk implication of an unusual occurrence of NaFe3+-amphibole: *Geology* v. 43, p. 63-66, doi:10.1130/G36199.1

National Institute for Occupational Safety and Health, 2011. Asbestos fibers and other elongate mineral particles: State of the science and roadmap for research. Current Intelligence Bulletin 62. https://www.cdc.gov/niosh/docs/2011-159/pdfs/2011-159.pdf (accessed Nov. 28, 2018).

Pfau, J.C., K.M. Serve, and C.W. Noonan, *Autoimmunity and asbestos exposure.* Autoimmune Dis, 2014. **2014**: p. 782045.

Reheis, M.C., and Kihl, R., 1995. Dust deposition in southern Nevada and California, 1984-1989: Relations to climate, source area, and source lithology. J. Geophysical Research, 100:D5:8893-8918.

Sheppard, R.A. (1996). Occurrences of erionite in sedimentary rocks of the western United States. U.S. Geological Survey Open-File Report 96–018, 24p.

Sheppard, R.A., Gude, A.J. III., and Munson, E.L. (1965) Chemical composition of diagenetic zeolites from tuffaceous rocks of the Mojave Desert and vicinity, California. *American Mineralogist* **50**, 244-249.

Sheppard, R.A. and Gude, A.J. III. (1973) Zeolites and associated authigenic silicate minerals in tuffaceous rocks of the Big Sandy Formation, Mohave County, Arizona. *U. S. Geological Survey, Professional Paper* **830**, 36 pp.

Smith, E.I. 1984. Geologic map of the Boulder Beach quadrangle, Nevada: Nevada Bureau of Mines and Geology Map 81, scale 1:24000.

Smith, E., Honn, D., and Johnsen, R., 2010, Volcanoes of the McCullough Range, southern Nevada, in, P.J. Umhoefer et al., editors, Miocene tectonics of the Lake Mead region, Central Basin and Range: Geological Society of America Special Paper 463, p. 203–219.

Tetra Tech Inc. 2014. Phase 1 Site Characterization Report for Boulder City Bypass Naturally Occurring Asbestos (NOA) Project Phase 1 (Railroad Pass to Silverline Road) (Accessed Nov 17, 2018). http://i-11nv.com/wp-content/uploads/2015/05/Final-NDOT-Phase-I-Report-10-6-14.pdf

Tschernich, R.W. (1992) *Zeolites of the World*. Geoscience Press, Phoenix, Arizona, USA.

Turk, J.K., and R.C. Graham. 2011. Distribution and properties of vesicular horizons in the western United States. *Soil Sci. Soc. Am. J.* 75:1449–1461. doi:10.2136/sssaj2010.0445

U.S. EPA, 2014. Toxicological Review of Libby Amphibole Asbestos. U.S. Environmental Protection Agency, EPA/635/R-11/002F

Van Gosen, B.S., 2007. The geology of asbestos in the United States and its practical applications. *Environmental & engineering Geoscience* v. XIII, No. 1, pp. 55-68.

Van Gosen, B.S, Lowers, H.A, Sutley, SJ, 2004, A USGS Study of Talc Deposits and Associated Amphibole Asbestos within Mined Deposits of the Southern Death Valley Region, California. US Geological Survey Open-File Report 2004-1092

Van Gosen, B.S., and Clinkenbeard, J.P., 2011, Reported historic asbestos mines, historic asbestos prospects, and other natural occurrences of asbestos in California: U.S. Geological Survey Open-File Report 2011-1188, 22 p., 1 pl.

Van Gosen, B. 2008. Reported historic asbestos mines, historic asbestos prospects, and natural asbestos occurrences in the southwestern United States (Arizona, Nevada, and Utah). USGS Open-File Rep. 2008-1095. USGS, Denver, CO.
Williams, M.M. 2003. Depositional history of the Black Mountain conglomerate, Mohave County, Arizona: Sedimentary response to Miocene extension. M.S. thesis. Univ. of Nevada, Las Vegas.

Volborth, A., 1972, Geology of the granite complex of the Eldorado, Newberry, and northern Dead Mountains, Clark County, Nevada: Nevada Bureau of Mines and Geology Bulletin 80, scale 1:125000.

Wagner, J. C., Skidmore, J. W., Hill, R. J., & Griffiths, D. M. (1985). Erionite exposure and mesotheliomas in rats. *British Journal of Cancer*, 51(5), 727–730.

Wells, S.G., L.D. McFadden, J. Poths, and C.T. Olinger. 1995. Cosmogenic 3He surface-exposure dating of stone pavements: Implications for landscape evolution in deserts. *Geology* 23:613–616.

Williams, A.J., Buck, B.J., Beyene, M.A. 2012. Biological Soil Crusts in the Mojave Desert, USA: Micromorphology and Pedogenesis. *Soil Science Society of America Journal* 76:1685–1695. doi:10.2136/sssaj2012.0021

Zebedeo, C.N., Davis, C., Pena, C., Ng, K.W. and Pfau, J.C., 2014. Erionite induces production of autoantibodies and IL-17 in C57BL/6 mice. Toxicology and Applied Pharmacology, 275:257-264.

Chapter 5:

Quantitative Assessment of Naturally-Occurring Asbestos (NOA) in Unpaved Roads and Playas in Southern Nevada

Brenda J Buck[1]
Brett T. McLaurin[2]
Rodney V. Metcalf[1]

[1]Department of Geoscience, University of Nevada Las Vegas, 4505 South Maryland Parkway, Las Vegas, Nevada 89119-4010
[2]Department of Environmental, Geographical and Geological Sciences, Bloomsburg University of Pennsylvania, 400 East Second Street, Bloomsburg, Pennsylvania 17815, USA

Introduction

Naturally-occurring asbestos (NOA) has been found to occur in and around the Las Vegas metropolitan area as a natural component of rocks and soils (Buck et al., 2013; Metcalf and Buck, 2015) (Figure 5-1). The geologic source of the NOA are hydrothermally-altered, Neogene granitic plutons that crop out in and around Boulder City, Black Hill, the McCullough Range in Nevada, and across the Colorado River in the Wilson Ridge area in northwestern Arizona (Buck et al., 2013; Metcalf and Buck, 2015) (Figure 5-1). The NOA fibers present in these areas belong to the amphibole mineral group. Calcic amphiboles actinolite and magnesiohornblende are found in the plutons in Nevada (Buck et al., 2013), whereas sodic amphiboles winchite, magnesioriebeckite, and richterite dominate the Wilson Ridge area in Arizona (Metcalf and Buck, 2015).

Erosion of these plutons has distributed the NOA into surrounding alluvial fan deposits and soils. These alluvial deposits can range in age from the late Miocene/Pliocene (e.g., Black Mountain conglomerate in Arizona; Williams, 2003; Metcalf and Buck, 2015) to modern alluvium in drainages emanating from any NOA-containing materials in Nevada or Arizona (Figure 5-2) (Buck et al., 2013; Kleinfelder, 2014; Tetra Tech, 2014, Metcalf and Buck, 2015). The arid climate of the Mojave Desert limits vegetation so that many of the NOA-containing soils are prone to wind erosion (Figure 5-3), especially if the delicate desert surfaces are disturbed.

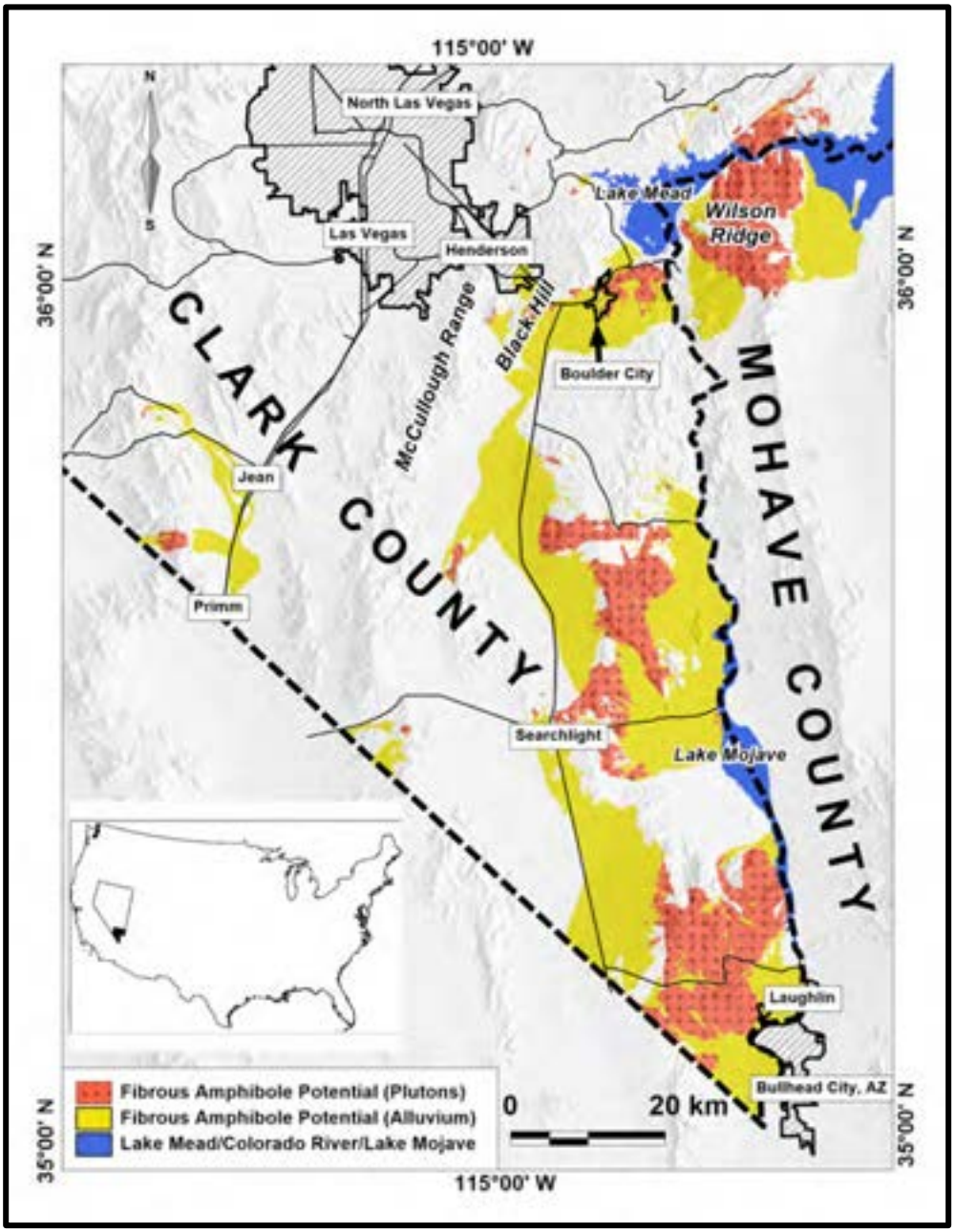

Figure 5-1. Map of southern Nevada and western Arizona, modified from Buck et al., 2013. Map delineates bedrock exposures of plutonic rock that is considered to have fibrous amphibole potential. Areas of fibrous amphibole potential in alluvium represent where erosion of plutonic rock would likely distribute fibers along drainages.

Figure 5-2. Example of NOA-containing alluvium from Wilson Ridge region in Lake Mead National Recreation Area, northwestern Arizona. Sediments in the foreground (with road) are recent/late Holocene alluvium; whereas the hills in this photo are older Miocene/Pliocene alluvium (Black Mountain conglomerate).

Additionally, a recent study of mesothelioma mortality found a significantly increased proportion of mesothelioma in young people and women in southern Nevada (Baumann et al., 2015a,b; Pinheiro and Jin, 2015). This work suggests that environmental exposure to fibrous minerals in southern Nevada may be causing disease.

Inhalation of NOA fibers is the most important human exposure pathway. Human exposure to NOA fibers is a concern because both regulated and non-regulated fibrous amphiboles are known to cause many diseases, including mesothelioma, asbestosis, interstitial pulmonary fibrosis, pleural effusion, pleural plaques, and lung, ovarian, and laryngeal cancer (ATSDR, 2001; USEPA, 2014). Exposure to these fibers has been correlated to other health effects including gastrointestinal, colorectal, throat, kidney, esophagus, gallbladder, pharyngeal and stomach cancer, and cardiovascular disease (ATSDR, 2001; USEPA 2014). Additionally, there is evidence that these fibrous minerals may cause autoimmune disorders, such as lupus, rheumatoid arthritis, and scleroderma (Pfau et al., 2014; Pfau, 2018). A recent study found that the fibrous amphibole fibers found in Wilson Ridge area of Lake Mead National Recreation Area are as toxic as those found in Libby, Montana when tested in mice for autoimmune reactions (Pfau et al., 2017).

Figure 5-3. Wind-generated dust from Roach Lake, the dry lakebed (playa) north of Primm, Nevada. During such events, asbestos fibers present in the soil can become airborne, which can lead to human exposures.

Many residents of the Las Vegas metropolitan area participate in numerous recreational activities in and around the areas where NOA has been found. Activities such as horseback riding, off-road vehicle (ORV) driving, bicycling, running, and hiking in areas that contain NOA (Figure 5-4), can cause fibers to become airborne, which increases the potential for NOA exposure. Once airborne, NOA fibers can cling to clothing, pets, cars, and other equipment, which could result in additional secondary exposures (Buck et al., 2013).

Figure 5-4. An off-road-driving enthusiast at the El Dorado dry lake bed (playa) west of Boulder City. Notice the amount of dust generated even though the lake bed is wet (see standing water in the foreground). This dry lake bed contains NOA (Buck et al., 2013; 2016)

Outdoor recreational activities in southern Nevada largely take place on federally-managed public lands. One of the most popular activities is driving vehicles including four-wheel drive, all-terrain vehicles (ATVs), motorcycles, and other vehicles on unpaved roads and playas (Figure 5-4). This is a very popular activity across the United States, where an estimated 44 million people age 16 and older engage in these recreational activities (Cordell et al., 2008). One of the potential health risks from such activities is to inhale fugitive dust (Buck et al., 2013; Goossens and Buck, 2009; Goossens et al., 2012; Padgett et al., 2008). Driving on unpaved surfaces can significantly increase the amount of total suspended particles including PM10 and PM2.5 (particulate matter with an average diameter of 10 μm and 2.5 μm), which are well-known for their detrimental health effects when inhaled (e.g. Plumlee et al., 2006; Morman and Plumlee, 2013). The size, shape, mineralogy, and chemistry of these particulates, and therefore their health effects if inhaled, can vary greatly depending on the geologic processes that have occurred in specific areas.

Recently, Wolfe et al. (2017) reviewed existing literature relevant to off-road recreation and naturally-occurring asbestos (NOA). They found that individuals who operate ORV's in regions where NOA is a component of the soil or unpaved road may have elevated exposures to mineral fibers. They found that approximately 80% of the known NOA occurrences in five western states were located within 20 miles of an ORV trail and nearly a third were located within one mile (Wolfe et al., 2017).

The goal of this study was to quantify NOA concentrations in southern Nevada soils in areas where people frequently drive on existing dirt roads, or on dry playas. As part of this goal, we obtained quantitative data using the Fluidized Bed Asbestos Segregator (FBAS) with analyses of fibers using the Transmission Electron Microscope (TEM). This

is a new method developed by the EPA to quantitatively measure very small amounts of asbestos in soils (Januch et al., 2013). This method can accurately measure concentrations of asbestos with detection limits 0.002% to 0.005% by weight, which is approximately 100-times lower than the detection limits that are usually achieved using other analytical methods for asbestos in soil and other solid media. This is important because soils with very low concentrations of asbestos, even those that test as non-detect using the traditional methods of quantification, can still generate hazardous concentrations in the air when disturbed (e.g. Addison et al., 1988; USEPA, 2010). Therefore, it is vitally important to be able to measure asbestos concentrations to extremely low levels in soils.

We analyzed for all amphibole mineral fibers, including those minerals that are legally regulated as asbestos, and those that are known carcinogens but are not regulated as asbestos minerals. We also analyzed for the zeolite mineral erionite, which is a well-known carcinogen that is also unregulated (e.g. Carbone et al., 2011).

Methods

Field sampling was performed using safety gear including level 3 Tyvek suits, and respirators (Figure 5-5). Ten samples were collected for analyses using FBAS and TEM analyses (Table 5.1; Figure 5-6). Unless otherwise described below, all 10 samples were taken from approximately the upper < 1 cm surface of either dirt roads commonly used by the public, or on dry lake beds also commonly used for recreational purposes such as off-road-driving (ORV). All 10 samples were compound samples taken from several subsamples within a specific area along a road bed or playa. We chose not to perform incremental sampling methodology (ISM) in this study because the current literature suggests that it does not improve the accuracy results when testing for asbestos, unlike for heavy metals (Wroble et al., 2017). Sites were chosen based on results in Chapter 4, and known areas where the authors have seen high levels of visitation and use by people.

Figure 5-5. Fieldwork performed in level 3 Tyvek suits and respirators.

All samples were sieved in the field using a 3 mm aluminum wire mesh to remove coarse fragments. Subsamples were thoroughly mixed prior to analyses. All samples were contained in double-bagged and sealed plastic bags and stored in air-tight containers. Samples are only opened at UNLV after being placed in special asbestos

hoods. Samples were sent to EMSL Analytical Inc., an accredited laboratory offering FBAS analyses. Each sample was analyzed in triplicate (Table 5.1). Samples were prepped using the FBAS methodology (Januch et al., 2013) and then analyzed using Transmission Electron Microscopy (e.g. Januch et al., 2013). EMSL's description of their methods is copied herein: *"TEM FBAS Level C (<25,000 s/g). Each soil sample was size-segregated by sieving and the fine fraction was then homogenized prior topreparation with the segregator. Small particles, nominally 10 micrometer (µm) aerodynamic equivalent diameter (AED) and smaller, are elutriated from the bulk sample and collected onto a filter. The filter is prepared and analyzed by transmission electron microscopy (TEM) for asbestos. Fibers are counted using the rules specified in the ISO 10312 analytical method. The concentration of asbestos in the soil is expressed as releasable asbestos structures per gram (g) of soil. The limit of detection (LOD) for the method is estimated to be 3 times the analytical sensitivity (A.S.) The A.S. (and therefore also the LOD) can be lowered by increasing the mass of soil elutriated and/or by increasing the area analyzed of the resulting filter. There is an upper limit to the mass of soil that can be used for elutriation due to overloading and obscuration of fibers. There is no theoretical limit to the amount of grid openings that can be analyzed however there is a practical limit based on the analytical effort required. The more grid openings analyzed the lower the sensitivity achieved. For samples in this set, elongate mineral particles were identified as fibers if they had: parallel or stepped sides, a length greater than or equal to 0.5 microns and an aspect ratio of at least 3:1 (modified from 5:1). The mineral classification procedure employed for these samples is based on a successive inspection of the morphology, selected area electron diffraction (SAED) and qualitative and semi-quantitative energy dispersive x-ray analysis. Fibers can often be found as complex aggregates with other fibers or particulate. These particles and fibers can interfere with SAED and EDXA analysis. Per our discussion, EMSL has attempted to identify the elongate mineral particles encountered on the filter as regulated asbestos, Non–Regulated Amphibole (NRA), or Erionite. The classification of regulated asbestos was performed as outlined in ISO 10312. For the classification of Non–Regulated Amphibole, we identified the mineral species by SAED and semi-quantitative EDXA using the IMA 2012 naming convention. In order to be classified as erionite, minerals would present a fibrous, acicular or needle-like habit with a length to width ratio of at least 3:1, chemistry consistent with erionite (Sodium, Calcium or Potassium rich alumino-silicate) and a crystal inter-row spacing of approximately 15.05 Angstroms. It should be noted that these identifications could be open to interpretation due to interference with other particulate, the lack of local reference standards and the limitations of TEM EDXA on determining the Iron phase (Fe2 or Fe3). Quality Control Performed One recount different QC analysis was completed with acceptable results. Lab blanks, process blanks, and sand blanks were also analyzed and no asbestos was detected. Quality Control for this project was performed in compliance with EMSL's Quality Assurance Manual."*

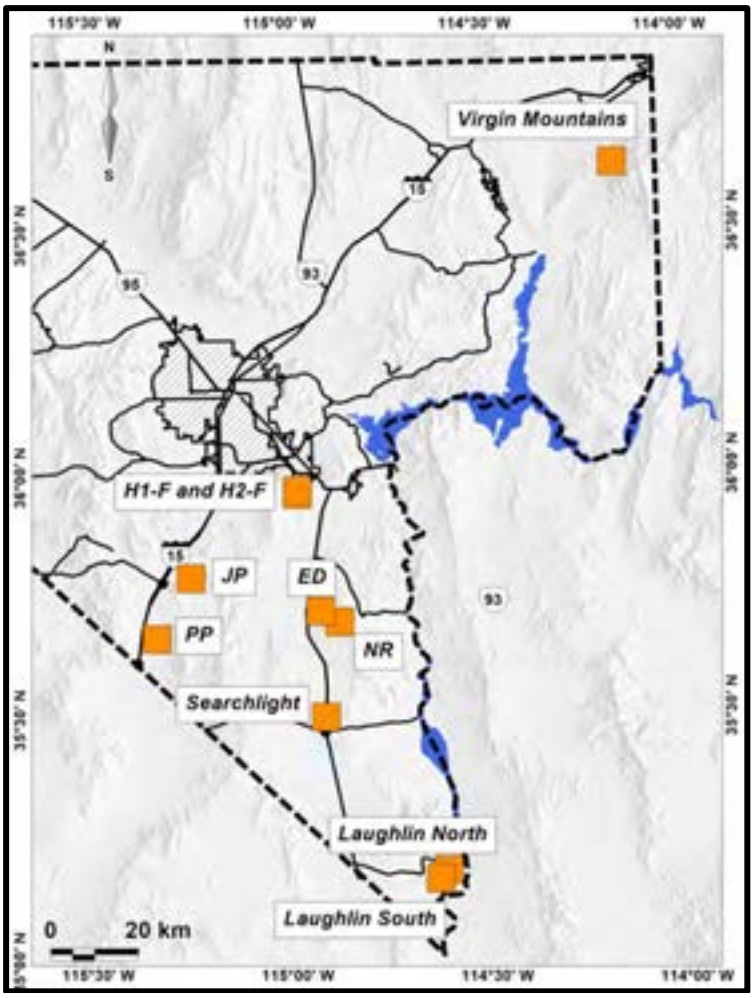

Figure 5-6. Map showing locations of soil samples analyzed using the FBAS/TEM method to quantify NOA in soils. All sites are on roads or playas where recreational driving commonly occurs. H1-F and H2-F are sites on dirt roads just south of Henderson, JP = Jean Playa; PP = Primm Playa; ED = El Dorado at Keyhole Canyon; NR = Nelson Road, Searchlight = dirt road just north of Searchlight; Virgin Mountains = dirt road in Virgin Mountains; Laughlin North and Laughlin South are dirt roads just west of the town of Laughlin, often used for ORV races and other recreational activities.

Henderson Sites

Soil from the surfaces of two dirt roads just south of Henderson NV were sampled and analyzed: H1-F and H2-F. At each site, a composite sample was created by taking multiple surface soil samples along dirt roads (Figures 5-7 to 5-9). Sample H1 was created by combining 16 sub-samples, all approximately the same volume of sample, taken from the surface road between the two marked locations, sieved through an approximately 3 mm wire mesh to remove coarse fragments. H2-F was sampled in the same way except it was created from 11 sub-samples. Both sites contain visible blue amphibole minerals on nearby bedrock and both sites are frequently visited by ORV recreationists and people driving vehicles on these dirt roads (Figure 5-10).

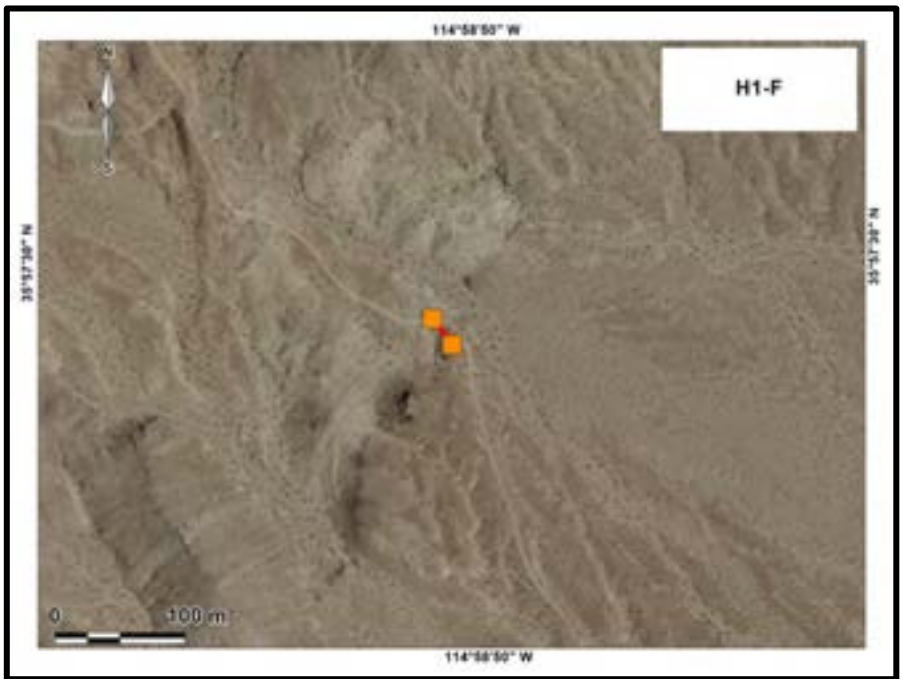

Figure 5-7. Map showing location of dirt road sampled for FBAS analyses: H1-F.

Figure 5-8. Map showing location of dirt road sampled for FBAS analyses: H2-F.

Figure 5-9. Map showing relative locations of dirt roads sampled for FBAS analyses south of Henderson. H1-F is the site in the south and H2-F is the site in the north of this image.

Figure 5-10. Photo of ORV riders on dirt roads south of Henderson, near the sites H1-F and H2-F.

Jean Playa (Jean Dry Lake)

A composite soil sample for the dry lake bed (playa) northeast of Jean, Nevada, was created by combining approximately equal volumes of 9 surface (< 2 cm depth) soil sub-samples (Figures 5-11 to 5-13) from the following locations on the surface of the playa northeast of Jean Nevada (see Figure 5-13). All sub-samples were sieved through an approximately 3 mm wire mesh to remove coarse fragments. In this case, the depth of sampling had to be slightly deeper (e.g. < 2 cm instead of < 1 cm) due to the very hard surface crust present at the time of sampling.

Figure 5-11. View to the north, from the Jean dry lake bed (playa).

Figure 5-12. One of the sub-samples from the Jean dry lake bed (playa) used for FBAS/TEM analyses.

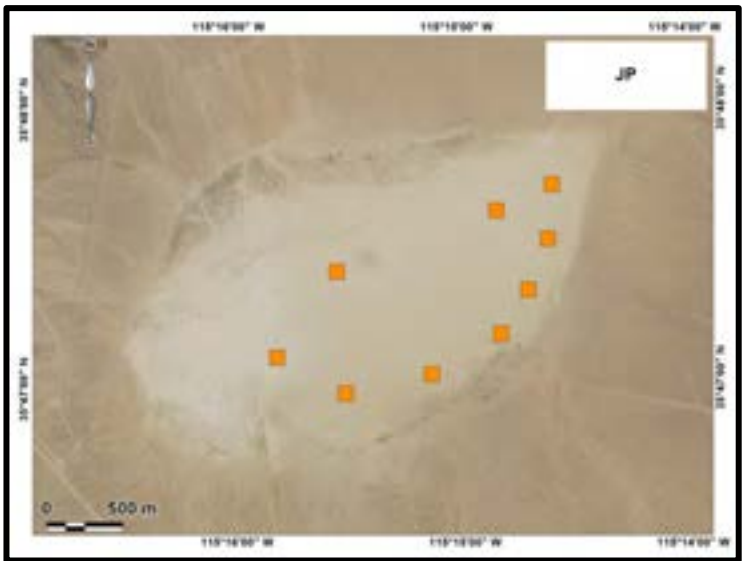

Figure 5-13. Map showing locations of sub-samples for FBAS analyses of the Jean Playa.

<u>El Dorado/Keyhole Canyon</u>

Soil from the surfaces of the dirt roads at the mouth of Keyhole Canyon (Figure 5-14), south of Boulder City NV, were sampled and analyzed. A composite sample was created by taking 19 approximately equal volume sub-samples, from < 1 cm depth, along the dirt road between the four marked locations (Figure 5-15). All sub-samples were sieved through an approximately 3 mm wire mesh to remove coarse fragments. This area is frequently visited by recreationists who hike and climb on the nearby rocks, walk through the canyon, and drive on these dirt roads.

Figure 5-14. Parking lot area at Keyhole Canyon where sediment was collected for FBAS/TEM analyses.

Figure 5-15. Map showing locations of sample collection for FBAS analyses at Keyhole Canyon, Nevada.

Nelson Road

Soil that was collected from the surface of the dirt road that links the town of Nelson to Highway 93 and Searchlight, was sampled and analyzed. A composite sample was created by taking 14 approximately equal volume sub-samples from < 1 cm depth from the dirt road between the two marked locations on Figure 5-16. All sub-samples were sieved through an approximately 3 mm wire mesh to remove coarse fragments. This road is frequently driven on by local residents, and many different types of outdoor recreationists.

Figure 5-16. Map showing location along the Nelson dirt road that was sampled for FBAS analyses. Area sampled lies between two squares.

Primm Playa (aka Roach Lake)

A composite soil sample for the playa northeast of Primm, Nevada (aka Roach Lake, Figures 5-17 to 5-20), was created by combining approximately equal volumes of 18 surface (< 1-3 cm depth) soil sub-samples from the following locations on the surface of the playa northeast of Primm Nevada (Figure 5-20). All sub-samples were sieved through an approximately 3 mm wire mesh to remove coarse fragments. In this case, the depth of sampling had to be slightly deeper (e.g. sometimes up to 3 cm) due to the very hard surface crust present in some areas at the time of sampling. Four of the 18 sub-samples were collected at 0-3 cm depths; three sub-samples were collected between 0-2.5 cm depths; one at 0-2 cm depth; 6 at 0-1.5 cm depths; and 4 at 0-0.5 cm depths.

Figure 5-17. View to the south from Roach Lake, a playa north of Primm, NV that was sampled for FBAS/TEM analyses. Dust caused by ORV riders (not shown).

Figure 5-18. View to the N/NW from the northern fringe of Roach Lake.

Figure 5-19. View to the southwest of dust being emitted from the surface of Roach Lake.

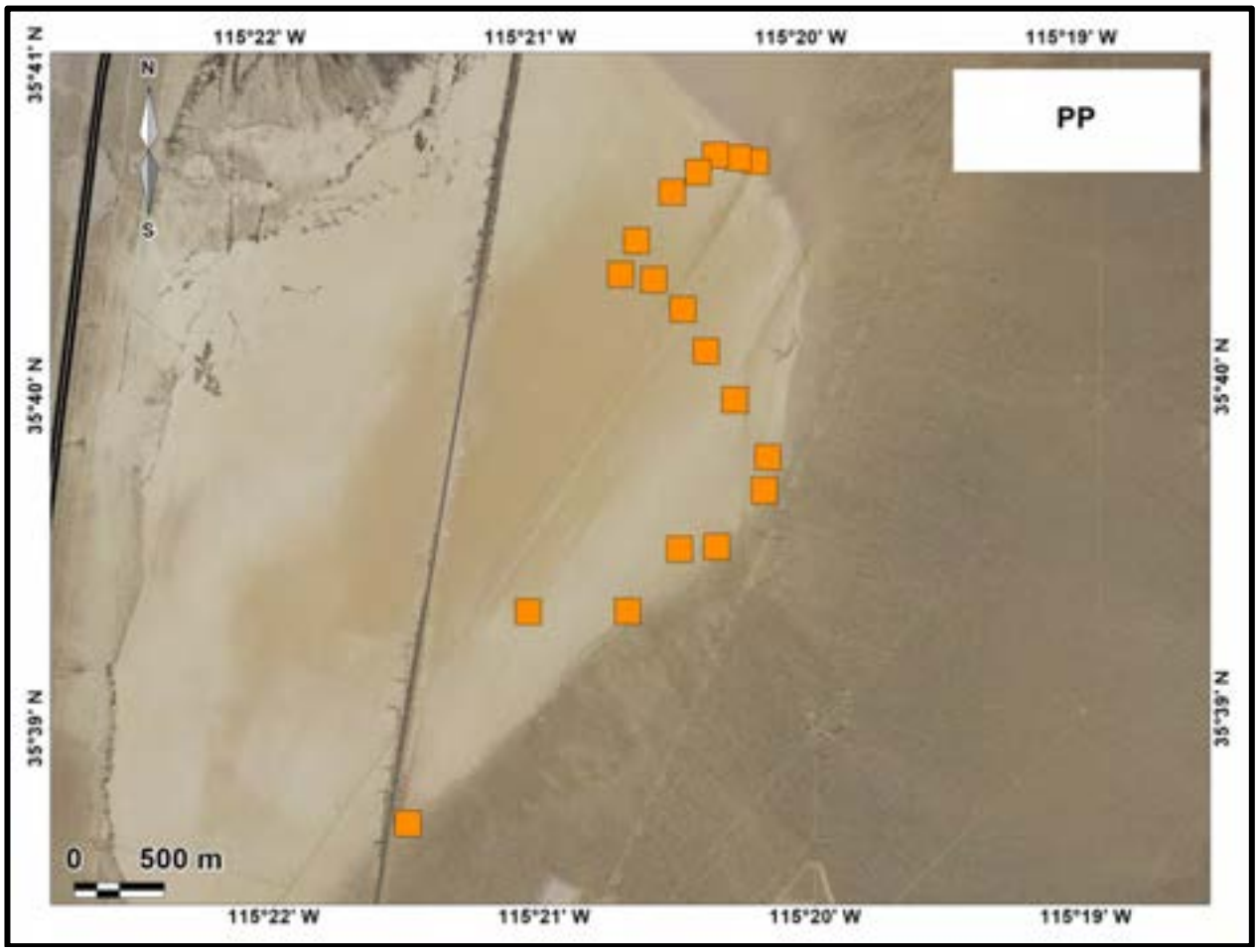

Figure 5-20. Map showing locations of sub-samples taken in the playa northeast of Primm, Nevada

Virgin Mountains Dirt Road

Surface soil that was collected from the surface of a dirt road in the Virgin Mountains, south of Mesquite NV, was sampled and analyzed. A composite sample was created by taking 18 approximately equal volume sub-samples from < 1 cm depth from the dirt road between the two marked locations on Figure 5-21. All sub-samples were sieved through an approximately 3 mm wire mesh to remove coarse fragments. This road is frequently driven on by local residents, and many different types of outdoor recreationists.

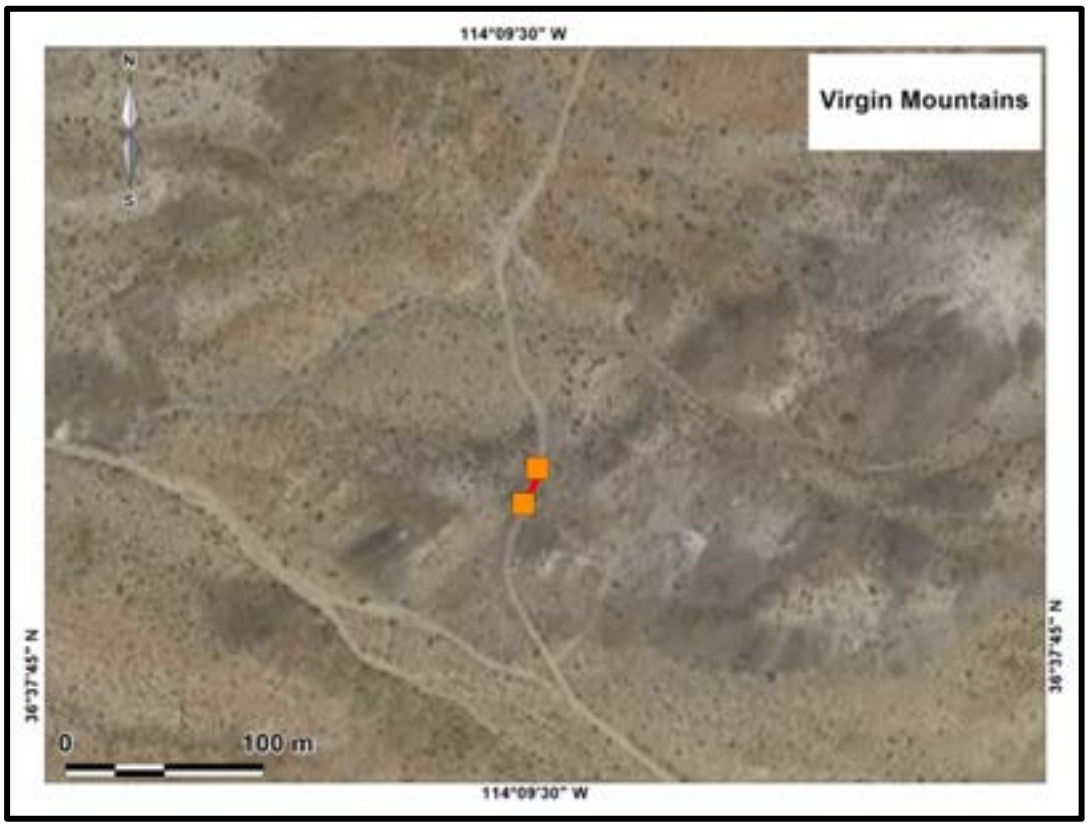

Figure 5-21. Map showing location of dirt road sampled in the Virgin Mountains for FBAS analyses. Area sampled is the portion of the road between the two squares.

Searchlight Road

Soil that was collected from the surface of a commonly utilized the dirt road (Figure 5-22) just north of Searchlight NV, was sampled and analyzed. A composite sample was created by taking 17 approximately equal-volume sub-samples from < 1 cm depth from the dirt road between the four marked locations on Figure 5-23. All sub-samples were sieved through an approximately 3 mm wire mesh to remove coarse fragments. This road is frequently driven on by local residents who live nearby, and many different types

of outdoor recreationists who use it to access many different areas of publically-managed lands in this region.

Figure 5-22. Dirt road north of Searchlight sampled for FBAS/TEM analyses.

Figure 5-23. Map showing location of dirt road sampled north of Searchlight for FBAS analyses. Area sampled lie between the 4 squares.

Laughlin Area

Soil from the surfaces of two dirt roads west of Laughlin NV, were sampled and analyzed: Laughlin North (LN) and Laughlin South (LS) (Figures 5-24 to 5-28). A composite sample was created by taking multiple surface soil samples along the dirt roads between the two marked locations on Figures 5-25 and 5-28. Sample LN was created by combining 16 sub-samples, all of approximately the same volume of sample, taken from the surface road between the two marked locations, sieved through an approximately 3 mm wire mesh to remove coarse fragments. Sample LS was sampled in the same way except it was created from 24 sub-samples and those could not be sieved due to being wet and already fine-grained at the time of collection. Laughlin North (LN) is a site commonly used for ORV-racing each year as well as numerous other uses by people using this dirt road to access many areas on public land west of Laughlin. Laughlin South is a retention basin and also commonly used by people driving in those areas west of Laughlin.

Figure 5-24. Dirt road sampled for Laughlin North FBAS/TEM analyses. A heavy rain had occurred the night before sampling.

Figure 5-25. Map showing location of dirt road sampled for Laughlin North FBAS analyses.

Figure 5-26. Dirt road in retention basin sampled for FBAS/TEM analyses at Laughlin South. View to the south. It had rained the night before, normally these roads are dry.

Figure 5-27. View up drainage, looking towards the west/northwest from the site of Laughlin South.

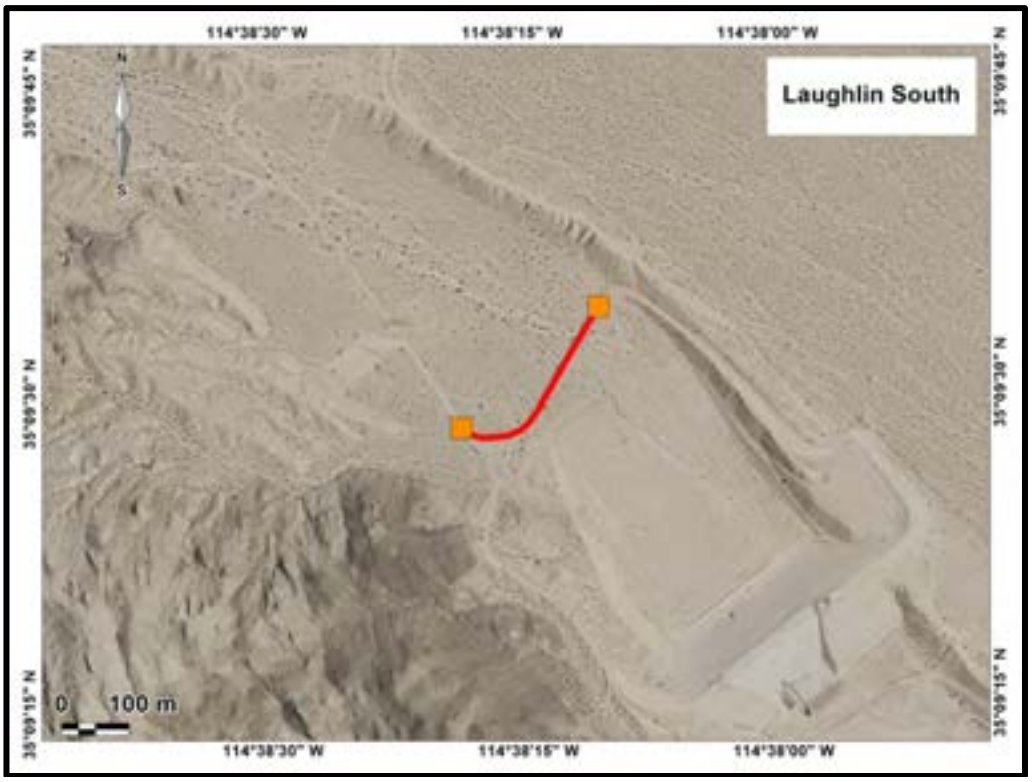

Figure 5-28. Map showing locations of dirt roads sampled for FBAS analyses, labeled Laughlin South

Results and Discussion

The results are shown in Table 5.1. All 10 sites contained amphibole NOA, but no erionite was measured in any of the samples. The highest concentration of amphibole NOA was found just south of Henderson at site H1 with a total average concentration of 2.3E+06 s/g (Table 5.1). The next highest concentrations were found along the Nelson road (9.7E+05 s/g) and just outside of Keyhole Canyon (3.7E+05 s/g), both sites of popular use for recreation and driving on dirt roads (Table 5.1).

Sites H2 south of Henderson (9.2E+04 s/g), and Laughlin North (8.3E+04) have similar concentrations of NOA followed by the Virgin Mountains dirt road (5.1E+04 s/g), Laughlin South (3.4E+04 s/g), and the Primm Playa (2.9E+04 s/g) (Table 5.1).

The two sites with the lowest average NOA concentrations were the dirt road north of Searchlight (8.0E+03 s/g) and the Jean Playa (2.1E+03 s/g) (Table 5.1).

Table 5.1. Asbestos mineralogy and concentrations (AC = actinolite, AN = anthophyllite, CR = crocidolite, AM = Amosite, OA = other amphibole, CH = chrysotile). Site locations described in text.

Soil Concentration (s/g, dw)								Mean Soil Concentration (s/g, dw) across filter replicates							
Site	**AC**	**AN**	**CR**	**AM**	**OA**	**CH**	**Total Asbestos**	**AC**	**AN**	**CR**	**AM**	**OA**	**CH**	**Total Asbestos**	**Total Asbestos PCMe**
H1	2.1E+06	2.2E+05	0.0E+00	0.0E+00	7.4E+04	0.0E+00	2.4E+06	1.9E+06	2.3E+05	4.1E+04	8.3E+03	1.1E+05	0.0E+00	**2.3E+06**	5.8E+05
	1.7E+06	1.5E+05	2.5E+04	0.0E+00	7.4E+04	0.0E+00	2.0E+06								
	2.0E+06	3.2E+05	9.8E+04	2.5E+04	1.7E+05	0.0E+00	2.6E+06								
NR	3.7E+05	0.0E+00	0.0E+00	0.0E+00	2.5E+05	0.0E+00	6.1E+05	6.4E+05	0.0E+00	0.0E+00	0.0E+00	3.1E+05	0.0E+00	**9.7E+05**	2.9E+05
	5.4E+05	0.0E+00	0.0E+00	0.0E+00	5.6E+05	0.0E+00	1.1E+06								
	1.0E+06	0.0E+00	0.0E+00	0.0E+00	1.2E+05	0.0E+00	1.2E+06								
ED	4.4E+05	0.0E+00	0.0E+00	0.0E+00	0.0E+00	0.0E+00	4.4E+05	2.9E+05	0.0E+00	0.0E+00	0.0E+00	7.3E+04	0.0E+00	**3.7E+05**	1.2E+05
	3.7E+05	0.0E+00	0.0E+00	0.0E+00	1.2E+05	0.0E+00	4.9E+05								
	1.2E+05	0.0E+00	0.0E+00	0.0E+00	9.7E+04	0.0E+00	2.2E+05								
	2.4E+05	0.0E+00	0.0E+00	0.0E+00	7.3E+04	0.0E+00	3.2E+05								
H2	7.3E+04	0.0E+00	0.0E+00	0.0E+00	0.0E+00	0.0E+00	7.3E+04	8.6E+04	0.0E+00	0.0E+00	0.0E+00	6.0E+03	0.0E+00	**9.2E+04**	3.1E+04
	4.9E+04	0.0E+00	0.0E+00	0.0E+00	2.4E+04	0.0E+00	7.3E+04								
	1.5E+05	0.0E+00	0.0E+00	0.0E+00	0.0E+00	0.0E+00	1.5E+05								
	7.3E+04	0.0E+00	0.0E+00	0.0E+00	0.0E+00	0.0E+00	7.3E+04								
V	0.0E+00	0.0E+00	0.0E+00	0.0E+00	5.0E+04	0.0E+00	5.0E+04	4.0E+03	0.0E+00	0.0E+00	0.0E+00	4.7E+04	0.0E+00	**5.1E+04**	3.1E+04
	1.2E+04	0.0E+00	0.0E+00	0.0E+00	1.9E+04	0.0E+00	3.1E+04								
	0.0E+00	0.0E+00	0.0E+00	0.0E+00	7.3E+04	0.0E+00	7.3E+04								
LN	0.0E+00	0.0E+00	0.0E+00	0.0E+00	4.9E+04	0.0E+00	4.9E+04	2.5E+04	0.0E+00	0.0E+00	0.0E+00	5.6E+04	0.0E+00	**8.3E+04**	1.7E+04
	4.9E+04	0.0E+00	0.0E+00	0.0E+00	0.0E+00	0.0E+00	4.9E+04								
	2.5E+04	0.0E+00	0.0E+00	0.0E+00	1.2E+05	0.0E+00	1.5E+05								
S	0.0E+00	0.0E+00	0.0E+00	0.0E+00	6.1E+03	0.0E+00	6.1E+03	0.0E+00	0.0E+00	0.0E+00	0.0E+00	8.0E+03	0.0E+00	**8.0E+03**	0.0E+00
	0.0E+00	0.0E+00	0.0E+00	0.0E+00	2.4E+04	0.0E+00	2.4E+04								
	0.0E+00	0.0E+00	0.0E+00	0.0E+00	0.0E+00	0.0E+00	0.0E+00								
PP	0.0E+00	0.0E+00	0.0E+00	0.0E+00	0.0E+00	6.3E+03	6.3E+03	2.1E+03	2.1E+03	0.0E+00	0.0E+00	2.1E+04	2.5E+04	**2.9E+04**	8.3E+03
	0.0E+00	6.3E+03	0.0E+00	0.0E+00	5.7E+04	6.3E+04	6.3E+04								
	6.3E+03	0.0E+00	0.0E+00	0.0E+00	6.3E+03	6.3E+03	1.9E+04								
JP	0.0E+00	0.0E+00	0.0E+00	0.0E+00	0.0E+00	6.2E+03	6.2E+03	0.0E+00	0.0E+00	0.0E+00	0.0E+00	0.0E+00	2.1E+03	**2.1E+03**	0.0E+00
	0.0E+00	0.0E+00	0.0E+00	0.0E+00	0.0E+00	0.0E+00	0.0E+00								
	0.0E+00	0.0E+00	0.0E+00	0.0E+00	0.0E+00	0.0E+00	0.0E+00								
LS	0.0E+00	0.0E+00	0.0E+00	0.0E+00	3.1E+04	0.0E+00	3.1E+04	4.1E+03	0.0E+00	0.0E+00	0.0E+00	2.9E+04	0.0E+00	**3.4E+04**	1.7E+04
	6.2E+03	0.0E+00	0.0E+00	0.0E+00	2.5E+04	0.0E+00	3.1 E+04								
	6.2E+03	0.0E+00	0.0E+00	0.0E+00	3.1E+04	0.0E+00	3.7E+04								

We compare these new results with previous FBAS data from a study with the EPA in which 6 samples in and around Boulder City were analyzed (from Buck et al., 2016); and with data collected from Libby Montana in which the sites were not contaminated from mining but are areas in which the asbestos occurs through natural geologic processes (Figure 5-29).

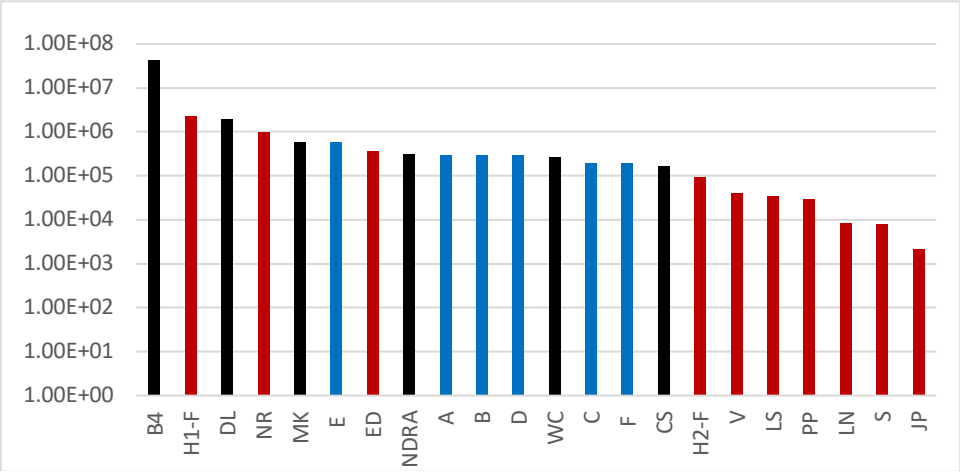

Figure 5-29. Graph of NOA concentrations as measured by FBAS & TEM (notice log scale) of six sites sampled as part of a previous study in the Boulder City Area (shown in black) which includes Martha P. King Elementary School (MK), East end of Adams Blvd (B4), Boulder City Bypass construction site, south of Boulder City (WC), Colorado Street lot (CS), El Dorado Dry Lake Bed (DL) and Nellis Dunes Recreational Area (NDRA) (Buck et al., 2016); six sites in Libby Montana (A, B, C, D, E, F – shown in blue – from USEPA 2010), and the 10 new sites in this study (shown in red) which include: Henderson (H1-F, H2-F); Virgin Mtns (V), El Dorado (ED), Nelson Road (NR), Laughlin North (LN), Laughlin South (LS), Primm Playa (PP), Jean Playa (JP), Searchlight (S).

The highest concentration in this dataset is site B4, which is a site at the end of Adams Blvd, east side of Boulder City. The second highest concentration is H1-F, a site on a dirt road managed by the BLM, just south of Henderson. The third highest concentration is the El Dorado Dry Lake bed, a playa on Boulder City land which is highly emissive for dust and is a popular destination for numerous outdoor recreational activities including off-road-driving (ORV). The fourth highest concentration is the dirt road to Nelson, which is on BLM-managed lands. The fifth highest concentration is the Martha King Elementary School in Boulder City (MK). The 6th, 9th, 10th, 12th, and 13th highest concentrations are soils in Libby Montana. The 7th highest concentration is Keyhole Canyon (ED) just southeast of the El Dorado Dry Lake Bed. The 8th highest concentration is Nellis Dunes Recreational Area (NDRA). The 11th highest concentration is WC, a site south of Boulder City along the Interstate-11 construction route. The 14th highest concentration is a vacant lot in Boulder City near Colorado Street (CS). The 15th

highest concentration is another site south of Henderson on BLM-managed lands (H2-F). The 16th highest concentration is a site in the Virgin Mtns, south of Mesquite, NV (V). The 17th highest concentration is Laughlin South (LS), a retention basin near Laughlin. The 4th lowest concentration is the Primm Playa (PP), the 3rd lowest site is a site on BLM-managed lands west of Laughlin, NV (LN). A dirt road north of Searchlight is the second-lowest site measured thus far (S), and the lowest concentration was found in the Jean Playa (JP).

Figure 5-30. Photo of Laughlin/Bullhead City from the west looking east. Notice the large areas of land disturbance (e.g. bare soil), which increases likelihood of dust emissions from natural wind, including asbestos fibers where present.

The presence of NOA in surface soils suggests that these mineral fibers can become airborne during or following disturbance providing the potential for human exposure via inhalation of these fibers (Figure 5-30). Unfortunately, there is still no way to directly correlate soil concentrations of NOA to airborne fiber concentrations (e.g. human exposures). Soils that test as non-detect using PLM (polarized light microscopy) can still produce hazardous airborne levels of fibers when disturbed (e.g. Addison et al., 1988; EPA, 2010). The concern when comparing asbestos concentrations from Libby to those in Southern Nevada is that southern NV has significantly increased aridity, which results in less vegetation, less soil organic matter, and therefore more dust generation with less soil disturbance or weaker natural winds. *Therefore, soils with low concentrations of asbestos may still generate significant airborne asbestos concentrations when disturbed by human activities or through natural wind erosion*. *Therefore, all the sites tested in this study have the potential to possibly generate harmful concentrations of fibers in the air when disturbed.*

What is needed in southern Nevada are many more studies to better understand the risks to specific populations through occupational or recreational activities, or due to living in areas that contain NOA. Activity-based-sampling (ABS) could be performed to better understand human exposures when driving on these dirt roads (for work or for recreation); or other common recreational activities such as hiking, cycling, ORV driving,

camping, and other popular activities. This work reported herein can be used to better choose the sites in which these ABS studies could be performed.

A recent review of the known literature on NOA and ORV activities found that riding behind others, driving faster, and sitting lower (e.g. children) result in greater exposures to mineral fibers (Wolfe et al. 2017). This study found that exposures can range between 0.01-5.6 f/cc, and in a study of 5 western states in the USA, many (approximately 80%) ORV activities occur within 20 miles of known sites of NOA, and nearly one-third occur within one mile (Wolfe et al., 2017). The Wolfe et al. (2017) paper concluded that public health awareness initiatives are needed to help ORV riders make more informed choices of where they perform these activities This study also found that geological hazard maps such as those created in this report, are very much needed. In particular, soil maps are needed since the footprint of the natural hazard (e.g. NOA) is much bigger when soils are included rather than just bedrock (See previous chapters). In addition, fibers can much more easily become airborne when soils are disturbed as compared to when bedrock is disturbed because the minerals are held tightly within the lithified rock as compared to soil. Also, people tend to interact with soils more than they do with bedrock, and therefore knowing where the hazard occurs can greatly help people make better-informed decisions regarding land management, recreational or occupational activities, and other choices that affect their exposures to these hazards.

Summary

Naturally-occurring asbestos (NOA) occurs in many areas in southern Nevada and northwestern Arizona (Buck et al., 2013; Metcalf and Buck, 2015). The primary route of human exposure is through inhalation of NOA that has become airborne through natural wind erosion or human disturbance. Since driving on dirt roads and dry playas are a common recreational (and occupational) activity in southern Nevada, the goal of this study was to quantify NOA concentrations in southern Nevada soils in areas where people frequently drive on existing dirt roads, or on dry playas. Ten composite samples from 10 sites that were known or predicted to contain NOA were sampled and analyzed in triplicate. All 10 sites tested positive for amphibole NOA at average concentrations that varied between 2.3E+06 to 2.1E+03 s/g. No erionite was measured in any of the samples.

Unfortunately, there is still no way to directly correlate soil concentrations of NOA to airborne fiber concentrations (e.g. human exposures). Soils that test as non-detect using PLM (polarized light microscopy) can still produce hazardous airborne levels of fibers when disturbed (Addison et al., 1988; USEPA, 2010). Therefore, soils with low concentrations of asbestos may still generate significant airborne asbestos concentrations when disturbed by human activities or through natural wind erosion. *In this study, all the sites tested have the potential to possibly generate harmful concentrations of fibers in the air when disturbed.*

References

Addison, J., Davies, LST, Robertson, A., Willey, R.J., 1988. The release of dispersed asbestos fibres from soils. World Health Organization Historical Research Report TM/88/14. http://www.iom-world.org/research/libraryentry.php

Agency for Toxic Substances and Disease Registry. 2001. Toxicological profile for asbestos. ATSDR, Atlanta, GA. https://www.atsdr.cdc.gov/toxprofiles/tp61.pdf (accessed 17 Nov. 2018).

Baumann, F., Buck, B. J., Metcalf, R. V., McLaurin, B. T., Merkler, D., Carbone, M. 2015a. The presence of asbestos in the natural environment is linked to mesothelioma in young individuals and women in Southern Nevada. *Journal of Thoracic Oncology*. 10: 731–737

Baumann F, Buck B**,** Metcalf R, McLaurin BT, Merkler D and Carbone M., 2015b. Answer to the Letter to the Editor: No increased risk for mesothelioma in relation to natural-occurring asbestos in Southern Nevada. *Journal of Thoracic Oncology* v. 10 ; e64-e65. DOI: 10.1097/JTO.0000000000000565; ISSN: 1556-0864/15/1007-0e64*.*

Buck, B.J., Metcalf, R.V., Berry, D., McLaurin, B., Kent, D., Goossens, D., Januch, J., 2016. Naturally occurring asbestos in soils, southern Nevada: Interpretations for wind distribution and human exposure. Geological Society of America Abstracts with Programs. Vol. 48, No. 7 doi: 10.1130/abs/2016AM-278831

Buck, B.J., Goossens, D. Metcalf, R.V., McLaurin, B., Ren, M., and Freudenberger*, F*.,* 2013*,* Naturally occurring asbestos: Potential for human exposure, southern Nevada USA, *Soil Science Society of America Journal,* 77:2192-2204. doi:10.2136/sssaj2013.05.0183

Carbone, M., Baris¸, Y. I., Bertino, P., Brass, B., Comertpay, S., Dogan, A. U., et al. (2011). Erionite exposure in North Dakota and Turkish villages with mesothelioma. *Proceedings of the National Academy of Sciences of the United States of America,* 108(33), 13618–13623.

CDM Smith. 2014. *Final Background Soil Summary Report, Libby Asbestos Superfund Site*. Denver, Colorado: CDM Federal Programs Corporation and Tetra Tech. Report prepared for U.S. Environmental Protection Agency. February 4.

Cordell, K.B., CJ, Green, G.T., Stephens, B., 2008. Off-Highway Vehicle Recreation in the United States: A National Report from the National Survey on Recreation and the Environment (NSRE) (Accessed Nov 17, 2018) http://www.srs.fs.usda.gov/trends/pdf-iris/IRISRec1rptfs.pdf.

Goossens, D., and Buck, Brenda, 2009, Dust Emission by Off-Road Driving: Experiments on 17 Arid Soil Types, Nevada, USA, *Geomorphology, v. 107, p.118-138* doi:10.1016/j.geomorph.2008.12.001

Goossens, D., Buck, B.J., McLaurin, B., 2012, Contributions to atmospheric dust production of natural and anthropogenic emissions in a recreational area designated for off-road vehicular activity (Nellis Dunes, Nevada, USA), *Journal of Arid Environments* 78:80-99.

Januch, J., Brattin, W., Woodbury, L., and Berry, D., 2013. Evaluation of a fluidized bed asbestos segregator preparation method for the analysis of low-levels of asbestos in soil and other solid media. *Anal. Methods* 5:1658-1668.

Kleinfelder, 2014. Interstate 11 – Boulder City Bypass Phase 2 Design Build Project Geologic Evaluation, Sampling and Testing for naturally-occurring asbestos, Boulder City, Clark County, Nevada (Accessed Nov. 17, 2018) http://www.rtcsnv.com/wp-content/uploads/2012/07/LAS14R02679-Final-Text-thru-Appendix-A.pdf.

Metcalf, R.V., and Buck, B.J., 2015, Genesis and health risk implication of an unusual occurrence of NaFe3+-amphibole: *Geology* v. 43, p. 63-66, doi:10.1130/G36199.1

Morman, S.A., and Plumlee, G.S., 2013. The role of airborne mineral dusts in human disease. *Aeolian Research* 9:203-212.

Padgett, P.E., Meadows, D., Eubanks, E., Ryan, W.E., 2008. Monitoring fugitive dust emissions from off-highway vehicles traveling on unpaved roads and trails using passive samplers. *Environ. Monit. Assess*. 144:93-103.

Pfau, J.C., *Serve, K.M., and Noonan, C.W., 2014. Autoimmunity and Asbestos Exposure, Autoimmune Diseases* v. 2014, 11 p., http://dx.doi.org/10.1155/2014/782045

Pfau, J.C., Buck, B.J., Metcalf, R.V., Kauish, Z., Stair, C., Rodriguez, M., and Keil, D.E., 2017. Comparative health effects in mice of Libby amphibole asbestos and a fibrous amphibole from Arizona. *Toxicology and Applied* Pharmacology 334:24-34.

Pfau, J.C., 2018. Immunotoxicity of asbestos, *Current Opinion in Toxicology* 10:1-7

Pinheiro, P., and Jin, H., 2015. Letter to the editor: No increased risk for mesothelioma in relation to natural-occurring asbestos in southern Nevada. *Journal of Thoracic Oncology*, v. 10, no 7. P. e62-e63.

Plumlee, G.S., Morman, S.A., and Ziegler, T.L., 2006. The toxicology and geochemistry of earth materials: An overview of processes and the interdisciplinary methods used to understand them. Reviews in Mineralogy and Geochemistry, Mineralogical Society of America, v. 64, p. 5-57

Tetra Tech Inc. 2014. Phase 1 Site Characterization Report for Boulder City Bypass Naturally Occurring Asbestos (NOA) Project Phase 1 (Railroad Pass to Silverline Road) (Accessed Nov 17, 2018). http://i-11nv.com/wp-content/uploads/2015/05/Final-NDOT-Phase-I-Report-10-6-14.pdf

U.S. Environmental Protection Agency (EPA), 2010. Activity-Based Sampling Summary Report Operable Unit 4, Libby, Montana, Superfund Site. Region 8

U.S. Environmental Protection Agency (EPA), 2014. Toxicological Review of Libby Amphibole Asbestos: In support of summary information on the integrated risk information system (IRIS) United States Environmental Protection Agency.

Williams, M.M. 2003. Depositional history of the Black Mountain conglomerate, Mohave County, Arizona: Sedimentary response to Miocene extension. M.S. thesis. Univ. of Nevada, Las Vegas.

Wolfe, C., Buck, B., Miller, A., Lockey, J., Weis, C., Weissman, D. Jonesi, A., and Ryan, P., 2017, Exposure to naturally occurring mineral fibers due to off-road vehicle use: a review. *International Journal of Hygiene and Environmental Health*. pii: S1438-4639(16)30583-1. https://doi.org/10.1016/j.ijheh.2017.07.003

Wroble J., Frederick T., Frame A., Vallero D., 2017. Comparison of soil sampling and analytical methods for asbestos at the Sumas Mountain Asbestos Site: Working towards a toolbox for better assessment. PLoS ONE 12(7): e0180210. https://doi.org/10.1371/journal.pone.0180210

Appendix A

This fact sheet was written by the **Agency for Toxic Substances and Disease Registry (ATSDR)**, a federal public health agency. ATSDR's mission is to serve the public by using the best science, taking responsive public health actions, and providing trusted health information to prevent harmful exposure and disease related to toxic substances.

Asbestos

Limiting Environmental Exposure to Asbestos in Areas with Naturally Occurring Asbestos

Who should read this fact sheet

Read this fact sheet if you or someone you know currently lives, works, attends school, or plays in areas with asbestos in the soils, or has done so in the past.

Purpose of this fact sheet

This fact sheet answers the following questions:

- What is asbestos?
- How could asbestos exposure make you sick?
- What can you do to reduce your exposure to asbestos?
- Where can you get more information?

What is asbestos?

Asbestos defined

Asbestos is the name given to a group of six different fibrous minerals that occur naturally in the environment. Asbestos fibers are too small to be seen by the naked eye. They do not dissolve in water or evaporate. They are resistant to heat, fire, and chemical or biological degradation.

Naturally occurring asbestos refers to those fibrous minerals that are found in the rocks or soil in an area and released into the air by one of the following methods:

- Routine human activities
- Weathering processes

If naturally occurring asbestos is not disturbed and fibers are not released into the air, then it is not a health risk. Asbestos is used in many commercial products, including insulation, brake linings, and roofing shingles.

Classes of asbestos

The two general classes of asbestos are chrysotile (fibrous serpentine) and amphibole. Chrysotile asbestos has long, flexible fibers. This type of asbestos is most commonly used in commercial products. Amphibole fibers are brittle, have a rod or needle shape, and are less common in commercial products. Although exposure to both types of asbestos increases the likelihood of developing asbestos-related illness, amphibole fibers tend to stay in the lungs longer. They also are thought to increase the likelihood of illness, especially mesothelioma, to a greater extent than chrysotile asbestos.

Where asbestos is found in your environment

Asbestos is commonly found in ultramafic rock, including serpentine rock, and near fault zones. The amount of asbestos typically present in these rocks ranges from less than 1% up to about 25%, and sometimes more. Asbestos can be released from ultramafic and serpentine rock if the rock is broken or crushed.

In California, ultramafic rock, including serpentine rock, is found in the Sierra foothills, the Klamath Mountains, and the coast ranges. This type of rock is present in at least 44 of California's 58 counties. Not all ultramafic rock contains asbestos; it only has the potential to contain asbestos. Environmental testing can determine if a rock contains asbestos.

How you might be exposed to asbestos

You might be exposed to asbestos through routine activities that crush asbestos-containing rock or stir up dust in soils that contain asbestos fibers. The following are some examples of these activities:

- Working in your yard or garden
- Digging or shoveling dirt
- Riding bicycles on unpaved surfaces
- Riding off-road vehicles such as four wheelers and dirt bikes
- Running and hiking on unpaved surfaces
- Driving over unpaved surfaces

How could asbestos exposure make you sick?

Important!

Being exposed to asbestos does not mean you will develop health problems. Many things need to be considered when evaluating whether you are at risk for health problems from asbestos exposure. A doctor can help you determine whether you are at risk for health problems from asbestos exposure.

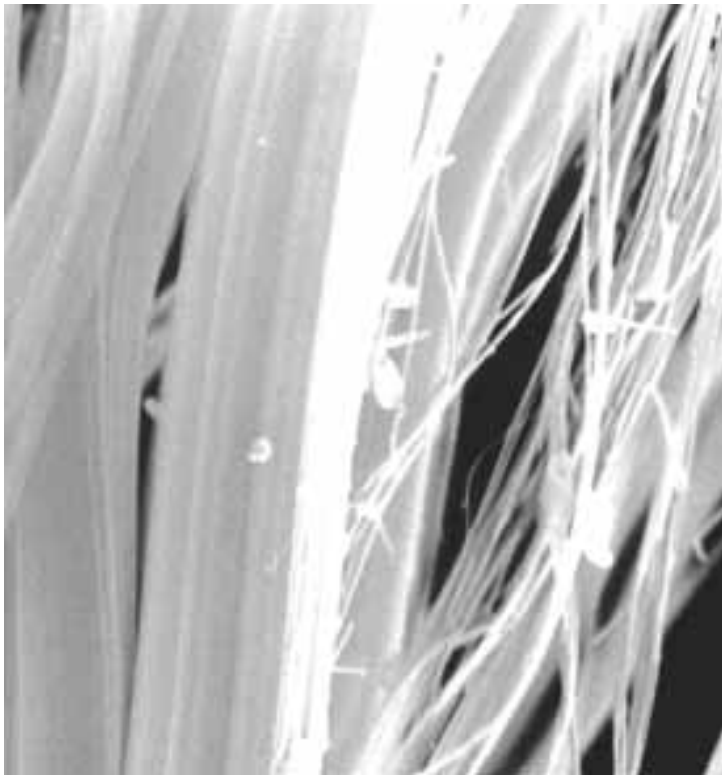

Magnification of Asbestos Fibers

Asbestos exposure and health

Asbestos is made up of fibers that are so small that you cannot see them. If asbestos fibers are in the air you breathe, you might get asbestos fibers in your lungs. Breathing in the fibers is the primary way that people are exposed to asbestos.

Asbestos fibers may remain in the lungs for a lifetime. In some cases, the fibers might damage the lungs or the membranes that cover the lungs, leading to illness and even death. Most people don't show any signs or symptoms of asbestos-related disease until 10 to 20 years or more after they were exposed.

For more information about asbestos-related disease, refer to ATSDR's fact sheet titled:
"Asbestos and Health: Frequently Asked Questions"

What can you do to reduce your exposure to asbestos?

Take steps right now

Limit exposure by taking the following steps if you live in an area where naturally occurring asbestos has been disturbed and is likely to become airborne:

- Walk, run, hike, and bike only on paved trails.
- Play only in outdoor areas with a ground covering such as wood chips, mulch, sand, pea gravel, grass, asphalt, shredded rubber, or rubber mats.
- Pave over unpaved walkways, driveways, or roadways that may have asbestos-containing rock or soil
- Cover asbestos-containing rock or soil in gardens and yards with asbestos-free soil or landscape covering.
- Pre-wet garden areas before digging or shoveling soil. Keep pets from carrying dust or dirt on their fur or feet into the home.
- Remove shoes before entering your home to prevent tracking in dirt.
- Use doormats to lower the amount of soil that is tracked into the home.
- Keep windows and doors closed on windy days and during nearby construction.
- Drive slowly over unpaved roads.
- Use a wet rag instead of a dry rag or duster to dust.
- Use a wet mop on non-carpeted floors.
- Use washable area rugs on your floors and wash rugs regularly.
- Vacuum your carpet often using a vacuum with a high efficiency HEPA filter.

Where can you get more information?

Stay informed

If you want more information about how to limit environmental exposure to asbestos, or if you have specific questions, contact ATSDR:

Toll free call:
800-CDC-INFO (800-232-4636)
TTY 888-232-6348

Online:
http://www.atsdr.cdc.gov/contacts.html

Some of the information in this fact sheet comes from the brochure Asbestos-Containing Rock and Soil—What California Homeowners and Renters Need to Know, California Air Resources Board, 2002. Accessed online at http://www.arb.ca.gov/cap/pamphlets/asbestosbrochure.pdf on April 26, 2005.

ATSDR
AGENCY FOR TOXIC SUBSTANCES
AND DISEASE REGISTRY

Appendix B

Naturally Occurring Asbestos: Approaches for Reducing Exposure

Purpose and Intended Audience

This fact sheet provides an overview of approaches for reducing exposures to naturally occurring asbestos (NOA). It is intended to make general information about management options available to state and local government officials, project managers, and environmental professionals. The information should serve as a starting point for identifying current NOA management practices. In general, selecting an appropriate approach to reduce NOA exposure should be determined on a location-specific basis.

NOA management approaches can reduce but may not completely eliminate potential exposures to naturally occurring asbestos.

Information contained in this fact sheet was obtained from the currently available literature, including state and local government publications. To obtain more information on NOA management approaches, including their performance and frequency of use, refer to the resources provided at the end of this fact sheet.

Naturally Occurring Asbestos

NOA occurs in rocks and soil as a result of natural geological processes. Natural weathering and human activities may disturb NOA-bearing rock or soil and release mineral fibers into the air, which pose a greater potential for human exposure by inhalation.

The U.S. Geological Survey (USGS) has an ongoing project to map the locations of historical asbestos mines, former asbestos exploration prospects, and natural asbestos occurrences. At least 35 states have reported NOA locations. To locate NOA areas in a specific part of the country, begin by consulting the USGS reports (see below) and contact a state geologist.

U.S. Geological Survey	• Eastern United States http://pubs.usgs.gov/of/2005/1189/ • Central United States http://pubs.usgs.gov/of/2006/1211/ • Rocky Mountain States http://pubs.usgs.gov/of/2007/1182/ • Southwestern United States http://pubs.usgs.gov/of/2008/1095/
California Geological Survey	Asbestos Reports, Maps, and Guidelines for Geologic Investigations • http://www.conservation.ca.gov/cgs/minerals/hazardous_minerals/asbestos/Pages/Index.aspx

This fact sheet is intended solely to provide general information on approaches that may be useful when addressing naturally occurring asbestos (NOA). It is not intended, nor can it be relied upon, to create any rights enforceable by any party, including any party in litigation with the United States. EPA considers NOA to be in an altered form if it has been disturbed by human activity; NOA is not considered to be altered if modified solely through naturally occurring processes or phenomena, from a location where it is naturally found. This fact sheet may be revised periodically without public notice. Use or mention of trade names does not constitute endorsement or recommendation for use.

In this fact sheet, NOA does not refer to commercially processed, asbestos-containing material, such as insulation and fire protection in buildings or automobile brake linings. Information about commercial asbestos-containing products is available in other publications, including the resources mentioned on EPA's asbestos Web page http://www.epa.gov/asbestos.

Approaches for Mitigating Exposures to NOA

The following general approaches to mitigate inhalation exposures to NOA are aimed at reducing NOA releases from rock or soil into the air:

- Leave NOA material in place and undisturbed
- Cover or cap NOA material
- Limit dust generating activities
- Excavate and dispose of NOA material

Approaches for reducing NOA exposure are similar to practices used for asbestos-containing materials in commercial applications.

Depending on the situation, a combination of engineering controls, work practices, and institutional (administrative) controls may be needed to implement an approach and reduce potential exposures to NOA. Selecting an approach depends on factors including:

- Accessibility of NOA (ground surface vs. below ground surface)
- Types of activities that disturb NOA (construction project vs. gardening)
- Climate and weather conditions
- Current and future land uses
- Technical and administrative feasibility of the approach

Typical engineering controls involve the use of covers and caps, vegetation, fencing, landscaping, and in some conditions, the application of water to suppress dust. Local factors, such as climate, influence the extent to which these approaches are implemented. For example, areas with dry or windy conditions may need more dust control than those with humid or less windy conditions.

Common work practices include limiting activities on NOA-containing areas, reducing driving speed on unpaved roads that may contain NOA, and cleaning vehicles driven over NOA. For example, during road construction or maintenance activities on unpaved areas where NOA is present, the Asbestos Airborne Toxics Control Measure (ATCM) for Construction, Grading, Quarrying, and Surface Mining Operations of the California Air Resources Board (ARB) requires that vehicle speeds not exceed 15 miles per hour.[1] Worker health and safety measures that include respiratory protection may be warranted. For information, consult with Occupational Safety and Health Administration Asbestos Standards for the General Industry and Asbestos Standards for the Construction Industry (http://www.osha.gov/SLTC/asbestos/hazards.html).

Examples of Engineering and Work Practices that Reduce Exposure to NOA

Excavation, Grading, or Utility Work at Construction Projects	• Wet road surfaces with water using trucks, hoses, or sprinklers[1] • Wet piles of excavated material and cover them with tarps, plastic sheeting, or other items[1] • Continuously mist the work area[1] • Install wind barriers around the work area[1] • Clean or decontaminate equipment and vehicles to ensure that no equipment or workers track soil out of the work area (a gravel pad, tire shaker, or wheel wash system may be used to clear soil from vehicles)[1] • Wet the work area using a spray system attached directly to rock cutting or drilling equipment, such as a fine-mist sprayer or a variable-rate fogger nozzle (similar to those used in fire fighting)[2] • Excavate utility trenches to an adequate depth and backfill them with clean soil so that future repair work will not need excavation into potential NOA-containing materials[3] • When transporting NOA-containing materials, avoid overloading trucks; keep the material below the top of each truck compartment and cover material with a tarp[4] • Limit personnel and vehicle access to the work area[5] • Identify NOA-containing areas with signs[2] • Reduce driving speed[1] • Reduce drilling or excavating speeds[6] • Excavate during periods of calm or low winds[1]
Roads and Parking Areas (unpaved and gravel roads)	• Cover roads with non-NOA-containing rock, chemical sealants or dust suppressants, chip seals, limestone aggregate, petroleum sealants, or asphalt cement paving[1, 7, 8] • Wet road surfaces with water[1] • Install windbreaks or berms[1] • Reduce driving speed[1] • Avoid dusty areas, especially in windy conditions[1]

Around Communities (playgrounds, ball fields, pathways, and gardens)	• Cover areas of rock and soil with clean soil, rock, vegetation, or other material (see next section, General Considerations for Using Covers or Caps)[3, 9] • Pave over unpaved walkways, driveways, or roadways containing NOA[1, 10] • Landscape areas with vegetation, such as NOA-tolerant plants, and add a layer of organic mulch or NOA-free soil. Water plants often until they are established to minimize erosion[9] • Water garden areas before digging[9] • Keep windows and doors closed on windy days and during periods when nearby rock or soil may be disturbed, such as during construction[9] • Limit track-in by using entryway (door) mats, and wipe down pets before they enter buildings to reduce the amount of soil tracked indoors[4, 9] • Allow children to play in outdoor areas only if the area has a ground covering, such as wood chips, mulch, sand, pea gravel, grass, asphalt, shredded rubber, or rubber mats[4] • Relocate outdoor activities to areas that do not contain NOA (walk, run, hike, and bike only on paved trails)[4] • Avoid dusty areas, especially in windy conditions[11]

General Considerations for Using Covers or Caps

One of the most common engineering controls is to place a cover system over the NOA. Cover materials may include clean soil or rock, concrete, chemical sealants or dust suppressants, chip seals, limestone aggregate, petroleum sealants, asphalt paving, geotextiles, wood chips, mulch, sand, pea gravel, shredded rubber, rubber mats, and vegetation.

The complexity of cover systems can vary from simple (e.g., a single soil layer) to complex (e.g., multiple layers of varying materials). Several factors, including cover material properties and site characteristics, affect the type of cover system appropriate for a particular area.

The availability of materials may influence the type of cover used. Materials that are readily available and close to the NOA area may be more desirable and cost effective than materials found farther away. For example, artificial turf and other imported materials may be more expensive than locally available soils. The cover material will likely need to be assessed for NOA or other undesirable constituents. Expected lifetime, maintenance, and monitoring requirements also affect the cost of covers.

The slope of the NOA area may influence the type and thickness of the cover material used. For example, steep slopes may need vegetation or shotcrete (concrete or mortar sprayed onto a surface with a pressurized hose) to promote slope stabilization. Steep slopes typically have a higher potential for erosion and therefore may demand thicker cover material.

The thickness of the cover material should provide a safety factor sufficient to ensure that airborne releases will not occur. Thicker covers may be needed in areas where there is a significant potential for erosion. The surface of a cover should protect against erosion by wind and rain. Materials used for erosion control typically include a layer of topsoil and vegetation. In areas where adequate vegetation is not possible, gravel, admixtures, or riprap may be used for the surface layer. The thickness of the cover may also depend on the presence of other cover components, such as irrigation lines.

A geotextile, which is a geosynthetic material made of polymer fabric, may be placed below the cover material to mark the presence of NOA and serve as an erosional indicator. Geotextiles also can provide protection, reinforcement, drainage, and separation when applied to the soil surface or between layers of materials. The California Department of Toxic Substances Control (DTSC) recommends that landscaped areas and play fields at schools include a geotextile marker covered by sufficient cover material to provide an effective barrier to reduce NOA exposures.[3] Placement of geotextile markers will demand additional time and expertise.

Long-Term Management Approaches

For long-term management of areas with NOA, institutional controls (ICs) and a maintenance plan may be desirable. In areas where NOA poses potential health concerns, local and state government officials should consider providing educational material to supplement engineering approaches for reducing exposures to NOA. The Agency for Toxic Substances and Disease Registry has developed a fact sheet about asbestos and NOA for the general public entitled "Asbestos and Health: Frequently Asked Questions."[4]

Institutional Controls

For additional information about ICs, refer to the Land Use Controls Web site at http://www.lucs.org

Generally, ICs are administrative or legal mechanisms that are designed to help minimize the potential for human exposure to contamination. They also protect the integrity of the engineering measures. ICs are generally divided into four categories:

- *Government controls* include laws and permits (such as local zoning laws and permits required for excavating or digging). Work that may disturb NOA-containing soil may require government approval and may be subject to local or state construction guidelines. In California, the ATCM of the California ARB requires owners and operators to notify the local air quality management district within one business day of discovering NOA, serpentine mineral, or ultramafic rock in an area to be disturbed by construction, grading, quarrying, or surface mining operations.[1] In Virginia, the Fairfax County Health Department requires a compliance plan that includes air monitoring to ensure effective dust control during construction in areas containing NOA.[2]
- *Proprietary controls* include property use restrictions based on private property laws, such as land use easements or covenants.
- *Enforcement tools* include legally binding documents that require individuals or companies to conduct or prohibit specific actions.
- *Informational devices* include deed notices, public advisories, and other measures (such as warning signs and worker health and safety awareness training) that alert and educate people about an area.

Maintenance Plan

A maintenance plan can help ensure that engineering controls and work practices remain effective. In California, for example, DTSC and school districts enter into an agreement to develop and implement an approved long-term operation and maintenance plan under DTSC oversight. These plans generally contain information about the following topics:[3]

- Building locations, utility line locations, and the thickness of cover material across the area
- Routine inspections

- Maintenance work, including erosion and storm water control
- Procedures for repairing cover damage
- Monitoring activities, such as perimeter or personal air monitoring
- Reporting format and frequency
- Restrictions on future activities that may expose NOA
- Management of imported soil and future excavation or trenching activities

Additional Information	
	• Agency for Toxic Substances and Disease Registry - http://www.atsdr.cdc.gov/NOA
	• California Air Resources Board - http://www.arb.ca.gov/toxics/asbestos/asbestos.htm
	• El Dorado County, California - http://www.co.el-dorado.ca.us/emd/apcd/asbestos.html
	• Fairfax County, Virginia - http://www.fairfaxcounty.gov/hd/asb
	• Sacramento County, California - http://www.airquality.org/compliance/asbestosNaturallyOccurring.shtml
	• U.S. Environmental Protection Agency - http://www.epa.gov/asbestos/pubs/clean.html

References

1. California Environmental Protection Agency (Cal/EPA) Air Resources Board (ARB). 2002. Asbestos Airborne Toxic Control Measure for Construction, Grading, Quarrying, and Surfacing Mining Operations. Final Regulation Order. Section 93105. July 22. http://www.arb.ca.gov/toxics/atcm/asb2atcm.htm

2. Fairfax County Health Department. Undated. "Control and Prevention of Asbestos Exposure from Construction in Naturally Occurring Asbestos." http://www.fairfaxcounty.gov/hd/asb/pdf/tbrdpubfin.pdf

3. Cal/EPA Department of Toxic Substances Control (DTSC). 2004. Interim Guidance: Naturally Occurring Asbestos (NOA) at School Sites. September 29. http://www.dtsc.ca.gov/Schools/upload/SMBRP_POL_Guidance_Schools_NOA.pdf

4. Agency for Toxic Substances and Disease Registry. Undated. "Asbestos and Health: Frequently Asked Questions." U.S. Department of Health and Human Services. http://www.atsdr.cdc.gov/NOA/Asbestos-and%20Health.pdf

5. El Dorado County. 2003. Naturally Occurring Asbestos and Dust Protection. Ordinance. Chapter 8.44. June 12. http://www.co.el-dorado.ca.us/emd/apcd/PDF/Naturally_Occuring_Asbestos_June_12.pdf

6. Fairfax County Health Department. Undated. "Basic Elements for a Naturally Occurring Asbestos Compliance Plan." http://www.fairfaxcounty.gov/hd/asb/pdf/asb50.pdf

7. Cal/EPA ARB. 2002. "Fact Sheet #3: Ways to Control Naturally-Occurring Asbestos Dust." January. http://www.arb.ca.gov/toxics/asbestos/3control.pdf

8. Cal/EPA DTSC. 2005. "DTSC Recommends Resurfacing of Serpentine Gravel Roads Based on Garden Valley Study." April. http://www.dtsc.ca.gov/SiteCleanup/Projects/Garden_Valley.cfm

9. Cal/EPA ARB. 2002. "Asbestos-Containing Rock and Soil – What California Homeowners and Renters Need to Know." Compliance Assistance Program. CAP 03-035. http://www.arb.ca.gov/cap/pamphlets/asbestosbrochure.pdf

10. Cal/EPA DTSC. 2006. "Fact Sheet: Recommended Housekeeping Activities to Reduce Exposure to Naturally-Occurring Asbestos in Schools." October. http://www.dtsc.ca.gov/Schools/upload/Recommended_Housekeeping_for_NOA_102306.pdf

11. University of California Cooperative Extension. Undated. "Lake County Serpentine Landscape Demonstration Garden." Asbestos Serpentine Soils Education Program. http://www.capcoa.org/noa/%5B5%5D%20Lake%20County%20Serpentine%20Landscaping.pdf

List of Acronyms

ARB	Air Resources Board
ATCM	Airborne Toxic Control Measure
DTSC	Department of Toxic Substances Control
ICs	institutional controls
NOA	naturally occurring asbestos
USGS	U.S. Geological Survey

Appendix C

United States Department of Agriculture
Forest Service, Pacific Southwest Region

Naturally Occurring Asbestos

What Visitors to National Forests Need to Know

General Information

Asbestos is the name given to a group of fibrous minerals that occur naturally in rock formations in the environment. Naturally occurring asbestos is the term applied to the natural geologic occurrence of various types of asbestos, and has been found to be present in the majority of counties in California. It is commonly found in ultramafic rock formations, including serpentine, and in the soils where these rock types are located. Serpentine, the California State Rock, is found widely throughout the state. It is typically grayish-green to bluish-black in color and its surfaces often have a shiny or wax-like appearance and a slightly soapy feel.

Presence on National Forests

The Forest Service has prepared maps which identify the locations of ultramafic and serpentine rock formations on national forest lands. Not all ultramafic and serpentine rock contains asbestos. Maps also identify locations where naturally occurring asbestos has been detected to date. These maps should not be considered as providing the definitive locations of all naturally occurring asbestos on the national forests in California but they should give you an idea of where potential risks may exist. The maps were prepared based on best available information from federal and state agencies such as the California Air Resources Board, California Geological Survey, U.S. Geological Survey, and Forest Service and will be updated as new information becomes available. The maps are available hard copy at local Forest Service offices and online at: *www.fs.fed.us/r5/noa*.

Asbestos Exposure & Health Facts

Naturally occurring asbestos may be a health risk if disturbed and asbestos fibers are released into the air. When asbestos-containing rocks are crushed or broken through natural weathering processes or through human activities, asbestos-containing dust can be generated. Once asbestos fibers are released into the air, they may remain airborne or in the soil for a long time. Airborne asbestos fibers may pose a health hazard because of the potential risks associated with inhalation of the fibers.

When these fibers are inhaled, over time they may cause mesothelioma (a rare cancer directly associated with asbestos exposure), lung cancer (smoking significantly increases the risk of lung cancer if one is exposed to asbestos), and non-cancer diseases such as asbestosis. All forms of asbestos fibers can cause cancer and are classified as known human carcinogens. Any exposure to a carcinogenic compound involves some risk; therefore, no "safe" exposure level has been established for asbestos. No one knows how many fibers are needed to cause cancer or other lung disease.

Examples of Serpentine Rocks

Diseases caused by asbestos may not be observed for twenty or more years. Being exposed to asbestos does not necessarily mean you will develop health problems. Many factors influence a person's chances of developing disease. A doctor can help you find out whether you are at risk for health problems from asbestos exposure.

Since naturally occurring asbestos is present on some national forest lands, there is a potential for your exposure to asbestos fibers on your visit to national forests in California. Natural weathering and routine human activities may disturb asbestos-bearing rock or soil and release asbestos fibers into the air. Examples of dust-generating activities include, but are not limited to:

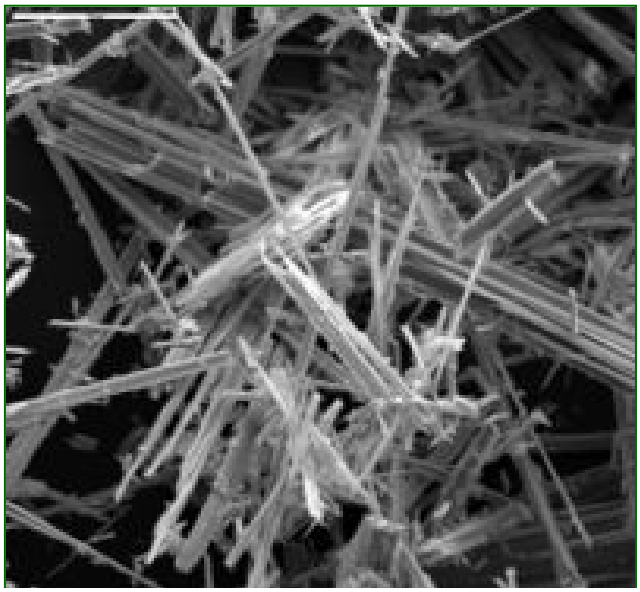

Magnification of Asbestos fibers

- Driving over unpaved roads, trails or soils
- Riding horses or moving livestock on unpaved roads, trails, or soils
- Recreational activities on unpaved roads, trails, or soils where dust may be generated, such as riding off-road vehicles, riding bicycles, running or hiking
- Digging or shoveling dirt
- Mining and quarrying operations

Health risks associated with exposure to naturally occurring asbestos are not yet fully understood. Recent studies and investigations by the U. S. Environmental Protection Agency in El Dorado County and at the Bureau of Land Management's Clear Creek Management area near Hollister, the U. S. Agency for Toxic Substances and Disease Registry, and by the University of California at Davis are increasing our understanding of the potential health risks associated with naturally occurring asbestos.

Reducing Your Exposure to Naturally Occurring Asbestos

Health risks to people are dependent upon their exposure to asbestos. The longer a person is exposed to asbestos and the greater the intensity of the exposure, the greater the chances for a health problem. If naturally occurring asbestos is not disturbed and asbestos fibers are not released into the air, then it will not pose a health risk. National forest visitors wishing to reduce their potential exposure to naturally occurring asbestos should consult the maps produced by the Forest Service or the State of California which identify the currently known areas of ultramafic and serpentine rock and naturally occurring asbestos and use the following best management practices in these areas to *Reduce Your Risk by Reducing Your Exposure:*

- Be aware of windy conditions and avoid dusty conditions to reduce exposure
- Limit dust generating activities, such as riding off-road vehicles, riding bicycles, running or hiking, riding horses or moving livestock, etc.
- Avoid handling or disturbing loose asbestos-containing rock types
- Drive slowly over unpaved roads, with windows and vents closed, to minimize dust generation (California Air Resources Board recommends that vehicle speeds not exceed 15 miles per hour on unpaved roads where asbestos is present)
- Avoid or minimize the tracking of dust into vehicles
- Do not use compressed air for cleaning your vehicles after your visit. Use a wet rag to clean the interior

These best management practices are based on guidance from various federal and state agencies such as the U. S. Environmental Protection Agency; U. S. Department of Health and Human Services, Agency for Toxic Substances and Disease Registry; and the California Air Resources Board. This list should not be considered as being all inclusive.

This information was obtained from state and federal resources listed below.

For more information, visit:

- U. S. Environmental Protection Agency.
  www.epa.gov/asbestos/pubs/clean.html
- U. S. Department of Health and Human Services
  www.atsdr.cdc.gov/noa/
- California Air Resources Board
  www.arb.ca.gov/toxics/asbestos/asbestos.htm
- California Geological Survey
  www.conservation.ca.gov/cgs/minerals/hazardous_minerals/asbestos/Pages/Index.aspx
- California Office of Environmental Health Hazard Assessment
  www.oehha.ca.gov/air/toxic_contaminants/Asbes_F.html
- California Department of Toxic Substances Control
  www.dtsc.ca.gov/HazardousWaste/upload/OAD_FS_Asbestos.pdf
- El Dorado County Environmental Management Dept.
  www.co.el-dorado.ca.us/emd/apcd/asbestos.html
- University of California, Davis Health System
  www.ucdmc.ucdavis.edu/newsroom/releases/archives/cancer/2005/asbestos_cancer7-2005.htm

The U.S. Department of Agriculture (USDA) prohibits discrimination in all its programs and activities on the basis of race, color, national origin, age, disability, and where applicable, sex, marital status, familial status, parental status, religion, sexual orientation, genetic information, political beliefs, reprisal, or because all or part of an individual's income is derived from any public assistance program. (Not all prohibited bases apply to all programs.) Persons with disabilities who require alternative means for communication of program information (Braille, large print, audiotape, etc.) should contact USDA's TARGET Center at (202) 720-2600 (voice and TDD). To file a complaint of discrimination, write to USDA, Director, Office of Civil Rights, 1400 Independence Avenue, S.W., Washington, D.C. 20250-9410, or call (800) 795-3272 (voice) or (202) 720-6382 (TDD). USDA is an equal opportunity provider and employer.

October 2008 **R5-RG-147**